Structural Investigation of Human PP2A Regulation by Protein Methylation

Meng-Lin Tsai

Institute of Structural and Molecular Biology

University College London

Submitted in fulfillment of the requirements for the degree of Doctor of Philosophy, September 2010

I, Tsai, Meng-Lin confirm that the work presented in this thesis is my own. Where information has been derived from other sources, I confirm that this has been indicated in the thesis.

Abstract

PP2A (protein serine/threonine phosphatase 2A), a conserved protein found in different species, was involved in various cellular processes including cell cycle, signal transduction, DNA replication, transcription, protein synthesis and apoptosis. Deregulation of PP2A methylation is linked to Alzheimer's disease and increased susceptibility to pathogen infection. PP2A was identified as to be an important tumour suppressor protein and hence a potential target for cancer therapeutic strategies. PP2A comprises a core structure of a 65 kDa scaffolding subunit A ($PP2A_A$) and a 36 kDa catalytic subunit C ($PP2A_C$), which associates with a variable regulatory subunit B to form a heterotrimeric holoenzyme. Different heterotrimeric compositions influence the enzyme's cellular location and substrate specificity.

Leucine carboxyl methyltransferase 1 (LCMT1) and protein phosphatase methylesterase 1 (PME1) are involved in PP2A's methylation and de-methylation respectively. Recent research has demonstrated that methylation of PP2A subunit C at the carboxyl-terminus, residue Leu309, by LCMT1 is related to the selection of the regulatory subunit to form a triple complex with the PP2A AC core enzyme ($PP2A_D$). In contrast, PME1 is thought to associate with and stabilize the inactivated form of PP2A complex.

The crystallographic structure of PME1-PP2A complex was solved in 2008 and was suggested that PME1 only associates with the catalytic subunit of PP2A; however, both PME1 and PP2A scaffolding subunit are not native form. In this

study, we used isothermal titration calorimetry (ITC) and surface plasmon resonance (SPR) methods to verify the association of PME1 and $PP2A_A$ and measured thermodynamic parameters of PME1-$PP2A_A$ interaction.

Finally, we have solved an X-ray crystal structure of human LCMT1 protein in complex with the co-factor S-adenosylmethionine (AdoMet) to resolution of 2 Å. The structure enables us to postulate a mode of interaction with protein phosphatase PP2A and it provides a platform for further functional studies of the methylation regulation of PP2A.

Acknowledgements

First, I sincerely thank my supervisor, Dr. Snezana Djordjevic, for her encouragement, patience, and guidance during the past four years. Because of her understanding and support, I could overcome the difficulties of this project. I would also like to thank Professor Paul Driscoll and Professor Ivan Gout for their useful suggestions and directing me in my PhD studies.

Secondly, I would like to thank Dr. Nora Cronin, Dr. Jean Paul Delgado, Dr. Sunita Sardiwal, Dr. Roger George and Dr. Syeed Hussain for their help in my project over the last few years. I would also like to show my gratitude to the people working in Darwin building.

Finally, I would like to thank my parents, Tsai, Ruei-Jen and Hou, Shu-Jiuan, and my wife, Yu-Ting, for their full support, love and patience.

Table of Contents

Chapter Two

Chapter Four

Chapter Five

List of Figures

Chapter One

Chapter Two

Chapter Three

Chapter Four

Chapter Five

Chapter Six

Chapter Seven

List of Tables

Abbreviations

4E-BP1	Eukaryotic initiation factor 4E binding protein 1
AD	Alzheimer's disease
BAD	Bcl-2-associated death promoter protein
BAX	Bcl-2-associated X protein
Bcl2	B Cell CLL/Lymphoma 2
bp	Base pair
CaM	Calmodulin
CD	Circular dichroism
Cdc	Cell division cycle protein
Cdk2	Cyclin-dependent kinase 2
Cdt1	chromatin licensing and DNA replication factor 1
CIP2A	Cancerous inhibitor of PP2A
DSC	Differential scanning calorimetry
E. coli	Escherichia coli
eRF	Eukaryotic release factor
ERK	Extracellular regulated kinase
HEAT	Huntingtin-Elongation-A subunit-TOR
IPTG	Isopropyl-2-Dthiogalactopyranoside
ITC	Isothermal titration calorimetry
JNK	c-Jun NH_2-terminal kinase
kDa	kilodalton
l	Litre
LCMT1	Leucine carboxyl methyltransferase 1
M	Molar
MAPK	Mitogen activated protein kinases
MPF	M Phase promoting factor
MW	Molecular weight
NFκB	Nuclear factor-κB
OA	Okadaic acid
PCR	Polymerase chain reaction
PKA	Protein Kinase A
PKB	Protein kinase B
PKC	Protein kinase C

PKR	Double-strand-RNA-dependent protein kinase
PME1	Protein phosphatase methylesterase 1
PMSF	Phenylmethanesulfonylfluoride
PP1	Protein phosphatase 1
PP2A	Protein Phosphatase 2A
$PP2A_A$	Scaffolding subunit of PP2A
$PP2A_B$	Regulatory subunit B family
$PP2A_{B'}$	Regulatory subunit B' family
$PP2A_{B''}$	Regulatory subunit B" family
$PP2A_{B'''}$	Regulatory subunit B'" family
$PP2A_C$	Catalytic subunit of PP2A
$PP2A_D$	Scaffolding subunit and catalytic subunit, PP2A core enzyme
$PP2A_T$	PP2A core enzyme with regulatory subunit
PPM	The metal dependent protein phosphatases
PPM1	Protein phosphatase methyltransferase 1
PPPs	Phosphoprotein phosphatases
PSPs	Protein serine/threonine phosphatases
PTPs	Protein tyrosine phosphatases
SAH	S-adenosyl Homocysteine
SAM	S-adenosyl methionine
SAPK	Stress-activated protein kinase
SDS-PAGE	Sodium dodecyl sulfate polyacrylamide gel electrophoresis
Sf9	Spodoptera frugiperda-9
SG2NA	S/G_2 nuclear autoantigen
SPR	Surface plasmon resonance
SV40	Simian vacuolating virus 40
TGF-β	Transforming growth factor-β
TOR	The target of rapamycin
WD	Tryptophan-aspartate

Chapter One

Introduction

1.1 Protein Phosphatase 2A

1.1.1 Classification of Protein Phosphatases

Protein phosphatases and kinases represent almost 3 % of human genome, including 518 putative protein kinases, 107 putative protein tyrosine phosphatases (PTPs) and far fewer other protein phosphatases. Together, these proteins regulate almost 30 % of the cellular proteins via reversibly protein phosphorylation [1-3].

Protein phosphatases (PPs), primary effectors of dephosphorylation, can be grouped into two major superfamilies, protein tyrosine phosphatases (PTPs) and protein serine/threonine phosphatases (PSPs), based on distinct substrates, amino acid sequences, three dimensional structures, and the catalysis mechanisms [4]. According to amino acid sequence of the catalytic domain, the PTPs superfamily can be further grouped into four families, Class I Cys-based PTPs (classical PTPs and dual specificity phosphatases (DSPs)), Class II Cys-based PTPs (18 kDa low molecular weight tyrosine phosphatase (LMPTP)), Class III Cys-based PTPs (CDC25a, CDC25b and CDC25c), and Asp-based PTPs (Eya) [5;6]. The PSPs superfamily contains the phosphoprotein phosphatases (PPPs) family, the metal dependent protein phosphatases (PPMs) family and the aspartate-based phosphatases, represented by FCP/SCP (TFIIF-associating component of RNA polymerase II CTD phosphatase/small CTD phosphatase). The FCP/SCP subfamily uses the aspartate-based catalytic mechanism to de-phosphorylate the C-terminal domain of RNA polymerase II. There are seven members in the PPPs family

comprising PP1, PP2A, PP2B, PP4, PP5, PP6 and PP7. The catalytic subunit of each member associates with various regulatory subunits. The metal dependent protein phosphatases (PPMs) family comprises PP2C and pyruvate dehydrogenase phosphatases (PDPs), which rely on Mg^{2+} and Mn^{2+} activation. Unlike the PPPs family, the members of PPMs family have no regulatory subunits but contain additional domains and conserved motifs which are related to their substrate specificity (Figure 1-1) [4;6]. This thesis focuses on the structure and methylation regulation of protein serine/threonine phosphatase 2A (PP2A) which belongs to the PPPs family of PSPs superfamily.

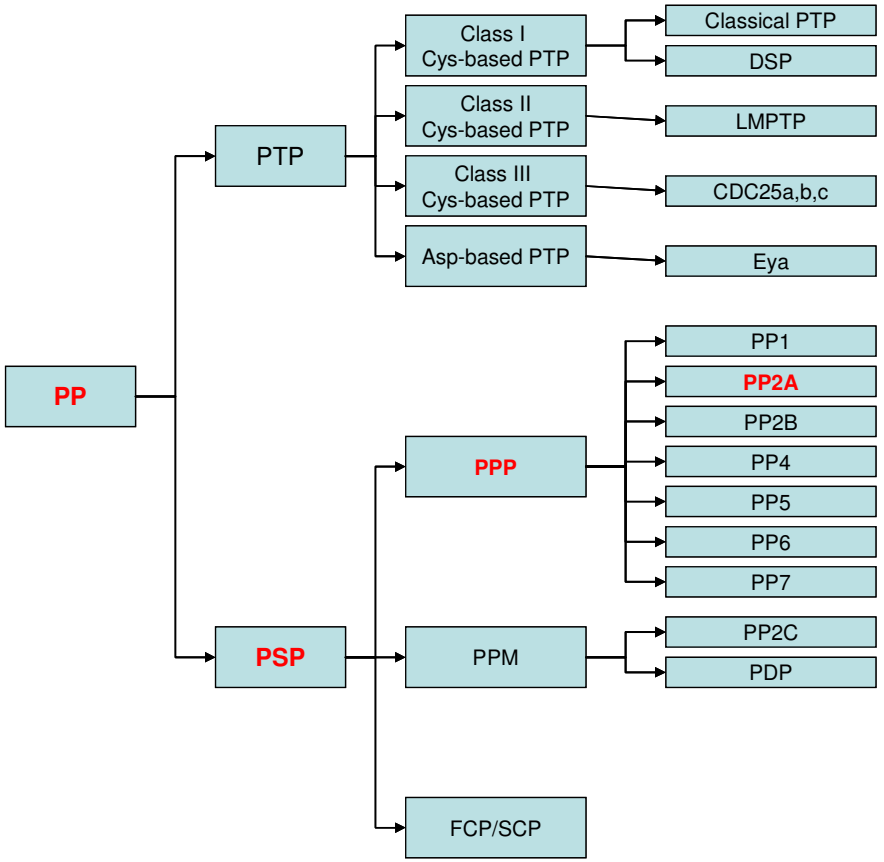

Figure 1-1. Classification of Protein Phosphatase Members. Protein phosphatases comprise two superfamilies, protein tyrosine phosphatases (PTPs) and protein serine/threonine phosphatases (PSPs). PP2A is classified into the phosphoprotein phosphatases (PPPs) family of PSPs superfamily [4-6].

1.1.2 Structure of PP2A

The core enzyme of PP2A is a dimer ($PP2A_D$) that consists of a highly conserved 65 kDa scaffolding subunit A ($PP2A_A$) and a 36 kDa catalytic subunit C ($PP2A_C$). Each subunit has two isoforms, α and β, which share high sequence similarity [7-9]. The core enzyme combines with one of the variable regulatory subunits to form a triple complex ($PP2A_T$). The regulatory subunits, at least 17 of them, belong to four families, B (PR55), B' (PR61), B" (PR48/PR59/PR72/PR130), and B'" (PR93/PR110) [10;11]. The regulatory B subunits will determine substrate specificity, cellular location and enzymatic activity of PP2A. In addition, the expression levels of the various regulatory subunits are highly diverse among different cell types and tissues [10;11].

1.1.2.1 Scaffolding Subunit A ($PP2A_A$)

The PP2A scaffolding subunit A exists in two forms, Aα and Aβ, which are 86% identical and consists of 15 tandem repeats, Huntingtin-Elongation-A subunit-TOR (HEAT) motifs, which are organized into a horseshoe shape [12]. A HEAT repeat is a loosely conserved sequence motif that has been identified in the huntingtin protein, elongation factor 3, the PP2A scaffolding subunit, lipid kinase (TOR), the nuclear pore transport protein importin β, and the splicing factor SAP155 [13-16]. Each HEAT repeat is composed of about 39 amino acids that are folded into a pair of anti-parallel α helices connected by an intra-repeat loop. Adjacent HEAT repeats are connected by inter-repeat turns. Left-handed rotations at several inter-repeat interfaces generate an L-shaped super helical conformation (Figure 1-2a [12]). When the scaffolding subunit

A interacts with the catalytic subunit C and regulatory subunit, significant bending of HEAT repeats 12-15 toward the amino terminus of the scaffolding subunit A was observed (Figure 1-2b [17]). Assembly of $PP2A_D$ results in significant changes in HEAT repeat 13 of the scaffolding subunit A [18]. The additional conformational rearrangement in the scaffolding subunit A, caused by the breakage of a hydrogen bond in HEAT repeat 11, is present in the $PP2A_T$ but not $PP2A_D$. The flexible structure of the PP2A scaffolding subunit A may be an important feature for the $PP2A_D$ to accommodate multiple families of regulatory subunits [19]. The scaffolding subunit A interacts with the catalytic subunit C via the intra-repeat loops of HEAT repeats 11-15 (Figure 1-2c [17;19]). The interaction between the subunit A and C is dominated by an extensive hydrogen bonds network that probably explains the high affinity of this interaction. Eight mutants of subunit A are linked to lung and colon cancers and all mutations in subunit A are defective in binding either subunit B or C [20]. With the reference to the crystal structures it could be noted that the amino acids related to these cancer-associated mutations directly participate in subunit interactions. This observation could be used to postulate that loss of normal regulation of PP2A activity might be caused by disruption of $PP2A_T$ formation and thus contributing to carcinogenesis [17-19].

a.

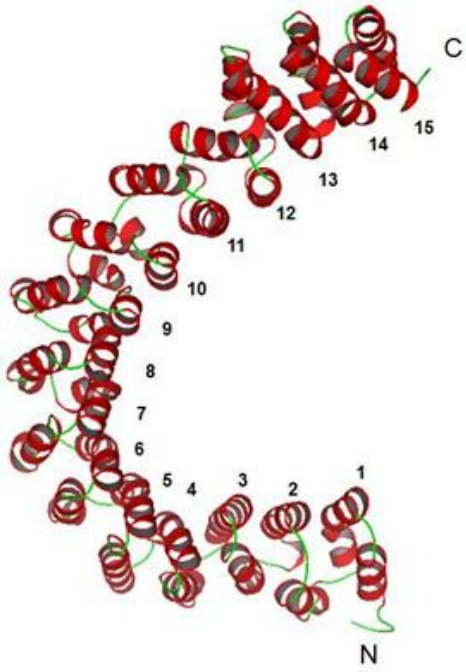

b.

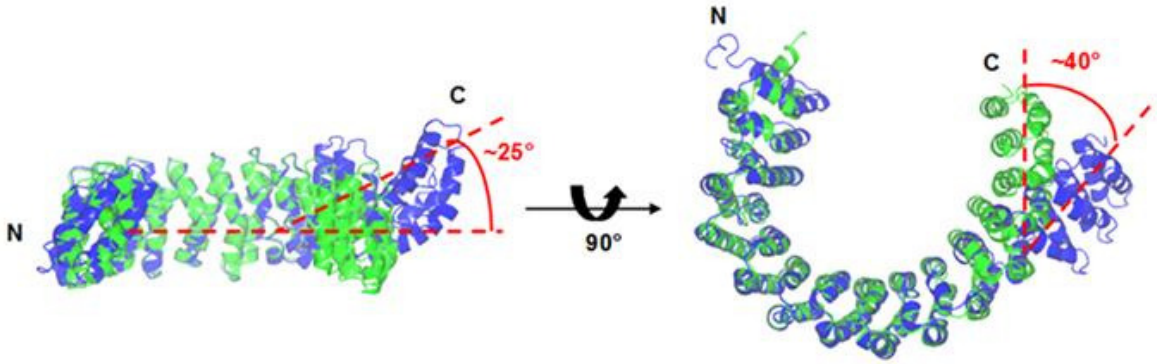

c.

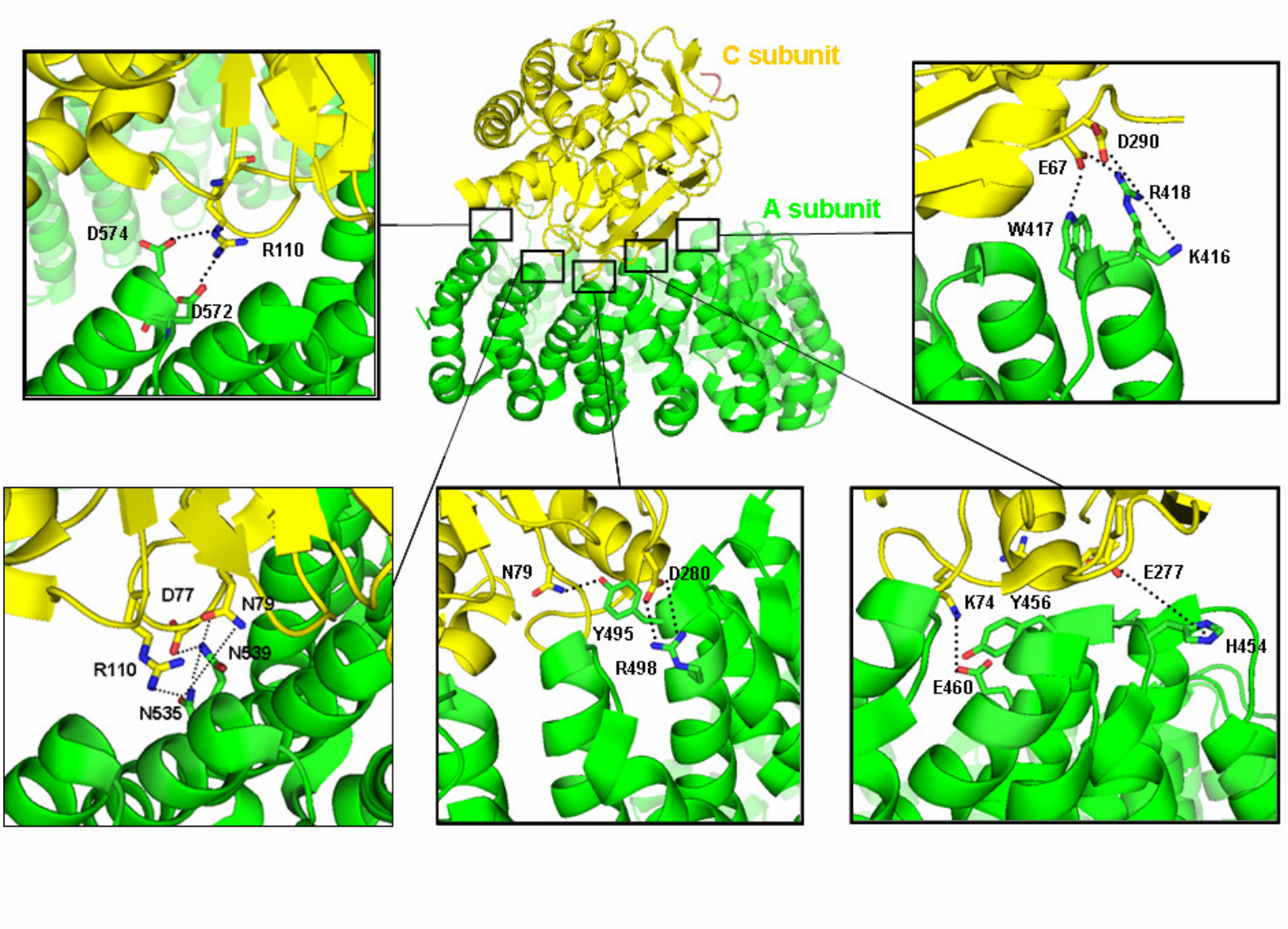
C subunit
A subunit
D574
R110
D572
D290
E67
R418
W417
K416
D77
N79
R110
N539
N535
N79
D280
Y495
R498
E277
K74
Y456
H454
E460

d.

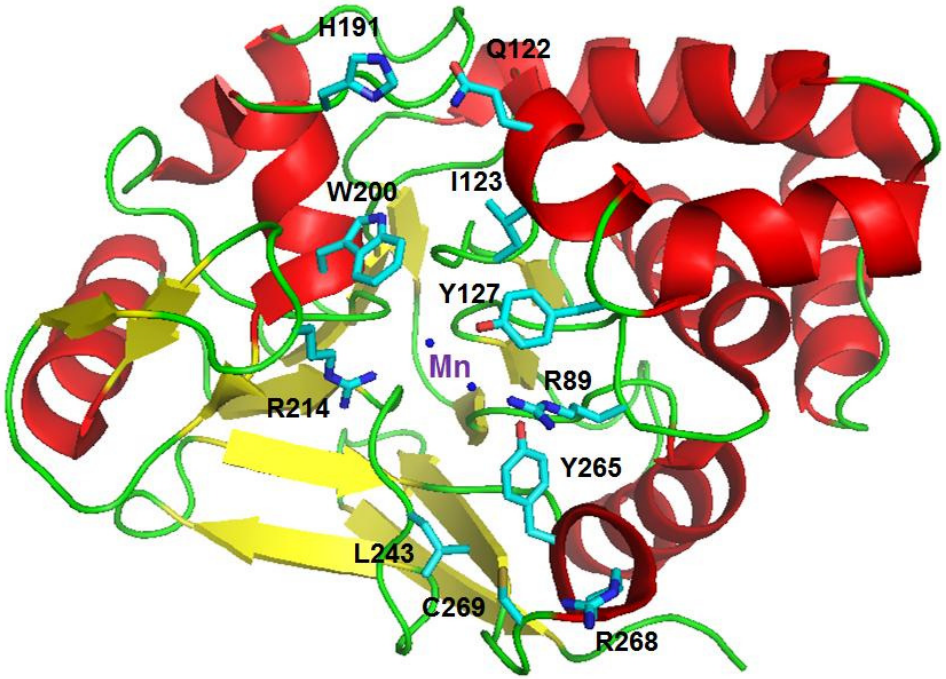

Figure 1-2. The Structure of $PP2A_A$ and $PP2A_C$. (a) Ribbon diagram of $PP2A_A$ generated with PyMOL viewer *(DeLano Scientific LLC*). $PP2A_A$ is composed of 15 HEAT repeats and forms a horse-shoe shaped fold [12]. (b) The structure superimposition of $PP2A_A$ (blue) (PDB: 1B3U) and $PP2A_T$ (green) (PDB: 2IAE) using Coot 0.6.1. and presented by PyMOL viewer. The association of regulatory subunit and catalytic subunit with $PP2A_A$ will cause the conformational change of $PP2A_A$ [17]. (c) Interface of $PP2A_A$ (green) and $PP2A_C$ (yellow) generated with PyMOL viewer. $PP2A_A$ interacts with $PP2A_C$ through hydrogen bonds at the intra-repeat loops of HEAT repeat 11-15 [17;19]. Dashed black lines represent hydrogen bonds. (d) The structure of $PP2A_C$ (PDB: 2IE3) generated with PyMOL viewer shows the active site of the enzyme and the substrate binding pocket located above the two manganese atoms [18].

1.1.2.2 Catalytic Subunit C ($PP2A_C$)

PP2A catalytic subunit C, composed of 309 amino acids, also contains two closely related iso-forms, Cα and Cβ, which share 97% sequence identity [21]. $PP2A_C$ contains an α/β fold catalytic domain and two manganese ions at the active site and shows high sequence identity to the catalytic subunit of PP1 (43% sequence identity) (Figure 1-2d [18]). Moreover, the residues participating in catalysis are highly conserved exhibiting similar catalytic mechanisms [21;22]. The active site is positioned away from the ridge of $PP2A_A$ and tilted toward the regulatory subunit B binding site of $PP2A_A$. Although the overall structure of $PP2A_C$ is conserved to other serine/threonine phosphatases in PPPs family, the local conformation of the solvent exposed surface loops are quite different. These differences might explain the functional diversity between PP2A and other protein phosphatases [17;19].

The carboxyl terminal residues 294-309 of $PP2A_C$ play an important role in the regulation of PP2A of subunit C and are highly conserved among all other serine/threonine phosphatases. Thus, the mechanism of regulation may be similar in all other serine/threonine phosphatases [17;19].

1.1.2.3 Regulatory Subunits ($PP2A_B$, $PP2A_{B'}$, $PP2A_{B''}$, and $PP2A_{B'''}$)

In contrast to subunit A or C, members of the four families of the PP2A regulatory subunits exist in several isoforms (Figure 1-3 [10;11]). Each type of the regulatory subunit imparts specific functions to the PP2A holoenzymes. In recent reports it was

suggested that the role of the PP2A regulatory subunits is to tether the $PP2A_T$ to its substrate rather than modify the catalytic site to accommodate different substrates [23].

1.1.2.3.1 Regulatory Subunit B ($PP2A_B$)

Regulatory subunit B family is involved in the dephosphorylation of Tau protein related to Alzheimer's disease [24]. In mammalian cells there are four isoforms encoded by four related genes in this family, PR55α, PR55β, PR55γ and PR55δ. PR55α and PR55δ have a widespread tissue distribution, whereas PR55β and PR55γ are enriched in the brain [25-27]. According to molecular structure the B family adopts a seven-bladed β-propeller fold, also known as tryptophan-aspartate (WD) repeats containing an acidic, substrate-binding groove located in the centre of the propeller [24] (Figure 1-4a). WD repeats are commonly found in proteins which engage in multiple protein-protein interactions [28]. For example, PR55α and PR55δ have been shown to interact with transforming growth factor-β (TGF-β) receptors and suppress and activate signaling pathway, respectively [29;30]. In addition to the core structure of β-propeller fold, PR55α also contains two β hairpins and two α helices which extend out of the β-propeller fold and form a β hairpin arm that grabs on to the A subunit (Figure 1-4a [24]). Unlike the B' family, there are very few interactions between B family and $PP2A_C$. The only contact is via residue Leu87 of PR55α, which interacts with $PP2A_C$ residues Val126 and Tyr127 via van der Waals (Figure 1-4b [24]) type of interactions. In addition, there is no interaction between C-terminal tail of $PP2A_C$ and PR55α. However, the association of $PP2A_A$ and PR55α are more extensive and stable. The β hairpin arm makes interactions with HEAT repeat 1 and 2 of $PP2A_A$

through van der Waals and the β-propeller fold also associates with $PP2A_A$ at the ridge of HEAT repeat 3 to 7 (Figure 1-4b [24]). All amino acids in PR55α forming H-bond to residues in $PP2A_A$ are highly conserved in other isoforms of regulatory subunits B family and share an identical mode of interaction with $PP2A_A$ [24].

1.1.2.3.2 Regulatory Subunit B' ($PP2A_{B'}$)

Five distinct mammalian genes encode members of the B' (PR61) family, called PR61α, β, γ, δ, and ε, generating at least eight isoforms [31-35]. All members of the family B' contain a highly conserved sequence in the central region (80% identity) but diverge at the C- and N-terminal portions suggesting that the conserved region is required for interaction with the A-C ($PP2A_D$) complexes, whereas the C- and N-terminal sequences may be responsible for different purposes, such as regulation of substrate specificity and subcellular targeting [35]. The PR61α and PR61γ1–γ3 are mainly expressed in the heart and skeletal muscle [34;36], whereas PR61β and δ are mainly expressed in the brain [32;33].

The two structures of the $PP2A_T$ reveal that the regulatory subunit B'(PR61γ1) is composed of eight pseudo-HEAT repeats and forms a solenoid-shaped structure similar to the HEAT repeats [17;19]. However, the protein sequence of PR61γ1 does not share apparent sequence similarity to any other HEAT-repeats-containing proteins. PR61γ1 interacts with subunit C near the active site and can determine the substrate specificity of PP2A by shielding a substantial surface of the $PP2A_C$ to provide a new surface. There are three main interfaces formed between $PP2A_C$ and PR61γ1 (Figure 1-5a [17]). The conserved residue Arg268 in the β12-β13 loop of $PP2A_C$ make

interactions with acidic residues in the intra-repeat loop 2 of PR61γ1 and form the first interface. The helical subdomain of $PP2A_C$ forms the second interface with the intra-loop of pseudo-HEAT repeats 6-8 of PR61γ1. The third interface is formed between the C-terminal tail of $PP2A_C$ and pseudo-HEAT repeats 4-6 of PR61γ1. The interactions of PR61γ1 with $PP2A_A$ are between the intra-repeat loops of the HEAT repeats 2–8 of $PP2A_A$ and the convex side of the PR61γ1 pseudo-HEAT repeats 2, 4, and 5 (Figure 1-5b [17]).

1.1.2.3.3 Regulatory Subunit B" ($PP2A_{B"}$)

The B" family contains two Ca^{2+} binding sites formed by an E-F hand motif. Two different isoforms have been described, PR72 and PR130, which are the splicing products from the same gene. Previous studies demonstrated that the family B" (PR72) is expressed exclusively in the heart and skeletal muscle, whereas PR130 was detected in almost all of the tissues analyzed, with the highest levels observed in the heart and muscle [37]. A recent report shows that the PR72 subunit is highly expressed in striatal tissue and possibly plays a role in the regulation of dopaminoceptive neurons, dopamine- and cAMP-regulated protein (DARPP-32) dephosphorylation by PP2A [38].

A regulatory subunit PR59, identified as an interaction partner of the retinoblastoma-related p107 protein, shares 56% identity with PR72; however the expression patterns of the two proteins differ completely. When PR59 and p107 were

co-expressed, overexpression of PR59 resulted in inhibition of cell cycle progression in the G_1 phase. This observation may be related to an increase in the amount of the hypo-phosphorylated p107 contributing to the activation of p107 [39].

PR48 shares 68% sequence similarity with PR59 and was found to interact with Cdc6, a protein required for the initiation of DNA replication [40;41]. Over-expression of PR48 causes a G_1 arrest suggesting that PP2A keeps the Cdc6 in the dephosphorylated form, a prerequisite for binding to the origins of DNA replication [42].

1.1.2.3.4 Regulatory Subunit B''' ($PP2A_{B'''}$)

Striatin (PR110) and S/G_2 nuclear autoantigen (SG2NA/PR93) were observed to form a stable complex with PP2A and were also identified as new members of a potential B''' family. Like the family B (PR55), they all contain the WD40 repeats and the association of striatin and SG2NA with $PP2A_D$ is independent of the C subunit carboxyl terminus. Striatin has been reported to associate with the post-synaptic densities of neurons, whereas SG2NA has been reported to be a nuclear protein expressed primarily during the S and G_2 phases of the cell cycle [43;44]. Both proteins also bind to calmodulin in a calcium-dependent manner, suggesting that these proteins that form PP2A triple-complexes may be involved in calcium-dependent signaling pathways and cellular events [45-48].

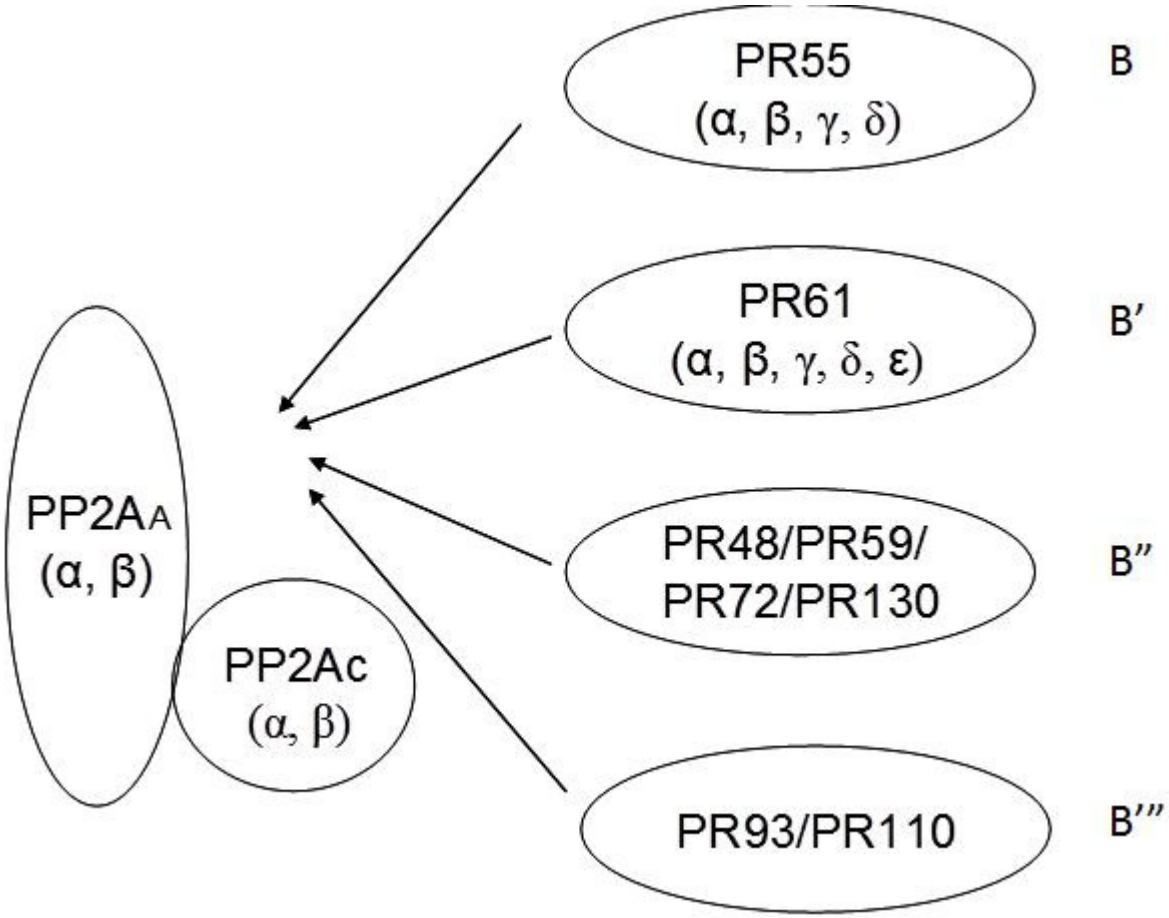

Figure 1-3. The Four Families of Regulatory Subunits. Based on the protein sequence, multiple B subunits, which have been grouped into four individual families (B (PR55), B' (PR61), B" (PR48/59/72/130) and B"' (PR93/110)), exist to target PP2A to distinct cellular compartments and/or substrates [10;11].

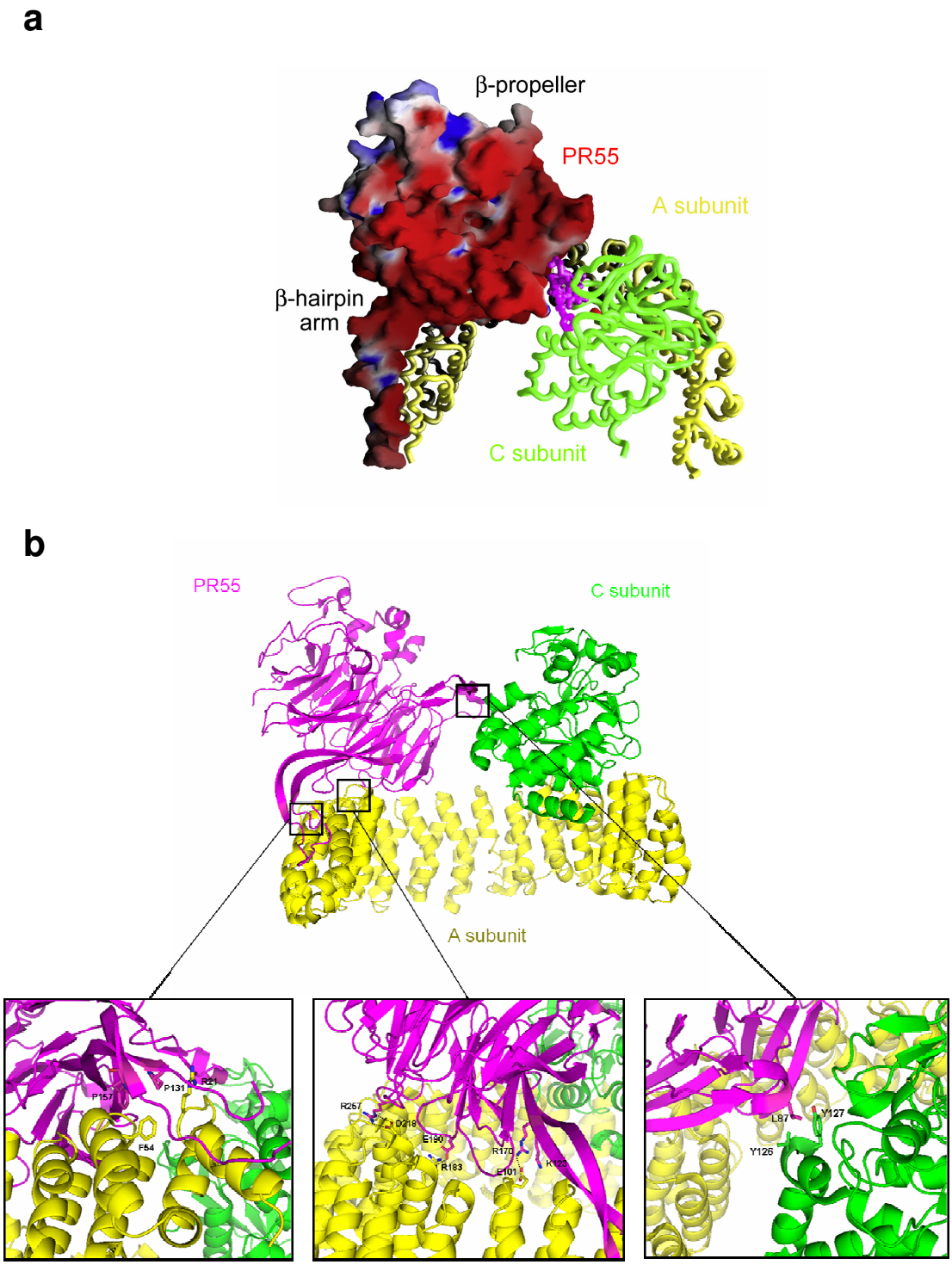

Figure 1-4. The Interaction of PP2A$_D$ and PR55. (a) The figure orginated from reference [24]. PR55 contains a seven-bladed β-propeller fold forming a highly acidic top face and additional a/β hairpin arm that interacts with the A subunit. (b) Ribbon diagram of PP2A$_D$-PR55 (PDB: 3DW8) generated with PyMOL viewer *(DeLano Scientific LLC*). The interaction between the hairpin arm of PR55 and HEAT repeats 1 and 2 of PP2A$_A$ is dominated by van der Waals, whereas the recognition between the

bottom face of PR55 and HEAT repeats 3-7 is dominated by hydrogen bonds (black dashed line). In addition, the residue Leu87 of PR55α contacts $PP2A_C$ residues Val126 and Tyr127 via van der Waals interactions [24].

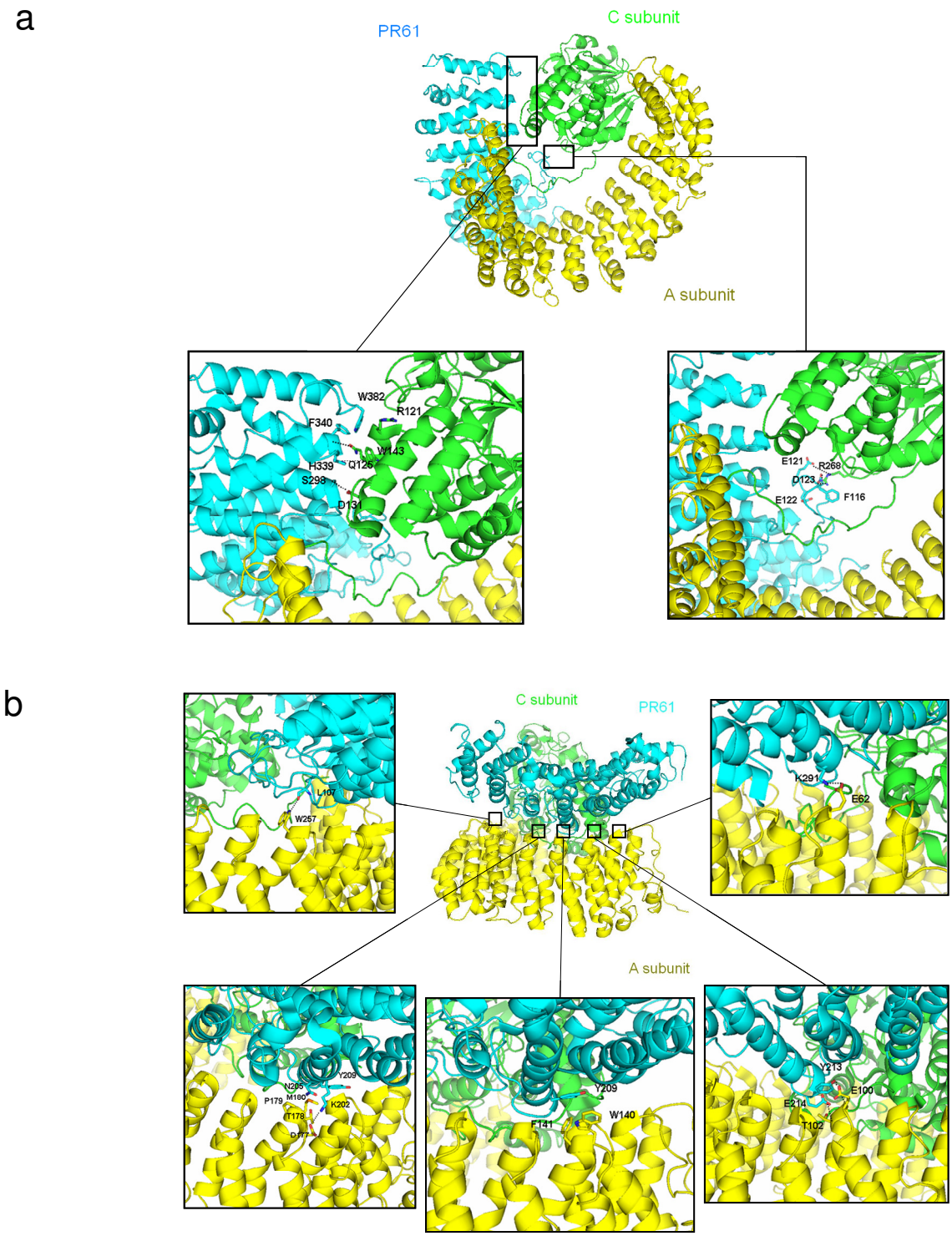

Figure 1-5. Interface of the PR61 with PP2A$_C$ and PP2A$_A$. Ribbon diagram of PP2A$_D$-PR61 (PDB: 2IAE) [17] represented by PyMOL viewer *(DeLano Scientific LLC)*. (a) Three main interfaces formed between PP2A$_C$ and PR61γ1contain a mixture of hydrogen bonds (black dashed line) and van der Waals contacts. (b) The interface of PP2A$_A$ and PR61γ1is dominated by van der Waals interactions [17].

1.1.3 Regulation of PP2A

1.1.3.1 Phosphorylation

PP2A can be phosphorylated by the epidermal growth factor (EGF), insulin receptor, and the tyrosine kinases including leukocyte-specific protein tyrosine kinase (LCK) and viral sarcoma (V-SRC) kinases [49]. The phosphorylation of the C-terminal tail of PP2A at Tyr307 will result in the inactivation of PP2A [50-53]. In addition to phosphorylation of $PP2A_C$, regulatory subunit B' family can also be phosphorylated. *In vitro*, phosphorylation of PR61δ by protein kinase A (PKA) regulates the activity and changes the substrate specificity of PP2A [54]. Phosphorylaton of PR61α by the double-strand-RNA-dependent protein kinase (PKR) promotes the activity of PP2A to associate with PKC-phosphorylated myelin basic protein and PKR-phosphorylated eukaryotic translation initiation factor 2α, *in vitro* [55].

1.1.3.2 Methylation

In addition to Tyr307 for phosphorylation, the $T^{304}PDYFL^{309}$ motif of $PP2A_C$ also contains a target site for methylation by a novel carboxyl methyltransferase [56-58]. All $PP2A_C$ sequences share this highly conserved motif at their C-terminal and the reversible methylation occurs on the carboxyl group at Leu309 [59;60]. In *Saccharomyces cerevisiae*, loss of the protein phosphatase methyltransferase 1 (PPM1), a homolog of leucine carboxyl methyltransferase 1 (LCMT1), results in loss of PP2A methylation, indicating that yeast PPM1 is probably the major methyltransferase responsible for methylating PP2A [61]. In parallel, it was demonstrated that the

mammalian LCMT1 and protein phosphatase methylesterase 1 (PME1) were also the major mammalian methyltransferase and methylesterase of PP2A [62;63]. Although many hypotheses were generated regarding the cellular function of the reversible methylation of PP2A, definitive description of a role that methylation of PP2A plays remained elusive.

Initially, the main function of methyltransferase was thought to be to methylate and further activate PP2A [64], with methylesterase reverse role to de-methylate and inactivate PP2A [63]; however, this hypothesis was soon disputed by two other groups which obtained opposing data with respect to the effect of $PP2A_C$ methylation. One group suggested that the methylation was not related to the activity of $PP2A_C$ [62] while others indicated that methylation leads to a decrease in $PP2A_C$ activity [65]. Therefore, methylation of $PP2A_C$ may impact on other properties of PP2A rather than catalytic activity directly.

After it was shown that methylation of Leu309 is necessary for $PP2A_D$ to associate with regulatory subunit PR55, *in vitro* [66] further evidence for the role of methylation in heterotrimeric assembly emerged. For example, it was demonstrated that fully-methylated $PP2A_T$ recruits B" (PR72) or B'" subunit *in vivo*. In a separate study though $PP2A_T$ was not always fully methylated when associated with B subunit (PR55) [62]. This result was soon confirmed by others that showed that the loss of carboxyl methyltransferase activity decreases but does not eliminate the formation of the $PP2A_T$ with PR55 [67;68]. Furthermore, an additional player in PP2A assembly and activation was identified – the protein phosphatase 2A activator (PTPA) protein, a peptidyl-prolyl cis/trans-isomerase. *In vitro* Studies have shown that the inactivated

$PP2A_C$ forming a complex with PME1 can only be reactivated by PTPA but not by methyltransferase [69;70] thus creating an even more complex picture of PP2A regulation and the specific function that methylation step plays in this process.

In 2006, the crystal structure of the PP2A holoenzyme was determined by two groups independently. Based on the PP2A three dimensional structure, the methylation of the C-terminal tail of subunit C at Leu309 was predicted to neutralize the negatively charged surface present at the A-C interface and thus recruit subunit B' (PR61) to form a stable holoenzyme [17] (Figure 1-6). This result might explain how methylation could assist in the formation of the PP2A holoenzyme and why methylation is always required for PP2A to recruit B' subunit (PR61). In 2007, another research group supported the view that methylation of the C-terminal tail of the PP2A subunit C is not required for either catalytic activity or the binding of the B subunit (PR55), *in vitro* [71]. In contrast a recent work indicated that methylation of the PP2A subunit C is not absolutely required for the binding of B' (PR61) or B" (PR72) family, but necessary for the binding of B (PR55) family, *in vivo* [72]. Taken everything together, it could be concluded that the methylation state of the catalytic subunit imparts on and regulates holoenzyme assembly. However due to the contradictory evidence it remains unclear how the methylated status of $PP2A_C$ results in an acquired selectivity for binding of regulatory subunit B, B' or B'".

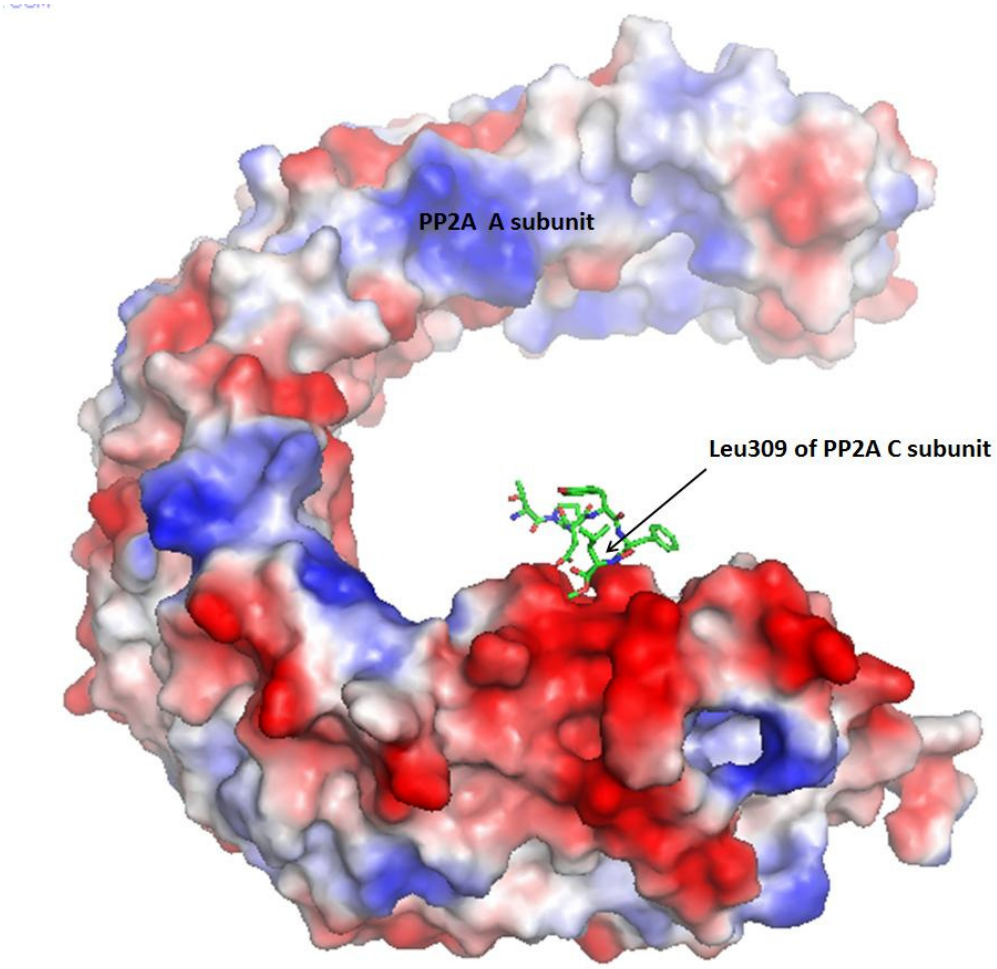

Figure 1-6. Methylation of PP2A$_C$. Qualitative representation of surface electrostatic potential of PP2A$_A$ (PDB: 2IAE) as generated in PyMOL viewer (*DeLano Scientific LLC*). The C-terminal tail of PP2A$_C$ is positioned in the middle of negatively charged region (red) of PP2A$_A$. When the C- terminal tail of PP2A$_C$ is methylated by LCMT1, charge repulsion is neutralized and the methylated C-terminal tail can settle down on the A-B interface [17;18].

1.1.4 Biological Role of PP2A

Protein serine/threonine phosphatase 2A (PP2A) is a conserved protein found in many different species and it constitutes 1% of total cellular proteins. Together with protein phosphatase 1 (PP1), PP2A contributes to 90% of all Serine/Threonine phosphatase activity in tissues and cells [73]. PP2A plays an important role in various cellular processes [10;74;75] including cell cycle regulation [76-80], DNA replication [42;81;82], mRNA translation [83-86], signal transduction [87-89] and apoptosis [90-95]. The deregulation of PP2A methylation is linked to Alzheimer's disease and increased susceptibility to pathogen infections [96-98]. PP2A was identified as an important tumour suppressor protein and hence a potential target for cancer therapeutic strategies [99;100]. In addition, okadaic acid (OA), a PP2A non-specific inhibitor, is the main marine toxin implicated in the diarrhetic shellfish poisoning (DSP) in humans after consumption of contaminated bivalve molluscs. Therefore, PP2A could be used in an inhibitor assay for assessing okadaic acid contamination [101].

1.1.4.1 The Role of PP2A in Cell Cycle Regulation

The cell cycle, composed of four distinct phases (G1, G2, interphase and mitosis), takes place in a cell leading to its division and duplication [102]. M Phase promoting factor (MPF) composed of the cell division cycle 2 (Cdc2) kinase and cyclin B is involved in the G_2/M transition [103]. In the cell cycle progression, PP2A negatively regulates Cdc2 kinase forming a complex with cyclin B in G2/M transition [104-107]. The activity of Cdc2 kinase relies on phosphorylation at residue Thr161, and PP2A is

related to its de-phosphorylation and inactivation [108;109]. In addition, phosphorylation at two other sites, Thr14 and Tyr15 of Cdc2 kinase is controlled by Wee1 kinase while the Cdc25 dual-specificity phosphatase activates the activity of the Cdc2 kinase. PP2A indirectly inactivates the Cdc2 by both the activation of the Wee1 kinase, which phosphorylates the cdc2 kinase at Tyr15, and by the inactivation of the Cdc25 dual-specificity phosphatase, which remove s phosphate from both Thr14 and Tyr15 of the Cdc2 kinase [78;110;111] (Figure 1-7).

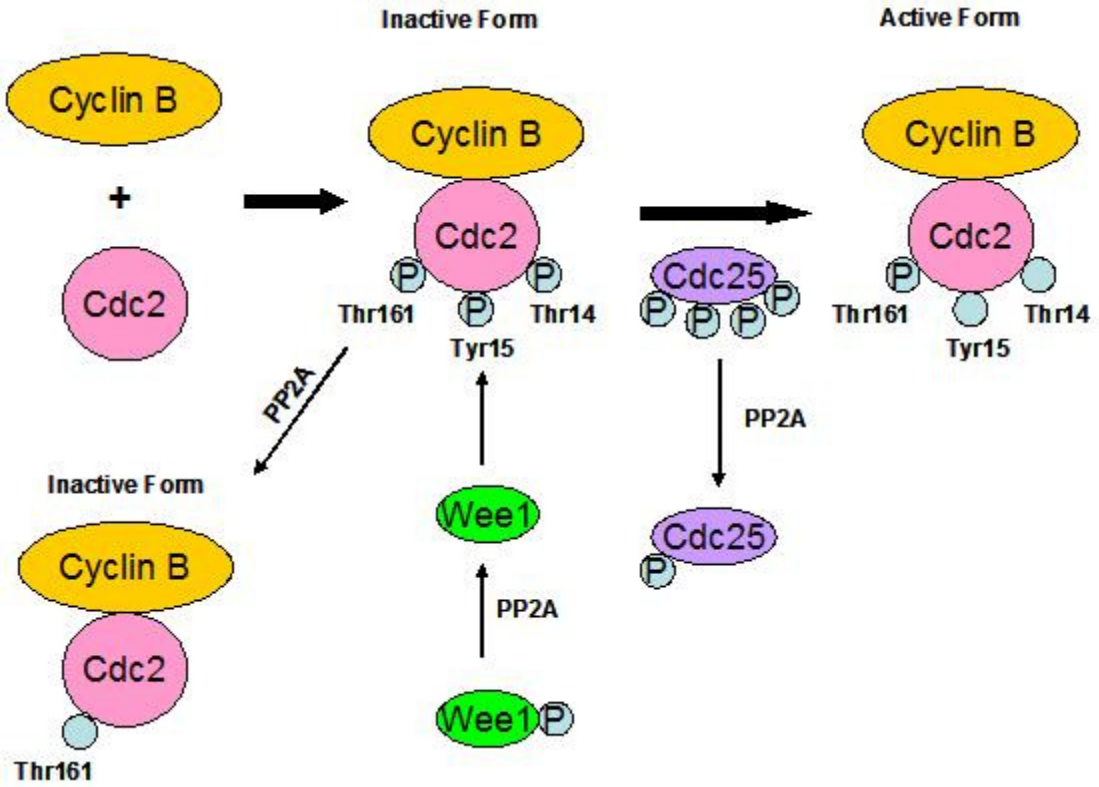

Figure 1-7. The Role of PP2A in Cell Cycle. In early G2 phase, PP2A is required to keep cyclin B-Cdc2 complex in its inactive form by inhibiting CAK (Cdc2 activating kinase) and activating Wee1 kinase. In addition, PP2A inhibits Cdc25 phosphorylation. Finally, PP2A is implicated in the exit from mitosis where PP2A participate in cyclin B degradation and in dephosphorylation of mitotic substrates of active cyclin B-Cdc2 complex [78;104-111].

1.1.4.2 The Role of PP2A in DNA replication

Previous studies indicated the relationship between PP2A and viral DNA replication, *in vivo* or *in vitro*. The Simian vacuolating virus 40 (SV40) large T antigen possesses site-specific DNA binding, ATPase and DNA unwinding activities [112]. The association of the various PP2A complexes with large T antigen is related to the activity of large T function. $PP2A_C$ and $PP2A_D$-B" family or -B' family are involved in SV40 large T antigen dephosphorylation at Ser120, Ser123, Ser677, and Ser679 sites that stimulates large-T-dependent origin unwinding and DNA replication [113;114]. In contrast, $PP2A_D$ and $PP2A_D$-B family will inactivate large T antigen by dephosphorylating the Cdc2 target site, Thr124 site [115].

In eukaryotic cells, cell division cycle 6 protein (Cdc6) is a member of the pre-replication complex together with the origin recognition complex, chromatin licensing and DNA replication factor 1 (Cdt1) and the mini-chromosome maintenance (MCM) complex. Cdc6 is recruited for loading MCM proteins onto the DNA [116;117]. It was demonstrated that $PP2A_D$-B" family interacts with Cdc6 and modulates DNA replication. The phosphorylation of Cdc6 by cyclin-dependent kinase 2 (Cdk2) is necessary for DNA replication and export of Cdc6 from the nucleus. $PP2A_D$-B family, existing in the cell nucleus, has a role in maintaining levels of dephosphorylated Cdc6 until replication is triggered by Cdk2 [42;82].

1.1.4.3 The Role of PP2A in mRNA Translation

1.1.4.3.1 The Initiation of Translation

The target of rapamycin (TOR), a serine/threonine kinase, is highly conserved from yeast to mammals [118;119]. TOR regulates the cell growth and metabolism in response to growth factors, nutrients and stress conditions [120-122]. In eukaryotic cells, there are two distinct multimeric complexes, TORC1 and TORC2. TORC1, sensitive to rapamycin, regulates temporal processes of cell growth while TORC2, which is insensitive to rapamycin, controls spatial aspects of cell growth such as yeast actin polarization, the membrane-localized actin patching concentrate at a previously selected and marked bud site after the initiation of a new cell cycle [120;123;124]. In yeast, Tap42 is a direct target of TORC1 phosphorylation that binds to $PP2A_C$ without A subunit and B subunit [125]. When nutrients are abundant phosphorylated Tap42-$PP2A_C$ localizes to the cell membrane and interacts with TORC1. Under this condition, Tap42-$PP2A_C$ will not dephosphorylate and activate Maf1, a repressor of the RNA Polymerase III. In addition, TORC1 will also phosphorylate Sch9 and promote ribosome biogenesis via the expression of Ribi and RP regulons [126]. However, in response to nutrient deprivation or rapamycin treatment, Sch9 phosphorylation is inhibited and ribosome biogenesis is turned off. At the same time, the Tap42-$PP2A_C$ will be disrupted and $PP2A_C$ will dephosphorylate Maf1, leading to inhibition of RNA Polymerase III [127].

In mammalian cells, an α4 protein, a homologue of Tap42, also binds to $PP2A_C$ independently of $PP2A_A$ and regulatory subunit [128-130]. The function of mTOR is related to the phosphorylation of the translation inhibitor, eukaryotic initiation factor 4E binding protein 1 (4E-BP1), and p70 S6 kinase and eventually causes the

phosphorylation of the 40 S ribosomal protein S6 and initiation of the translation [131]. Like yeast, the nutrient deprivation or rapamycin treatment also leads to the dissociation of α4 and $PP2A_C$. Free $PP2A_C$ can dephosphorylate mTOR-phosphorylated 4E-BP1 and finally inhibit translation [132].

1.1.4.3.2 The Termination of Translation

In addition to the importance of the initiation of translation, $PP2A_C$ also participates in the termination of translation via the association with a translation termination factor, eukaryotic release factor 1 (eRF1), which cooperates with eukaryotic release factor 3 (eRF3) to terminate protein synthesis in ribosomes [84;133;134].

1.1.4.4 The Role of PP2A in Signal Transduction

In signal transduction, PP2A can negatively modulate the activities of several protein kinase cascades, in particular protein kinase B (PKB) [135], protein kinase C (PKC) [136], p70 S6 kinase [137], Ca^{2+} calmodulin dependent kinases [138-140], mitogen activated protein kinases (MAPK), nuclear factor-κB (NF-κB) [141] and the B cell CLL/lymphoma 2 family [142].

1.1.4.4.1 Protein Kinase B (PKB) and p70 S6 kinase

Protein kinase B (PKB) is involved in cellular survival pathways by inhibiting apoptosis

processes [143] and also in the induction of protein synthesis [144]. Phosphoinostide 3-kinase (PI 3-kinase) is related to an extraordinarily diverse group of cellular functions and generates lipid secondary messengers phosphatidylinositol 3,4-bisphosphate (PtdIns(3,4)P_2) and phosphatidylinositol 3,4,5-trisphosphate (PtdIns(3,4,5)P_3). Both of these two messengers bind to the PH domain of PKB and bring about recruitment of PKB to the membrane. Under these conditions, 3-phosphoinositide dependent protein kinase-1 (PDK1) and Ser473 kinase will phosphorylate and activate PKB [145]. PP2A de-phosphorylates and thus inactivates PKB [135].

P70 S6 kinase is also activated by PDK1 but without the assistance of any lipid secondary messengers and inactivated by PP2A. P70 S6 kinase, a serine/threonine kinase, participates in the phosphorylation of S6 ribosomal protein and then induces protein synthesis [137;146-148].

1.1.4.4.2 Protein Kinase C

Protein kinase C (PKC) superfamily plays key roles in a multitude of cellular processes including control of fundamental cellular autonomous activities such as cell proliferation and organismal functions such as memory [149]. PKC contains several isoforms which share three highly conserved phosphorylation sites. One is required for its activity and the others are related to maintenance of the enzyme stability. The activated PP2A which contains PR55 will interact with PKC leading to its inhibition [136;150;151].

1.1.4.4.3 Ca^{2+}-Calmodulin-Dependent Kinase (CaM Kinase)

The CaM kinase cascade is composed of three kinases: CaM-kinase kinase (CaMKK); and the CaM kinases CaMKI and CaMKIV. CAMKI and CAMKIV are phosphorylated and activated by CaMKK [152]. This cascade plays an important role in many cellular processes and has been implicated in various diseases. These processes include cell proliferation, apoptosis, neuronal growth, synaptic plasticity, proper function of the immune system including the inflammatory response, activation of T lymphocytes and hematopoietic stem cell maintenance, and the central control of energy balance that can lead to obesity and diabetes [153-155].

PP2A can not only dephosphorylate CaM kinase I, II and IV *in vitro*, but also CaM, which exists in several forms activating variety of target proteins [87]. Therefore, PP2A might indirectly or directly control the activity of CaM kinase by binding to CaM kinases or modulating interactions between CaM and CaM kinases [156].

1.1.4.4.4 B Cell CLL/Lymphoma 2 Family (Bcl2)

The PP2A is also linked to various mechanisms of apoptosis [157-159]. The Bcl-2-associated death promoter protein (Bad) and Bcl-2-associated X protein (Bax) are all pro-apoptotic molecules of the B cell CLL/lymphoma 2 family (Bcl2 family) [160-162]. Recently, it was shown that PP2A may function as the physiological Bax and Bad regulatory phosphatase that dephosphorylates Bax and Bad and further activates their pro-apoptotic functions [90;95]. The induction of neutrophil apoptosis is

an important event in the inflammatory process. PP2A promotes neutrophil apoptosis through two actions, firstly by dephosphorylating and inactivating p38 mitogen-activated protein kinase (p38 MAPK), a neutrophil survival factor, and thus inhibiting the phosphorylation of caspase 3 and secondly by dephosphorylating caspase 3, which has already been phosphorylated, thereby restoring its activity [94]. In addition, PP2A will dephosphorylate and inhibit the activity of Bcl2 resulting in activation of caspase 2 and thus triggering mitochondrial pathway of cell apoptosis [163].

1.1.4.4.5 Nuclear Factor-κB (NF-κB)

PP2A is also a key regulator of negative feedback regulation of nuclear factor-κB (NF-κB) [141]. NF-κB plays a paradoxical role in apoptosis [164]. Although NF-κB usually inhibits apoptotic process, upon activation by interleukin-1 (IL-1) it enhances ultraviolet-B radiation (UVB)-induced apoptosis [165]. UVB will inactivate the activity of PP2A which is responsible for persistent inhibitor of κB kinase β (IKKβ) activity [166]. The phosphorylation of IKKβ will lead to uncontrolled NF-κB activity. Chronic NF-κB activation will finally lead to cell death but not survival [141].

1.1.4.4.6 Mitogen-Activated Protein Kinase (MAPK)

MAPK pathways regulate a variety of physiological processes such as cell growth, differentiation, and apoptotic cell death [167]. Three MAPK pathways have been elucidated including the extracellular regulated kinase (ERK) pathway, the c-Jun

NH_2-terminal kinase (JNK)/ stress-activated protein kinase (SAPK) and p38 pathway [168-171].

PP2A plays both a positive and negative role in the regulation of ERK pathway [172]. The ERK pathway, related to cell growth, cell proliferation, and survival, is activated mainly in response to mitogens and growth factors [173-175]. Ras, a membrane-bound protein, will recruit Raf (MAPKKK), to the cell membrane for activation [176]. Three mammalian Raf proteins, A-Raf, B-Raf, and Raf-1, share the same downstream MAPKK substrate mitogen-activated protein kinase kinase 1,2 (MEK1,2). MEK1,2 phosphorylate and activate ERK1,2 which can phosphorylate several cytoplasmic and nuclear kinases [177]. PP2A has not only been reported to negatively regulate ERK1/2 activity [178-180], but has also been identified as a positive regulator of Raf1 [181-183] and Ksr - kinase suppressor of Ras [184]. In addition, the different activities of various heterotrimeric PP2A complexes in PP2A's regulation of the ERK1,2 pathway were investigated. For instance, in the human sympathetic neuron cell line PC6–3, overexpression of the PP2A regulatory subunit PR55γ induced ERK pathway activity, whereas PR55α or PR55δ directly promoted ERK1,2 dephosphorylation [183;185]. Recent studies also indicate that PP2A containing PR61β or PR61 γ could directly dephosphorylate and inactivate ERK [186].

The p38 pathway can be stimulated by inflammatory cytokines and mitogens [170]. All p38 MAPK protein isoforms, α, β, γ, δ, are activated by dual phosphorylation of a threonine and a tyrosine [187]. Phosphorylated p38 proteins can activate several transcription factors, including ATF-2, CHOP-1, MEF-2, p53, and Elk-1, and other kinases, such as MNK1,2, MSK1, PRAK, PRAK, MAPKAPK-2 and MAPKAPK-3. In

addition, activation of p38 pathway is also required for apoptosis induction in different cellular models and related to the promotion of cancer cell growth and survival [188-191]. PP2A regulates p38 pathway by association with and dephosphorylation of MEK3 - the activator of p38 MAPK [192].

1.1.4.4.7 Wnt Signalling Pathway

The Wnt signaling pathway comprises a complex network of proteins involved in embryogenesis [193;194]. The deregulation of Wnt pathway will lead to tumorigenesis due to the accumulation of β-catenin in the nucleus [195;196]. Like in ERK pathway, PP2A also plays dual role with dominant and negative effects in Wnt signaling [197]. In the absence of Wnt signal, β-catenin will form complex with adenomatosis polyposis coli (APC), Axin and GSK-3β in the cytosol [196-198]. GSK-3β will phosphorylate β-catenin resulting in the ubiquitination of β-catenin for degradation by proteosome. The binding of PR61α and PR61δ to APC or the binding of PR61α, PR61β and PR61γ to Axin will lead to decreased levels of β-catenin [194]. However, the mechanism of how PP2A negatively regulates the Wnt signaling pathway through the destabilization of β-catenin is still unclear.

The role of PP2A in positive regulation of Wnt signaling is even more complex. PP2A can directly stabilize β-catenin at plasma membrane. The inhibition of PP2A expression results in the degradation of β-catenin which is redistributed to the cytoplasma [194]. The activation of Wnt will lead to the degradation of APC-Axin-GSK-3β through Dishevelled (Dsh). Naked, one of the downstream target genes of the Wnt pathway, inhibits Dsh through a negative feedback mechanism.

Unlike PR72, PR130 will inhibit Naked resulting in the increased Dsh expression, which is also positively regulated by PR61ε. Both PR61ε and PR55 will destabilize the inhibitory properties of GSK-3β. PR61α also interacts with p63, a member of p53 family, and finally stabilizes β-catenin through the negative regulation of GSK-3β [199;200] (Figure 1-8).

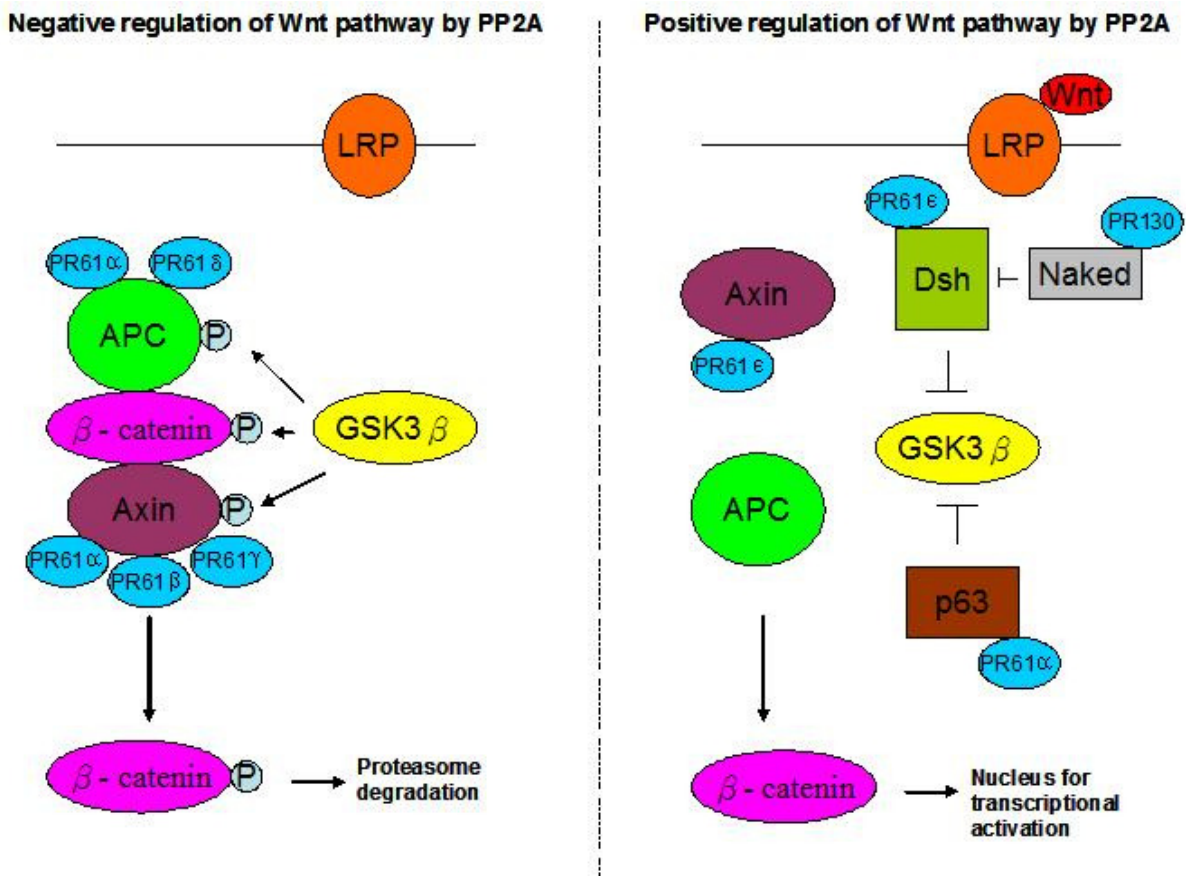

Figure 1-8. The Role of PP2A in Wnt Pathway. In the absence of Wnt signal, β-catenin will associate with APC and Axin which form complex with the members of PR61 family in the cytosol. GSK-3β will phosphorylate β-catenin resulting in the ubiquitination of β-catenin for degradation by proteosome; however, in the presence of Wnt signal, the APC, Axin, and GSK-3β complex is degraded by Dsh. Unphosphorylated β-catenin will move to the nucleus leading to the activation of Wnt target genes. Here, PP2A appears to play a role in the stabilization of β-catenin [194;199;200].

1.1.4.5 PP2A and Pathologies

1.1.4.5.1 Alzheimer's Disease

Alzheimer's disease (AD) is associated with two histopathological hallmarks in the brain, senile plaques and neurofibrillary tangles. Senile plaques are the accumulation of the amyloid-beta peptides derived from the abnormal processing of amyloid precursor protein (APP) whereas neurofibrillary tangles consist of hyperphosphorylated tau protein related to the low activity of phosphatases in the AD brain [201].

Recent research indicated elevated blood levels of the homocysteine are a significant risk factor for Alzheimer's disease. The PP2A catalytic subunit C can be methylated at Leu309 residue by the leucine carboxyl methyltransferase 1 and methylation is required for efficient assembly of the PP2A holoenzyme. The LCMT1 activity is dependent on the S-adenosylmethionine (SAM) and inhibited by the *S*-adenosylhomocysteine (SAH). The elevated SAH levels result in decreased PP2A methylation and may be related to subunit B downregulation and accumulation of the phosphorylated tau protein [202;203].

In addition, intracellular PP2A activity is regulated by two inhibitor proteins, called I_1^{PP2A} and $I_2^{PP2A,}$ found in mammalian tissues. It was suggested that I_1^{PP2A} and I_2^{PP2A} may be involved in Alzheimer neurofibrillary pathology through the inhibition of PP2A activity resulting in abnormal hyperphosphorylation of the tau protein [97;204].

1.1.4.5.2 Carcinogensis

The role of PP2A in carcinogenesis has been disputed for a long time and the protein was viewed as a tumour suppressor. However, there is a sufficient evidence that the inactivation and disruption of PP2A may be related to cancer formation [99;100;205]. For example, the PPP2R1B gene encoding the subunit A of the serine/threonine protein phosphatase was identified as a putative tumour suppressor gene in lung and colon cancer in the chromosome region 11q23. Four of the cancer-associated mutations were found and they have affected A subunit binding to other subunits. Moreover, a total absence or substantial reduction of the subunit A will cause the deregulation of PP2A and some human cancers [206;207]. In addition to subunit A, it was shown that truncation of the regulatory subunit B' (PR61γ) will lead to increased metastasis [208]. Recent data has shown that the expression of PR61γ is suppressed in melanomas compared with non-transformed melanocytic naevi [209]. PR61α also plays an important role as a regulator of c-myc. The dephosphorylation of Ser62 of c-myc by PR61α is modulated by a human oncoprotein, the cancerous inhibitor of PP2A (CIP2A) [210]. In addition, PR61α acts as both a negative and positive regulator of the tumor suppressor p53. The cyclin G, a p53 target, will recruit PP2A containing either PR61α or PR61β to form a quaternary complex with the E3 ligase MDM2 and activate the protein. Finally, MDM2 binds to p53 and ubiquitinates p53 leading to its degradation [211;212]. Although this discovery would not support that notion that PP2A is a tumor suppressor, PP2A is also a positive regulator of p53 signaling pathway. Namely, it was shown that PP2A directly dephosphorylates p53 at Ser37 or Thr55. While dephosphorylation of Ser37 decreases p53 transcriptional activity dephosphorylation of Thr55 stabilizes p53 protein resulting in increased apoptosis

[213;214]. PP2A containing PR55α was also implicated in dephosphorylation and inactivation of protein kinase B that has an important role in tumor-promoting pathways [215].

In another example, the SV40 small t antigen (ST) is an oncoprotein that disrupts the function of PP2A by binding to $PP2A_A$ and displacing the regulatory subunit [216]. Recently, the crystal structure of the SV40 small t antigen with the mouse $PP2A_A$ was determined. The small t antigen contains an N-terminal J domain and a unique C-terminal domain, formed by two zinc-binding motifs. Both the J domain and second zinc-binding motif interact with the intra-repeat loops of the HEAT repeats 3–7 of $PP2A_A$, whereas the first zinc-binding motif may directly interact with and inactivate the catalytic subunit $PP2A_C$ [217].

1.2 Protein Phosphatase Methylesterase 1 (PME1)

PME1, the first methylesterase found in humans, is a highly conserved protein found in different species [63]. In human cells, PME1 is most abundant in the nucleus, whereas the leucine carboxyl methyltransferase 1 (LCMT1) is mainly found in the cytoplasm. The subcellular localization of LCMT1 and PME1 is related to the methylation state of the PP2A subunit C [218].

Earlier studies indicated that PME1 is a PMSF-resistant, okadaic acid-sensitive PP2A methylesterase belonging to a functional family of serine carboxylesterases containing Ser-Asp/Glu-His triad; this triad is also found in lipases [60;63]. According to the

3D-PSSM fold recognition program [219] and the Pfam domain prediction database [220], PME1 contains an esterase domain (residue position from 47-238) thought to catalyze the demethylation of carboxylmethylester of Leu309 from PP2A.

In addition, inactive PP2A was found to tightly interact with PME1 and could only be re-activated by PP2A phosphatase activator (PTPA) but not by LCMT1, *in vitro* [69;70]. This discovery hints to a wider function of PME1 in PP2A regulation rather than just a hydrolysis of a methylester bond. Recently, structural studies suggested that the association of PME1 to PP2A results in inactivation of PP2A through removal of catalytic metal ions [221].

1.2.1 The Structure of PME1

Although PME1, composed of 386 amino acids, has been purified and well characterized more than10 years ago, only recently, its three dimensional structure forming complex with $PP2A_D$ was solved [221]. Based on the structure, PME1 was classified into α/β hydroxylase superfamily. This domain is composed of a nine stranded β sheet surrounded by six α helices, two on one side and four on the other side of the β core. The active site pocket containing catalytic residue Ser156 is located between the cap domain, composed of four additional α helices, and the α/β fold. This structural arrangement suggests that PME1 must undergo an activation process that might be mediated by binding to the PP2A core enzyme. This observation also explains why PME1 cannot interact with carboxyl-methylated peptide $T^{304}PDYFL^{309}$ and shows no reduction of methylesterase activity toward PP2A core enzyme when treated with a conventional a serine protease inhibitor, PMSF [221].

In the reported structure of PME1-PP2A$_D$ complex, PME1 only binds to PP2A$_C$ but not PP2A$_A$ (Figure 1-9 [221]). PME1 and PP2A$_C$ stack closely against each other and form an S-shaped interface, which is dominated by three networks of hydrogen bonds (Figure 1-9 [221]). The first network includes residue Arg214 of PP2A$_C$ which provides two intermolecular hydrogen bonds to the carbonyl oxygen atoms of residues 334 and 335 in PME1, and two intramolecular hydrogen bonds, one to Asp202 and the other to carbonyl oxygen of residue 241 in the PP2A$_C$. Two other hydrogen bonds networks stabilize both ends of the S-shaped interface. The residue Arg268 of the PP2A$_C$ forms three hydrogen bonds with several residues at the N-terminal of helix α9 in PME1. The other network was composed of a water molecule mediating hydrogen bonds between residue 213 in PP2A$_C$ and the side chains of Gln340, Arg369, and His370 in PME1 [221].

The interaction between PME1 and PP2A leads to marked conformational changes of active site in PME1 resulting in the widening of the active site pocket for PME1 to accommodate the C-terminal tail of PP2A$_C$ and the rearrangement of the catalytic triad residues, Ser156, His349, and Asp181, into an active conformation. On the other hand, the binding of PME1 to PP2A displaces the manganese ions from the active site of the PP2A$_C$ resulting in the inactivation of PP2A [221].

The crystal structure of PME1-PP2A$_D$ suggests that PME1 only interacts with PP2A$_C$. However the PME1 protein used in the study contains only residues 39-238 linked through a small EGK tripeptide to remaining protein residues 284-376 while and PP2A$_A$ subunit was engineered such that it included only HEAT repeats 1 and 11-15.

Even though this study showed the methylesterase activity of truncated form PME1 as only slightly different from that of full length PME1 the three dimensional arrangement of interaction between PME1 and PP2A may not be fully accounted for in the structure.

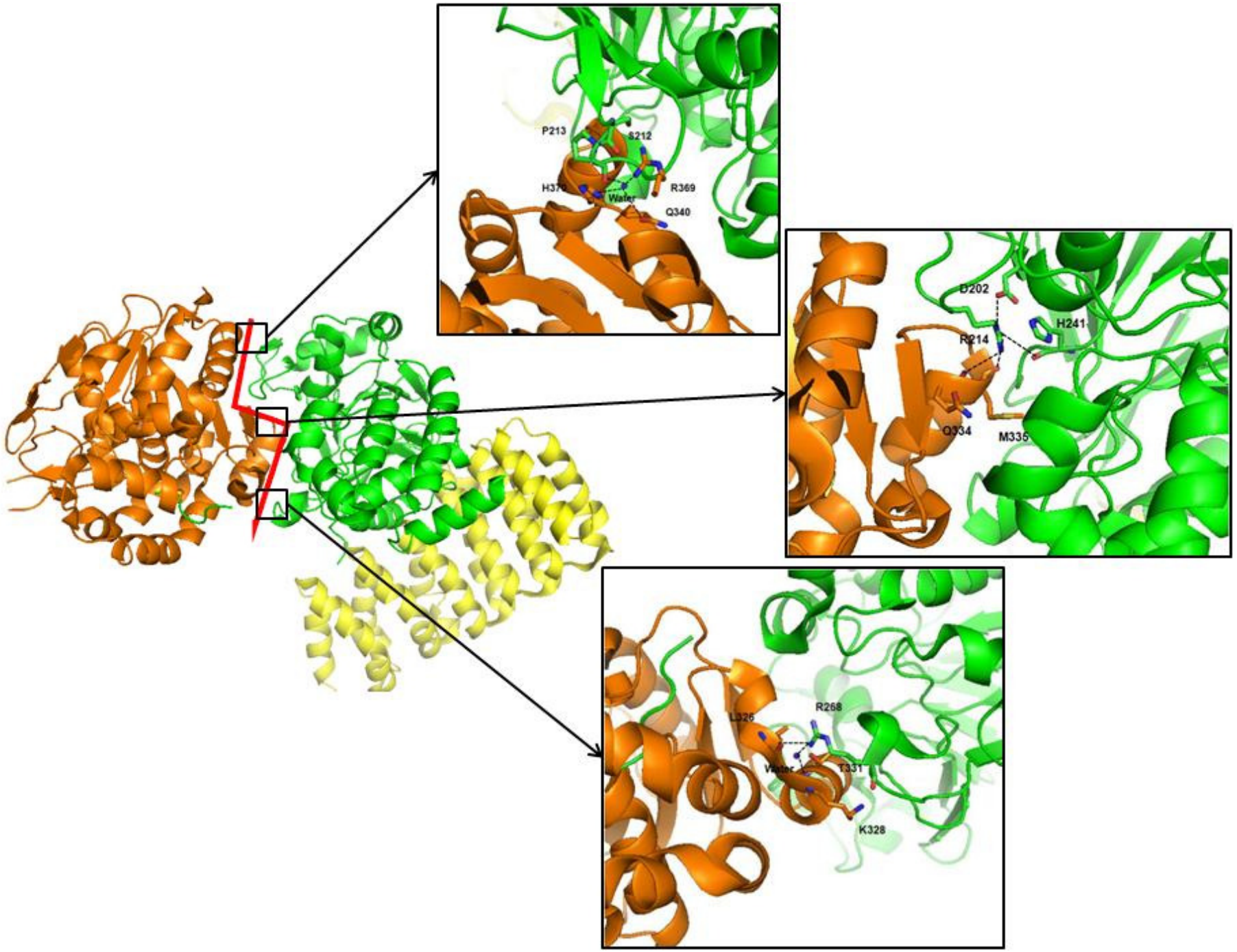
P213
S212
H37
R369
Water
Q340
D202
H241
R214
Q334
M335
L326
R268
Water
T331
K328

Figure 1-9. Interface between PME1 and PP2A$_C$. Ribbon diagram of PP2A$_D$-PR61 (PDB: 3C5W) represented by PyMOL viewer *(DeLano Scientific LLC*). The structure of PP2A$_D$-PME1 complex shows that PME1 (orange) only associates with PP2A$_C$ (green). In addition, PME1 and PP2A$_C$ form and S-shaped interface and the interaction between PME1 and PP2A$_C$ is dominated by hydrogen bonds (black dashed line) [221].

1.2.2 Biological Role of PME1

Although overexpression of PME1 causes a significant change in the methylation status of the PP2A subunit C, there is no significant effect on normal cell functioning [72]. However, knock-out of LCMT1 protein and co-overexpression of PME1 are associated with the hyper-phosphorylation of tau protein and cause a G1 arrest and ultimately apoptosis [222].

1.3 Leucine Carboxyl Methyltransferase 1 (LCMT1)

The gene for human leucine carboxyl methyltransferase 1 (LCMT1) encoding 334 amino acid residues has been sequenced and cloned [62]. Recently, it was shown that LCMT1 is important for normal progression through mitosis in mammalian cells and is necessary for embryonic development in mice [222]. Inhibition of LCMT1 expression will disrupt the formation of $PP2A_D$-PR55 and further induce cell apoptosis. With reference to these mechanisms, methylation of PP2A by LCMT1 may play an important role in cell functions [222].

1.3.1 The Structure of Protein Phosphatase Methyltransferase 1

Although the structure of human mammalian leucine carboxyl methyltransferase 1 was still unsolved, the three dimensional structure of protein phosphatase methyltransferase 1 found in *Saccharomyces cerevisiae* was solved in 2004 [223] and

demonstrated a leucine carboxyl methyltransferase domain involved in carboxy-methylation of the $PP2A_C$. PPM1 shares 28% sequence identity to the mammalian leucine carboxyl methyltransferase 1 based on the pairwise sequence alignment through ClustalW (*EMBL-EBI*). The core domain of PPM1 containing AdoMet and PP2A binding sites is characterized by alternate α/β secondary structure elements forming a central sheet containing seven β-strands (β1-β7). The six α-helices (αZ and αA-αE) are oriented roughly parallel and surrounding the β-strands (Figure 1-10a) [223]. The structure of the core domain is highly conserved among methyltransferases such as L-isoaspartate-O-methyltransferase, chemotaxis receptor methyltransferase, phenylethanolamine N-methyltransferase, glycine N-methyltransferase and Yeco methyltransferase (Figure 1-10b). However, their substrates are very diverse due to additional insertions and variations to the core domain [223]. In *Saccharomyces cerevisiae* PPM1, helix α1, helix α5, helix α8 and helix αZ of the core domain form the funnel-shaped cavity for the methyl donor group to situate at and specify the acceptor substrate which needs to penetrate deeply inside the cavity (Figure 1-10c) [223].

Based on the 3D-PSSM fold recognition program and sequence alignment, human LCMT1 shares the core domain and insertions with *Saccharomyces cerevisiae* PPM1. In addition, the *Saccharomyces cerevisiae* methyltransferase PP2A binding site and AdoMet binding site residues are highly conserved in methyltransferases of different species (Figure 1-10d). For that reason, we could propose that human LCMT1 has the same PP2A binding site and a similar function to *Saccharomyces cerevisiae* methyltransferase, and thus we could design human LCMT1 DNA constructs based on *Saccharomyces cerevisiae* methyltransferase structure using this structure as our

model for further studies.

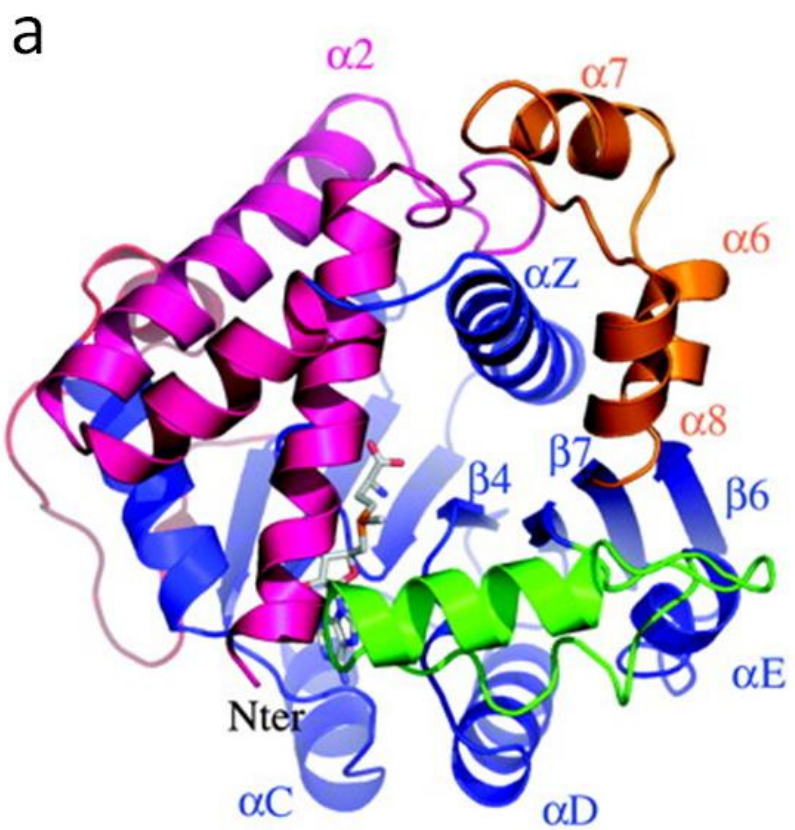
a
α2
α7
α6
αZ
α8
β7
β4
β6
αE
Nter
αC
αD

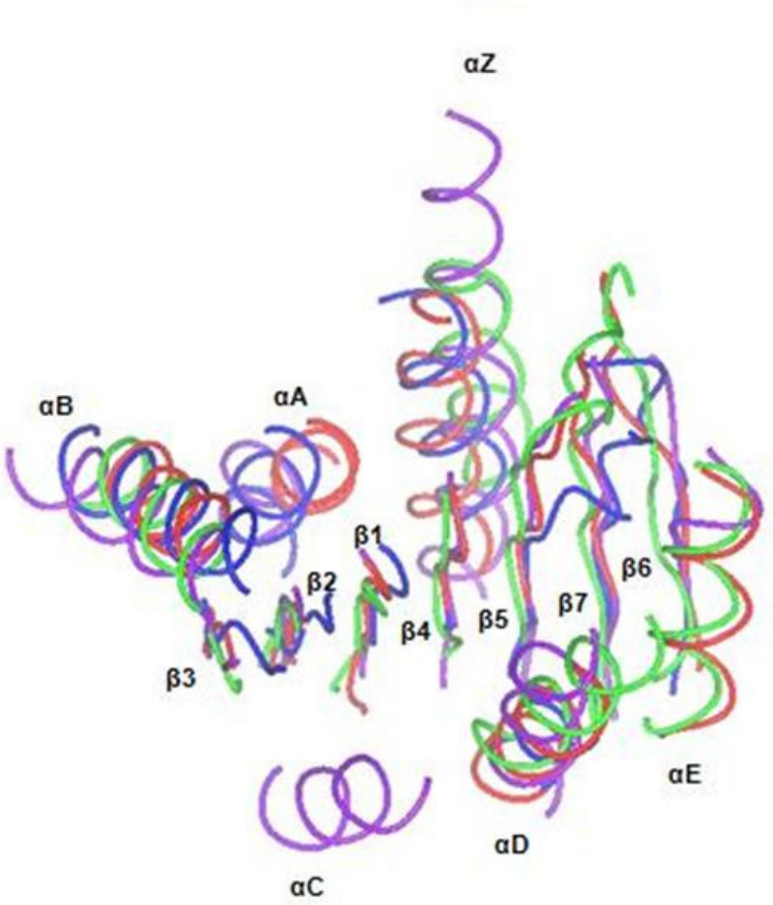
b
αZ
αB
αA
β1
β2
β6
β7
β5
β4
β3
αE
αD
αC

C

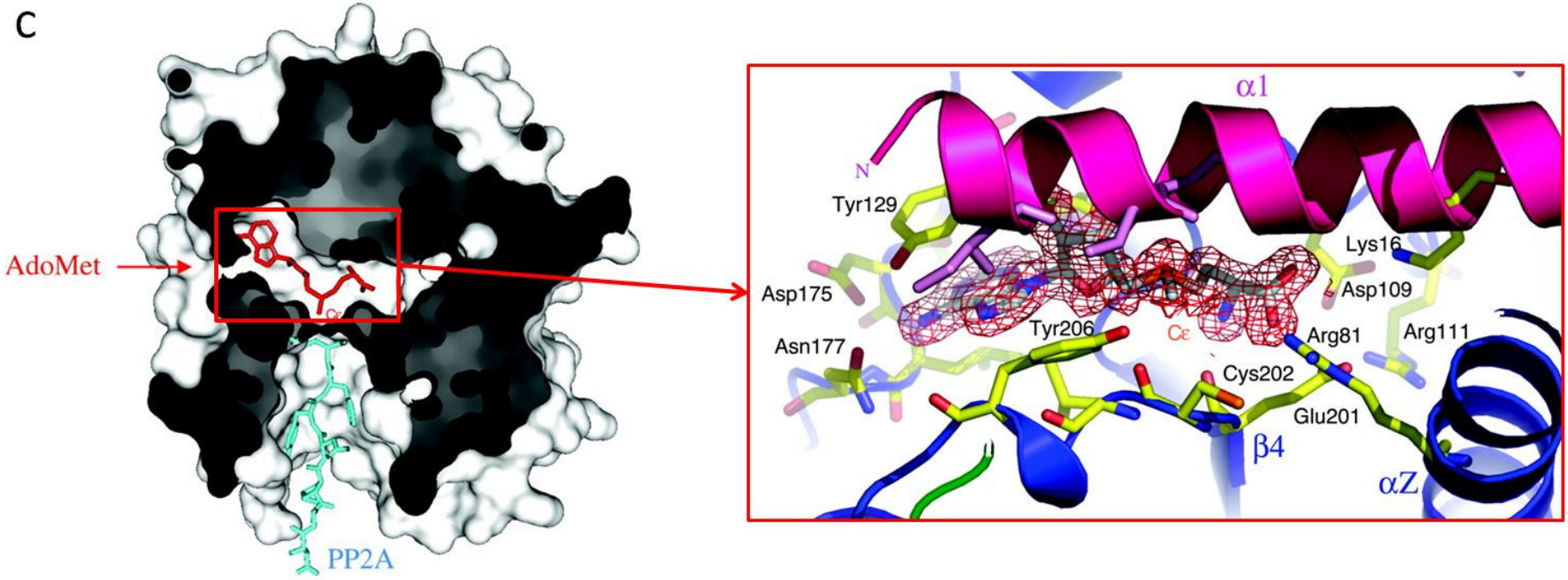
AdoMet
Cε
PP2A
α1
N
Tyr129
Lys16
Asp175
Asp109
Tyr206
Cε
Arg81
Arg111
Asn177
Cys202
Glu201
β4
αZ

d

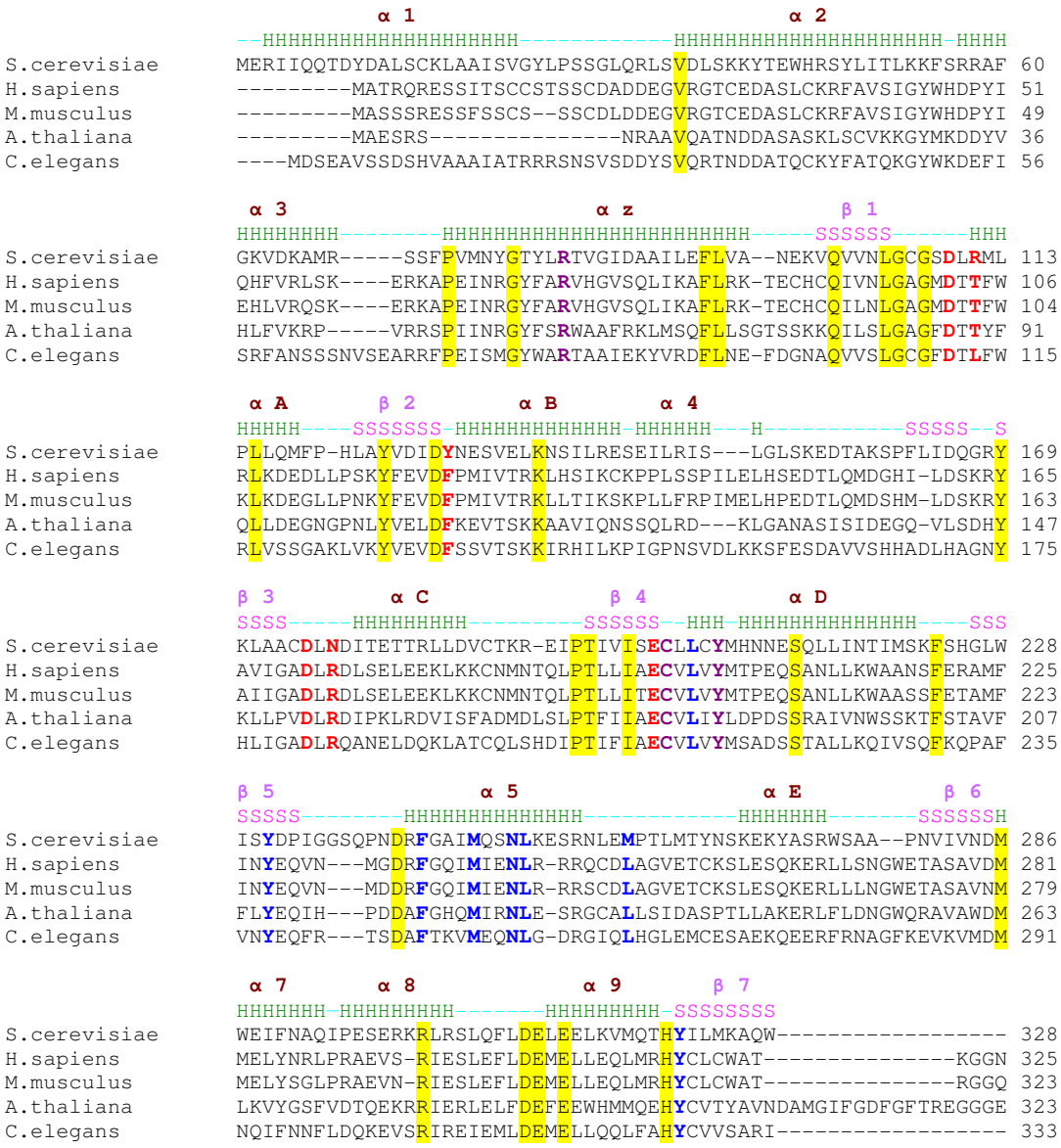

Figure 1-10. The Structure of PPM1 in *Saccharomyces cerevisiae.* (a) The core domain structure of PPM1 represented by ribbon diagram [223]. (b) A superimposition of MT core domain of yeast leucine carboxyl methyltransferase 1 (PDB code 1RJD, purple), L-isoasparate-o-methyltransferase (PDB code 1JG3, blue), Yeco methyltransferase (PDB code 1IM8, red) and Phenylethanolamine *N*-methyltransferase (PDB code 1HNN, green) shows that β strands are conserved [223]. (c) Sliced representation of the PPM1 surface originated from reference [223]. A conformational change is necessary for AdoMet to enter or for AdoHCys to exit the cavity. The methyl group is accessible through the second cavity perpendicular to the AdoMet binding cavity, which may constitute the binding site for the PP2A C-terminal tail. (d) Based on the multiple sequence alignment of LCMT1 from different species by ClustalW, the yeast PPM1 PP2A binding site residues (blue), and AdoMet binding site residues (red) are highly conserved in methyltransferases of different species.

1.3.2 Biological Role of LCMT1

Although LCMT1 and PP2A regulatory subunits are important in mammalian cells for the spindle checkpoint, which ensures proper spindle formation and chromosomal attachment prior to progression from M phase to G_1 phase, the precise role of various regulatory subunits in spindle checkpoint and mitosis still need to be elucidated [224]. The latest research indicated that both B family isoform PR55δ and the B' family isoform RR61γ are the negative regulators of sister chromatid separation. PR55δ is involved in stabilizing securin, which protect cohesins from the degradation by separase, a cohesion protease. PR61γ was also found to protect cohesion by binding to shugoshin and maintain cohesins in a more stable state [225;226]. LCMT1 knockdown in mammalian cells reduces both $PP2A_C$ methylation and the formation of PP2A heterotrimers and further influence the mitotic progression, *in vivo* [222].

In addition, B, B' regulatory family and LCMT1 play important roles in anti-apoptosis. The knockdown by small hairpin RNAs and monoclonal antibodies of both B subunit and LCMT1 in HeLa cells induced apoptosis and this phenotype was partially rescued by thymidine treatment. This study also indicates that LCMT1 is essential for development. Homozygous knockout of LCMT1 in mice will cause embryonic lethality, but the details of mechanism are still unclear [222].

Chapter Two

Materials & Methods

2.1 Informatics

2.1.1 Gene Annotation

2.1.1.1 Bioinformatic Prediction

In order to identify domains, protein secondary structure and related proteins, the full length sequences of Leucine carboxyl methyltransferase 1 (LCMT1) and Protein phosphatase methylesterase 1 (PME1) were submitted to the following webservers, SMART (simple modular architecture research tool [227], Pfam (protein families database of alignments and hidden Markov models) [220] and PSIPRED second structure prediction [228;229].

2.1.1.2 The Limited Proteolysis

Limited proteolysis is a commonly used method for probing conformational features of a protein. This method can be used to identify the most stable fragment or a domain in a protein structure, thus providing useful information that could direct choices in designing protein expression gene constructs [230].

Two proteases, trypsin and chymotrypsin (*Sigma*), were chosen for the

experiment. For the first experiment, the amount of protease should be about 1000 times less than the amount of target protein in mass units. For example, 1 µg of trypsin or chymotrypsin was added to the 1 mg of target protein. The sample was incubated at room temperature and the aliquots of the sample were removed for SDS-PAGE analysis at 10, 30, and 60 minutes, then at hourly intervals until the reaction has ended.

To identify the most stable fragment or domain in target protein for protein construct design, the sample after protease digestion was immobilised on a PVDF membrane (*GE Healthcare*) via transfer buffer (10 mM CAPS pH 11.0, 10% methanol) with a constant voltage of 250 milliamps (mA) for 2 hours and the target band of membrane, stained by CBB stain (0.025% Comassie Blue R-250, 40% methanol), was sent to Protein & Nucleic Acid Chemistry Facility (*PNAC*) of Cambridge University for the N-terminal protein sequence analysis (six residues). The molecular weight of a target segment or a domain, from the solution at the concentration of 1 mg/ml of the protein sample in 10mM ammonium acetate buffer pH 6.4, was determined by Mass Spectrometry analysis at the Institute of Structural and Molecular Biology (*ISMB*).

2.1.2 Protein Modeling

In order to study the catalytic mechanism and the putative three dimensional structure, human LCMT1 model was generated and assessed based on yeast protein phosphatase methyltransferase 1 (PPM1) (PDB: 1RJG) by Modeller

9v2 [231, 232]. The initial model of LCMT1 for molecular replacement covered ~75 % of the amino acid residues, including residues 62-108, residues 114-137, residues 157-231 and residues 258-321, present in the polypeptide chain used to obtain crystals. Further structural comparisons were accomplished by CCP4 Molecular Graphics v1.0 [233] and PyMOL Viewer (*DeLano Scientific LLC*).

2.2 Bacterial Strains

Escherichia coli DH5α or *Escherichia coli* XL1-blue were used for cloning of DNA expression vectors while *Escherichia coli* BL21 (DE3) pLysS, *Escherichia coli* Rosetta (DE3) pLysS, *Escherichia coli* BL21 (DE3), and *Escherichia coli* C41 (DE3) were used for the expression of proteins.

2.2.1 Growth Medium and Culture Conditions

Luria-Bertani (LB) growth medium (10 g/L tryptone, 5 g/L yeast extract and 5 g/L NaCl) was produced using deionised water from an Elga Maxima Ultra-pure water purification system and sterilized by autoclaving and used for liquid cultivation of *E. coli* strains. LB agar plates consisted of LB medium supplemented with 15 g/L agar.

LB medium for the cultures of *E. coli* DH5α, *E. coli* XL1-blue, *E. coli* BL21 (DE3)

and *E. coli* C41 (DE3) strains containing any pET30aTEV or pET28a expression vector (*Novagen*) was supplemented with 50 µg/ml kanamycin while the media for the growth of the cells containing any pET442b (*Birkbeck College*) or pGEX4T2 (*GE Healthcare*) expression vector was supplemented with 100 µg/ml ampicillin. In addition, 30 µg/ml chloramphenicol was included in media for the growth of any pLysS-containing *E. coli* strains.

2.2.2 Competent E. coli Cells for Cloning

One single colony of *E. coli* DH5α or *E. coli* XL1-blue cells was inoculated into 5 ml LB media and incubated at 37 ^{o}C with shaking at 200 revolutions per minute (rpm) for overnight until the culture becomes cloudy. 1 ml of the overnight culture was transferred to 100 ml LB and incubated at 37 ^{o}C with shaking at 200 rpm until mid log phase (OD_{600nm} = 0.45). The cells were put on ice for 5 minutes and then spun down by centrifugation at 3440 g for 5 minutes at 4^{o}C. The supernatant was decanted and the cell pellet was resuspended in 15 ml of cold, sterile Transformation Buffer 1 (TFB1) (30 mM potassium acetate pH 5.8, 100 mM RbCl, 50 mM $MnCl_2$, 10 mM $CaCl_2$, 15 % glycerol). The cells were incubated on ice for 2 hours and then spun down by centrifugation at 3440 g for 5 minutes at 4 ^{o}C. The TFB1 was decanted and the cell pellet was resuspended in 3 ml of cold, sterile Transformation Buffer 2 (TFB2) (10 mM MOPS pH 6.8, 10 mM RbCl, 75 mM $CaCl_2$, 15 % glycerol). The competent cells were aliquoted into 100 µl samples and then placed at -80 ^{o}C.

2.2.3 Competent E. coli Cells for Protein Expression

One single colony of *E. coli* BL21 (DE3) pLysS, or *E. coli* Rosetta (DE3) pLysS or *E. coli* C41 (DE3) or *E. coli* BL21 (DE3) cells was inoculated into 5 ml LB media and incubated at 37 ^{o}C with shaking overnight at 200 rpm until the culture becomes cloudy. The LB media contained 30 µg/ml chloramphenicol for the competent *E. coli* Rosetta (DE3) pLysS and *E. coli* BL21 (DE3) pLysS cells. 1 ml of the overnight culture was transferred to 100 ml LB and incubated at 37 ^{o}C with shaking at 200 rpm until OD_{600nm} = 0.6. The cells were spun down by centrifugation at 860 g for 10 minutes at 4 ^{o}C. The cell pellet was resuspended in one-half volume (50 ml) of cold, sterile 100 mM $CaCl_2$ and incubated on ice for 2 hours. The cells were spun down as before and gently resuspended in 4 ml of cold sterile 100 mM $CaCl_2$ containing 15 % sterile glycerol. The competent cells were aliquoted into 50 µl samples and then placed at -80 ^{o}C.

2.2.4 Nucleic Acid Methods

2.2.4.1 Purification of Plasmid DNA

A single colony from freshly transformed DH5α or XL1-blue cell culture was inoculated into 5 ml LB media containing antibiotics and grown at 37 ^{o}C with vigorous shaking at 200 rpm for overnight. Purification of plasmid was

performed using a QIAprep Spin Miniprep Kit (*Qiagen*). The bacterial cells were spun down and lysed in alkaline buffer. The lysate was subsequently neutralised and adjusted to high-salt binding conditions. The spin columns contain a unique silica membrane specific to the adsorption of DNA. Salts are removed by a wash buffer containing 80 % ethanol and then the plasmid eluted from the QIAprep spin column using elution buffer (Tris containing buffer, pH 7.0 – 8.5).

2.2.4.2 Agarose Gel Electrophoresis

For separation and identification of digested DNA fragments, DNA fragments were resolved on 1 % agarose gel using electrophoresis. Agarose was dissolved in TAE buffer (40 mM Tris-acetate and 1 mM ethylene-diamine-tetraacetic acid (EDTA)) containing 0.5 µg/ml ethidium bromide (EtBr) to detect the DNA. Gels were cast and set in the apparatus provided. DNA samples were prepared by the addition of 1x Orange Loading Dye Solution (*Fermentas*). The Quick-Load 100 bp and 1 kb DNA ladders (*New England Biolabs*) were used as molecular weight standards. Electrophoresis was carried out in TAE buffer at 100 V for 20-30 minutes and the resolved DNA bands were analyzed on UV-transilluminators.

2.2.4.3 Extraction of DNA from Agarose Gels

DNA fragments were extracted from the gel using the QIAquick Gel Extraction

Kit (*Qiagen*). The appropriate salt concentration and pH for adsorption of DNA to the silica-membrane of the spin column were provided by binding buffers. Salts are washed away by the ethanol-containing PE buffer. The DNA is subsequently eluted with buffer EB (10mM Tris, pH 8.5).

2.2.5 Manipulation of Constructs

Appropriate oligo-nucleotide primers were designed to amplify specific gene targets by polymerase chain reaction (PCR). The primers were designed to be at least 16 base pairs long with similar melting temperatures and included a stop codon in the reverse primer.

The DNA sequence for all constructs of LCMT1 was amplified by polymerase chain reaction (PCR) using human's full length LCMT1 as a template. PCR for all LCMT1 variants except LCMT17-334 and LCMT1SD20-334 was accomplished using primers designed to introduce the restriction site PciI (ACATGT) at the 5' end of the PCR fragments and a HindIII (AAGCTT) restriction site and stop codon at the 3' end. In order to generate DNA constructs for LCMT17-334 and LCMT1SD20-334, nested PCR protocol with two pairs of primers was used. The restriction site PciI was introduced at the 5' end of the PCR fragments while the reverse primer (5'-CTGTGACTCTAATGATTTGCCTTCGTTCACCTGTTCGTA-3') corresponded to complementary DNA strand of the amino acid sequence YEQVN-EG-KSLE, where YEQVN sequence comprises residues 228-232 of

LCMT1. The second pair of primers consisted of a forward primer (5'-TACGAACAGGTGAACGAAGGCAAATCATTAGAGTCACAG-3') coding for YEQVN-EG-KSLE amino acid sequence and a reverse primer that introduced HindIII restriction site and a stop codon at the 3' end of the fragment. Combination of the two fragments yielded a PCR amplicon encoding residues 20-232 linked through the EG dipeptide to residues 259-334 of the human LCMT1. The amplified PCR products were cloned into a pET30aTEV expression vector (*Novagen*) with an N-terminal six histidine affinity tag and a tobacco etch virus (TEV) protease cleavage site to allow the removal of the affinity tag.

For constructs of PME1, majority of PCR products were designed to contain the NcoI (CCATGG) restriction site at the 5' end and a HindIII (AAGCTT) restriction site and the stop codon at the 3' end. However for the production of PME1_$GE_{239-283}$ and PME1_$ET_{239-283}$ constructs, PCR primers were designed to incorporate the restriction site BamHI (GGATCC) at the 5' end of the PCR fragments and a NotI (GCGGCCGC) restriction site and the stop codon at the 3' end. All methods and protocols for molecular cloning of PME1 variant were similar except for $PME1_{39-376}$ which contains residues 39-238, a small linker EGK, followed by PME1 residues 284-376 (1). Nested PCR protocol with two pairs of primers was used to generate this construct. Two primers for residues 39-238 of PME139-376 were designed to introduce the restriction site PciI (ACATGT) at the 5' end of the PCR fragments and KQC-EGK-PYT site (GGTGTATGGTTTGCCTTCACACTGTTT) at the 3' end and another two primers for residues 284-376 of PME139-376 were set up to apply the

KQC-EGK-PYT site (AAACAGTGTGAAGGCAAACCATACACC) at the 5' end of the PCR fragments and the HindIII (AAGCTT) restriction site and stop codon at the 3' end. All PCR products were digested and cloned into pET30aTEV vector except PME1_GE239-283 and PME1_ET239-283 which were cloned into pGEX4T2 and pET442b vector respectively. In addition, few PME1 expression constructs, designed for isothermal titration calorimetry measurements, included a BamHI (GGATCC) site at the 5' end and a NotI (GCGGCCGC) site at the 3' end and these PCR amplicons were cloned into a pET442b (*Birkbeck College*) with *E. coli* NusA protein tag (NusA tag) or pGEX4T2 (*GE Healthcare*) with glutathione-S-transferase tag (GST tag).

PCR amplification of the A subunit of Protein phosphatase 2A ($PP2A_A$) was carried out with the primers that introduced NdeI (CATATG) and NotI (GCGGCCGC) restriction sites at the 5' and 3' ends of the amplified fragment respectively. The amplified PCR product was cloned into a pET28a expression vector with thrombin cleavage site and an N-terminal six-histidine affinity tag. The names of all expression constructs that were produced and described in this thesis, and the primers used to generate them are shown in Table 1.

Construct name	Vector	5' to 3' Forward Primer	3' to 5' Reverse Primer
$LCMT1_{61-334}$	pET30a	CGCGACATGTCTAGGAAAGCCCCTGAAATC	CGCGAAGCTTTTAATAAGTTATCTCC
$LCMT1_{1-321}$	pET30a	GGCGCGACATGTCTATGGCCACTAGGCAGAGG	GCTCATTAAGCTTCTAGGTTGCCCAGCAAAG
$LCMT1_{9-321}$	pET30a	GGGAGGGACATGTCTATCACCTCCTGCTG	GCTCATTAAGCTTCTAGGTTGCCCAGCAAAG
$LCMT1_{16-321}$	pET30a	CACCTCCTACATGTCTACCTCGAGCTG	GCTCATTAAGCTTCTAGGTTGCCCAGCAAAG
$LCMT1_{20-321}$	pET30a	GTATTTCAGGGCGCCATGGACGAGAACGACGAGGGCGTG	GCTCATTAAGCTTCTAGGTTGCCCAGCAAAG
$LCMT1_{20-334}$	pET30a	GTATTTCAGGGCGCCATGGACGAGAACGACGAGGGCGTG	ACCCGACTTCCTCTATTGAATAATTTTAAGCACGAGGCAG
$LCMT1_{1-334}$	pET30a	GGCGCGACATGTCTATGGCCACTAGGCAGAGG	ACCCGACTTCCTCTATTGAATAATTTTAAGCACGAGGCAG
$LCMT1_{7-334}$	pET30a	1. CCGGCAACATGTCTGAATCCTCTATCACCTCC 2. TACGAACAGGTGAACGAAGGCAAATCATTAGAGTCACAG	1. CTGTGACTCTAATGATTTGCCTTCGTTCACCTGTTCGTA 2. GGTTCAAGCTTTTAATAAGTTATCTCCTTCAG
$LCMT1_{SD20-334}$	pET30a	1. CCGGCAACATGTCTGACGCAGACGACGAGGGC 2. TACGAACAGGTGAACGAAGGCAAATCATTAGAGTCACAG	1. CTGTGACTCTAATGATTTGCCTTCGTTCACCTGTTCGTA 2. GGTTCAAGCTTTTAATAAGTTATCTCCTTCAG
$LCMT1_{7-232}$	pET30a	CCGGCAACATGTCTGAATCCTCTATCACCTCC	GGTTCAAGCTTTTAGTTCACCTGTTCGTAGTT
$PME1_{51-370}$	pET30a	GAGTCCATGGAGTCCATGGAAGATGTAGAA	GATGGGTTCAAGCTTCTAGTGCCGGAT
$PME1_{53-370}$	pET30a	GAGTCCATGGAAGATGTAGAAGTAGAGAAT	GATGGGTTCAAGCTTCTAGTGCCGGAT
$PME1_{56-370}$	pET30a	GAGTCCATCCATGGTAGAAGTAGAGAATG	GATGGGTTCAAGCTTCTAGTGCCGGAT
$PME1_{65-370}$	pET30a	GAATGAAACCCATGGATACTTTTCGAGTCTAC	GATGGGTTCAAGCTTCTAGTGCCGGAT
$PME1_{88-370}$	pET30a	CATGTAGGCCATGGCGTCTGCCCTTTC	GATGGGTTCAAGCTTCTAGTGCCGGAT
$PME1_{51-386}$	pET30a	GAGTCCATGGAGTCCATGGAAGATGTAGAA	CTAACAAAGCTTCTAACAGCCAGGAAACAC
$PME1_{53-386}$	pET30a	GAGTCCATGGAAGATGTAGAAGTAGAGAAT	CTAACAAAGCTTCTAACAGCCAGGAAACAC
$PME1_{1-382}$	pET30a	CGCGCCATGGGTATGTCGGCCCTC	CTAACAAAGCTTCTACACACACTGGAATCCACC
$PME1_{24-382}$	pET30a	CCGGCACCATGGGCAGTCAGAGC	CTAACAAAGCTTCTACACACACTGGAATCCACC
$PME1_{26-382}$	pET30a	GCAGCGCCATGGGTCAGAGCGGA	CTAACAAAGCTTCTACACACACTGGAATCCACC
$PME1_{44-382}$	pET30a	ACTTTTCCATGGTTCCTTGGAGTCAGTATTTTGAG	CTAACAAAGCTTCTACACACACTGGAATCCACC
$PME1_{1-386}$	pET30a	CGCGCCATGGGTATGTCGGCCCTC	CTAACAAAGCTTCTAACAGCCAGGAAACAC
$PME1\_ET_{239-283}$	pET442b	CGCGGATCCGAAGGAATTACAAGTCCAGAA	TTCCTTTTGCGGCCGCTCAATGGTCTTTCTTGGTCTCCAT
$PME1\_GE_{239-283}$	pGEX4T2	CGCGGATCCGAAGGAATTACAAGTCCAGAA	TTCCTTTTGCGGCCGCTCAATGGTCTTTCTTGGTCTCCAT
$PME1_{39-376}$	pET30a	1. CCGGCAACATGTCTCGGGATTTTCCCCT 2. AAACAGTGTGAAGGCAAACCATACACC	1. GGTGTATGGTTTGCCTTCACACTGTTT 2. GGTTCAAGCTTTCAGATGGGTTCTGCAAA
$PP2A_A\_Full$	pET28a	GGAATTCCATATGGCGGCGGCCGACGGC	CGCGGAATGCGGCCGCTCAGGCGAGAGACAGAACAGTCA

Table 2-1. The Forward and Reverse Primers of all PME1, LCMT1 and $PP2A_A$ Constructs for *E. coli* Strains.

2.2.5.1 Amplification of Genes Using Polymerase Chain Reaction

PCR amplification was performed in 50 µl reaction volumes containing 1x Phusion HF buffer (*FINNZYMES*), 3 % DMSO, 1 µM of forward primer, 1 µM of reverse primer, 0.5 µg DNA template and 0.02 units (U) Phusion DNA Polymerase (*FINNZYMES*). The cycling conditions of PCR reactions were carried out using the guideline (*FINNZYMES*) as follows: initial denaturation at 98 ^{o}C for 5 minutes was followed by performing 30 cycles that consisted of denaturation step at 98 ^{o}C for 1 minute, 1 min annealing step at the appropriate temperature and an extension step at 72 ^{o}C that lasted for 30 seconds per 1000 base pairs to amplify the required stretch of DNA. Annealing temperatures were chosen based on the melting temperature value (Tm) of primers. Final extension step was carried out at 72^{o}C for 10 minutes and the reactions were at the end held at 4 ^{o}C. The PCR amplified products were analysed on an agarose gel, and extracted using QIAquick gel extraction kit (*Qiagen*).

2.2.5.2 Restriction Enzyme Digestion

All restriction enzymes were purchased from New England Biolabs. The plasmid pET30aTEV was double digested with NcoI and HindIII while the double cleavage of pET28a plasmid was carried out using NdeI and NotI enzymes. The pET442b and pGEX4T2 vector were digested with BamHI and

NotI enzymes. All LCMT1 PCR products were double digested with PciI and HindIII while PME1 PCR fragments were double digested with NcoI or PciI and HindIII except for those PCR amplicons that were subsequently cloned into pET442b and pGEX4T2 vectors which were double digested with BamHI and NotI. The PCR fragments of $PP2A_A$ were double digested with NdeI and NotI. All DNA digestion reactions were performed using the protocol guideline. Reactions were performed in 20-50 µl volumes and incubated at appropriate temperature based on the optimal activity of enzymes used for overnight reactions. Cleavage products were electrophoresed on an agarose gel and subsequently extracted and purified using QIAquick Gel Extraction Kit (*Qiagen*).

2.2.5.3 DNA Ligations and Transformations

Ligations were carried out in 10 µl or 20 µl volumes using insert:vector molar ratios of 3:1 or 5:1, 1x T4 DNA ligation buffer (*New England Biolabs*) (50 mM Tris-HCl pH 7.5, 10 mM $MgCl_2$, 10 mM dithiothreitol (DTT), 1 mM ATP, 25 µg/ml bovine serum albumin (BSA)) and 400 U of T4 DNA ligase (*New England Biolabs*) at 25 ^oC, overnight.

100 µl aliquots of competent cells were thawed on ice. 10 µl of ligation mixture or 1 µl of constructed plasmid were added to the thawed cells and left on ice for 30 minutes. The cells were then heat shocked at 42 ^oC for 45 seconds and then left on ice for at least 2 minutes. 500 µl of LB broth were subsequently added to

the cells that were then incubated at 37 ^{o}C and 200 rpm for 1 hour. 200 µl of transformation mixture was plated onto agar plate with the appropriate antibiotic and incubated overnight at 37 ^{o}C.

Constructed plasmids were verified by restriction enzyme digestion to confirm the presence and size of an insert and by sequencing via Eurofins MWG Operon Company.

2.2.5.4 Preparation of Glycerol Stocks

A single colony from an agar plate was inoculated into 5 ml of LB with the appropriate antibiotic. Cells were incubated overnight at 37 ^{o}C with shaking at 200 rpm. 1 ml of each culture was transferred into a cryogenic vial along with 700 µl of 70 % glycerol and stored at -80 ^{o}C.

2.2.6 Protein Expression

The summary of all LCMT1, PME1 and $PP2A_A$ variants protein expression results are listed in Table 2-2.

2.2.6.1 Small Scale Protein Expression Tests in 100 ml LB Medium

A single colony selected from an agar plate of freshly transformed *E. coli* BL21

(DE3) pLysS or *E. coli* Rosetta (DE3) pLysS or *E. coli* C41 (DE3) or *E. coli* BL21 (DE3) was inoculated in 5 ml of LB media containing antibiotics and the culture was incubated overnight at 37 ºC and 200 rpm. 1 ml of overnight culture was transferred to 100 ml of LB medium containing antibiotics and incubated at 37 ºC and 200 rpm until OD_{600nm} = 0.6. The expression of protein was initiated by addition of isopropyl-β-D-thiogalactopyranoside (IPTG) to a final concentration of 1 mM and the protein expression was carried out at 37 ºC for further 4 hours. The cell cultures were spun down at 20000 g in a Sorvall SS-34 rotor and the pellets were resuspended with Tris buffer (25mM Tris pH 8.0) to obtain an OD of 0.6. The cells were disrupted by mild sonication and then spun down at 20000 g in a Sorvall SS-34 rotor. Finally, supernatant and cell debris/insoluble fraction of each sample were analysed by SDS polyacrylamide gel electrophoresis to assess protein expression and its solubility.

2.2.6.2 Large Scale Protein Expression of all LCMT1 Constructs

In order to enhance production of soluble protein, *E. coli* C41 (DE3) cells were cotransformed with pBADESL plasmid containing GroES/GroEL (chaperonin) genes in addition to various LCMT1 recombinant clones [234]. Alternatively, LCMT1 expression clones were expressed in BL21 (DE3) pLysS cells. Protein expression in C41 (DE3) cells was carried out in batches of 6 L LB medium containing kanamycin (50 μg/ml) and ampicillin (100 μg/ml) and L-arabinose (2 mg/ml) for induction of GroES/EL expression. For protein expression in BL21 (DE3) pLysS cells, 50 μg/ml kanamycin and 30 μg/ml chloramphenicol were

added to the media. The cells were incubated at 37 ^{o}C and 200 rpm and grown to an OD_{600nm} of 0.6. The cultures were then supplemented with 1 mM IPTG for protein induction. After 5 hours of induction, the cells were harvested at 4 ^{o}C and 5000 g in a Sorvall SLA-3000 rotor for 15 minutes. The cell pellets were stored at -20 ^{o}C.

2.2.6.3 Large Scale Protein Production of all PME1 Constructs

The transformed *E. coli* BL21 (DE3) pLysS, *E. coli* Rosetta (DE3) pLysS or *E. coli* BL21 (DE3) cells from glycerol stock were inoculated into 100 ml of fresh medium containing suitable antibiotics and incubated overnight at 37 ^{o}Ct. The cell cultures were then aliquoted into 6 L LB medium and grown at 37 ^{o}C until OD_{600nm} = 0.6 when protein expression was induced by 0.5 mM IPTG at 30 ^{o}C and 180 rpm for 5 hours. After 5 hours of induction, the cells were harvested at 4 ^{o}C by centrifugation at 5000 g in a Sorvall SLA-3000 rotor for 15 minutes. The cell pellets were stored at -20 ^{o}C until the time of protein purification.

2.2.6.4 Large Scale Protein Expression of the $PP2A_A$ Construct

Large scale protein expression from transformed *E. coli* BL21 (DE3) cells was performed in batches of 6 L LB medium containing kanamycin (50 μg/ml). Cell cultures were incubated at 37 ^{o}C with shaking at 180 rpm and grown to an OD_{600nm} of 0.6. For induction of protein expression, the cultures were then

supplemented with 0.1 mM IPTG at 18 ^{o}C. After 18 hours of induction, the cells were harvested by centrifugation at 4 ^{o}C and 5000 g in a Sorvall SLA-3000 rotor for 15 minutes [12;17]. The cell pellets were stored at -20 ^{o}C until the time of protein purification.

Construct Name	Protein Sequence	Protein Expression	Protein Expression Temperature (^{o}C)	Ammount of Protein Purified from 1 L of *E. coli* Cell Culture (mg)
$LCMT1_{61-334}$	residues 61-334	Soluble	37	10
$LCMT1_{1-321}$	residues 1-321	Insoluble	-	-
$LCMT1_{9-321}$	residues 9-321	Insoluble	-	-
$LCMT1_{16-321}$	residues 16-321	Insoluble	-	-
$LCMT1_{20-321}$	residues 20-321	Insoluble	-	-
$LCMT1_{20-334}$	residues 20-334	Soluble	37	1.5
$LCMT1_{1-334}$	residues 1-334	Soluble	37	2.5
$LCMT1_{7-334}$	residues 7-232, a linker EG, and residues 259-334	Soluble	37	4
$LCMT1_{SD20-334}$	residues 20-232, a linker EG, and residues 259-334	Soluble	37	4
$LCMT1_{7-232}$	residues 7-232	Insoluble	-	-
$PME1_{51-370}$	residues 51-370	Insoluble	-	-
$PME1_{53-370}$	residues 53-370	Insoluble	-	-
$PME1_{56-370}$	residues 56-370	Insoluble	-	-
$PME1_{65-370}$	residues 65-370	Insoluble	-	-
$PME1_{88-370}$	residues 88-370	Insoluble	-	-
$PME1_{51-386}$	residues 51-386	Insoluble	-	-
$PME1_{53-386}$	residues 53-386	Insoluble	-	-
$PME1_{1-382}$	residues 1-382	Insoluble	-	-
$PME1_{24-382}$	residues 24-382	Soluble	30	2

$PME1_{26-382}$	residues 26-382	Soluble	30	2
$PME1_{44-382}$	residues 44-382	Insoluble	-	-
$PME1_{1-386}$	residues 1-386	Soluble	30	2
$PME1\_ET_{239-283}$	NusA and residues 239-283	Soluble	30	3
$PME1\_GE_{239-283}$	GST and residues 239-283	Soluble	30	2.5
$PME1_{39-376}$	residues 39-238, a small linker EGK, and residues 284-376	Soluble	30	2.5
$PP2A_A$_Full	Residues 1-589	Soluble	18	1

Table 2-2. Summary of LCMT1, PME1, and $PP2A_A$ Protein Expression and Production.

2.3 Baculovirus Expression System

Baculovirus expression systems are powerful systems for high-level, recombinant protein expression in insect cells. Target genes placed under the transcriptional control of the strong polyhedrin promoter of the *Autographa california* nuclear polyhedrosis virus (AcNPV) are expressed during the late stages of infection. Bac-to-bac baculovirus expression system (*Invitrogen*) and BacMagic transfection system (*Novagen*) were used for the expression of the full length C subunit of protein phosphatase 2A ($PP2A_C$).

2.3.1 Insect Cell Lines

Two insect cell lines were used for baculovirus expression system. Sf9 cells (*Novagen*) are derived from pupal ovarian tissue of *Spodoptera frugiperda* and used for the transfection, amplification and quantification of virus. High Five cells (*Invitrogen*) that are commonly recommended for protein expression, originate from the ovarian cells of the cabbage looper *Trichoplusia ni*. Sf9 cells were grown in protein-free Insect-Xpress medium (*Lonza*) while High Five cells were grown in protein-free EX-CELL 405 medium containing L-glutamine (*Sigma*).

2.3.1.1 Initiation of Cell Culture from Frozen Stock

A vial of cells from liquid nitrogen was incubated in a water bath at 37 ^{o}C until cells were all thawed. The vial was decontaminated outside using 70 % ethanol and placed on ice. 4 ml of Insect-Xpress medium or EX-CELL 405 medium was added to a 25 cm^2 tissue culture flask (*Sigma*). 1 ml of cells was transferred into the flask and incubated at 27 ^{o}C for 30 minutes. After the cells were attached the medium was replaced with 5 ml of fresh medium and the cells were further incubated at 27 ^{o}C for 24 hours. The health of the cells was assessed by viability which should be greater than 70 %. The cells were incubated until they formed a confluent monolayer.

2.3.1.2 Suspension Cultures of Cells

5 ml of the cells from tissue culture flask was transferred to 250 ml erlenmeyer flask with a 43 mm vent cap (*Corning*) containing 50 ml fresh medium with 5 % fetal bovine serum (FBS) (*Biosera*) and antibiotics and incubated in shaking incubator at 27 ^{o}C and 125 rpm. The cells were checked daily and split when the log phase cell density of Sf9 or High Five cells exceeded 4 million cells per ml.

2.3.1.3 Long Term Storage of Insect Cells

For the storage, cell viability, used to assess healthy cells content in cell

population, needs to be at least 90 %, as nearly 30 % of cells are lost during the recovery process. The freezing medium for Sf9 cells contains 60 % Insect-Xpress medium, 30 % FBS and 10 % DMSO and for freezing of High Five cells the medium includes 42.5 % old EX-CELL 405 medium from original cell culture, 42.5 % fresh EX-CELL 405 medium, 5 % FBS and 10 % DMSO. Sterile cryovials were placed on ice. The cells were spun down at 4 ^{o}C and the supernatant was decanted to be used later for the preparation of freezing medium for High Five cells. The cells were resuspended in freezing medium and 1 ml of the cell mixture was transferred to sterile cryovials, placed at -20 ^{o}C for 1 hour and then incubated at -80 ^{o}C for 24 hours. Sterile cryovials with insect cells were finally stored in liquid nitrogen.

2.3.2 Bac-to-Bac Baculovirus Expression System (Invitrogen)

To produce the baculovirus for the expression of $PP2A_C$ and improve the stability of protein, target gene was cloned into the pFastBacHTa vector with an uncleavable HA tag or 8 histidine tag and introduced D88N mutation in the active sites of the enzyme [235].

2.3.2.1 Cloning of $PP2A_C$

Conventional molecular biology procedures and techniques were used for cloning and DNA constructs manipulation in bacterial strains. DNA gene

expression constructs and primers designed for insect cells expression system are shown in Table 2-3. The primers used to generate the expression constructs of $PP2A_C$ encompass an NcoI (CCATGG) site at the 5' end and a HindIII (AAGCTT) site at the 3' end. pFastBacHTa plasmid (*Invitrogen*) and the full length $PP2A_C$ DNA fragment were digested overnight at 37°C with NcoI and HindIII restriction enzymes. After ligation using T4 DNA Ligase (*New England Biolabs*) overnight at room temperature, the recombinant plasmid was transformed into *E. coli* DH5α cells. The recombinant plasmid was finally verified by using diagnostic restriction enzyme reaction and by DNA sequencing (*Eurofins MWG*).

Construct name	Vector	5’ to 3’ Forward Primer	3’ to 5’ Reverse Primer
$PP2A_C$_Full with 8 His Tag	pFastBacHTa	CCGCGCCATGGCTCATCACCATCACCATCACCATCACGAGAAGGTG	GGCCAAGCTTTTATTACAGGAAGTAGTCTGG
$PP2A_C$_Full with 8 HA Tag	pFastBacHTa	CCGCGCCATGGCTTACCCATACGACGTCCCAGACTACGACGAGAAGGTGT	GGCCAAGCTTTTACAGGAAGTAGTCTGGGG
$PP2A_C$_Full with 8 His Tag	pBAC4x-1	CGGGATCCATGCACCACCACCACCACCACCACCACGACGAGAAGGTGTTC	GGCCGCATGCTTACAGGAAGTAGTCTGGGG
$PP2A_A$_Full	pBAC4x-1	TCCCCCGGGATGGCGGCGGCCGAC	GACTAGTTCAGGCGAGAGACAGAA

Table 2-3. Forward and Reverse Primers of all $PP2A_C$ and $PP2A_A$ DNA Constructs for Baculovirus Expression System.

2.3.2.2 Transposition of Target Genes

For transposition of target DNA, the recombinant plasmid is transformed into *E. coli* DH10Bac competent cells (*Invitrogen*) containing the bacmid with a mini-*att*Tn7 target site and the helper plasmid (Figure 2-1).

Luria agar plates containing 50 μg/ml kanamycin, 7 μg/ml gentamicin, 10 μg/ml tetracycline, 100 μg/ml bluo-gal, and 40 μg/ml IPTG were prepared and 50 μl of *E. coli* DH10Bac competent cells were thawed on ice. Approximately 1 ng of recombinant plasmid was added to the DH10Bac competent cells and incubated on ice for 30 minutes. The mixture was heat shocked at 42 ^{o}C for 45 seconds and then chilled on ice for 2 minutes. 900 μl of SOC medium (*Invitrogen*) was added to the mixture and then the cells were placed in a shaking incubator at 37^{o}C and 250 rpm for 4 hours. 200 μl of transformation mixture was plated evenly onto Luria agar plate and incubated at 37 ^{o}C for 24 to 48 hours.

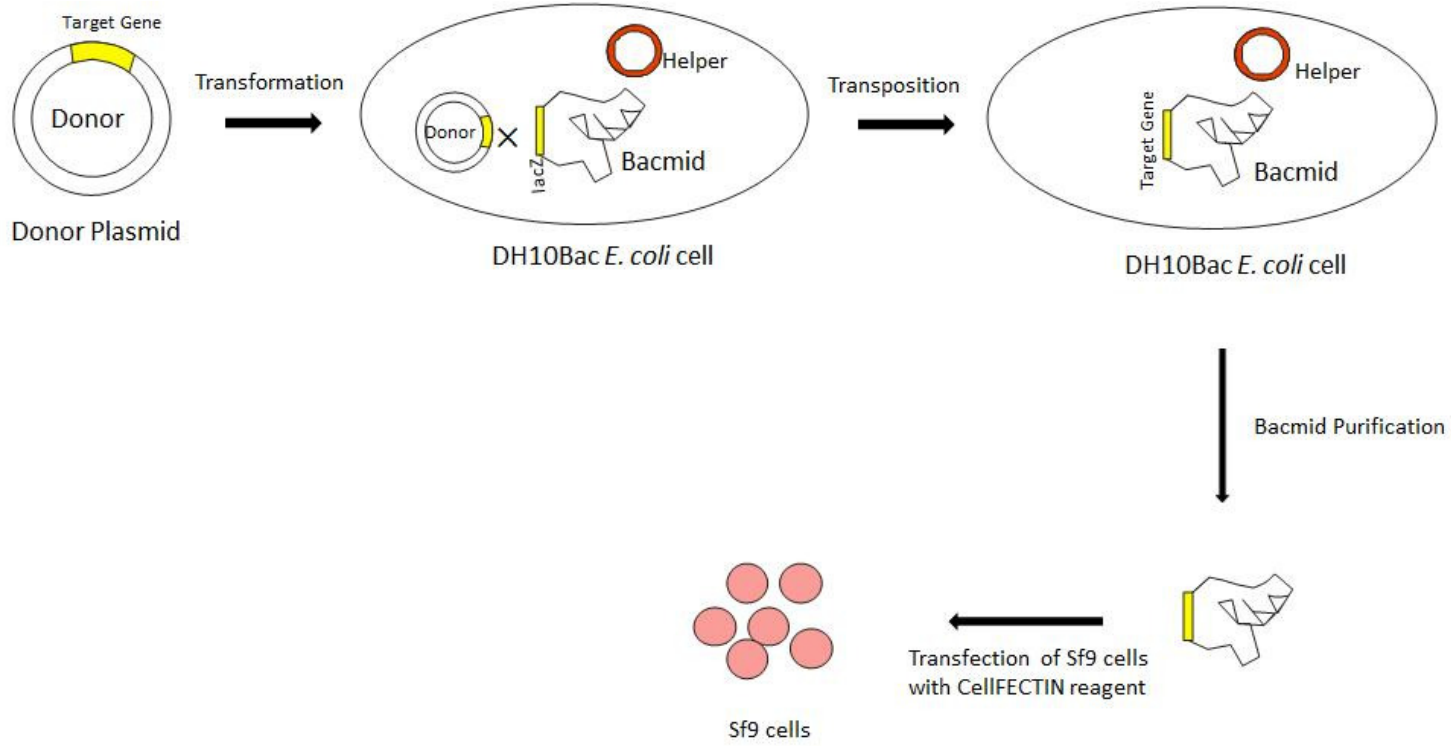

Figure 2-1. Bac-to-Bac Baculovirus Expression System (*Invitrogen*). The target gene is cloned into a pFastBac donor plasmid (Invitrogen), followed by transformation into DH10Bac competent cells (Invitrogen). The cells contain the bacmid with a mini-attTn7 target site and the helper plasmid. The target gene can be transposed to the mini-attTn7 target site in the presence of transposition proteins provided by the helper plasmid. Bacmid with target gene can be further identified by colony's color due to disruption of the lacZ gene. Bacmid was purified and used to transfect insect cells.

2.3.2.3 Purification of Recombinant Bacmid

White colonies containing the recombinant bacmid are selected from plates and inoculated into 5 ml LB media containing antibiotics, 50 µg/ml kanamycin, 7 µg/ml gentamicin, and 10 µg/ml tetracycline, and grown overnight at 37 ^{o}C with vigorous shaking at 200 rpm. 1 ml of each sample was transferred into a cryogenic vial along with 500 µl of 70 % glycerol and stored at -80 ^{o}C.

The cells were spun down at 3440 g for 10 minutes and the supernatant was decanted. The pellet was resuspended using 0.3 ml of solution I (15 mM Tris pH 8.0, 10 mM EDTA, and 100 µg/ml RNase A) and lysed upon addition of 0.3 ml of solution II (0.2 M NaOH, and 1 % SDS). The lysate was gently mixed and incubated at room temperature for 5 minutes. 0.3 ml of solution III (3 M potassium acetate pH 5.5) was added for precipitating protein and isolating genomic DNA. The sample was placed on ice for 10 minutes and then spun down at 16060 g for 10 minutes. The supernatant was transferred to the tube containing 0.8 ml of absolute isopropanol. The sample was mixed gently and placed on ice for 10 minutes. After incubation, the mixture was spun down for 10 minutes, the supernatant was removed, and the pellet was washed with 0.5 ml of 70 % ethanol. The pellet was air dried for 10 minutes and dissolved in 40 µl of TE buffer (10 mM Tris pH 8.0, and 1 mM EDTA). The bacmid was stored at 4 ^{o}C.

2.3.2.4 Transfection of Sf9 Insect Cells (Novagen)

1 million Sf9 cells in 2 ml of Insect-Xpress protein-free medium (*Lonza*) containing 7 μg/ml gentamicin were seeded in 2 ml cell dish and allowed to attach at 27 ^{o}C for 1 hour. For each transfection, solution A (100 μl Insect-Xpress protein-free medium without antibiotics, and 10 ng of bacmid DNA) and solution B (100 μl Insect-Xpress protein-free medium without antibiotic, and 6 μl CellFECTIN Reagent (*Invitrogen*)) were prepared and mixed thoroughly. Two solutions were combined and incubated at room temperature for 45 minutes. The cells were washed once using 2ml of Insect-Xpress protein-free medium without antibiotics. Solution C was formed such that 0.8 ml of Insect-Xpress protein-free medium without antibiotics was added to tube containing the mixture of solution A and B. Wash medium was removed from the cell dish and then 1 ml of solution C was overlaid over the cells. The cells were incubated at 27 ^{o}C for 5 hours. After incubation, the tansfection mixture was decanted and 2 ml of the fresh Insect-Xpress protein-free medium containing 7 μg/ml gentamicin was added. The cells were incubated at 27 ^{o}C for 72 hours. After 72 hours transfection, the viruses were harvested from the cell culture medium containing 2 % FBS and stored at 4 ^{o}C, protected from light.

2.3.2.5 Amplification and Quantification of Viruses

2 million cells per ml in 50 ml suspension culture were infected using 100 μl of a

viral stock and incubated in shaking incubator at 27 ^{o}C for 72 hours. The cells were spun down at 860 g and 4 ^{o}C. 50 ml of the supernatant containing viruses were filtered and supplemented with 1 ml FBS for further quantification of viruses.

For efficient titer of viral inoculum, the FastPlax Titer Kit (*Novagen*) utilizing a monoclonal antibody specific to an external epitope of baculovirus glycoprotein 64 (GP64) was used. The GP64 envelope fusion protein is an integral membrane protein which could be detected on the surface of the infected cells at 8-24 hours post-infection.

Following the manufacturer protocol, infected cells are fixed after 20-30 hours post-infection by serial diluted viral stock (10^{-5}, 10^{-6}, and 10^{-7}) and FastPlax antibody is added to the cells for GP64 detection. Goat Anti-Mouse IgG β-Galactosidase Conjugate and X-Gal/NBT were used for colorimeric antibody detection. The cells infected by baculovirus are distinguished by their dark blue color. The number of well isolated dark blue cell was count for the calculation of the viral titer. The titer was calculated with the following formula:

Plaque-forming unit per ml = 5 x (# infected cells and foci) x (dilution factor) (2.1)

dilution factor = dilution of viral stock (10^{-5}, 10^{-6}, and 10^{-7})

2.3.2.6 Optimization of Infection Conditions for High Five Cells

For multiplicity of infection (MOI) optimization and the time course of infection, 2 million cells per ml in 50 ml suspension culture were infected at varying MOIs and 5 ml of cells from each MOI sample were harvested at the following time intervals: 24, 36, 48, 60 and 72 hours.

Each sample of different MOI and time intervals was lysed using 1 ml of FastBreak Cell Lysis Reagent (*Promega*) and incubated on ice for 30 minutes. The cell lysate was pelleted at 16060 g and 4 ^{o}C. The supernatant of each sample was analyzed using SDS-PAGE electrophoresis and verified by His-Tag AP Western Reagent Kit (*Novagen*).

2.3.3 BacMagic Transfection System (Novagen)

BacMagic DNA is a faster method than bac-to-bac baculovirus expression system for generating recombinant baculoviruses by eliminating the steps of bacmid generation and purification. The BacMagic DNA (*Novagen*) and pBAC4x-1 plasmid with target gene were co-transfected into insect cells through GeneJuice transfection reagent (*Novagen*). The homologous recombination of the pBAC4x-1 plasmid and BacMagic DNA takes place in insect cells thus restoring the function of virus (Figure 2-2).

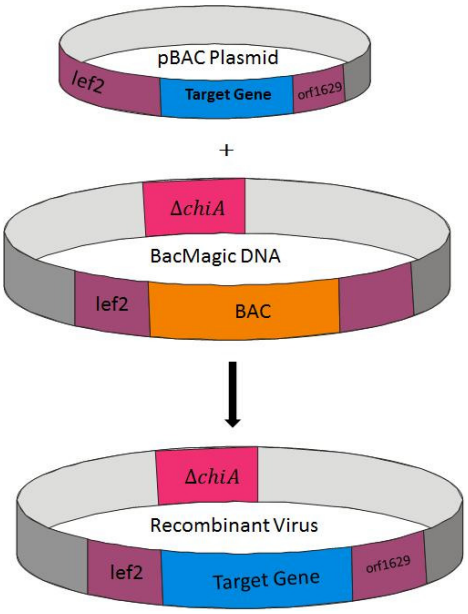

Figure 2-2. The BacMagic System (*Novagen*). The BacMagic DNA, an AcNPV genome, contains a portion of the open reading frame (ORF) 1629 and a bacterial artificial chromosome (BAC) in place of the polyhedrin (polh) coding region. The target gene is cloned into pBAC transfer plasmid and further co-transfected with BacMagic DNA into insect cells. Homologous recombination within the cells restores the function of the virus ORF1629 while the target coding sequence replaces the BAC sequence.

2.3.3.1 pBAC4x-1 with $PP2A_C$

To improve the stability of $PP2A_C$ protein, target gene was cloned into the pBAC4x-1 plasmid (*Novagen*) with uncleavable 8 His tag and D88N mutation was introduced in the active site of the enzyme. The primers for constructs of $PP2A_C$ include a BamHI (GGATCC) site at the 5' end and a SphI (GCATGC) site at the 3' end. For cleavage of DNA, pBAC4x-1 plasmid and the full length $PP2A_C$ DNA fragment were both digested overnight at 37°C by BamHI and SphI (*New England Biolabs*). The pBAC4x-1 and the full length $PP2A_C$ DNA fragments were ligated using T4 DNA Ligase (*New England Biolabs*) at and the

recombinant plasmid was transformed into *E. coli* DH5α. The recombinant plasmid was finally verified using restriction enzyme digestion and sequencing (*Eurofins MWG*).

2.3.3.2 pBAC4x-1 with $PP2A_A$ and $PP2A_C$

The pBAC4x-1 vector contains four promoters and cloning sites for a large scale expression of multiple target genes in the same cell. For co-expression of $PP2A_C$ and $PP2A_A$ protein, pBAC4x-1 plasmid containing $PP2A_C$ sequence was used. For PCR amplification of $PP2A_A$ sequence, pET28a plasmid containing $PP2A_A$ sequence ($PP2A_A$_Full), described in section 2.2.5, was used as a template and the primers were introduced SmaI (CCCGGG) and SpeI (ACTAGT) restriction sites at the 5' and 3' ends of the amplified fragment respectively. Both $PP2A_C$-containing pBAC4x-1 plasmid and the PCR product were digested overnight at 25 ^oC using restriction enzyme, SmaI and SpeI (*New England Biolabs*). The plasmid and the insert were ligated overnight using T4 DNA Ligase (*New England Biolabs*) at room temperature and the recombinant plasmid was transformed into *E. coli* DH5α. The DNA sequence was verified by restriction enzyme digestion and through sequencing (*Eurofins MWG*).

2.3.3.3 Transfection of Sf9 Cells

1 million Sf9 cells in 2 ml of Insect-Xpress protein-free medium (*Lonza*)

containing 7 μg/ml gentamicin were seeded in 2 ml cell dish and incubated at 27 ^{o}C for 1 hour. During incubation period, transfection mixture containing 1 ml Insect-Xpress protein-free medium without antibiotics, 5 μl Insect GeneJuice (*Novagen*), 100 ng of BacMagic DNA, and 500 ng of recombinant plasmid were prepared and gently mixed. To allow lipid complexes formation, the mixture was incubated at room temperature for 30 minutes. The medium was removed from the cells and 1 ml of the transfection mixture was added drop by drop to the centre of cell dish. The cells were incubated overnight at 27 ^{o}C. After the initial incubation period, 1 ml Insect-Xpress protein-free medium with 7 μg/ml gentamicin was added to the cell dish and incubated at 27 ^{o}C for another five days after which, the medium containing recombinant baculovirus was harvested and filtered.

2.3.3.4 Amplification of Recombinant Virus

2 million Sf9 cells per ml in 100 ml suspension culture were infected using 500 μl of a viral stock and incubated in shaking incubator at 27 ^{o}C for 5 days. The cells were spun down and the supernatant containing viruses were filtered and supplemented with 5 ml FBS for further quantification of viruses using the FastPlax Titer Kit (*Novagen*).

2.4 Detection of Protein

2.4.1. Western Blot

The western blot analysis was carried out with the His Tag AP Western Reagent Kit (*Novagen*). Proteins were separated on a 10 % SDS-PAGE gel and PageRular Prestained Protein Ladder (*Fermentas*) was used for approximating molecular weight of proteins. Hybond-P Polyvinylidene Difluoride (PVDF) membrane (*GE Healthcare*) was activated in 100 % methanol for 10 seconds and then washed in distilled water for 10 minutes. The SDS-PAGE, PVDF membrane, filters and sponge were rinsed in western transfer buffer (25 mM Tris-HCl, pH 8.3, 190 mM glycine, and 20 % methanol) for 5 minutes and then the electroblotting cassette was assembled in western transfer buffer. Proteins were transferred to a PVDF membrane in Mini Protean II (*Bio-Rad*) by electroblotting in transfer buffer with a constant voltage of 250 milliamps (mA) for 2 hours. Membranes were washed using 30 ml of TBS buffer (10 mM Tris pH 7.5 and 150 mM NaCl) and then incubated for 1 hour in 15 ml of blocking buffer (10 mM Tris pH 7.5, 150 mM NaCl and 3 % BSA) to block the remaining protein binding sites on the membrane. After the blocking step, the membrane was washed in 40 ml of TBSTT buffer (20 mM Tris pH 7.5, 500 mM NaCl, 0.2 % Triton X-100, 0.05 % Tween -20) and then 15 ml of TBS buffer.

The primary mouse Anti His-tag monoclonal antibody (*Clontech*) was added at a dilution of 1:1000 to 10 ml of blocking buffer. Alternatively, mouse anti-$PP2A_C$ antibody (*BD Biosciences*) was used as primary antibody at a dilution of 1:20000 to 10 ml of blocking buffer for $PP2A_C$ detection. After incubation for 2

hours with primary antibody, membranes were washed with 40 ml of TBSTT buffer and15 ml of TBS buffer and then incubated in blocking buffer with 1:5000 Goat Anti-Mouse IgG AP Conjugate (*Novagen*) for 1 hour. Following the final washing step in 100 ml of TBSTT buffer the membranes were incubated in a developing solution at room temperature until colour developed. Developing solution was prepared by adding 60 µl NBT (42 mg/ml in 100 % dimethylformamide) and 60 µl BCIP (83 mg/ml in 100 % dimethylformamide) to 1x Alkaline phosphatase (AP) buffer.

2.4.2. Sodium Dodecyl Sulphate – Polyacrylamide Gel Electrophoresis (SDS-PAGE)

SDS-PAGE separates proteins based on their molecular weights. SDS disrupts the folded structure of proteins by forming complexes with proteins through binding to hydrophobic patches of a polypeptide chain SDS-PAGE composed of a 5 % stacking layer and a 10 % or 15 % resolving layer was used in all experiments. Electrophoresis was carried out using the MiniProtean II gel apparatus (*BioRad*) connected to a PowerPac 300 power supply (*BioRad*). SDS loading dye (0.5 M Tris-HCl pH 6.8, 0.5 % bromophenol blue, 10 % SDS, and 50 % glycerol) was added to each sample which were then heated to 95 ^{o}C for 5 minutes and centrifuged at 16060 g for 1 minute. Unstained Precision Plus Protein standards (*BioRad*) were used as molecular weight markers. Polyacrylamide gels were electrophoresed at a constant voltage of 100 V through the stacking layer and 150 V through the resolving layer.

Following electrophoresis the gel was stained in a solution containing a Coomassie dye (0.25 % brilliant blue R Coomassie, 40 % methanol, 7 % acetic acid and 52 % H_2O). Protein bands were visualized by washing the gel in a de-staining solution (40 % methanol and 10 % acetic acid in distilled water) for 30 minutes.

2.4.3. Silver Staining Method

There are two types of silver staining methods: those based on silver amine complex and those using silver nitrate solutions as the silvering agent. Silver amine method depends on the formation of silver diamine complexes with ammonium hydroxide. These complexes bound to proteins are subsequently reduced to metallic silver with formaldehyde in acidic environment. Silver nitrate method involves the reaction of silver ions with protein under weak acidic conditions, followed by the reduction of silver ion to metallic silver by formaldehyde under alkaline conditions [236].

ProteoSilver^{TM} Kits (*Sigma*) based on silver nitrate method which detects at least 0.1 ng of protein per mm^2 was used for the visualization of protein bands.

2.5 Purification of Protein

2.5.1 LCMT1 and PME1 with an N-terminal Histidine Tag

2.5.1.1 Metal Affinity Chromatography

The cells were defrosted on ice and resuspended in a sonication buffer (50 mM Tris pH 8.0, 50 mM NaCl, 3 mM β-mercaptoehanol, and complete EDTA-free cocktail inhibitor (*Roche*)) and then lysed by sonication (20 x 30 seconds bursts with 1 minute intervals). The lysate was spun down at 20000 g for 30 minutes. The supernatant (soluble fraction) was incubated with 0.5 – 2 ml Ni Sepharose 6 Fast Flow (*GE Healthcare*) by rolling for 2 hours. The beads were washed 7 times with 30 resin volumes of wash buffer (50 mM Tris pH 8.0, 50 mM NaCl, 3mM β-mercaptoethanol, and 25 mM imidazole). The protein was eluted in elution buffer (50 mM Tris pH 8.0, 50 mM NaCl, 3 mM mercaptoehanol, and 300 mM imidazole) and the eluted samples were analysed by SDS-PAGE. Histidine-tagged TEV protease was added in a 1:10 dilution of the total amount of protein present and the solution left to dialyse overnight at 4^{o}C in dialysis buffer (50 mM Tris pH 8.0, 50 mM NaCl, and 3 mM β-mercaptoehanol). In order to remove the cleaved six histidine tag and TEV protease, the dialysed samples were incubated with Ni-NTA agarose (*Qiagen*) by rolling at 4 ^{o}C for 2 hours and then spun down at 2600 g. The supernatant was stored at 4 ^{o}C for further purification.

2.5.1.2 Size Exclusion Chromatography

Further purification of proteins based on protein size was carried out using Hi Load 16/60 Superdex 200 Prep Grade column (*GE Healthcare*) and ÄKTA FPLC system (*Amersham Biosciences*) at 4 ^{o}C. The column was pre-equilibrated with buffer C (50 mM Tris pH 8.0, 50 mM NaCl, 1 mM DTT). Upon concentrating protein solution using concentrator (10,000 Da cutoff membrane), the protein samples (1-5 ml) were injected into the pre-equilibrated column at a flow rate of 2 ml per minute with 2 ml fractions collected. Total volume for an elution was approximately 160 ml. Eluted protein was detected using UV absorbance at 280 nm and verified by SDS-PAGE analysis.

2.5.2 PME1 with GST Tag or NusA Tag

2.5.2.1 Purification of PME1 with GST Tag

The cells were defrosted on ice and resuspended in phosphate buffered saline (PBS) and then lysed by sonication (20 x 30 seconds bursts with 1 minute intervals). The lysate was spun down at 20000 g for 30 minutes. The supernatant (soluble fraction) was incubated with suitable amount of Glutathione Sepharose™ 4 Fast Flow beads (*GE Healthcare*), with the binding capacity of approximately 10 mg GST tag protein per ml medium, by rolling for

one hour. The glutathione beads were washed 6 times with 30 resin volumes of PBS buffer. The protein was eluted in elution buffer (50 mM Tris pH 8.0, 50 mM NaCl, and 10 mM reduced glutathione) and the eluted samples were analysed by SDS-PAGE and prepared for isothermal titration calorimetry experiments.

2.5.2.2 Purification of PME1 with NusA Tag

Although there are no commercial beads especially for NusA protein, the pET442b plasmid also includes the six hisitidine tag sequence; therefore, the same procedure of histidine tag protein purification for LCMT1/PME1 variants can also be used in the purification of PME1 with NusA tag. In addition, anion exchange chromatography on Q FF Fast Flow column (*Amersham Pharmacia*) was included in the procedure for further purification. The method was described in section 2.5.3.2.

2.5.3 $PP2A_A$

2.5.3.1 Metal Affinity Chromatography

The frozen cells were thawed on ice and resuspended in a sonication buffer (50 mM Tris pH 8.0, 50 mM NaCl, 3 mM β-mercaptoehanol, and complete EDTA-free cocktail inhibitor (*Roche*)) followed by the sonication (20 x 30 seconds bursts with 1 minute intervals). The cell lysate was centrifuged at

20000 g for 30 minutes. The supernatant was incubated with 0.5 – 2 ml Ni Sepharose 6 Fast Flow (*GE Healthcare*) by rolling for 2 hours. Non-specifically bound proteins were removed, by washing the beads 7 times with 30 resin volumes of wash buffer (50 mM Tris pH 8.0, 50 mM NaCl, 3mM β-mercaptoethanol, and 25 mM imidazole). The protein was eluted in elution buffer (50 mM Tris pH 8.0, 50 mM NaCl, 3 mM mercaptoehanol, and 300 mM imidazole) and the eluted samples were analysed by SDS-PAGE. Due to the irregular cleavage of $PP2A_A$ by thrombin protease (*Sigma*), six histidine tag of $PP2A_A$ was not removed.

2.5.3.2 Anion Exchange Chromatography

Separation and purification of proteins using ion exchange chromatography is based on differences in the ionic properties of surface amino acids. At a given pH that is below its pI value, a protein exhibits more positive overall net charge that becomes more negative at a higher pH above the protein's pI. Target protein containing a positive or negative net charge displaces a low molecular weight ion from an ion exchange matrix and binds to the matrix. An increase in the counter-ion concentration or a decrease in the protein net charge by change in a buffer pH causes the bound protein to be released from the ion exchange matrix in favour of the counter-ion.

Anion exchange chromatography with HiTrap Q FF Fast Flow column (*Amersham Pharmacia*) at the buffer pH of 8.0, was selected as the isoelectric

point (pI) of $PP2A_A$ is 5.6 The column was equilibrated with 10 bed column volumes of buffer A (50 mM Tris pH 8.0, 1 mM DTT) and the protein samples (5 ml) were then injected into the pre-equilibrated column. Total volume for a salt gradient elution was approximately 50 bed column volumes. The gradient elution was carried out using the lower ionic strength buffer A and higher ionic strength buffer B (50 mM Tris pH 8.0, 1 M NaCl, 1 mM DTT) on an ÄKTA FPLC system (*Amersham Biosciences*). The fractions were analyzed by SDS-PAGE electrophoresis.

2.5.3.3 Size Exclusion Chromatography

Further purification of $PP2A_A$ was achieved by using Hi Load 16/60 Superdex 200 Prep Grade column (*GE Healthcare*) and ÄKTA FPLC system (*Amersham Biosciences*) at 4 ^{o}C. The column was pre-equilibrated with buffer C (50 mM Tris pH 8.0, 50 mM NaCl, 1 mM DTT). Concentrated protein sample was injected into the pre-equilibrated column at a flow rate of 2 ml/minute with 2 ml fractions collected. Total volume of an elution buffer was approximately 120 ml. The eluted protein was analyzed by SDS-PAGE.

2.5.3.4 Ammonium Sulphate Precipitation

The appropriate volume of solid ammonium sulphate was added to $PP2A_A$ protein sample to get the desired concentration and the sample was incubated

at 4 ℃ for 30 minutes with constant rolling. The protein sample was then centrifuged at 20000 g for 15 minutes to pellet out the ammonium sulphate - precipitated protein. The supernatant was mixed with additional solid ammonium sulphate to make up the next concentration and the sample was again centrifuged after the incubation. All pellets from different fractions were dissolved in buffer C (50 mM Tris pH 8.0, 50 mM NaCl, 1 mM DTT) for further analysis by SDS-PAGE electrophoresis. Fraction containing $PP2A_A$ protein was dialyzed in buffer C at 4 ^oC overnight.

2.5.4 $PP2A_C$

2.5.4.1 Ethanol Precipitation Method

High Five cells expressing $PP2A_C$ stored at -80 ^oC were resuspended in buffer D (20 mM Tris pH 7.5, 2 mM EGTA, 0.5 mM DTT and 0.1 mM PMSF) and disrupted using a homogenizer. After centrifugation at 20000 g for 20 min at 4 ^oC, five volumes of 99% ethanol were added to the protein mixture and centrifuged immediately at 4250 g for 15 minutes at 4 ^oC. The pellet was resuspended in buffer D and homogenized for three times; this was followed by centrifugation at 20000 g for 20 min at 4 ^oC. The supernatant containing $PP2A_C$ was dialyzed in buffer A (50 mM Tris pH 8.0, 1 mM DTT) for further purification.

2.5.4.2 Size Exclusion Chromatography for the assembly of PP2A

The assembly of $PP2A_C$ and $PP2A_A$ was carried out using Hi Load 16/60 Superdex 200 Prep Grade column (*GE Healthcare*) and ÄKTA FPLC system (*Amersham Biosciences*) at 4 ^oC. The column was pre-equilibrated with buffer C (50 mM Tris pH 8.0, 50 mM NaCl, 1 mM DTT). The $PP2A_C$ was mixed in the molar ratio 1:1 with $PP2A_{A.}$ The protein mixture was concentrated using a concentrator with 10,000 Da cut-off membrane and the protein mixture (5 ml) was injected onto the pre-equilibrated column at a flow rate of 2 ml per minute with 2 ml fractions collected. Total volume of an elution buffer was approximately 120 ml. Eluted proteins were examined by SDS-PAGE analysis and the immunoblotting.

2.6 Quantification of Protein Concentration

2.6.1 BioRad Protein Assay

Protein concentration was determined using the BioRad (*BioRad*) protein assay kit following the manufactures protocol.

The Coomassie Brilliant Blue G-250 dye will change colour when it associates with the residues tryptophan, tyrosine, arginine, histidine and phenylalanine. Free dye in solution has absorption maxima at 470 and 650 nm, but when

bound to protein the absorption maximum is at 595 nm. The colour change can therefore be quantified at 595 nm with a spectrophotometer and a protein concentration could be determined from the linear dependence of the 595nm absorbance on the concentration of BSA that is used as a protein standard. A range of different BSA concentrations was used in order to generate the standard reference curve.

2.6.2 Absorbance Spectra

UV-visible absorbance spectra of the proteins were measured in a 1 ml quartz cuvette using BioSpec-1601E UV-Visible spectrometer (*Shimadzu*). Molar extinction coefficients were calculated based on the amino acid sequence of the various constructs along with their corresponding molecular weight (Da) using the program Expasy ProtParam. Protein concentration was calculated using the Beer-Lambert Law:

$$A_{280} = \varepsilon_{280} \times C \times L \qquad (2.2)$$

A_{280} = the absorbance of the protein at 280 nm

ε_{280} = the molar extinction coefficient at 280 nm ($M^{-1}cm^{-1}$)

C = the protein concentration (M)

L = the path length (cm)

2.7 Biophysical Analysis

2.7.1 Circular Dichroism (CD)

Circular dichroism (CD) spectroscopy measures differences of that a substance exhibits in the absorption of left-handed circular polarized light versus right-handed circular polarized light. This is a sensitive method for determining the extent of protein 'foldedness', and for characterizing a protein secondary structure. CD spectroscopy is also powerful in studying the conformational stability of a protein under different thermal and pH conditions.

Secondary structure can be analyzed using CD spectroscopy in the Far Ultra Violet (UV) spectral region (190-260 nm). At these wavelengths, the signal arises when the peptide bond is located in a regular and folded environment. Different secondary structures would give varying characteristic shapes and magnitude of CD spectrums [237].

Pure 1 mg/ml of protein was prepared for Far-UV CD spectra using Aviv 202SF spectropolarimeter (*Aviv Instruments Inc.*) connected to a thermostated water bath at 25 ^{o}C. Spectra were recorded between 190 nm and 300 nm in a 0.1 cm path length quartz cuvette, with 0.2 nm increments and subtracted from buffer scans. The data is represented as delta epsilons ($\Delta\varepsilon$) calculated from the following equation:

$$\Delta\varepsilon = (\theta_{obs} \times 0.1 \times \text{MRW}) / l \times c \times 3298 \quad (2.3)$$

θ_{obs}= observed ellipticity (millidegrees)

MRW = protein mean weight / number of residues

l = optical path length (cm)

c = protein concentration (mg/ml)

2.7.2 Isothermal Titration Calorimetry (ITC)

Isothermal Titration Calorimetry (ITC) is a thermodynamic method for measuring the energetics of biochemical reactions or molecular interactions. For ITC experiments, two binding partners in the same buffer are placed in the injection syringe and the ITC sample cell respectively. The ITC sample cell is kept at a small temperature difference compared to a reference cell filled with water.

When a protein sample in syringe is injected into the sample cell, the interaction of two proteins will generate or absorb heat. If this interaction is exothermic, the ITC uses less energy to heat the sample cell. On the contrary, if the interaction is endothermic, the ITC uses more energy to heat the sample cell in order to maintain the temperatures between the sample and the reference cell equal. The enthalpy changes of the system can be measured through the heat absorbed or generated by a system at constant pressure. To understand how ITC can be used to measure the enthalpy of a binding process through heat generation or absorbance, the equation of enthalpy evolved from the First Law

of Thermodynamics is applied as follows:

$$\Delta H = q_p \qquad (2.4)$$

Where ΔH is the change of enthalpy of binding reaction and q is the heat transferred to the system at constant pressure.

ITC directly measures this heat and determines association constants ($K_a = 10^2 - 10^9\ M^{-1}$), reaction stoichiometry (n), and enthalpy of binding (ΔH_b). In addition, through binding constants, ITC can indirectly calculate the value of free energy and entropy of binding reaction, thereby provide a complete thermodynamic profile of the molecular interaction in a single experiment [238;239]. The temperature dependence of the ΔH_b, measured by performing the titration at varying temperatures, will provide the information of heat capacity change (ΔC_p) which describes conformational changes, hydrogen bonding, hydrophobic interactions, and electrostatic interactions in molecular interactions.

The binding measurements were performed in reaction buffer (50 mM Tris pH 8.0, 50 mM NaCl, 1 mM DTT) using a VP-ITC titration calorimeter (*MicroCal, LLC*) with a reaction cell volume of 1.4 ml at different temperatures (10, 15, 20, or 25 ℃). Before running experiment, all protein samples were dialyzed in the same buffer and adjusted to the same pH value. In addition, all samples and solutions, as well as the buffer for heat dilution, were degassed and filtered just before loading into the calorimeter. 1.4 ml of target protein in the reaction cell was titrated by a 300 μl of analyte. At least 20 consecutive injections of 15 μl at

2 second/µl were applied at 4 or 5 minutes intervals, while stirring the reaction solution at 300 rpm constant speed. For heat dilution of the target protein, 1.4 ml of the reaction buffer alone in the reaction cell was titrated by a 300 µl of analyte and this value was subtracted from the measured heats of binding. Titration curves were analyzed with the Origin program provided by MicroCal, LLC, using a one-site binding model to fit the curves.

2.7.3 Differential Scanning Calorimetry (DSC)

Differential scanning calorimetry can be used to directly measure the differential power required to maintain the temperature of a sample at the same value as the solvent in a reference cell when the overall temperature of the system is increased or decreased at a fixed scan rate. In addition, DSC may also provide useful information for protein-ligand binding or protein-protein interaction which may affect thermal transitions.

The output from DSC experiment is a thermogram showing the excess heat capacity (C_P) as a function of temperature. The data is represented by the following formula [240]:

$$dQ_P/dt \text{ X } 1/\sigma M = C_P \qquad (2.5)$$

Q_P = the heat absorbed at constant pressure

t = time

σ = the scan rate (dT/dt)

T = temperature

M = the number of moles of sample in the sample cell

The C_P simply reflects the difference in heat capacity between the protein and the solvent, usually water, it has displaced. Since water has a high heat capacity compared to proteins, the apparent C_P in this region will normally be negative. The thermogram for a simple globular protein contains three regions: the pre-transition baseline, the endothermic unfolding transition, and the post-transition baseline. The pre-transition baseline represents a slightly positive slope, indicating a gradual increase in heat capacity with temperature. In a single cooperative unfolding process, the C_P increases as more heat energy is taken up in denaturing the protein, followed by reaching a peak at approximately the mid-point (T_m) temperature of the process, before dropping down to the high temperature baseline. The post-transition baseline, showing the relative heat capacity of an unfolded polypeptide, is usually found at a higher level and has a lesser slope than the pre-transition baseline [241].

The calorimetric enthalpy (ΔH_{cal}) is the total integrated area under the thermogram peak which represents the total heat energy uptake by the sample undergoing the transition and the van't Hoff Enthalpy (ΔH_{VH}) is an independent estimate of the enthalpy of the transition, based on an assumed model, a simple two-state model. The value of ΔH_{cal} and ΔH_{VH} should be similar in DSC experiment and could be revealing about factors such as the purity and

concentration of the sample in addition to providing information about the reversibility of the process [241].

The differential scanning calorimeter VP-DSC (*Microcal, LLC*) with cell volume of 500 µl was used for DSC analysis. Samples were prepared using a 25 µM target protein in the buffer containing 25 mM Tris, pH 8.0, 50 mM NaCl, also used as a reference buffer. All experiments were calibrated to the baseline obtained by scanning the reference buffer. All protein samples and solutions, as well as the reference buffer, were degassed and filtered just before loading onto the calorimeter. Scanning was performed at 1 °C/min between 10 and 80 °C and with filtering period of 16 sec. The calorimetric enthalpy change (ΔH_{cal}), determined by numerical integration of the area of the heat absorption peak to the area of calibration peak, was calculated using Microcal Origin software supplied with the instrument.

2.7.4 Surface Plasmon Resonance (SPR)

Surface Plasmon Resonance (SPR) occurs at metal surfaces (gold or silver) when an incident light beam strikes the surface at a particular angle. Depending on the thickness of a molecular layer at the metal surface, the intensity of the reflected light will change. In biomedical applications, the sensitivity of SPR to the refractive index of the medium next to the metal surface makes it possible to measure accurately the adsorption of molecules on the metal surface and their

interactions with ligand or proteins [242].

In SPR biosensors, like the BIAcore, monochromatic light with a broad distribution of incident angles is used and the reflected light reaches the detector at different points, depending on the angle of reflection. The detector continuously records the position of reduced light intensity and calculates the SPR angle of reflected light. The change in SPR angle θ of reflected light at a given wavelength is directly related by constants c_1 and c_2 to both the change in refractive index n at the surface and the change in thickness d of the layer, according to the formula [242-244]:

$$\Delta\theta(\lambda) = c_1\Delta n + c_2\,\Delta d \qquad (2.6)$$

Δd = the change in protein thicken

Δn = refractive index change

(according to the Lorentz-Lorenz relation)

The output of the SPR angle change is resonance units (RU). 1000 RU is correspondent to an angle change of 0.1 degree which is produced for most proteins by the binding on the sensing layer of approximately 1 ng/mm^2.

Real-time biomolecular interaction measurements were performed on a

BIAcore™ X-100 (*BIAcore Life Sciences*). A Ni-NTA sensorchip (*BIAcore Life Sciences*) which immobilized Ni^{2+} - nitrilotriacetic acid (NTA) was used. The $PP2A_A$ was analyzed for its capacity to bind free PME1 protein when $PP2A_A$ is immobilized to the sensor chip. For this purpose, 0.5 mM $NiCl_2$ was injected at 10 µl per minute for 1 min onto the agarose coated chip, which was followed by the injection of 50 nM histidine-tagged $PP2A_A$ in the buffer containing 10 mM HEPES, pH 7.8, 150 mM NaCl, 50 µM EDTA, and 0.005% surfactant P20 at the same rate. The association with analyte (PME1 or LCMT1 variants) was allowed to occur during 60 sec before the flow was switched to analyte-free buffer for dissociation measurement. The chip was regenerated with buffer containing 0.35 M EDTA.

2.7.5 Thermofluor

Thermoflour method was used as a high-throughput approach to efficiently identify optimal buffer condition or potential ligand for protein crystallization. Folded and unfolded protein can be distinguished through exposure to hydrophobic fluoroprobe which is quenched in an aqueous solution (of a folded protein) but associate with the exposed hydrophobic portion of an un-folded protein and generate fluorescence. Thermally induced unfolding would lead to a sharp decrease in quenching and readily detected fluorescence emission [245].

Thermofluor method was set up using a 96-well PCR plate (*BioRad*). Each well

contained 5 µl of 50 µM protein, 45 µl of test buffer and 0.025 µl of 300X Sypro Orange (*Molecular Probes*). The plates were sealed using Optical-Quality Sealing Tape (*BioRad*) and analyzed in iCycler iQ Real Time PCR Detection System (*BioRad*) from 20 ^{o}C to 95 ^{o}C in increments of 0.5 ^{o}C.

2.7.6 X-ray Crystallography

X-ray crystallography is the most successful method for the determination of protein structure. The protein must be crystallized for application of X-ray diffraction to a macromolecule. The crystals do not grow from a saturated solution. The system must be in a supersaturated state to provide the thermodynamic driving force for crystallization. The natural inclination of any system proceeding toward equilibrium is to maximize the entropy by freeing individual constituents from physical and chemical constraints; however, the formation of chemical bonds and interactions that generally provide negative free energy usually minimize the free energy of the system.

The high-quality relatively large crystal is necessary for a high resolution X-ray diffraction study. However, the crystallization step is also the primary obstacle in X-ray crystallography. Systematic search of protein crystallization condition is important for scanning the ranges of the individual parameters that impinge upon crystal formation. Commonly a set or multiple sets of these factors are found via high throughput pre-screening method that would yield some kind of crystals and then the variables are optimized to obtain the best possible crystals

for X-ray analysis.

2.7.6.1 Pre-screening Crystallization Condition of Proteins

Following large scale purification, proteins were concentrated to at least 10 mg/ml concentration and subjected to crystallization trials using sitting drop vapor diffusion method with commercial screening suites including: Index (*Hampton Research*), PGA Screen (*Molecular Dimensions*), PEG Suite (*Qiagen*), JBScreen PEG/Salt (*JENA Bioscience*), JCSG (*Qiagen*), JBScreen Classic II (*JENA Bioscience*) and Nextal Cryo Suite *(Qiagen*). TTP LabTech's mosquito which provides accurate sample placement for drop dispensing was used for automated high throughput pre-screening and 0.1 µl of proteins and 0.1 or 0.2 µl reservoir buffer sitting drops were set up in 96 well plates (*Qiagen*). All crystallization trays were incubated at 20 ^{o}C.

2.7.6.2 X-ray Diffraction and Data Collection

The crystal that was used to obtain the X-ray diffraction data was grown from the solution containing pentaerytrhritol ethoxylate and the crystal was flash frozen directly in a cold nitrogen stream. The X-ray diffraction data were collected on 300 mm Saturn 944+ CCD detector with AFC-11 4-axis partial χ goniometer with Rigaku MicroMax-007 HF rotating anode X-ray generator equipped with Varimax VHF optics. 180° of data was collected over 0.5°

oscillations and diffraction images were scaled, data merged and indexed using the program d*TREK [246].

2.7.6.3 Optimization of Protein Crystals

High resolution of diffraction pattern is highly desirable for X-ray crystallography structure determination. Therefore, the crystal quality is an important issue in X-ray crystallography. Diffraction pattern depends on unit cell type and unit the cell size. Unit cell size also depends on the protein size, the tightness of the packing of the protein and the symmetry. In addition, uniformity of the unit cells within the crystal lattice is also important.

For improvement of the quality of crystal and the diffraction pattern, several methods including dehydration, annealing, additive screening and seeding method were used.

2.7.6.3.1 Dehydration Method

Crystal dehydration is usually applied to remove the excess solvent content, to tighten the packing of the protein molecules and to reduce the size of the solvent channels. It sometimes improves crystal order and diffraction resolution at room temperature, especially for crystals with large initial solvent contents. Protein crystals sometime undergo structural rearrangements after dehydrating

and yield alternative crystal packing that may be difficult to achieve directly during crystal growth. Of course, dehydration often severely degrades diffraction properties, but original crystal order can usually be fully recovered just by re-hydrating [247;248].

To achieve the dehydration of protein crystals, four protocols are used and tested. In method I, protein crystals are gradually transferred to increasing concentration of ammonium sulphate (1.6 M, 1.8 M and 2.0 M) and exposed to air. In method II, 1.8 M ammonium sulphate solution was added to crystallization drop which was exposed to air. In method III, crystals were transferred to 1.8 M ammonium sulphate buffer and equilibrated over reservoir. In method IV, cover slip with protein crystals was transferred to reservoirs containing serial increase of ammonium sulphate solution. These methods were shown in Figure 2-3. All crystals were tested at room temperature (20 ℃) or low temperature (-173 ℃) by diffraction screening.

MicroRT™ capillary system (*MiTeGen*) was also used for protein crystal dehydration and room temperature diffraction screening. The method is based on the fact that saturated solutions of salts will maintain a fixed relative humidity that depends on the salt in an enclosed container at constant temperature. Protein crystals usually have relative humidities of 95-98%, so a good set of humidities to test is 93%, 86%, 79%, 75%, and 68% which are corresponding to a series of saturated salt solutions including potassium nitrate, potassium chloride, ammonium sulphate, sodium chloride, and cupric chloride.

Each saturated salt solution (30 µl) was injected into the MicroRT capillary, made of clear plastic that gives less background scatter than regular quartz X-ray capillaries tube, using a pipette with a gel-loading tip. The crystals were mounted on a goniometer base and covered by capillary with different salt solutions for X-ray diffraction at room temperature.

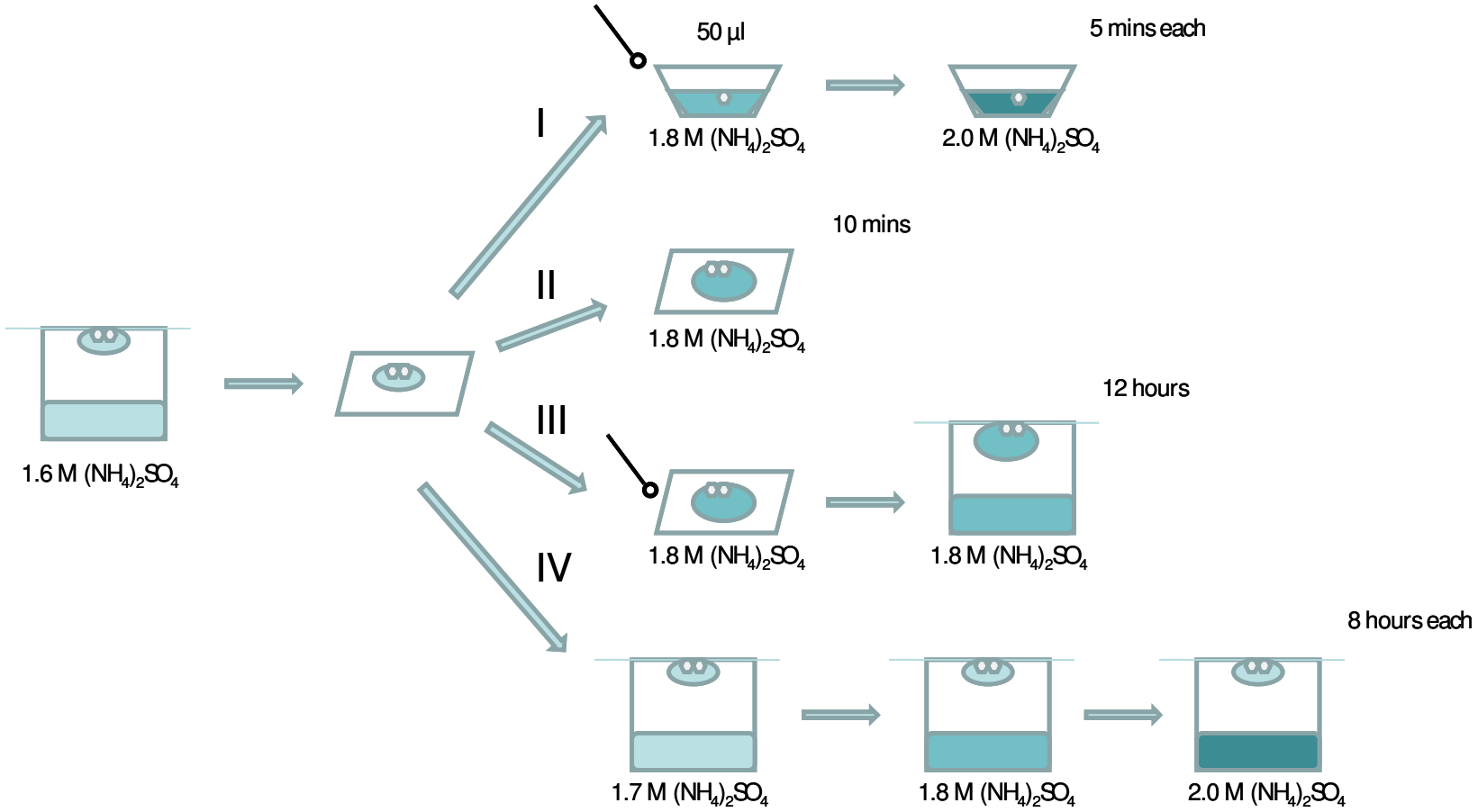

Figure 2-3. Four Methods for Dehydration of LCMT1$_{20\text{-}334}$ Protein Crystals.

2.7.6.3.2 Annealing Method

Flash cooling step can dramatically increase the mosaicity and crystal annealing sometimes will reduce the mosaicity of crystals without affecting molecular structure. Two annealing method protocols were tested. In method one, the crystals were frozen in a cryostream, brought back to the cryoprotectant solution at room temperature for 3 minutes, and re-frozen. In method two, the cold stream for crystals was blocked for 3 second and the crystal is then re-cooled. Both methods are shown in Figure 2-4 [249].

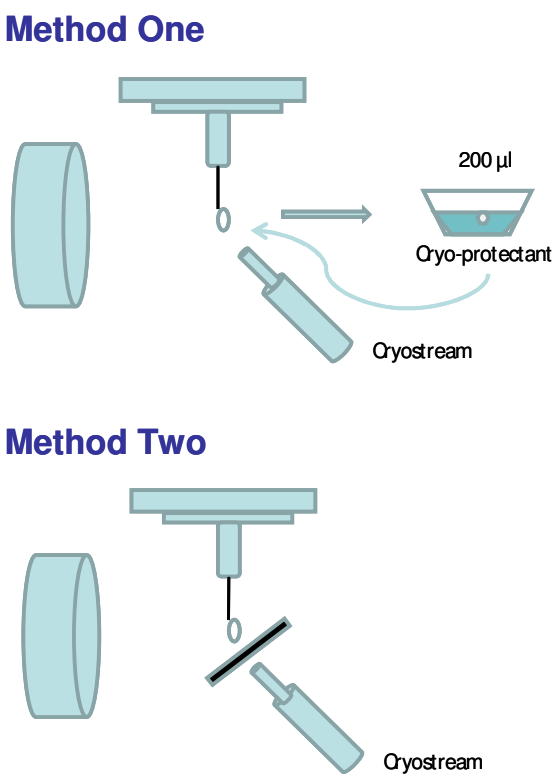

Figure 2-4. Two Methods for Crystal Annealing of LCMT1$_{20-334}$ Protein Crystals.

2.7.6.3.3 Additive Screening Method

Additive Screen (*Hampton Research*) and the Opti-Salt Suite (*Qiagen*) were used in screening for crystallization additives. In Additive Screen (*Hampton Research*), two separate methods were used for volatile and non-volatile additives. When non-volatile additives were tested, 1 ml of hit crystallization reagent was added directly into the reservoir and sample drop was set up using 1 µl of protein sample, 0.8 µl of reservoir solution and 0.2 µl non-volatile additives. Volatile additives were screen by mixing 100 µl of additive with 900 µl of hit crystallization reagent that were then added into the reservoir and 1 µl of protein sample was mixed with 1 µl of reservoir solution for the sample drop.

In Opti-Salt Suite (*Qiagen*), the reservoir solution was set up by mixing hit crystallization reagent in a ratio of 9:1 with Opti-Salt solutions. The sample drop was set up by mixing reservoir solution in a ratio of 1:1 or 2:1 with the protein sample.

2.7.6.3.4 Seeding Method

Preparation of the seed stock was carried out by placing the seed crystal in the microcentrifuge tube containing 50 µl of reservoir solution together with seed bead and the microcentrifuge tube was vortexed for 90 sec. Seed stock was diluted in the ratio of 1:10 with the reservoir solution for storage.

The Additive Screen HT (*Hampton Research*) and Seeding method were used together for large screening for optimal crystallization conditions. The reservoir condition were set up by mixing hit crystallization condition in a ratio of 9:1 with additives and the sitting drop was set up by mixing seed stock, reservoir solution with additives and the protein sample in a ratio of 1:2:1. High throughput screening was accomplished by using TTP LabTech's mosquito.

2.7.6.4 Structure Determination and Refinement

The structure of human LCMT1 was determined by the molecular replacement method using the programs Phaser and Molrep from CCP4 v6.1.3 Suite [250;251] (Collaborative Computational Project, Number 4, 1994) and a homology model for the core structure of LCMT1 that was based on the coordinates of *S. cerevisiae* protein phosphatase methyltransferase 1 (PDB: 1RJG) [223] as the starting model. The initial model covered ~75 % of the amino acid residues present in the polypeptide chain used to obtain crystals. The electron density for the cofactor not included in the molecular replacement model was clearly visible in the initial maps, providing confirmation of the molecular replacement solution. Structure refinement was carried out using the maximum likelihood restrained method with simple scaling in REFMAC5/CCP4 [252] as well as solvent flattening and density modification routines implemented in CCP4. Real space refinement/manual fitting of the electron density map and model building were carried out in Coot 0.6.1 [253].

The final model of LCMT1 includes residues 29-232, EG dipeptide linker, and residues 259-334. In addition, a single molecule of AdoMet and a glycerol molecule are included in the model. The model was validated using Coot, PROCHECK [254] and MolProbity [255]. No Ramachandran outliers were detected and the model generated a good MolProbity score of 2.1 with hydrogen atoms added prior to the analysis. MolProbity was very valuable in identifying significant number of poor rotamers, in particular those of Leu residues that were subsequently corrected such that the final model contains only 4 % of poor rotamers, many of which were constrained by the intramolecular interactions with other residues in the structure. While the core of the structure fitted well into the electron density, there were regions that exhibited high level of disorder, in particular a large loop region (residues 303-313) and the C-terminal end (residues 325-334). Atomic coordinates for LCMT1 structure were deposited to Protein Data Bank (www.pdb.org) [256], PDBID 3O7W.

Chapter Three

Cloning, Protein Expression and Characterisation of PME1 and LCMT1

After many years of investigation it is now clear that the methylation state of the catalytic subunit provides a key mechanism for the assembly of a PP2A holoenzyme; however, the discrepancies in literature with respect to the relationship between the methylation state and the type of the regulatory subunit (B, B' or B'") found within the heterotrimeric complex emphasizes the need for further investigations of this phenomena. Although the major participants in methylation of PP2A, PME1 and LCMT1, are well recognized, at the time of starting the work for this dissertation the structure of human LCMT1 and PME1 had not been determined. And although, the structure of PME1-PP2A complex was solved in 2008 [221], there is uncertainty regarding the full extent of PME1 and PP2A interaction, as large segments of polypeptides from both PME1 and $PP2A_A$ were truncated in the reported complex structure.

The initial objective of this project was to generate a panel of soluble PME1 and LCMT1 protein constructs so that suitable candidates could be used for structure analysis and mechanistic studies. This chapter describes molecular cloning of the full length PME1, LCMT1 and truncated PME1 and LCMT1 genes in the expression vector pET30a-TEV/pGEX2T1/pET442b to generate DNA constructs encoding for protein variants with an N-terminal histidine tag or glutathione-s-transferase fusion proteins for the protein expression in *E.coli* cells. This chapter also includes the results of over-expression of cloned constructs, purification of each cloned construct, initial characterisation of the soluble proteins using biophysical instrumentation and high throughput screening of crystallization condition.

3.1 Human Leucine Carboxyl Methyltransferase

3.1.1 Construct Design

3.1.1.1 Bioinformatics Analysis of LCMT1

Proteins commonly contain flexible regions serving as linkers between structurally autonomous domains that could interfere with the production of a soluble protein. Based on the information from sequence alignments and secondary structure predictions, optimal DNA constructs that encode for structurally independent domains could be predicted and designed.

LCMT1 was predicted to contain leucine carboxyl methyltransferase domain (residues 24-322) using the Simple Modular Architecture Research Tool (SMART) [227]. This tool uses multiple sequence alignments to identify and annotate protein domains within the target sequence. The secondary structure of LCMT1 was also predicted using PSIPRED secondary structure prediction protocol (BCB, *UCL*) for construct design (Figure 3-1) [228;229]. In addition, the crystal structure of protein phosphatase methyltransferase 1 from *Saccharomyces cerevisiae* that was previously solved and that shares 28% sequence identity with human's LCMT1 [223] was used to carry out secondary structure alignment with the predicted secondary structure of human LCMT1. Based on the combined information from these comparisons, the expression constructs could be design to keep the core domain of the protein and to

potentially remove the putative flexible segments. Therefore, several residues preceding the first α helix of LCMT1 including Met1, Glu7, Ser9, Thr16 and Asp20 were chosen as an alternative N- terminus of protein products and residues following the last β strand of LCMT1 (Thr321 and Tyr334) were selected as the alternative C-terminus of the engineered proteins. In addition, it was considered that, based on the sequence alignment, the similarity of secondary structure of LCMT1 and PPM1 become more significant after the residue 61 of LCMT1 and thus, Arg61 of LCMT1 was also chosen as a potential candidate residue for the N-terminus.

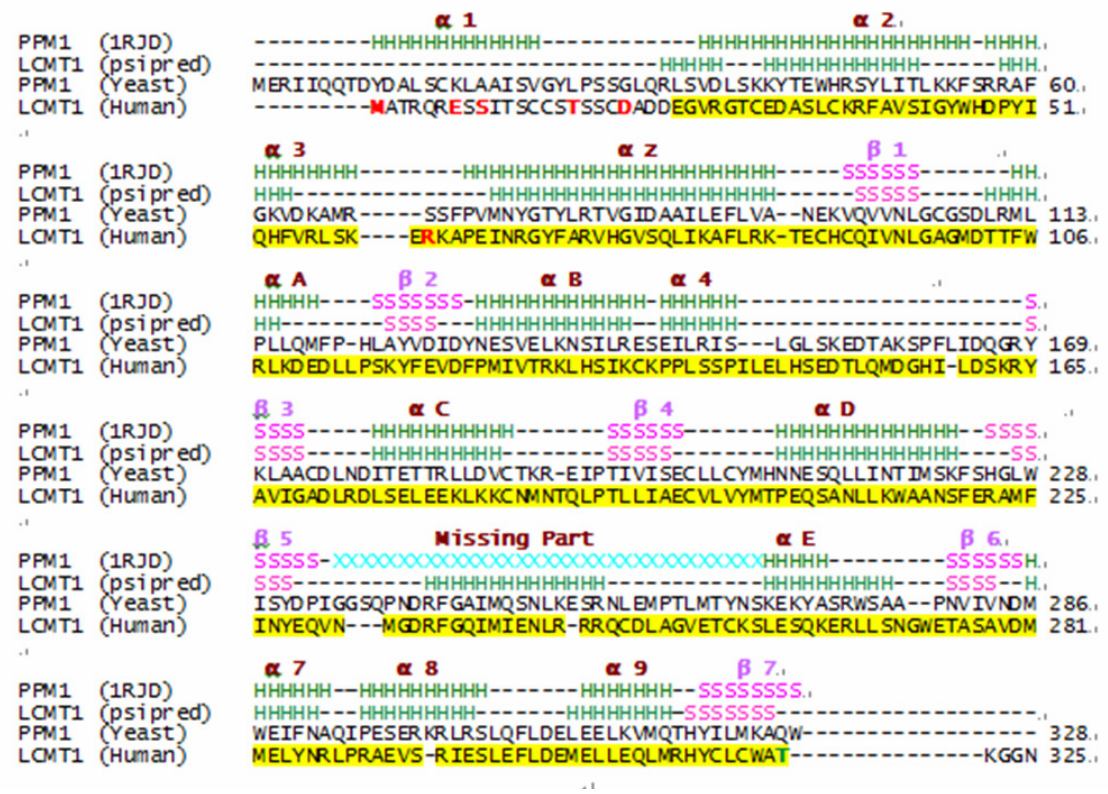

Figure 3-1. Comparison of the Secondary Structure Prediction of LCMT1 and the Secondary Structure of PPM1. The domain recognition (yellow region) and secondary structure prediction were accomplished respectively by simple modular architecture research tool [227] and psipred secondary structure prediction (BCB, *UCL*) [228,229]. The primary sequences of human LCMT1 and yeast PPM1 aligned through ClustalW (*EMBL-EBI*) [257] exhibit 28% sequence similarity. However, the secondary structure arrangements of LCMT1 and PPM1 are highly conserved. Residues shown in red and residues shown in green are chosen as alternative N-termini and C-termini respectively. The residues 234 to 267 of PPM1 protein in PDB file (1RJD) [223] were not observed in the electron density maps due to high flexibility of this region.

3.1.1.2 Limited Proteolysis of LCMT1

In order to facilitate crystallization and improve solubility of LCMT1, the limited proteolysis method was applied for detecting any putative flexible segments and internal loops of LCMT1. After the incubation of 1 mg of the full length LCMT1 with 1 μg of trypsin for 10, 30, 60, 120, 240, 480 minutes, a stable fragment of LCMT1 was generated and further analyzed by SDS-PAGE. The result shows that the molecular weight of this segment is about 30 kDa (Figure 3-2a). To characterize the first residue and molecular weight of this target segment, the samples were sent to Protein & Nucleic Acid Chemistry Facility (PNAC) of Cambridge University for the N-terminal protein sequence analysis and to the Institute of Structural and Molecular Biology (ISMB) for Mass Spectrometry analysis respectively. The protein sequencing result showed that the first six residues in the N-terminus are $E^{7}SSITS^{12}$ (where superscript 7 and 12 denote the residue number in the amino acid sequence) while the molecular weight of this target segment is 26.8 kDa, as verified by Mass Spectroscopy. These two analyses and the prediction of trypsin digestion site of LCMT1 suggested that the residue at the C-terminus of the fragment could be Arg236. In addition, sequence alignment of yeast PPM1 and Human LCMT1 by ClustalW [257], indicates that the residue Arg236 of human LCMT1 corresponds to the residue Arg242 at the flexible region in the PPM1 structure (Figure 3-2b). The combination of the prediction of secondary structure and the result of sequence alignment suggest that the protein sequence from Asn232 to Ser260 of human LCMT1 may be also a flexible segment (Figure 3-2b). Therefore, based on this information and the limited proteolysis studies, three

LCMT1 constructs were designed and generated. $LCMT1_{7\text{-}334}$ contains residues 7-232, a small linker EG, and residues 259-334, whereas $LCMT1_{7\text{-}232}$ protein variant only includes residues 7-232. $LCMT1_{20\text{-}334}$, with a truncation of the N-terminal 20 amino acids of LCMT1, previously formed weakly diffracting. Therefore, $LCMT1_{SD20\text{-}334}$ DNA expression construct was also designed to include DNA sequence coding for residues 20-232, a small EG dipeptide linker, followed by residues 259-334.

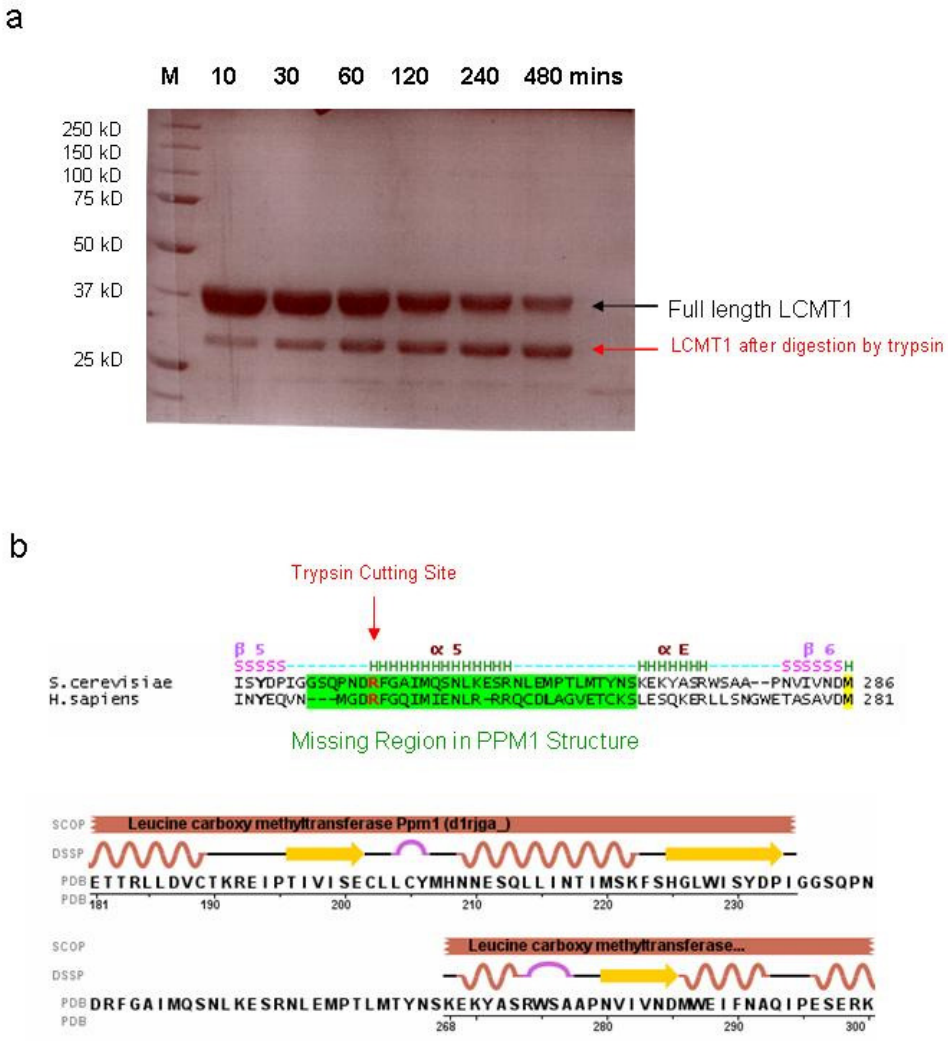

Figure 3-2. The Limited Proteolysis Analysis of LCMT1. (a) 1 mg of LCMT1 was incubated with 1 μg of trypsin and the digestion reaction was stopped at several time points (10, 30, 60, 120, 240, and 480 minutes). The results of 10 % acrylamide SDS-PAGE gel show more and more truncated segment of LCMT1 was generated with time. (b) The target trypsin cutting site (Arg236) was situated in the flexible region of human LCMT1 correspondent to the missing site in the structure of yeast PPM1 (PDB: 1RJG) [223].

3.1.2 Molecular Cloning and Protein Expression

The primer design for all LCMT1 variants and the conditions of PCR reactions were described in section 2.2.5. The PCR products were digested and cloned into pET30aTEV vector. The purification of DNA from agarose gel and ligation of plasmid and insertion were both described in sections 2.2.4.3, 2.2.5.2, and 2.2.5.3. All constructs were initially transformed into *E. coli* DH5a cells, a host without the T7 genes, thus eliminating plasmid instability due to the production of a cloned protein potentially toxic to the host cells. The detail of transformation was described in section 2.2.5.3. All clones were verified through DNA sequencing via Eurofins MWG.

The pET30a-TEV vector contains a kanamycin resistance gene. Within the pET expression systems, T7 RNA polymerase produced from an engineered *E. coli* strain will transcribe the recombinant gene. This polymerase is under control of a *lac* operon and expression of T7 polymerase gene is suppressed by the binding of *lac* repressor protein to the *lac* promoter. The addition of isopropyl-β-D-thiogalactopyranoside (IPTG), the analog of allolactose, will activate the T7 polymerase gene by dissociating *lac* repressor protein from the *lac* promoter.

For protein expression, $LCMT1_{7\text{-}334,}$ $LCMT1_{7\text{-}232}$ and $LCMT1_{SD20\text{-}334}$ were transformed to *E. coli* BL21 (DE3) pLysS cells, whereas other LCMT1 constructs were co-transformed with pBADESL plasmid that contains the

GroES and GroEL coding region, to *E. coli* BL21 (DE3) or *E. coli* C41 (DE3) cells. Previously, it was shown that GroEL/ES mediate LCMT1's folding and improve the production of LCMT1 [234]. The recombinant proteins contain an N-terminal six histdine tag and a tobacoo etch virus (TEV) protease cleavage site for removal of the tags and redundant amino acids. After removing histdine tag, only an additional glycine and alanine residues remained at the N-terminus of each LCMT1 variant.

Small scale expression tests were carried out in 100 ml cultures that were grown to an optical density (OD_{600nm}) of 0.6. The expression of the proteins was induced using IPTG to a final concentration of 1 mM. Several hours after the induction of protein expression un-induced and the induced cell cultures were individually sonicated and subjected to SDS-PAGE analysis to confirm protein expression as described in section 2.2.6.1. Only $LCMT1_{61-334}$ in *E. coli* BL21 (DE3), $LCMT1_{20-334}$ in *E. coli* C41 (DE3), $LCMT1_{7-334}$ and $LCMT1_{SD20-334}$ in *E. coli* BL21 (DE3) pLysS and $LCMT1_{1-334}$ in *E. coli* C41 (DE3) cells yielded soluble target protein at 37 ^{o}C.

3.1.3 Purification of LCMT1 for Protein Crystallization

Proteins cloned into the pET30aTEV vector carry the histidine tag sequence, a segment of six consecutive histidine residues that are expressed at the N-terminus of the proteins. The histdine tag binds to divalent cations, *e.g.* (Ni^{2+}, Co^{2+}), immobilised on tetra-dentate chelating adsorbent resin. Here, we used

the resin of Ni^{2+} Sepharose 6 (*GE Healthcare*), composed of highly cross-linked 6% spherical agarose that contains a proprietary chelator and comes pre-charged with nickel.

Before metal affinity chromatography, all *E. coli* cells were lysed through sonication. The cell lysate was centrifuged and then the soluble fraction was incubated with Ni Sepharose 6 which trapped all LCMT1 proteins with an N-terminal histidine tag. Any non-specifically bound of other proteins were removed by washing with 20 mM imidazole. All LCMT1 proteins were harvested by elution with 250 mM imidazole, which displaces the tagged proteins from the Ni Sepharose 6 beads.

All LCMT1 proteins were dialyzed in the presence of TEV protease, containing a non-cleavable N-terminal histidine tag, in order to cleave the histidine tag from all LCMT1 proteins. After TEV digestion, only an additional glycine and alanine residues remain at the N-terminus of each variant. To remove the cleaved histidine tag, un-cleaved protein and TEV protease, the solution was passed back over Ni-NTA resin and the unbound cleaved protein collected. The nitrilo-tri-acetic acid (NTA) occupies four of the six ligand binding sites in the coordination sphere of the nickel ion, leaving two sites free to interact with the histidine tag, which binds with high affinity to the histidine tagged proteins.

Each LCMT1 variant was discussed in the following sections while the details of the purification methods were described in section 2.5.1. Total amount of

soluble protein obtained from 1 litre of *E. coli* cells for each of the LCMT1 proteins was estimated using UV-visible absorbance spectra or BioRad protein assay as described in section 2.6.

Before setting crystallisation trays using TTP LabTech's mosquito and commercial screening kits, 20-30 mg/ml of protein was mixed with the ligand S-adenosylmethionine (Sigma) in a 1:1 molar ratio. 672 conditions were used for LCMT1 variant crystal screening as described in section 2.7.6.1. Only $LCMT1_{20\text{-}334}$ and $LCMT1_{SD20\text{-}334}$ protein could be crystallized. The protein production and crystallization condition of each LCMT1 variant were described and summarized in Table 3.1.

LCMT1 Variant	Production (mg per litre *E. coli*)	Crystallization Condition	Figure
$LCMT1_{20-334}$	1.5	0.1 M sodium citrate pH 5.6, 2% PEG400, and 1.8 M ammonium sulphate	Figure 3-3
$LCMT1_{61-334}$	10	-	Figure 3-4
$LCMT1_{1-334}$	2.5	-	Figure 3-5
$LCMT1_{7-334}$	4	-	Figure 3-6
$LCMT1_{SD20-334}$	4	A range of different precipitants including PEG 3350, PEG 5000, PEG 8000, ammonium sulfate, or Jeffamine ED-2001.	Figure 3-6 Figure 3-7

Table 3-1. The Protein Production and Crystallization Condition of Each LCMT1 Construct.

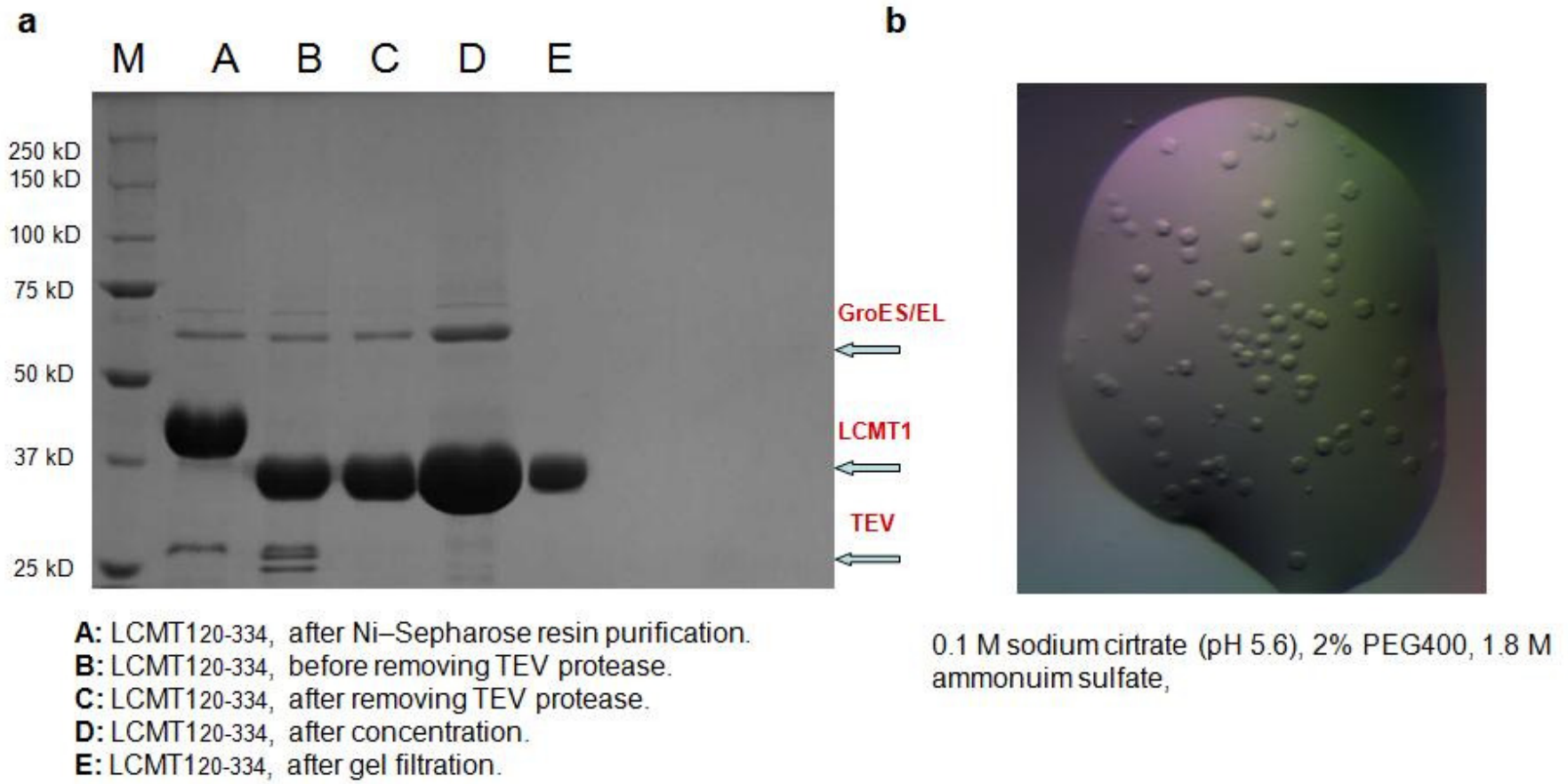

Figure 3-3. Purification and Crystallization of Truncated LCMT1 (residues 20-334). (a) 10% acrylamide SDS-PAGE analysis of the LCMT1 isolation with Coomassie Blue staining. The arrow denotes the recombinant LCMT1 protein at each purification step. (b) Small crystals of LCMT1 were formed in 0.1 M sodium citrate (pH5.6), 2% PEG400 and 1.8 M ammonium sulfate.

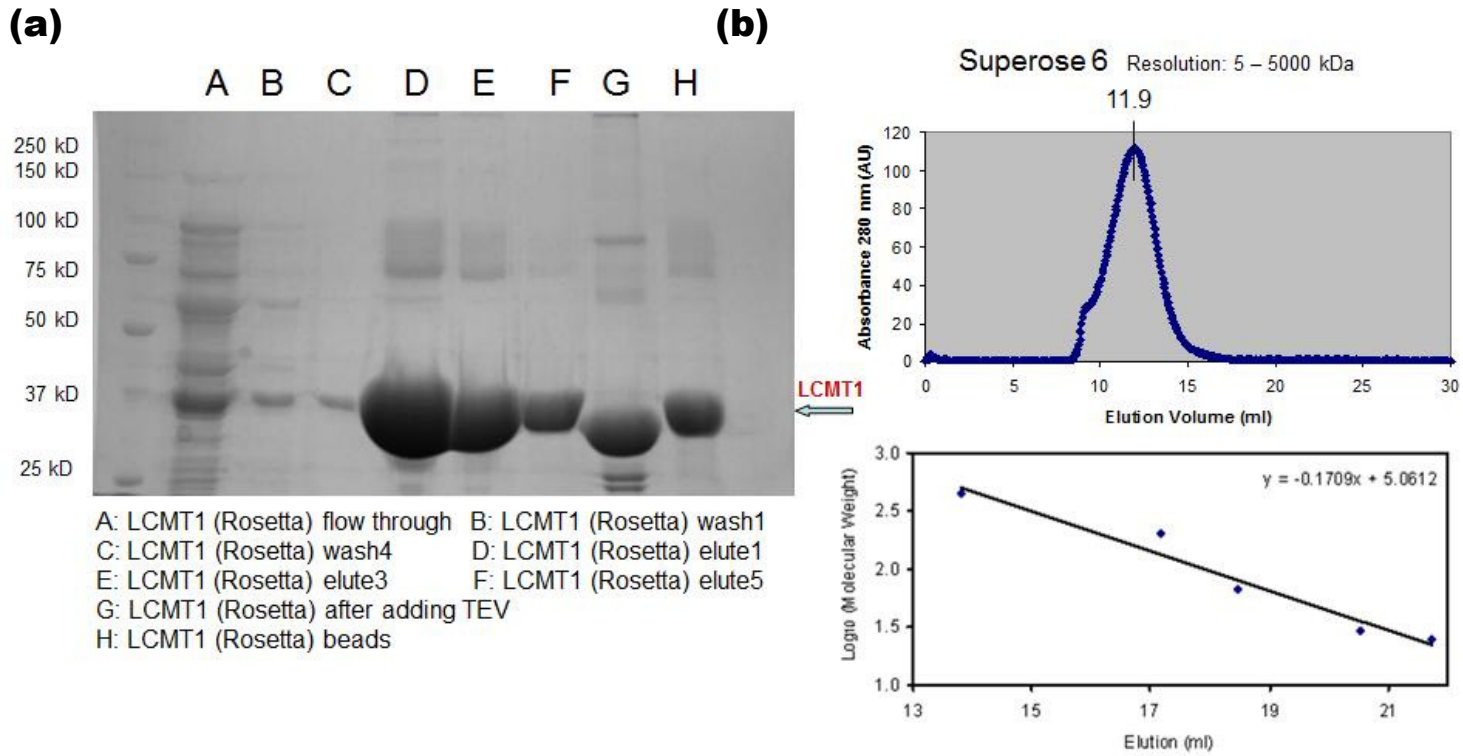

Figure 3-4. Purification and Gel Filtration of Truncated LCMT1 (residues 61-334). (a) 10 % acrylamide SDS-PAGE analysis of the LCMT1 isolation with Coomassie Blue staining. The arrow denotes the recombinant LCMT1 protein. Relatively high yield of purified protein - 10 mg of LCMT161-334 protein/L cells was obtained. However, this form of the N-terminally truncated protein was poorly soluble and it precipitated in a buffer containing glycerol (20 %) and a high salt concentration (500 mM). (b) Based on the calibration equation of the size exclusion chromatography Superose 6 column (separation range : 5 to 5000 kDa) (GE Healthcare), the $LCMT1_{61\text{-}334}$ (31 kDa) eluted at a high molecular weight of 773 kDa indicating that the N-terminal deletion of the polypeptide sequence resulted in an aggregated form of the protein.

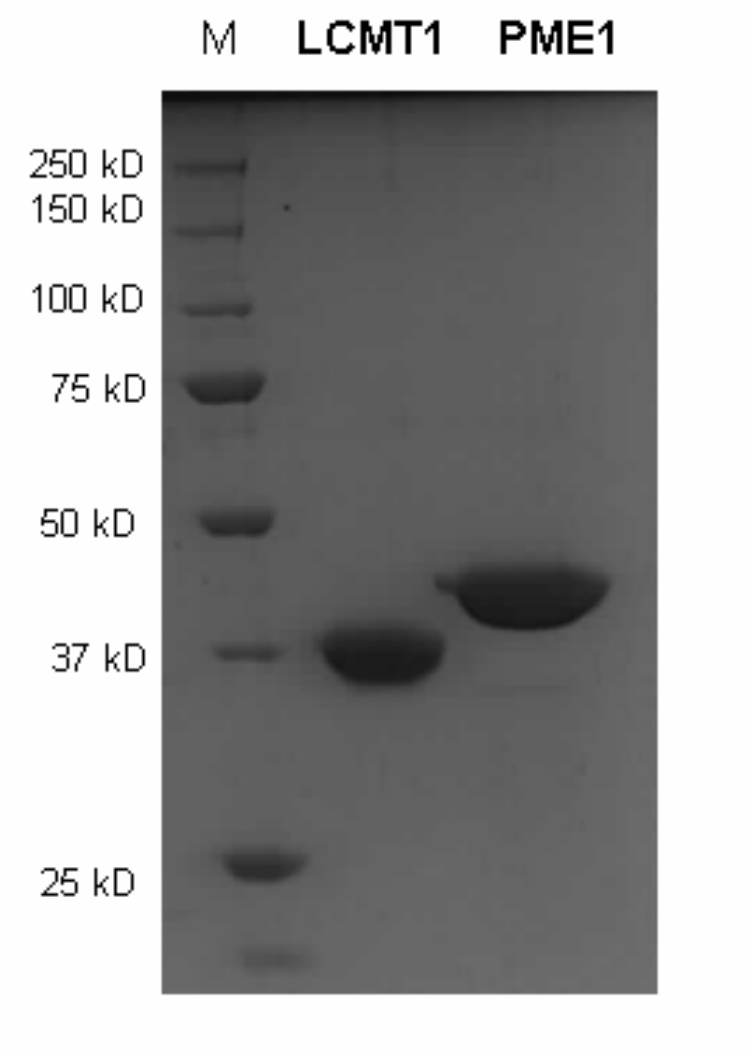

Figure 3-5. Purification of Full Length LCMT1 and PME1. Full length LCMT1 and PME1 were further purified using gel filtration column (Hi Load 16/60 Superdex 200 Prep Grade, *GE Healthcare*). The 10% acrylamide SDS-PAGE gel was visualized using Coomassie Blue staining method and showed the purified full length PME1 and LCMT1 after size exclusion chromatography column.

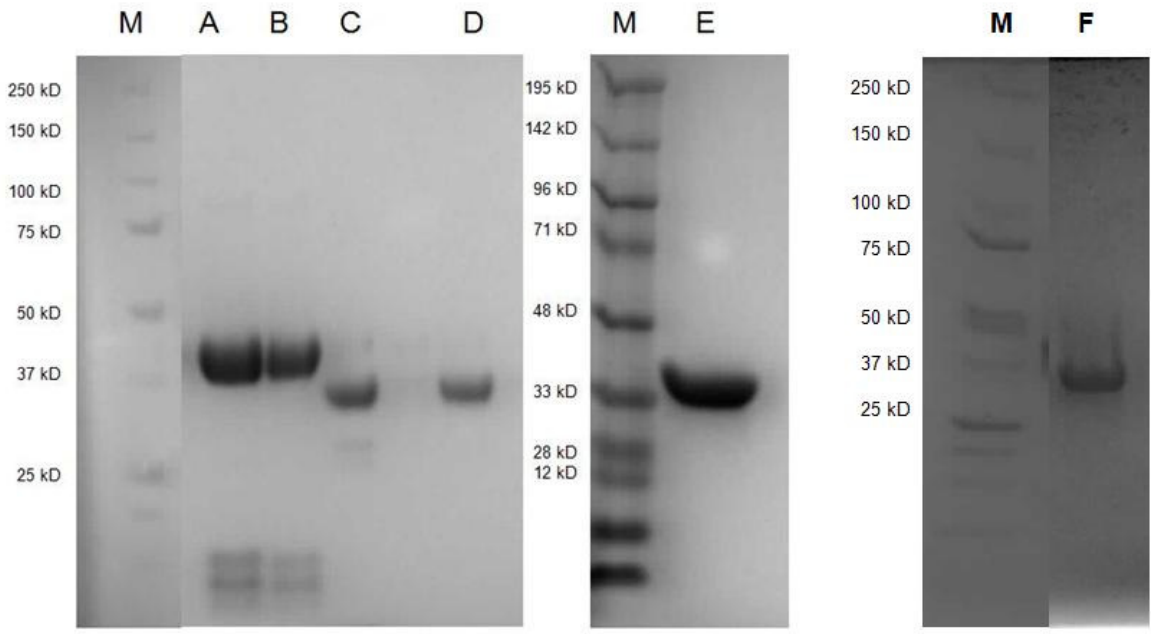

Figure 3-6. 10% Acrylamide SDS-PAGE Analyses of LCMT1$_{7-334}$ and LCMT1$_{SD20-334}$ Purification. Soluble LCMT1$_{7-334}$ and LCMT1$_{SD20-334}$ protein could be obtained after large scale protein purification.

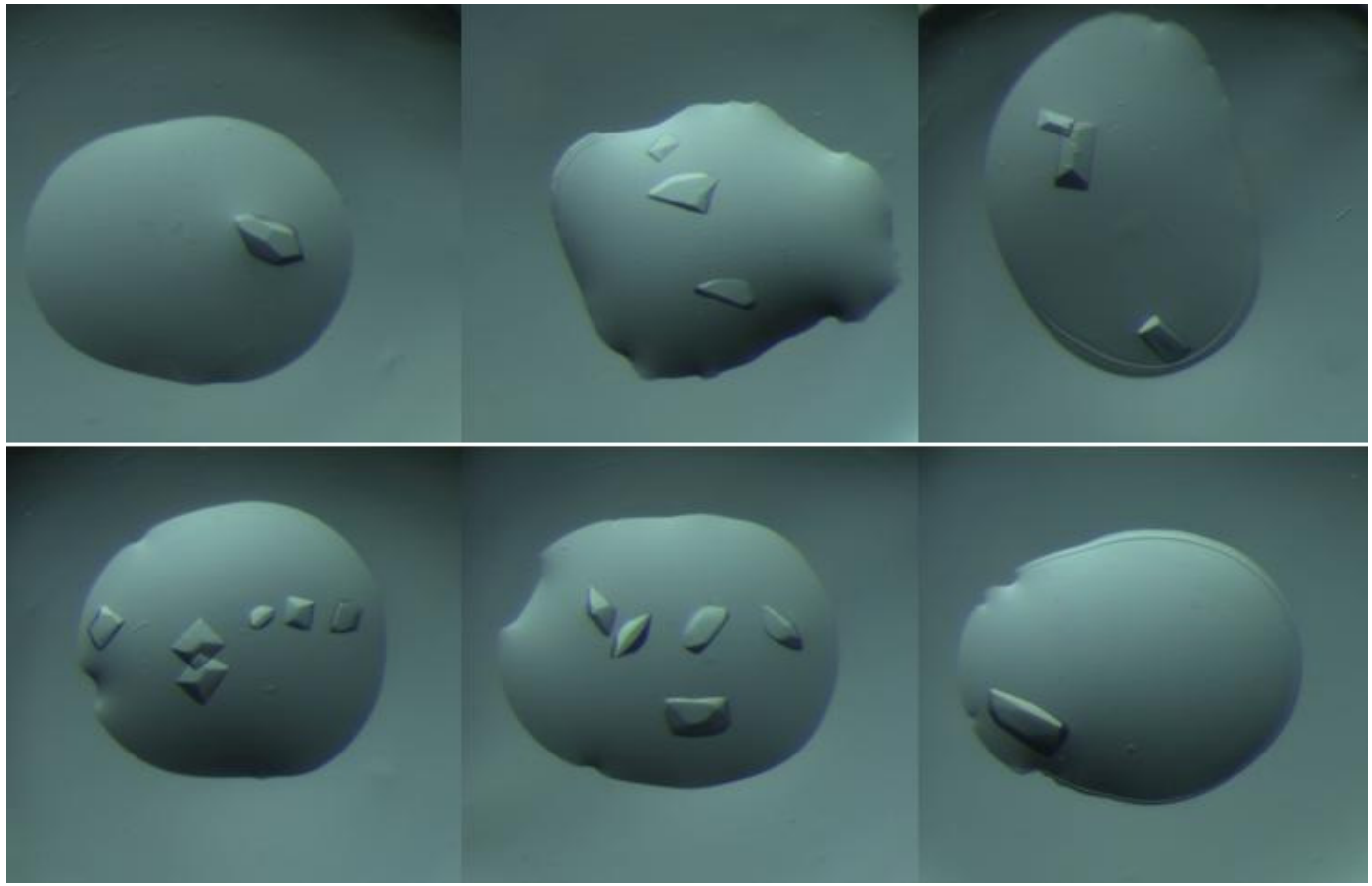

Figure 3-7. The Protein Crystals of LCMT1$_{SD20-334}$. In the initial screen of seven hundred crystallization conditions with the LCMT1$_{SD20-334}$ protein about hundred conditions produced crystals. The successful crystallization conditions contained a range of different precipitants including PEG 3350, PEG 5000, PEG 8000, ammonium sulfate, or Jeffamine ED-2001.

3.2 Protein Phosphatase Methylesterase 1

3.2.1 Gene Annotation and Construct Design

The protein construct deign of PME1 was carried out for two purposes, to generate the protein suitable for X-ray crystallography and to generate the protein for thermodynamic studies. To target the suitable domain or segment for protein crystallization, several bioinformatic websites or softwares were used to assist in gene construct design. According to 3D-PSSM fold recognition and Pfam domain prediction server [219,220], PME1 contains an esterase domain (residue position from 47 - 238) thought to catalyze hydrolysis of the carboxylmethylester of Leu309 from PP2A. With reference to protein sequence alignment by ClustalW [257], PME1 shares a consensus sequence IMLIGHSMGG with lysophospholipase [(I/V/R/F)X(L/V)(L/I/Y/F/A)GHSXGG] containing Ser-Asp(Glu)-His triad (Fig 3-8a). The secondary structure of PME1 was also predicted using PSIPRED secondary structure prediction protocol (*BCB, UCL*) [228,229] to find the suitable region of PME1 for constructs design (Fig 3-8b). Based on this prediction, there is a large flexible region in front of the residue Asp55 which I postulated may interfere with protein solubility or crystallization. For the protein constructs design, the residues Glu51, Met53, Val56, Asp65, and Ser88 were chosen as alternative N-termini, whereas the residues His370, Val382 and Cys386 were selected as alternative C-termini.

To clarify the interaction between PP2A and PME1 via thermodynamic studies,

$PME1_{39-376}$, the same construct of PME1 used by a group in Princeton University, was also made to compare with the full length PME1 in biophysical analysis [221]. In addition, to study the effect of protein engineering and the role of the specific polypeptide segment (residues 237-283) of PME1, additional two protein variants, $PME1\_GE_{239-283}$ and $PME1\_ET_{239-283}$, were generated and purified.

3.2.2 Molecular Cloning and Protein Expression

The PCR reactions were described in section 2.2.5.1. All PCR products were digested and cloned into pET30aTEV vector except $PME1\_GE_{239-283}$ and $PME1\_ET_{239-283}$ which were cloned into pGEX4T2 and pET442b vector respectively. The purification of DNA from agarose gel, ligation of plasmid and insertion, and transformation were all referred to in sections 2.2.4.3, 2.2.5.2, and 2.2.5.3.

100 ml of LB mediums were also prepared for each PME1 construct and grown to an optical density (OD_{600nm}) of 0.6. All samples were sonicated and subjected to SDS-PAGE analysis to confirm protein expression as described in section 2.2.6. Judged by SDS-PAGE analysis, small scale expression tests of each PME1 construct reveal that $PME1_{24-382}$ in *E. coli* Rosetta (DE3) pLysS, $PME1_{26-382}$ in *E. coli* Rosetta (DE3) pLysS, $PME1_{39-376}$ in *E. coli* BL21 (DE3) pLysS, $PME1\_ET_{239-283}$ in *E. coli* BL21 (DE3) pLysS, $PME1\_GE_{239-283}$ in *E. coli* BL21 (DE3) pLysS and the full length PME1 in *E. coli* BL21 (DE3) could express soluble protein at 30 ^{o}C.

(a)

```
Human PME1                      VEAMYGDLPPPIMLIGHSMGGAIAVHTASSNLVPSLLGLCMIDVVEGTAMDALNSMQNFLRGRPKTFKS
Mouse PME1                      VEAMYGDLPPPVMLIGHSMGGAIAVHTAAANLVPSLLGLCMIDVVEGTAMDALNSMQNFLRGRPKTFKS
carboxylic ester hydrolase      AreMGWEELPDLVLVGHSLGGAVITDVAKKeLGNKVLAYAVLDVVEGSAMDALQSMEKYLSTRPSRFPS
putative lipase                 LDSLHIE---KASLIGHSMGGKVAMQVAKQA-PTRVERLIVADMAPVAYPHA---------RHQNVFAG
putative esterase/lipase        LEHL---NLTSVVVIGHSMGGKVAMKLADIAA-EKVRQLVVLDMSPVAYSQ---------RRHDNVFAG

Human PME1                      LENAIEWSVKSGQIRNLESARVSMVGQVKQCEGITSPXXXXXXXXXXXXXXXXXXXXXXXXXXKRKKEDD
Mouse PME1                      LENAIEWSVKSGQIRNLESARVSMVGQVKQCEGITSPXXXXXXXXXXXXXXXXXXXXXXXXXXVNKRKKEDD
carboxylic ester hydrolase      LTSGVEWHTRSRTIRNRASARVSVPSLLYKEETPS-------------------------------
putative lipase                 LNATLAKM-----PKSRNEAETLLAEHIE-----------------------------IPGVRQFLLK
putative esterase/lipase        LEAVL-----VQKPTSRSEVMAILAQHIEQE-----------------------------GVRQFLGK

Human PME1                      METKKDHPYTWRIELAKTEKYWDGWFRGLSNLFLSCPIPKLLLLAGVDRLDKDLTIGQMQGKFQMQVLP
Mouse PME1                      METKKDHPYTWRIELAKTEKYWDGWFRGLSNLFLSCPIPKLLLLAGVDRLDKDLTIGQMQGKFQMQVLP
carboxylic ester hydrolase      ---DPAKPWVWRTNLSATKPFWEDWFIGLSRKFLEARGGKLLLLAGTDRLDKELMIGQMQGKYQLQVLP
putative lipase                 SFAKDGVDWGWRFNVAALEHSYAN-IMGWPDSQSRFDGPTLFIKGGESDYMLpeTVMAQFPAAKARVIA
putative esterase/lipase        SLMSEQNVMTWRFNVAALKAHYAEIL--GWDIIAKCRIPTLFIKGADSDYlhQPMVQAQFSQAKAHVIA

Human PME1                      QCGHAVHEDAPDKVAEAVATFLIRHRFAEPIGGFQCVFPGC
Mouse PME1                      QCGHAVHEDAPDKVAEAVATFLIRHRFAEPIGGFQCVFPGC
carboxylic ester hydrolase      EAGHFIQEDMPAKTAQILVDFYKRN----------------
putative lipase                 GTGHWLHAEKPVLFNKLVVDFLS------------------
putative esterase/lipase        NTGHWLHAEKPAEVIRAIRKFID------------------
```

(b)

PME1

```
1   msaleksmhlgrlpsrpplpgsggsqsgakmrmgpgrkrdfspvpwsqyfesmedveven 60
    ----HHHH-------------------------------------------------SSSSS-

61  etgkdtfrvyksgsegpvllllhggghsalswavftaaiisrvqcrivaldlrshgetkv 120
    ----SSSSSS-------SSSSS------HHHHHHHHHHHHHH---SSSSS----------

121 knpedlsaetmakdvgnvveamygdlpppimlighsmggaiavhtassnlvpsllglcmi 180
    -------HHHHHHHHHHHHHHH--------SSSSSS-HHHHHHHHHHHH------SSSSSS

181 dvvegtamdalnsmqnflrgrpktfkslenaiewsvksgqirnlesarvsmvgqvkqceg 240
    -------------HHHHHHH----HHHHHHHHHHHHH------HHHH----HHHH-----

241 itspegsksivegiieeeeedeegsesiskrkkeddmetkkdhpytwrielaktekywdg 300
    -----------HHHH-------HHHHHHHH------HHHHH---------HHHHHHHHHH

301 wfrglsnlflscpipkllllagvdrldkdltigqmqgkfqmqvlpqcghavhedapdkva 360
    HH-------------SSSSS--------HHHHHHH----SSSSS-------HHHHHHHHH

361 eavatflirhrfaepiggfqcvfpgc 386
    HHHHHHHHH-----------------
```

(PSIPRED)

Figure 3-8. Gene Annotation of PME1. (a) Sequence alignment of PME1 and several lipases was produced by 3D-PSSM fold recognition server [219]. PME1 shares a Ser-Asp(Glu)-His triad (Ser156, His349, and Asp181) with lipases and was classed as a serine hydrolase. (b) According to the domain (yellow region) and secondary structure prediction of PME1 by simple modular architecture research tool and psipred (*BCB, UCL*) [228;229], residues in red and residues in green are chosen as the alternative N and C termini of protein constructs.

3.2.3 Purification of PME1 for Protein Crystallization

3.2.3.1 $PME1_{24-382}$ & $PME1_{26-382}$

Following large-scale protein purification protocol as described in section 2.5.1, 2 mg of purified protein was obtained from 1 L cells (Figure 3-9a). In order to identify the optimal buffer condition for the crystallization of $PME1_{24-382}$, thermoflour method was utilized using a 96-well PCR plate (*BioRad*) with 52 different test buffers at the range of temperatures from 20 ^{o}C to 95 ^{o}C. The profile shows that $PME1_{24-382}$ is more stable at a high pH (>7.5) and in the presence of sodium phosphate (Figure 3-9b).

Different concentrations of $PME1_{24-382}$ and $PME1_{26-382}$ proteins (5, 10, 15, 20 mg/ml) were used to set up crystallization trails at different temperature (15 or 20 ℃) using hanging drop and sitting drop methods. Although different commercial crystallization screening kits and additive screening kits were used to test these truncated proteins, no crystal was observed. In addition, co-crystallization of PME1 with okadaic acid was attempted but no crystals were obtained from these experiments.

(a)

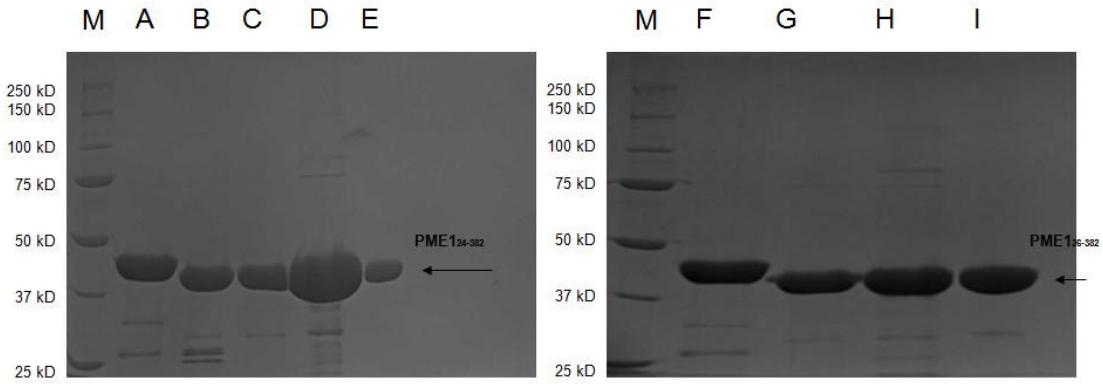

A : PME1 24-382, after Ni–Sepharose 6 beads purification.
B : PME1 24-382, before removing TEV protease.
C : PME1 24-382, after removing TEV protease.
D : PME1 24-382, after concentration.
E : PME1 24-382, after gel filtration.

F: PME1 26-382, after Ni–Sepharose 6 beads purification.
G: PME1 26-382, after removing TEV protease.
H: PME1 26-382, after concentration.
I: PME1 26-382, after gel filtration.

(b)

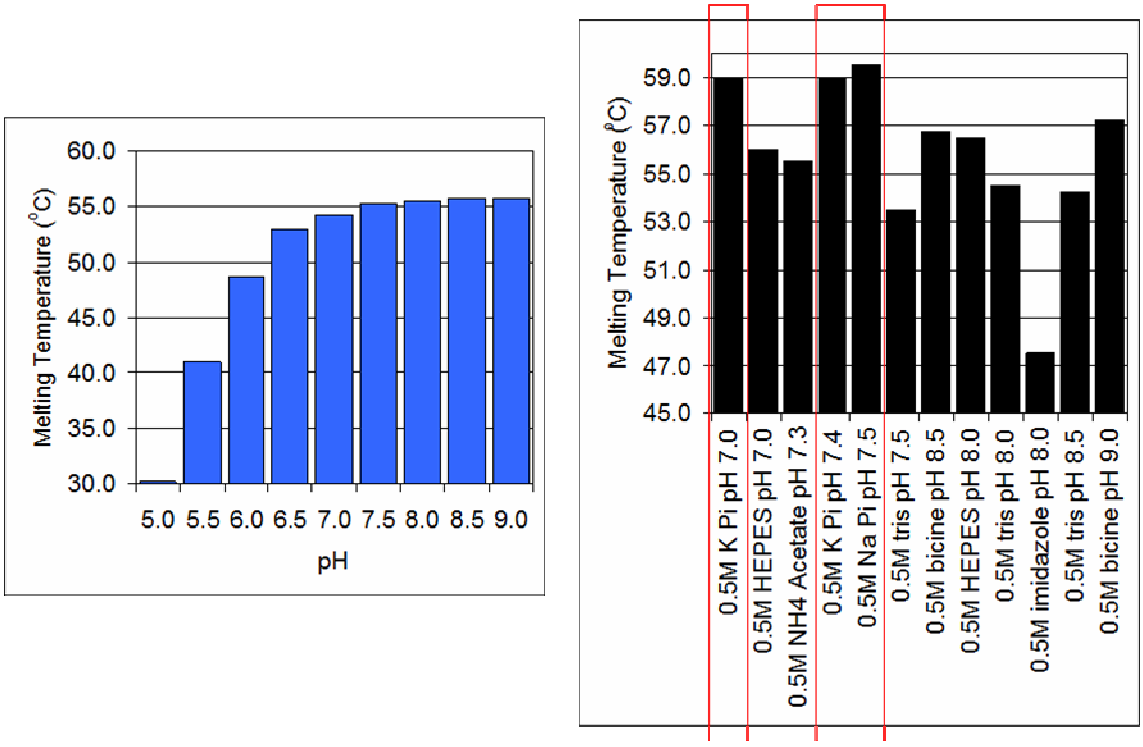

Figure 3-9. Purification and Thermoflour Analysis of PME1$_{24-382}$ and PME1$_{26-382}$. (a) The 10% SDS-PAGE analysis of the PME1$_{24-382}$ and PME1$_{26-382}$ stained by Coomassie Blue. The arrow denotes the recombinant PME1$_{24-382}$ and PME1$_{26-382}$ protein after the large scale purification. (b) Thermofluor analysis of buffer conditions. PME1$_{24-382}$ is more stable at higher pH and in the presence of sodium phosphate.

3.2.3.2 $PME1_{1\text{-}386}$

2 mg of protein was obtained from 1 L cells after the schedule of purification as described in section 2.5.1 (Figure 3-5). Purified protein was concentrated to 20 mg/ml and subjected to a series of sparse matrix crystallisation screens using TTP LabTech's mosquito. However, no hits were obtained for the full length PME1.

3.2.4 Purification of PME1 for Thermodynamic Studies

3.2.4.1 $PME1_{39\text{-}376}$

2.5 mg of protein could be harvested from 1 L cells after large scale purification as described in section 2.5.1 (Figure 3-10a).

3.2.4.2 $PME1\_ET_{239\text{-}283}$ & $PME1\_GE_{239\text{-}283}$

For the $PME1\_GE_{239\text{-}283}$ protein (31.6 kDa) with glutathione-s-transferase tag (GST tag), the Glutathione Sepharose™ 4 Fast Flow beads (*GE Healthcare*) column was used for the initial purification of $PME1\_GE_{239\text{-}283}$. To improve the protein solubility and stability, the GST tag (27.7 kDa) was retained on the protein. 2.5 mg of PME_GE_{239} protein was purified from 1 L of *E. coli* cell cultures (Figure 3-10b). The schedule of purification was described in section 2.5.2.1.

It was previously reported that NusA protein [258], 65.4 kDa, is superior in improving protein solubility compared to other protein tags, such as maltose binding protein (MBP) or glutathione-s-transferase (GST), used to generate fusion proteins. However, there is no commercial resin for NusA tag fusion protein purification. Therefore, NusA tag was linked six histidine tag at the N-terminus in order to facilitate protein purification. Ni Sepharose 6 beads were therefore utilized for purification of PME1_$ET_{239-283}$, (64.7 kDa). After further purification as described in section 2.5.2.2, 3 mg of PME1_$ET_{239-283}$ protein was purified from 1 L of cell cultures (Figure 3-10c).

Calibration of the size exclusion chromatography column (Hi Load 16/60 Superdex 200 Prep Grade, *GE Healthcare*) using both low and high molecular weight standards (LMW and HMW Calibration Kit *GE Healthcare*) (Figure 3-11a), confirmed that native glutathione-s-transferase and NusA protein form dimer and tetramer molecule respectively. However, both PME1 fusion proteins described here, PME1_$GE_{239-283}$ (GST tag) and PME1_$ET_{239-283}$ (NusA tag), were tetrameric in solution (Figure 3-11b) suggesting that the specific PME1 protein segment favours oligomerisation.

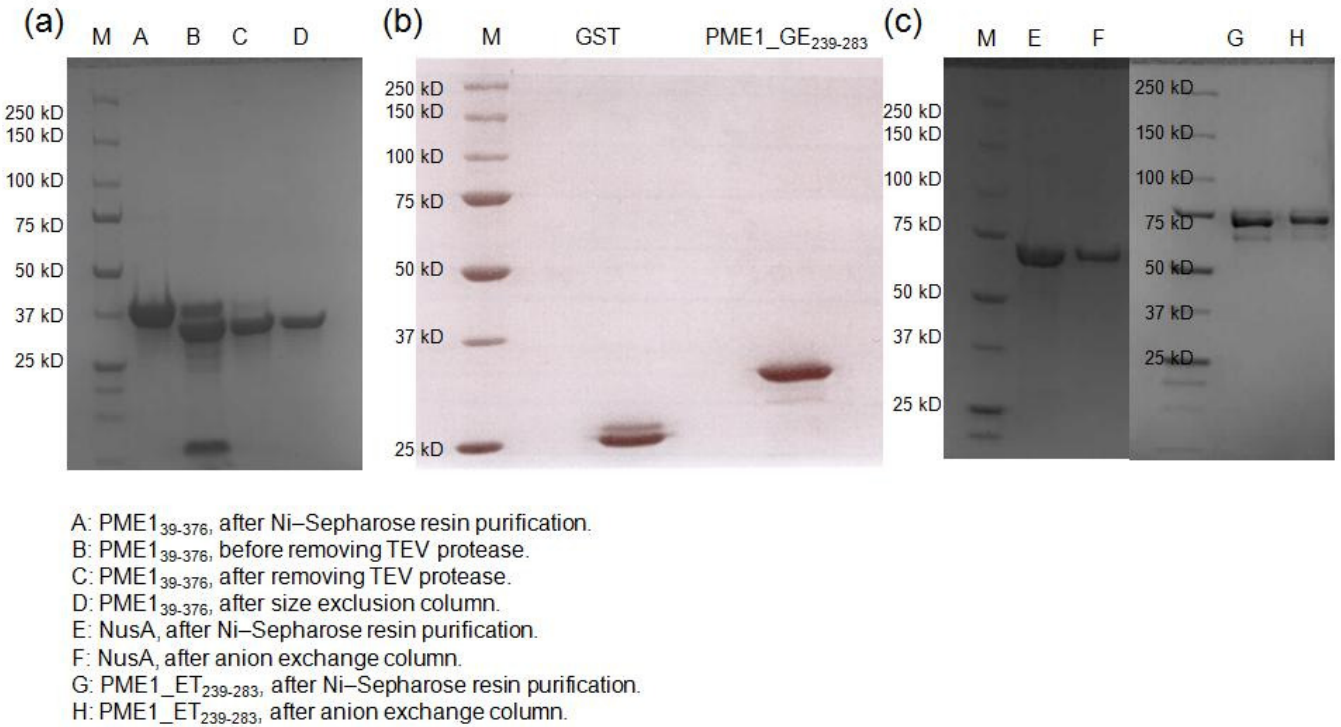

Figure 3-10. 10% Acrylamide SDS-PAGE Analyses of the Purification of PME1$_{39-376}$, PME1_GE$_{239-283}$ and PME1_ET$_{239-376}$. (a) The arrow denotes the recombinant PME1$_{39-376}$ after large scale purification including Ni-Sepharose 6, removal of the histidine tag, and size exclusion chromatography. (b) GST tag and PME1_GE$_{239-283}$ were both purified using Glutathione Sepharose™ 4 Fast Flow beads. (c) NusA and PME1_ET$_{239-376}$, containing six histidine tag, were purified using Ni^{2+} beads, anion exchange and size exclusion chromatography.

(a)

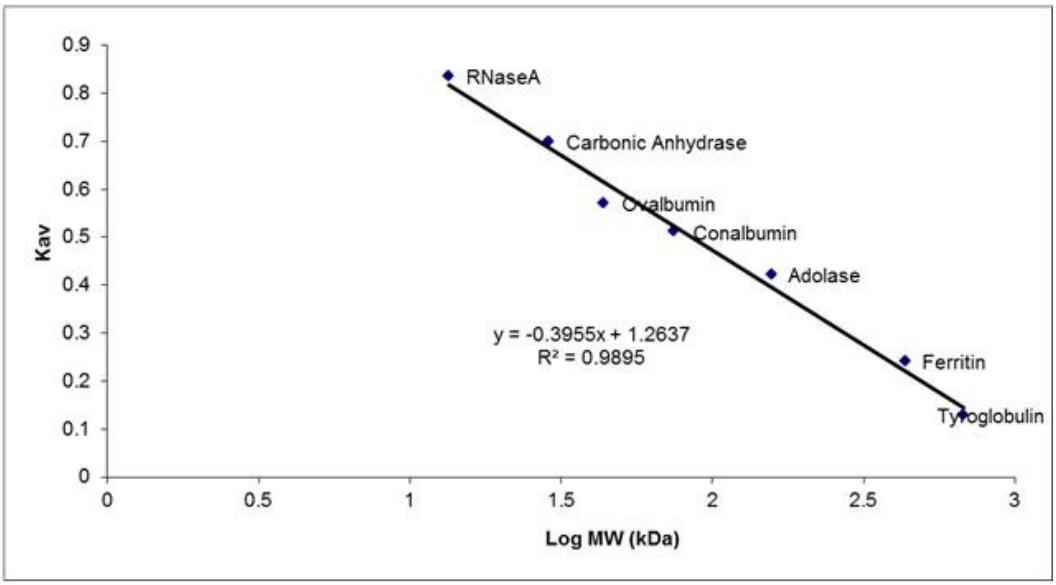

(b)

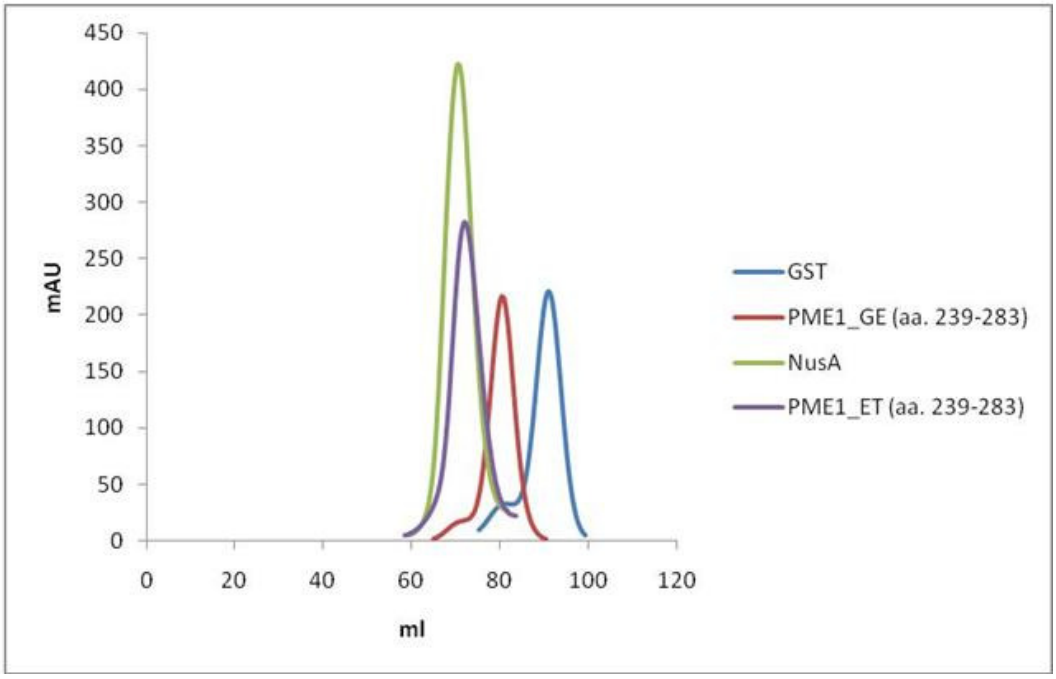

Figure 3-11. Size Exclusion Chromatography Analysis of GST, NusA, PME1_GE$_{239-283}$ and PME1_ET$_{239-283}$. (a) Multiple proteins from LMW and HMW calibration kits (GE Healthcare) were applied to Hi Load 16/60 Superdex 200 Prep Grade column (*GE Healthcare*). The K_{av} value (V_e-V_o/V_t-V_o, V_o= void volume, V_t = total column volume, V_e = elution volume) and log molecular weight values were calculated for calibration curve. (b) Based on the calibration curve, GST (27 kDa) and PME1_GE$_{239-283}$ (31.6 kDa) proteins were eluted at 55 kDa and 126 kDa region respectively, whereas NusA (65 kDa) and PME1_ET$_{239-283}$ (64.7 kDa) were both eluted at approximately 260 kDa region.

3.3 Initial Analysis of PME1 and LCMT1 Variants

3.3.1 Analytical Size Exclusion Chromatography

In addition to $LCMT1_{61-334}$ protein discussed in section 3.1.3, PME1 and LCMT1 variants, including $LCMT1_{20-334}$ (36.7 kDa), $LCMT1_{7-334}$ (35.2 kDa), $LCMT1_{SD20-334}$ (33.8 kDa), $PME1_{24-382}$ (39.7 kDa) and $PME1_{26-382}$ (39.6 kDa), were all analyzed using high resolution size exclusion column, Superdex 200 10/300GL (separation range: 10 - 600 kDa) (*GE Healthcare*) prior to crystallization trials. Calibration of this column was carried out using the LMW Calibration Kit (*GE Healthcare*) (Figure 3-12a).

Based on the calibration curve and trend equation, $LCMT1_{20-334}$, $LCMT1_{7-334}$, $LCMT1_{SD20-334}$, $PME1_{24-382}$ and $PME1_{26-382}$ were eluted in region of 30 - 44 kDa, thus demonstrated a monomeric form of the proteins (Figure 3-12b).

(a)

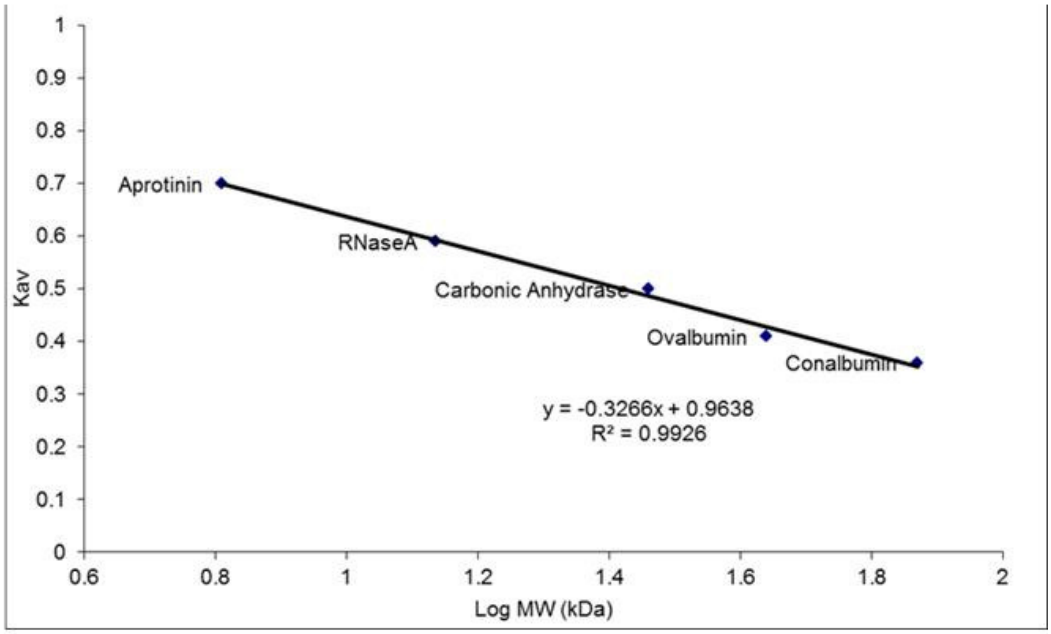

(b)

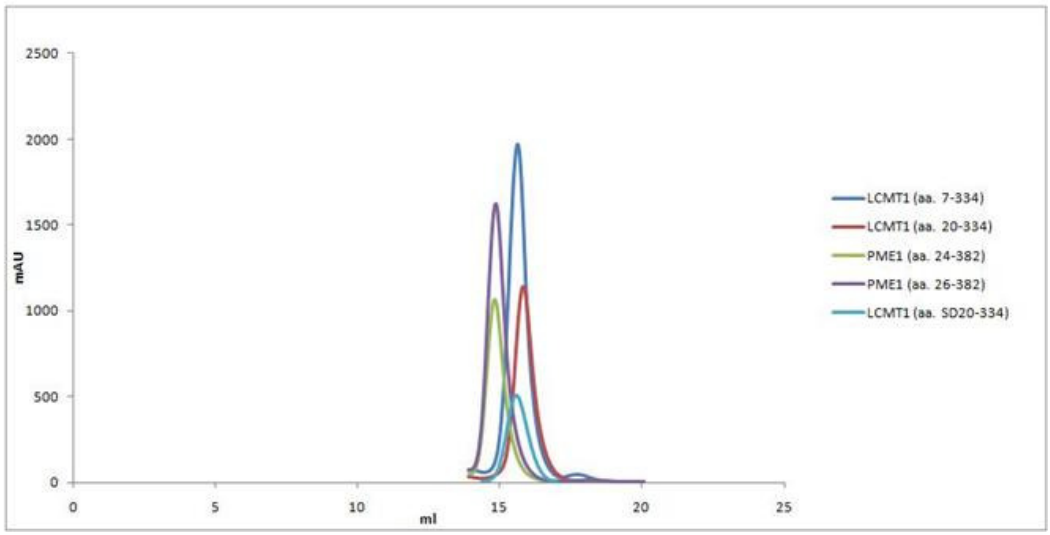

Figure 3-12. Analytic Superdex 200 10/300 GL Column Analysis of LCMT1 and PME1 Variants. (a) The column was calibrated with LMW Calibration Kit (*GE Healthcare*). To obtain the trend equation, the K_{av} value (V_e-V_o/V_t-V_o, V_o= void volume, V_t = total column volume, V_e = elution volume) and log molecular weights were calculated and the calibration curve generated. (b) PME1 and LCMT1 variants were eluted at region 30 - 44 kDa were the monomeric forms of the proteins would be expected to elute.

3.3.2 Circular Dichroism Spectroscopy Analysis

In order to ensure that PME1 and LCMT1 variants for setting crystal tray are well folded, $LCMT1_{20\text{-}334}$ (36.7 kDa), $LCMT1_{7\text{-}334}$ (35.2 kDa), $LCMT1_{SD20\text{-}334}$ (33.8 kDa), $LCMT1_{61\text{-}334}$ (31.7 kDa), and $PME1_{24\text{-}382}$ (39.7 kDa) were analyzed using circular dichroism (CD) spectroscopy. All data were interpreted through CDtool program (*Birkbeck College*).

Based on the curves of CD wavelength scans, all LCMT1 and PME1 variants appear to be well folded. Two negative peaks (208 and 222 nm) and one positive peak (195 nm) demonstrate that LCMT1 and PME1 variants are mixture of α-helix and β-sheet (Figure 3-13).

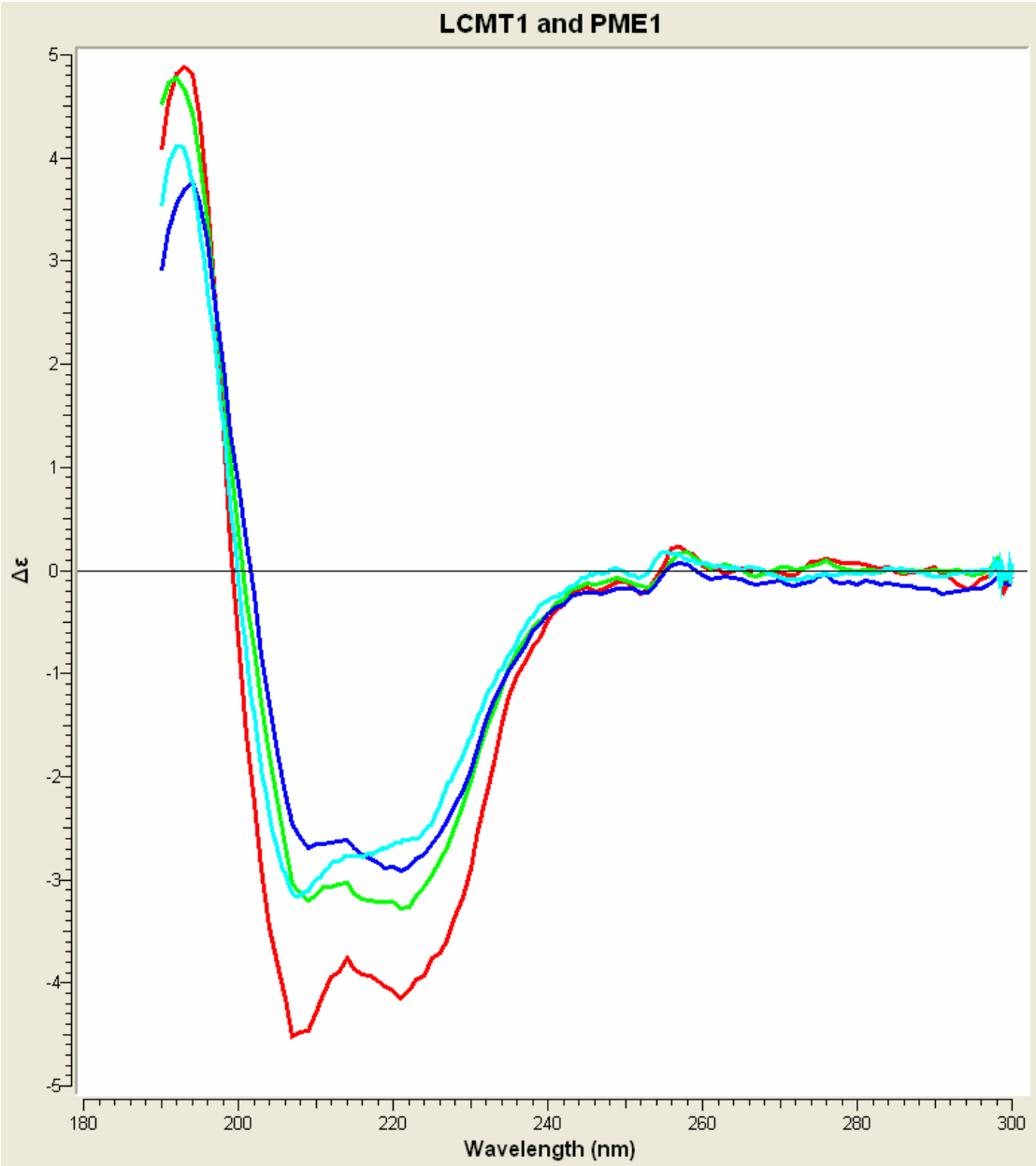

Figure 3-13. Circular Dichroism Analysis of PME1 and LCMT1 Variants. 1 mg/ml of $LCMT1_{20\text{-}334}$ (green), $LCMT1_{7\text{-}334}$ (blue), $LCMT1_{61\text{-}334}$ (cyan) and $PME1_{24\text{-}382}$ (red) were analyzed via CD spectrum wavelength scan. All LCMT1 and PME1 variants contain a mixture of α-helices and β-sheets. Truncation of residues 233-258 ($LCMT1_{7\text{-}334}$) or the N-terminal 20 residues ($LCMT1_{20\text{-}334}$) in LCMT1 may not influence the core structure of LCMT1, as the spectra shared a similar signal curve; however, truncation of the N-terminal 60 residues of LCMT1 may affect the folding of the core structure.

3.4 Summary

Although the full-length human LCMT1 can be expressed in and purified from *E. coli*, no crystals were obtained of this form of the protein and further gene constructs for LCMT1 were designed. Amino acid sequence alignment with *S. cerevisiae* PPM1 using ClustalW [257] together with a comparison of human LCMT1 secondary structure prediction obtained by PSIPRED [228,229] and the secondary structure from the crystal structure of yeast PPM1 [223] were suggesting secondary structure conservation starting from the residue Asp 20 of LCMT1. Therefore, several residues preceding the first predicted α helix of LCMT1 including Arg6, Glu7, Ser9, Thr16 and Asp20 were chosen as a potential starting N-terminal residue of the protein products while the residues following the last predicted β strand of LCMT1 (Thr321 and Aspr329) were selected as alternative C-termini of the protein products to be generated for crystallization studies. Table 3-2 gives the summary of the protein products generated and their solubility properties; superscript denotes starting and ending residue in the full-length LCMT1 sequence. Truncation at the residue Thr321 at the C-terminus of LCMT1 rendered the resulting proteins insoluble. Yields of soluble proteins generated from other gene constructs were relatively low and their levels were enhanced through co-expression with chaperonin molecules (GroES/GroEL) [234]. $LCMT1_{20\text{-}334}$ was the only protein product that was crystalized in complex with the co-factor, *S*-adenosylmethionine from crystallization conditions of 0.1 M sodium citrate (pH5.6), 2% PEG400 and 1.8 M ammonium sulfate at 22 ^{o}C.

Limited proteolysis method was also utilized in order to detect any flexible segments and internal loops of human LCMT1 and to potentially identify stable protein domain. SDS-PAGE analysis showed that limited proteolysis of LCMT1 resulted in a single stable polypeptide band with migration properties corresponding to the molecular weight of approximately 27 kDa. N-terminal protein sequencing, mass spectrometry analysis and the prediction of trypsin digestion sites of LCMT1 suggested that the C-terminal residue of the main proteolytic product could be Arg236. Arg236 of human LCMT1 corresponds to the residue Arg242 in the previously reported flexible region of the *S. cerevisiae* PPM1 structure.

Three LCMT1 constructs were designed: $LCMT1_{7\text{-}334}$ containing residues 7-232, a small linker EG, and residues 259-334; $LCMT1_{7\text{-}232}$ construct including residues 7-232 only; and the $LCMT1_{SD20\text{-}334}$ construct including residues 20-232, a small linker EG, and residues 259-334. Similar strategy of excision of the flexible region has been previously employed in generating a suitable protein for crystallization of human PP2A methylesterase [221]. $LCMT1_{7\text{-}232}$ did not yield soluble protein. In contrast, both protein products that lacked a putative flexible region were soluble and the levels of soluble protein expression were significantly higher than previously obtained such that we were able to purify about 8 mg of protein per liter of cells in the absence of any chaperonin molecules. In the initial screen of seven hundred crystallization conditions with the $LCMT1_{SD20\text{-}334}$ protein more than hundred conditions produced crystals. The successful crystallization conditions contained a range of different precipitants including PEG 3350, PEG 5000, PEG 8000, ammonium

sulfate, or Jeffamine ED-2001.

For protein crystallization, PME1 constructs were also designed based on the secondary structure prediction. PME1 variants ($PME1_{24-382}$ and $PME1_{26-382}$) could be successfully expressed and purified. Thermofluor analysis of various buffer conditions identified alkaline pH and sodium phosphate salt as favouring stability of $PME1_{24-382}$ protein, however this finding id not help in identifying crystallization conditions for human PME1.

In addition to constructs for protein crystallization, three PME1 constructs, $PME1_{39-376}$, $PME1\_GE_{239-283}$, and $PME1\_ET_{239-283}$, were also designed for isothermal titration calorimetry analysis discussed in chapter five. The residues 239 to 283 of PME1, containing a stretch of acidic amino acids, that were excised from the protein used to generate reported crystals of PME1 [221] were generated as NusA or GST C-terminal fusion proteins. All protein constructs were successfully purified.

Construct	Amino Acid Sequence	Solubility	Crystallization
$LCMT1_{1-334}$	N 1 → 334 C	+	-
$LCMT1_{6-334}$	N 6 → 334 C	+	-
$LCMT1_{1-329}$	N 1 → 329 C	+	-
$LCMT1_{6-329}$	N 6 → 329 C	+	-
$LCMT1_{24-329}$	N 24 → 329 C	+	-
$LCMT1_{26-329}$	N 26 → 329 C	-	-
$LCMT1_{7-321}$	N 7 → 321 C	-	-
$LCMT1_{9-321}$	N 9 → 321 C	-	-
$LCMT1_{20-321}$	N 20 → 321 C	-	-
$LCMT1_{20-334}$	N 20 → 334 C	+	+
$LCMT1_{61-334}$	N 61 → 334 C	$+_a$	-
$LCMT1_{7-232}$	N 7 → 232 C	-	-
$LCMT1_{7-334}$	N 7 → ^{232}EG^{259} → 334 C	+	-
$LCMT1_{SD20-334}$	N 20 → ^{232}EG^{259} → 334 C	+	+

$+_a$ = The protein forms soluble aggregation

Table 3-2. LCMT1 Constructs.

Chapter Four

Heterologous Expression of $PP2A_A$ and $PP2A_C$ in Insect Cell

Following the publication of the crystal structure of $PP2A_D$ complex with okadaic acid in 2006 [18] the crystal structures of some other proteins that form complexes with PP2A were reported in 2007, such as $PP2A_D$ complex with B' subunit [17;19] or B subunit [24], and $PP2A_A$ with SV40 small T antigen [217]. Previous studies also demonstrate that SV40 small T antigen could tightly associate with PP2A [216] and the interaction between PME1 and PP2A was also observed *in vivo* [63]. Therefore, it might be possible to obtain crystals of PME1-PP2A or LCMT1-PP2A complexes. In an attempt to co-crystallize PME1 or LCMT1 with $PP2A_A$ or $PP2A_C$ or $PP2A_D$, purified $PP2A_A$ and $PP2A_C$ proteins were needed..

It was previously reported that $PP2A_A$ could be expressed in *E. coli* cells [12;17], whereas $PP2A_C$ could only be obtained from insect cells using baculovirus expression system [17;19;259]. This chapter includes the results from cloning of full length $PP2A_A$ gene in the expression vector pET28a to obtain N-terminally his-tagged protein in *E. coli* cells and the cloning of the full length $PP2A_C$ gene in the baculovirus expression vectors pEastBacHTa (*Invitrogen*) and pBAC4x-1 (*Novagen*) for the use in insect cells. In addition, full length $PP2A_A$ and $PP2A_C$ genes were cloned together into pBAC4x-1 for co-expression in insect cells. This chapter also describes the results of the over-expression of cloned constructs, as well as purification and assembly of $PP2A_A$ and $PP2A_C$.

4.1 The Scaffolding Subunit of PP2A ($PP2A_A$)

4.1.1 Molecular Cloning, Expression and Purification of $PP2A_A$

Following PCR protocol as described in section 2.2.5.1 the PCR products were cloned into a pET28a expression plasmid as described in sections 2.2.5.2 and 2.2.5.3. The recombinant protein included an N-terminal six histidine tag to aid protein purification and a thrombin protease cleavage site for removal of the tags. After the confirmation of the sequencing result and the small scale protein expression test (see section 2.2.6.1), a large scale expression and purification of $PP2A_A$ were carried out as described in sections 2.2.6.4 and 2.5.3. Routinely, about 15 mg of $PP2A_A$ was purified from 6 L culture of *E. coli* BL21 (DE3) plysS cells.The N-terminal 6 histidine tag of was not removed, as protein digestion of $PP2A_A$ by thrombin protease was nonspecific. Further purification of $PP2A_A$ was achieved through anion exchange column (Q FF, *GE Healthcare*) and size exclusion chromatography (Superdex 200) as described in sections 2.5.3.2 and 2.5.3.3.

At this stage it was expected that protein will be sufficiently pure as previously published protocol was followed; however, some contaminating proteins were observed (Figure 4-1) on SDS-PAGE gels. Therefore, to obtain pure $PP2A_A$, the ammonium sulphate precipitation and a protein purification using hydrophobic interaction column were tested.

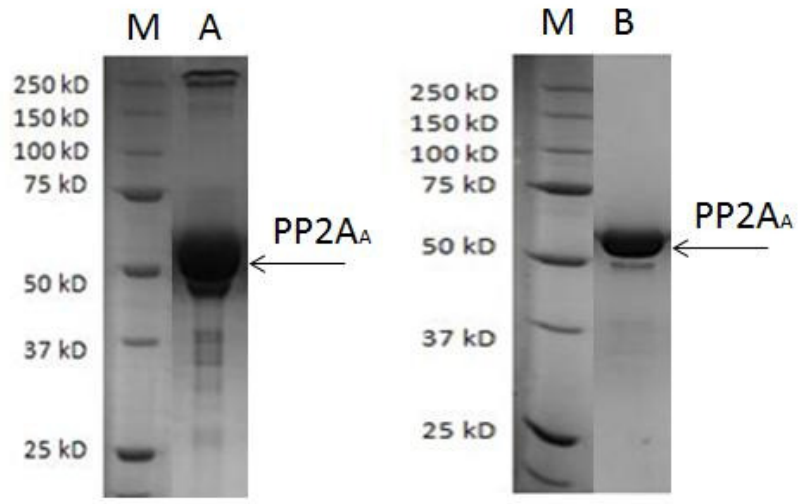

A: PP2AA, after Ni-Sepharose 6 and anion exchange chromatography purification
B: PP2AA, after Ni-Sepharose 6, anion exchange and size-exclusion chromatography purification

Figure 4-1. 10% Acrylamide SDS-PAGE Analyses of PP2A$_A$ Purification by Former Studies. PP2A$_A$ was applied to Ni Sepharose 6 (*GE Healthcare*), anion exchange column (Q FF, *GE Healthcare,* eluted on a linear gradient between 120 and 400 mM NaCl) (lane A) and finally size exclusion chromatography column (Hi Load 16/60 Superdex 200 Prep Grade, *GE Healthcare,* eluted at 65-70 kDa region) (lane B). Peak fractions were loaded onto a SDS-PAGE gel stained by Coomassie Blue.

Figure 4-2a shows the results of ammonium sulphate precipitation of $PP2A_A$ protein that was previously purified by Ni Sepharose 6 Fast Flow (*GE Healthcare*) and anion exchange chromatography. Protein fraction containing $PP2A_A$ was applied to 20% to 40 % ammonium sulphate solution and incubated at 4 ^{o}C for 15 minutes as described in section 2.5.3.4.

The result of the SDS-PAGE analysis suggested an enhancement in purity of the protein and therefore the ammonium sulphate precipitation step was included in the purification protocol. Finally, the protein was dialyzed in buffer, 25 mM Tris (pH 8.0), 50 mM NaCl and 2 mM BME for overnight at 4 ^{o}C. The total protein amount of $PP2A_A$ obtained after above purification was about 1 mg from 1 litre of cell culture (Figure 4-2b).

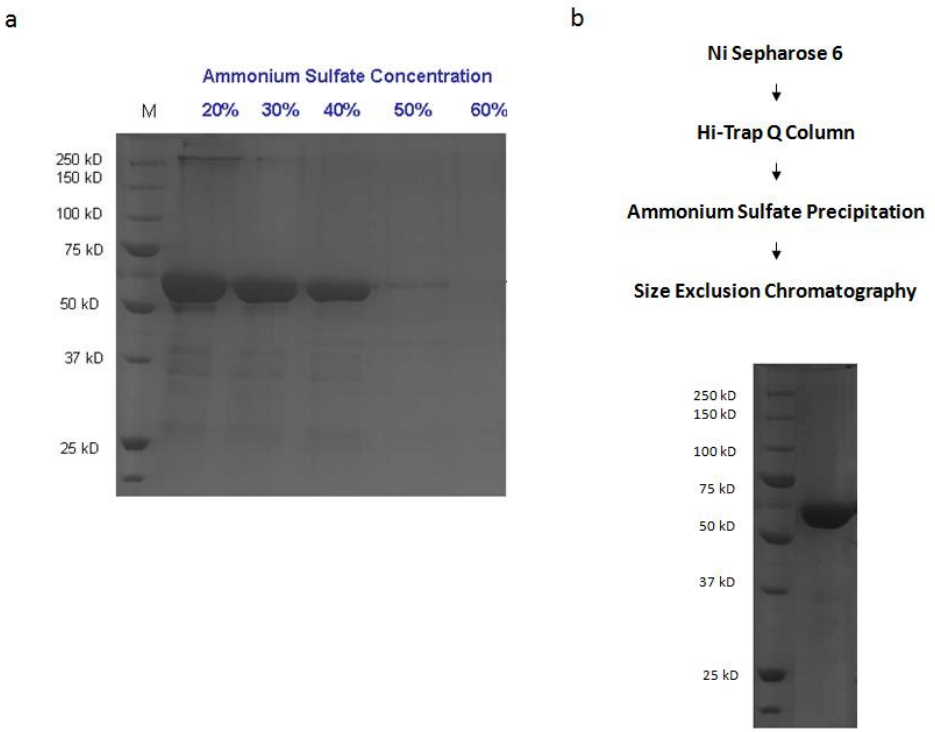

Figure 4-2. The Ammonium Sulphate Precipitation of $PP2A_A$. (a) The 10% acrylamide SDS-PAGE analysis visualized by Coomassie Blue staining showed that 40% ammonium sulphate solution was successful in removing contaminating proteins. (b) New $PP2A_A$ purification protocol and the 10% acrylamide SDS-PAGE analysis of the purified $PP2A_A$ after the final dialysis step.

4.2 The Catalytic Subunit of PP2A ($PP2A_C$)

4.2.1 Molecular Cloning and Viral Expression of $PP2A_C$

4.2.1.1 Bac-to-Bac Expression System (*Invitrogen*)

Following PCR reactions as described in section 2.2.5.1 desired PCR fragment was cloned into the pFastBacHTa plasmid (*Invitrogen*) such that expressed protein would contain an N-terminal six histidine tag and a TEV cleavage site as described in section 2.3.2.1. In additionspecific D88N mutation was introduced in the active site [235] using site-directed mutagenesis kit QuikChange (*Stratagene*). To obtain bacmids of this mutant, the plasmid was transformed to *E. coli* DH10Bac cells containing the bacmid with a mini-*att*Tn7 target site and the helper plasmid. The mini-Tn7 site of the pFastBacHTa donor plasmid could transpose to the mini-*att*Tn7 target site on the bacmid in the presence of transposition proteins produced by the helper plasmid. For further transfection, the bacmids were verified by PCR analysis and 1% agarose gel electrophoresis.

After amplification of virus, recombinant virus was quantified using FastPlax Titer Kit (*Novagen*) which can efficiently detect the GP64 envelope fusion protein of sf9 cells (*Novagen*) after 8-24 hours post-infection by virus. It was estimated that the concentration of viral stock was about 3×10^8 pfu/ml.

Although sf9 cells perform well in cell transfection and viral titer, the doubling time (72 hours) and protein production of sf9 cells are not as convenient as that of High Five cells (*Invitrogen*). The doubling time of High Five cells is usually 18 hours and the protein production of High Five cells are usually 5 to 10 fold higher than that of sf9 cells. Therefore, High Five cells were chosen as more suitable for protein expression.

For small scale expression test, High Five cells in EX-405 cell medium (*Sigma*) at a density of 2×10^6 cells/ml were infected with recombinant virus from the stock at multiplicity of infection (MOI) of 3 and 6 for 24, 48 and 72 hours. The result of this test suggested that the optimal infection was achieved with multiplicity of infection of 3 for 48 hours (Figure 4-3a).

4.2.1.2 BacMagic Transfection System (*Novagen*)

In BacMagic system, PCR was carried out using primers designed to introduce the restriction site BamHI (GGATCC), start codon (ATG), and un-cleavable 8 histdine tag at the 5' end of the PCR fragments and a SphI (GCATGC) restriction site and stop codon at the 3' end. The PCR reaction was described in section 2.2.5.1 and target sequence was observed and verified on a 1 % agarose gel stained with ethidium bromide. PP2Ac with D88N mutation was cloned into the pBAC4x-1 plasmid (*Novagen*) as described in section 2.3.3.1 [235]. For transfection, 100 ng of BacMagic DNA and 500 ng of recombinant

plasmid were co-transfected to *Spodoptera frugiperda* (Sf9) cells (*Novagen*). The BacMagic DNA is an AcNPV genome containing incomplete essential open reading frame (ORF) and a bacterial artificial chromosome (BAC) in place of the polyhedrin coding region. The target gene was cloned into the transfer vector containing parts of baculovirus DNA sequence and polyhedrin promoter. After homologous recombination of the transfer plasmid and BacMagic DNA in insect cells, the function of the virus ORF1629 was restored and the BAC was replaced by the target gene.

After amplification of virus, the FastPlax Titer Kit (*Novagen*) was used for efficient titer of viral inoculum. High Five cells (*Invitrogen*) was also used for small scale of expression test. It was found that the optimal condition were infection of a 50 ml culture at 2×10^6 cells/ml at MOI of 3 for 48 hours or at MOI of 7 for 36 hours (Figure 4-3b).

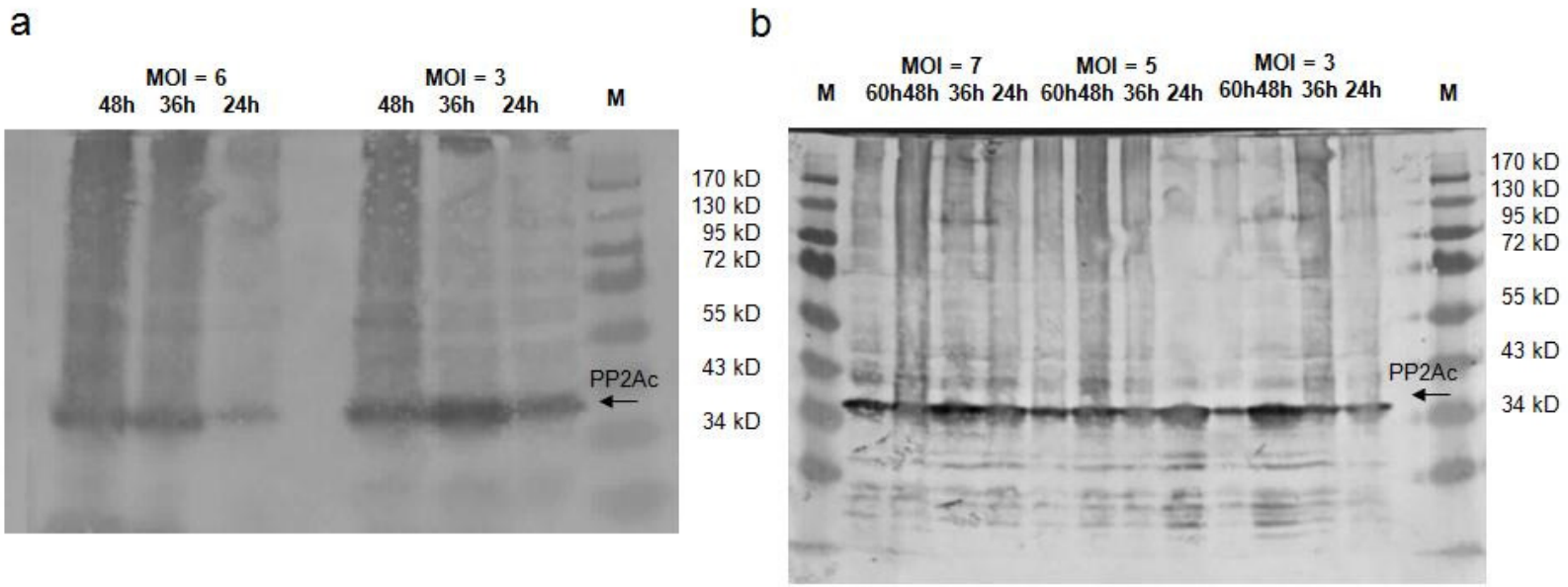

Figure 4-3. Transfection tests for PP2A C subunit. (a) After virus was successfully generated using bac-to-bac transfection system (*Invitrogen*), High Five insect cells were infected at varying MOI and time intervals. The western blot, using anti-His-tag-antibodies (*Clontech*), results showed that the optimal infection of cells was at MOI of 3 for 48 hours. (b) Sf9 cells were also transfected by using BacMagic transfect kit (*Novagen*). To find the ideal condition of infection, Sf9 insect cells were infected at varying MOI and time intervals. The western blot indicates that the optimal condition is MOI of 3 for 48 hours or at MOI of 7 for 36 hours.

4.2.2 Solublization of $PP2A_C$

The recombinant $PP2A_C$ proteins from pFastBacHTa expression construct contain cleavable N-terminal six histidine tag followed by un-cleavable eight histidine residues tag whereas proteins expressed from pBAC4x-1 construct only contain un-cleavable eight histidine residues tag at the N-terminus. The histidine tag binds to divalent cations immobilised on a metal chelation resin. The large scale purification of $PP2A_C$ from 1 litre insect cells using Ni-NTA (*Qiagen*) demonstrated a low production of soluble $PP2A_C$ which cannot be detected by Coomassie Blue staining in SDS-PAGE. However, a significant amount of $PP2A_C$ was observed in insoluble form (Figure 4-4); therefore, the solubility of $PP2A_C$ was considered to be a major problem for $PP2A_C$ purification. To solubilise $PP2A_C$, several detergents (Elugent detergent, Zwittergent detergent and MEGA-8) and non-detergents (EGTA, NDSB-211, Dodecanoylsucrose, Arginine, and Ethylene Glycol) were individually supplemented to the sonication buffer (20 mM Tris pH 8.0, 150 mM NaCl, 1 % Triton X-100 and 1 mM DTT) with the final concentration of detergent in buffer based on the critical micelle concentration (CMC). Each sample pellet from 10 ml cells was re-suspended in each testing buffer on ice. After incubation on ice for 20 minutes, each sample was spun and the supernatant and pellet was analyzed using electrophoresis. This analysis showed that most of detergents and non-detergents could be helpful to solubilise $PP2A_C$. While all of the additives appeared to have increased the solubility of the expressed protein, no additive was significantly superior and therefore, 5 mM EGTA was chosen to be included in further purification (Figure 4-5).

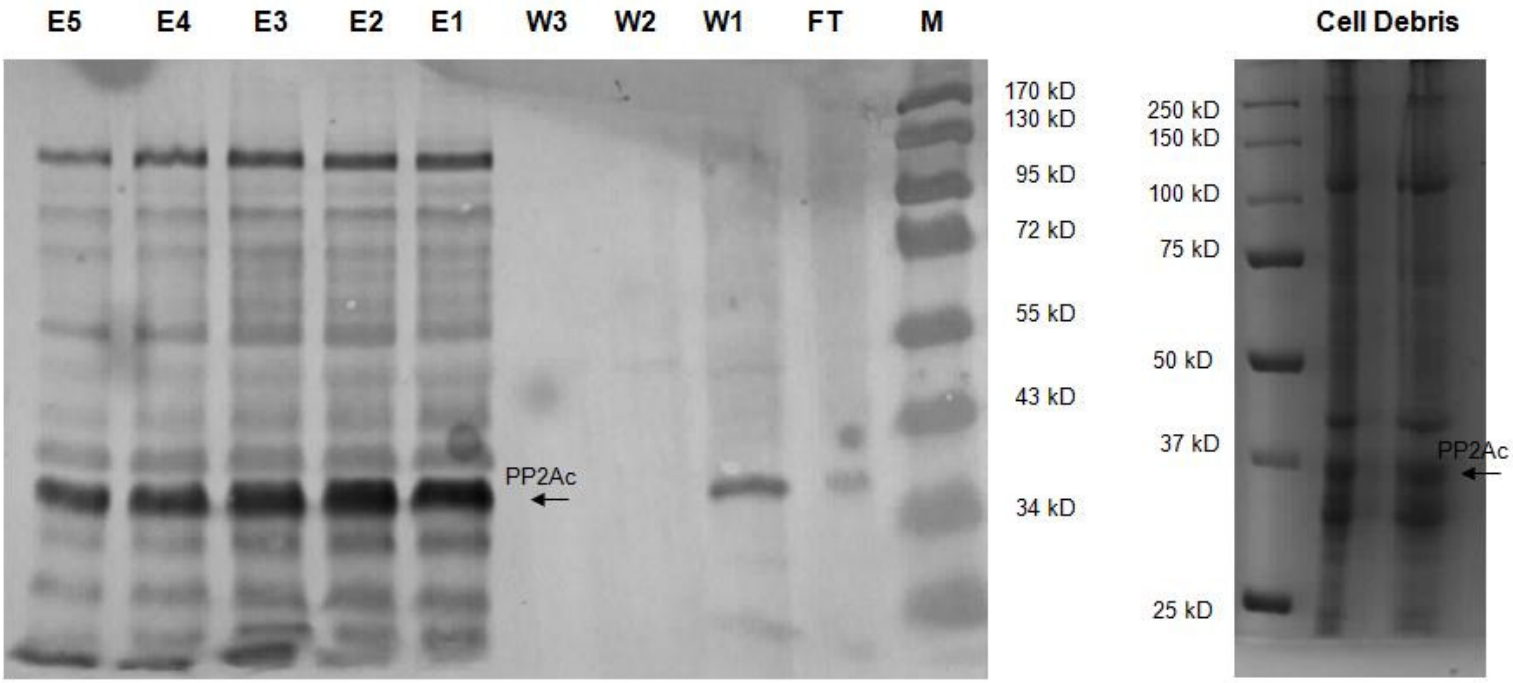

Figure 4-4. The Metal Affinity Purification of PP2A$_C$ from One Litre of Insect Cells. The sample from each step in Ni-NTA beads (*Qiagen*) purification was loaded onto 10 % acrylamide SDS-PAGE gel and further detected by the western blot method, using anti-His-tag-antibodies (*Clontech*). A low production of soluble PP2A$_C$ can only be observed (left picture) due to a majority of PP2A$_C$ protein associated with cell debris as shown by 10 % acrylamide SDS-PAGE analysis visualized by Coomassie Blue staining (right picture).

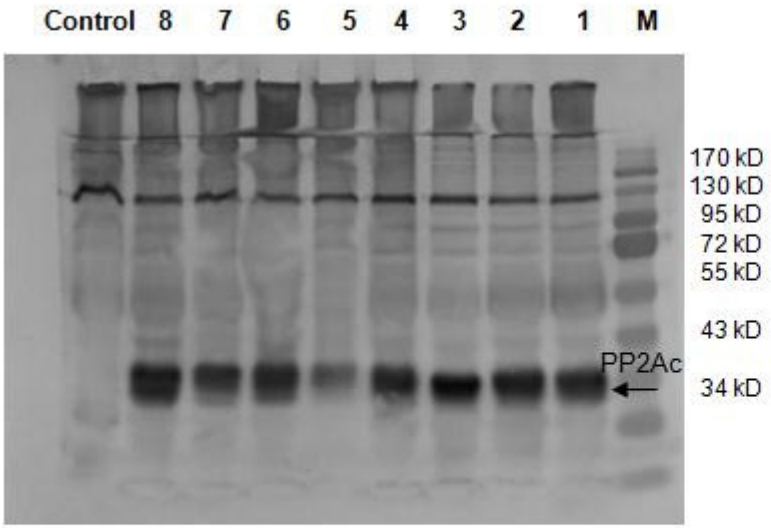

	Testing Buffer
1	20 mM Tris-HCl pH 8.0, 200 mM NaCl, 1% Triton X-100, 1 mM DTT and **5 mM EGTA**
2	20 mM Tris-HCl pH 8.0, 200 mM NaCl, 1% Triton X-100, 1 mM DTT and **200 mM NDSB-211**
3	20 mM Tris-HCl pH 8.0, 200 mM NaCl, 1% Triton X-100, 1 mM DTT and **10% Ethylene Glycol**
4	20 mM Tris-HCl pH 8.0, 200 mM NaCl, 1% Triton X-100, 1 mM DTT and **0.3 mM n-Dodecanoylsucrose**
5	20 mM Tris-HCl pH 8.0, 200 mM NaCl, 1% Triton X-100, 1 mM DTT and **4% Elugent Detergent (50% solution)**
6	20 mM Tris-HCl pH 8.0, 200 mM NaCl, 1% Triton X-100, 1 mM DTT and **30 mM Zwittergent 3-10 detergent**
7	20 mM Tris-HCl pH 8.0, 200 mM NaCl, 1% Triton X-100, 1 mM DTT and **50 mM MEGA-8**
8	20 mM Tris-HCl pH 8.0, 200 mM NaCl, 1% Triton X-100, 1 mM DTT and **200 mM Arginine**

Figure 4-5. Solubilisation of PP2A$_C$ subunit. Various detergents and non-detergents used to improve the solubility of PP2A$_C$ subunit analyzed by 10 % acrylamide SDS-PAGE. The gel was detected by western blot using anti-His-tag-antibodies (*Clontech*).

4.2.3 Purification of $PP2A_C$

4.2.3.1 Published Methods for $PP2A_C$ Purification

Various strategies were implemented in an attempt to purifiy $PP2A_C$; however, none of them was successful in obtaining purified $PP2A_C$. The methods used and the results that were obtained are summerised below:

1. $PP2A_C$ was initially purified using Ni-NTA beads (*Qiagen*) and then passed through ion exchange (DEAE and Q FF, *GE Healthcare*) and size exclusion chromatography (Hi Load 16/60 Superdex 200 Prep Grade) columns (Figure 4-6a). The SDS-PAGE analysis of the sample that was purified via this protocol clearly shows $PP2A_C$ is not sufficiently pure (1-3) [17;19].
2. $PP2A_C$ was also purified using Ni-NTA beads and followed by precipitation by increasing concentrations of ammonium sulphate, 20%, 30% and 40% (Figure 4-6b). The western blot indicates that most of $PP2A_C$ precipitates at 20% and 30% ammonium sulphate solution similarly to other contamination.
3. $PP2A_C$ subunit was first purified from the cell-lysate using Ni-NTA beads and the eluted fraction was the loaded on a hydrophobic interaction column (HIC) (*e.g.* Phenyl HP, GE Healthcare) (Figure 4-6c). In hydrophobic interaction chromatography, proteins are separated based on their different surface hydrophobic interactions with column resin that contains hydrophobic groups attached (*e.g.* phenyl-, octyl-, and butyl- groups). The surface hydrophobic characteristics of proteins are dominated by their amino acid side chains (*e.g.* Trp > ILE/Phe > Tyr > Leu > Val > Met).The

interaction between proteins and a HIC column is significantly influenced by the salt types and concentrations in running buffer. In contrast to ion exchange chromatography, a high salt concentration will enhance the interaction whereas low salt concentration will weaken the interaction. Amongst available hydrophobic interaction active groups, the strongest one is octyl- group followed by phenyl- group and then butyl- group. $PP2A_C$ was successfully purified using hydrophobic interaction column, HiTrap Phenyl HP; however, I was unable to repeat this result.

4. Cell lysate was applied to 55% ammonium sulphate solution and the precipitate was resuspended in a Tris buffer (20 mM Tris pH 8.0, 150 mM NaCl, 5mM EGTA and 1 mM DTT) and adjusted to 80% ethanol by quickly adding 5 volume of 95 % ethanol with 1 mM PMSF. The mixture was immediately centrifuged at 4200 g for 5 minutes and the pellet was extracted in a Tris buffer (20 mM Tris pH 8.0, 150 mM NaCl, 5 mM EGTA and 1 mM DTT) and centrifuged again for 5 minutes at 4200 g. The supernatant was subsequently precipitated by 65 % ammonium sulphate [259;260]. Unfortunately, in contrast to the published report $PP2A_C$ cannot be easily re-dissolved after ethanol precipitation.

Main problems encountered in purification of $PP2A_C$ were low levels of protein production and a low efficiency of histdine tag binding to Ni-NTA beads. In order to improve his tag binding efficiency, each dialysis buffer (20 mM Tris pH 8.0, 150 mM NaCl, and 1 mM DTT) was prepared with different type of salt ions at a range of concentrations. Usually, increasing ionic strength of a buffer composition aids in the removal of the non-specifically bound proteins to

Ni-NTA.

Effect of various salt concentrations in the Ni-NTA wash buffer was evaluated by dialysis of cell lysates from 10 ml cell cultures in each buffer and the lysates were then passed over Ni-NTA beads. The western blot analysis of these experiments confirmed that in this case, increased salt concentration does not result in a decreased amount of non-specifically bound proteins to the Ni-NTA resin (Figure 4-7).

4.2.3.2 Additional Methods Used for PP2A$_C$ Purification

Dr. Ikehara's group [259] used modified ethanol precipitation to purify PP2A$_C$ protein and according to their published protocol, ammonium sulphate precipitation preceded ethanol precipitation [259]. In our experience, while this procedure precipitated PP2A$_C$ the protein could not be re-dissolved in original buffer as suggested. Thus, ethanol precipitation step at that stage was abandoned from our experiments.

In a final attempt to improve purity of PP2A$_C$, proteins from the insect cell lysate were ethanol precipitated directly without initial ammonium sulphate addition and a Tris buffer (20 mM Tris pH 7.5, 2 mM EGTA, 0.5 mM DTT and 0.1 mM PMSF) was used to re-dissolve PP2A$_C$ using homogenizer. Subsequently, the protein sample was dialyzed in 50 mM Tris pH 8.0, 1 mM DTT at 4 ^oC overnight and then subjected to Ni-NTA purification (*Qiagen*). Purification details are described in section 2.5.4. The western blot and SDS-PAGE results showed a

significant increase in PP2AC purification when this method was used, however the efficiency of histidine-tagged $PP2A_C$ binding to Ni-NTA (Figure 4-8) was still very poor. PP2Ac was not detected in the elution fractions or on the resin either by mouse anti-histidine tag monoclonal antibody (*Clontech*) or mouse anti-$PP2A_C$ antibody (*BD Biosciences*) respectively. It is possible that the histidine tag is obstructed through an interaction with the rest of the $PP2A_C$ molecule and thus unavailable for binding to Ni resin.

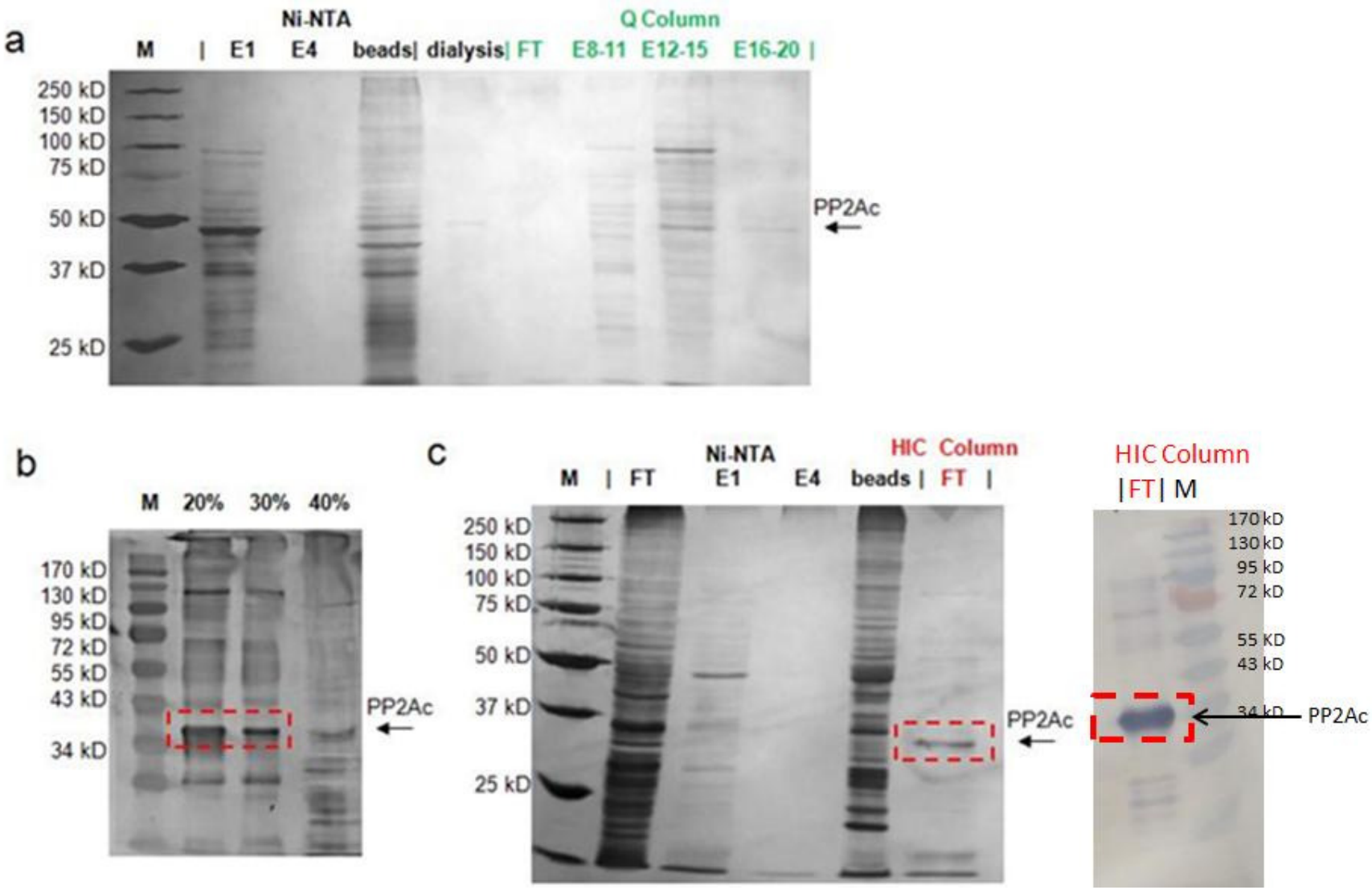
a
Ni-NTA
Q Column
M | E1 E4 beads| dialysis| FT E8-11 E12-15 E16-20 |
250 kD
150 kD
100 kD
75 kD
50 kD
37 kD
25 kD
PP2Ac
b
M 20% 30% 40%
170 kD
130 kD
95 kD
72 kD
55 kD
43 kD
34 kD
PP2Ac
c
Ni-NTA
HIC Column
M | FT E1 E4 beads | FT |
250 kD
150 kD
100 kD
75 kD
50 kD
37 kD
25 kD
PP2Ac
HIC Column
|FT| M
170 kD
130 kD
95 kD
72 kD
55 KD
43 kD
34 kD
PP2Ac

Figure 4-6. Purification of $PP2A_C$. (a) High Five insect cell lysate was applied to Ni-NTA (*Qiagen*) (lane E1, E4 and beads) and anion exchange column (Q FF, *GE Healthcare*, eluted on a linear gradient between 250 and 400 mM NaCl) (lane FT, E8-11, E12-15, and E16-20). Peak fractions were loaded onto a 10 % acrylamide SDS-PAGE gel stained by silver stain method (ProteoSilver Kits, *Sigma*). (b) High Five insect cell lysate was applied to Ni-NTA beads and followed by precipitation by increasing concentrations of ammonium sulphate, 20%, 30% and 40%. Supernatant of each fraction (20%, 30% and 40%) was loaded onto a 10 % acrylamide SDS-PAGE gel. $PP2A_C$ can be detected by the western blot method, using anti-His-tag-antibodies (*Clontech*). (c) High Five insect cell lysate was applied to Ni-NTA (*Qiagen*) (lane E1, E4 and beads) and HIC column (Phenyl HP, *GE Healthcare*, eluted on flow through fractions) (lane FT). Peak fractions were loaded onto a 10 % acrylamide SDS-PAGE gel stained by silver stain method (ProteoSilver Kits, *Sigma*) (right picture) and also detected by the western blot method, using anti-His-tag-antibodies (*Clontech*) (left picture). $PP2A_C$ was successfully purified using phenyl HP column; however, the result was not repeated.

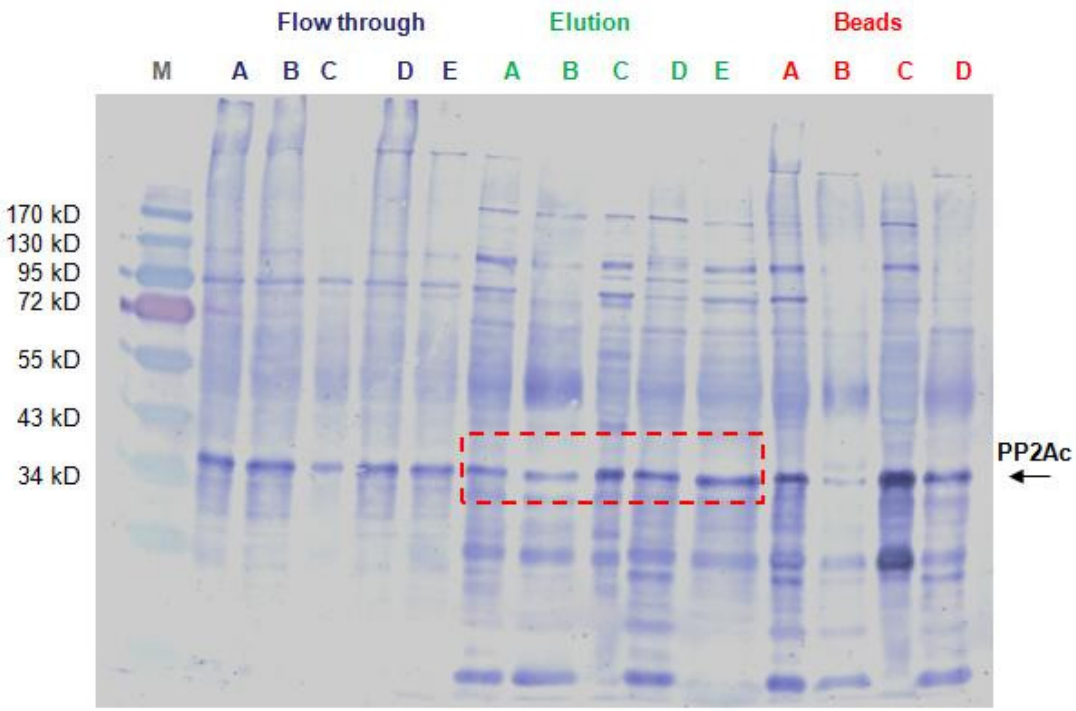

A. 0.5 M NaCl
B. 1 M NaCl
C. 10 mM $MgCl_2$
D. 0.5 M $(NH_4)_2SO_4$
E. 0.5 M Na_2HPO_4

Figure 4-7. Low Efficiency of His-tag Binding to Ni-NTA. High Five insect cell lysate was dialyzed and passed over Ni-NTA beads using different type of salt ions at a range of concentrations. Each sample was loaded onto 10% acrylamide SDS-PAGE gel and detected by the western blot method, using anti-His-tag-antibodies (Clontech). The result showed that lysis buffer (20 mM Tris pH 8.0, 150 mM NaCl, and 1 mM DTT) supplemented with different types of salts did not improve the efficiency of his tag binding to Ni-NTA.

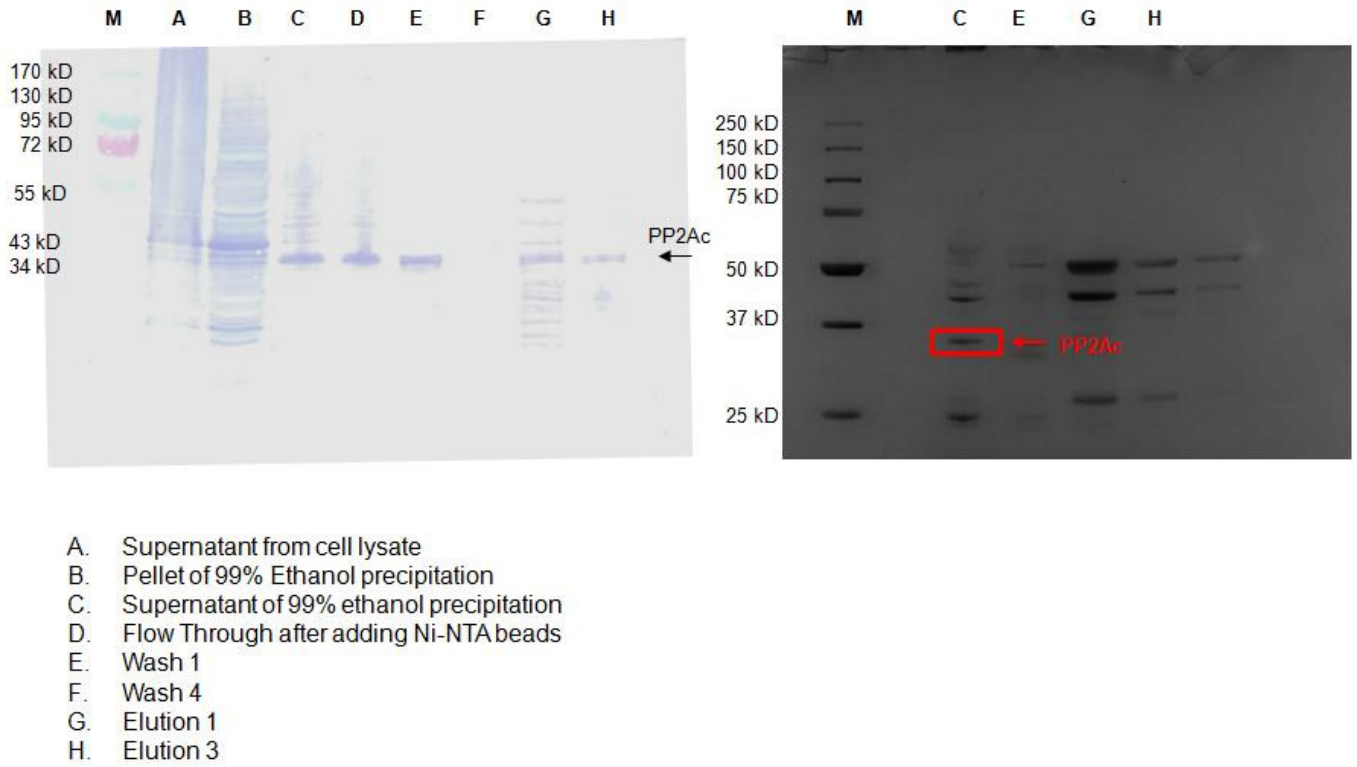

Figure 4-8. Purification of $PP2A_C$ by Ethanol Precipitation. The sample from each step in ethanol precipitation was loaded onto 10 % acrylamide SDS-PAGE gel and stained by Coomassie Blue. To identify $PP2A_C$, the gel was also detected by the western blot method, using mouse anti-$PP2A_C$ antibody (*BD Biosciences*).The western blot (left) and SDS-PAGE (right) analysis of the steps in protein purification showed that ethanol precipitation surprisingly improved the purity of $PP2A_C$. However, efficiency of his-tag binding to Ni-NTA resin remained low.

4.3 Co-expression of $PP2A_A$ and $PP2A_C$

The pBAC4x-1 plasmid contains four multiple cloning sites; therefore, $PP2A_C$ and $PP2A_A$ could be both cloned into this vector and co-expressed in insect cells using BacMagic Transfection System (*Novagen*). Co-expessing the two proteins might have an impact on soluble yields of PP2AC, as through protein-protein interaction between A and C subunit, the stability and folding of the C subunit might be improved.

Specific primers and the PCR reaction conditions were described in section 2.2.5.1. After the PCR products were verified $PP2A_A$ was cloned into the second multiple cloning site of pBAC4x-1 plasmid (*Novagen*) which already contained $PP2A_C$ gene in the first multiple cloning site (For details see section 2.3.3.2. 100 ng of BacMagic DNA and 500 ng of recombinant plasmid were co-transfected to *Spodoptera frugiperda* (Sf9) cells. After amplification of virus, and titer efficiency were determined small scale expression tests using sf9 cells were carried out. The western blot analysis of the expression tests showed that while $PP2A_A$ is found in soluble form in the cell lysates, unfortunately, in contrast to our expectations, majority of $PP2A_C$ was found in the fraction with the cell debris (Figure 4-9). Furthermore, the results suggest that co-expression of $PP2A_A$ and $PP2A_C$ did not assist in solubilisation of $PP2A_C$ but that the yields of expression of $PP2A_A$ in this system were relatively high. When High Five cells were used for co-expression of $PP2A_A$ and $PP2A_C$, significant cell death and diminished levels of $PP2A_A$ were observed.

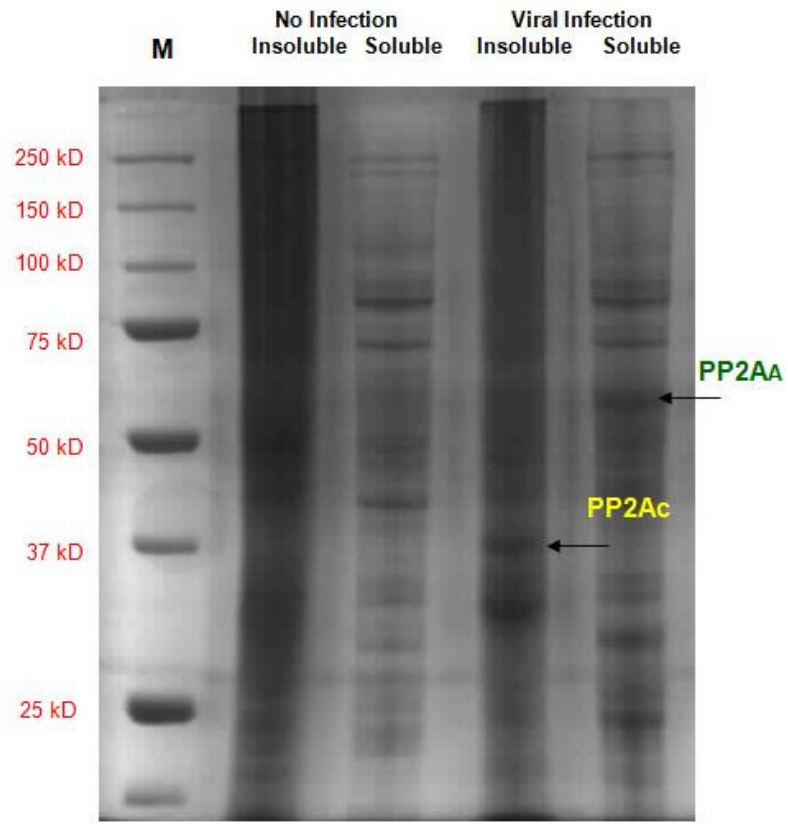

Figure 4-9. Co-expression of $PP2A_A$ and $PP2A_C$ in Sf9 Cells. Each sample was loaded onto 10 % acrylamide SDS-PAGE gel and stained by Coomassie Blue. The SDS-PAGE showed that co-expression of $PP2A_A$ and $PP2A_C$ in sf9 cells resulted in $PP2A_C$ subunit found only in an insoluble form.

4.4 Assembly of $PP2A_A$ and $PP2A_C$

To obtain PP2A AC complex, partially purified $PP2A_C$ was mixed with 100 μg purified $PP2A_A$ and applied to the size exclusion column (Hi Load 16/60 Superdex 200 Prep Grade, *GE Healthcare*). Samples from each of the fractions collected were analyzed using SDS-PAGE electrophoresis and the western blot analysis, using mouse anti-$PP2A_C$ antibody (*BD Biosciences*). There were two main peaks in the gel filtration elution profile. Based on the calibration of Hi Load 16/60 Superdex 200 Prep Grade column (GE Healthcare), the first peak (fraction 38, ~200 kDa) could be interpreted as containing dimeric PP2A AC complex that in a 1:1 stoichiometry would have a molecular weight of 104.1 kDa while I would suggest that the second peak (fraction 47, ~65 kDa), contains monomeric form of $PP2A_A$ (67.5 kDa) (Figure 4-10). However, to clarify the association of $PP2A_A$ and $PP2A_C$ in gel filtration column, both samples should be advanced analyzed through other biophysical instruments such as Mass Spectrometry.

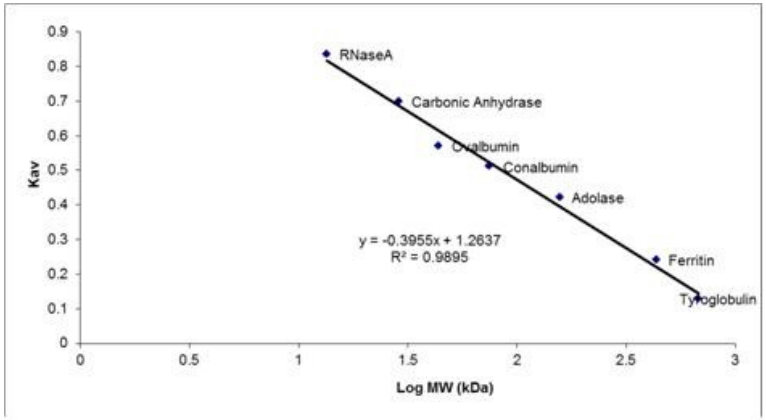
RNaseA
Carbonic Anhydrase
Ovalbumin
Conalbumin
Adolase
Ferritin
Tyroglobulin
y = -0.3955x + 1.2637
R² = 0.9895
Kav
Log MW (kDa)

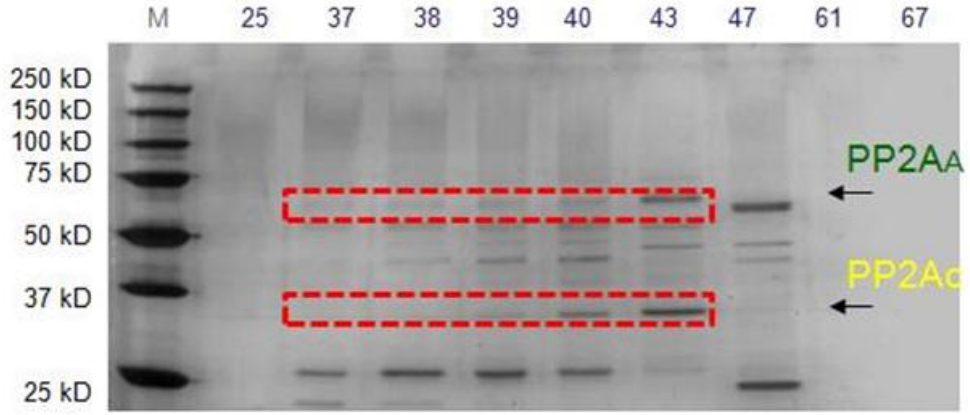
M
25
37
38
39
40
43
47
61
67
250 kD
150 kD
100 kD
75 kD
50 kD
37 kD
25 kD
PP2AA
PP2Ac

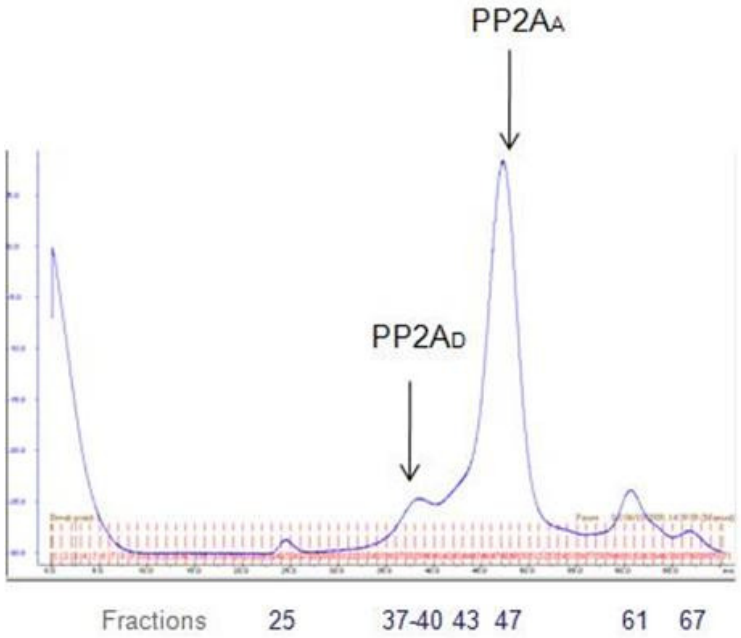
PP2AA
PP2AD
Fractions
25
37-40
43
47
61
67


M
40
43
170 kD
130 kD
95 kD
72 kD
55 kD
43 kD
34 kD
PP2Ac

Figure 4-10. Assembly of $PP2A_A$ and $PP2A_C$ in Superdex 200 Column. Multiple proteins from LMW and HMW calibration kits (*GE Healthcare*) were applied to Hi Load 16/60 Superdex 200 Prep Grade column (*GE Healthcare*). The K_{av} value (V_e-V_o/V_t-V_o, V_o= void volume, V_t = total column volume, V_e = elution volume) and log molecular weight values were calculated for calibration curve. Based on the calibration curve, two peaks were observed at 200 kDa and 65 kDa region respectively. The first peak (fraction 38) could be interpreted as containing dimeric PP2A AC complex (~104 kDa) or oligomeric $PP2A_C$ while the second peak (fraction 47) could contain monomeric form of $PP2A_A$ (67.5 kDa). However, to identity the proteins both samples should be further analyzed. The fractions of gel filtration were verified using 10 % acrylamide SDS-PAGE gel. To identify $PP2A_C$, the gel was also detected by the western blot analysis, using mouse anti-PP2AC antibody (*BD Biosciences*).

4.5 Summary

The full-length A subunit of PP2A was successfully expressed in an *E. coli* expression system, whereas $PP2A_C$ was expressed using baculovirus expression system. The purification procedure of $PP2A_A$, including Ni sepharose 6, anion exchange chromatography (Q FF), size exclusion chromatography and 40% ammonium sulphate precipitation, was used to reproducibly obtain mg quantities of the protein with high level of purity (>99 %). Purification of the C subunit was less successful. The best purification protocol for $PP2A_C$ incorporated ethanol precipitation step that was originally reported in purification of the phosphatase from animal tissues [261;262]. However, the efficiency of histidine tag binding to Ni-NTA was persistently low and precluded obtaining a protein of the desired purity.

Although $PP2A_A$ and $PP2A_C$ were both expressed in insect cells using BacMagic transfection system, co-expression of $PP2A_A$ and $PP2A_C$, in contrast to what was expected, decreased the solubility of $PP2A_C$.

Finally, to obtain $PP2A_D$, $PP2A_A$ and $PP2A_C$ were mixed, assembled and partially purified using size exclusion chromatography.

Chapter Five

Biophysical Studies of $PP2A_A$ and PME1 Interaction

The structure of PME1-PP2A complex was solved in 2008 and demonstrated that the association of PME1 with $PP2A_C$ will activate PME1 and lead to the inactivation of PP2A [221]. Based on the X-ray crystal structure, this study implied that PME1 only interacts with $PP2A_C$ but not $PP2A_A$ subunit. However, neither PME1 nor $PP2A_A$ used to form the molecular complex structure were not in their native form. $PP2A_A$ protein construct used in the study had HEAT repeats 2-10 deleted while $PME1_{39\text{-}376}$ protein construct contained only residues 39-238, a small tri-peptide linker EGK, and residues 284-376 at the C-terminus. Although the authors insist that deletion of HEAT repeats 2-10 from the $PP2A_A$ molecule has no detectable impact on the interaction between PME1 and the PP2A core enzyme, in the absence of any supporting data, it was suggested that the HEAT repeats 2-10 were very important for $PP2A_A$ interaction with B and B' subunits [19,24]. It was previously reported that $PP2A_A$ HEAT repeats 2, 4 and 5 are involved in PR61-$PP2A_A$ interaction, while HEAT repeats 3 to 7 are engaged in PR55-$PP2A_A$ interaction. In addition, not only regulatory subunits but also small T antigen was shown to interact with the intra-loops of HEAT repeats 3-7 of $PP2A_A$. Although no structural similarity was found among PR61, SV40 small T antigen and PME1, PR61 and SV40 small T antigen interact with $PP2A_A$ at similar HEAT repeats region [217].

To evaluate putative association of full the length PME1/LCMT1 molecules and $PME1_{39\text{-}376}$ with $PP2A_A$, isothermal titration calorimetry (ITC), differential scanning calorimetry (DSC) and surface plasmon resonance (SPR) techniques were used. In addition, as it was previously reported that PME1 is a PMSF-resistant, okadaic acid-sensitive PP2A methylesterase in vivo [60,63], association of okadaic acid with PME1 was tested *in vitro*.

This chapter focuses on thermodynamic studies of PME1/LCMT1 and $PP2A_A$ interaction using ITC and DSC. This chapter also includes SPR experiments to confirm the observations from ITC measurements. Finally, the interaction between PME1 and okadaic acid was analyzed using ITC method.

5.1 Analysis of PME1/LCMT1 and $PP2A_A$ Interaction

5.1.1 Thermodynamic Studies

Isothermal Titration Calorimetry (ITC) is a thermodynamic technique for monitoring the energetics of biochemical reactions or molecular interactions including ligand-binding reactions, enzyme-substrate interactions, and interactions among components of multi-molecular complexes. By monitoring directly the energy required to maintain temperature of the sample cell during several ligand injections allows for the calculation of free energy, enthalpy of binding (ΔH_b), entropy (ΔS), binding constants (K_b), and reaction stoichiometry (n) of binding from one single experiment, thereby providing a complete thermodynamic profile of the molecular interaction in a single experiment. In addition, unlike NMR or SPR method, the reaction can be measured without immobilization or labelling of the binding partners. Today's ITC instrument, VP-ITC titration calorimeter (*MicroCal, LLC*), is so sensitive that can detect very weak association (Ka = 100 M^{-1}). Therefore, it's a suitable biophysical instrument to investigate the interaction between PME1/LCMT1 and PP2A.

5.1.1.1 Does PME1/LCMT1 Interact with $PP2A_A$?

In order to obtain an optimal binding curve, relative concentrations of binding partners should be first considered. The c value in the following formula is used for the estimation of required protein concentrations.

$$c = Ka \times [M] \times n \tag{5.1}$$

Here, Ka is the binding constant, [M] is the concentration of the macromolecule in the sample cell, and n is the stoichiometry of the binding reaction. The optimal c value is between 10 and 100 in ITC experiments. The concentration of the binding partner in the syringe is estimated as follows:

$$\text{Binding partner concentration} = 10 \times [M] \times n \tag{5.2}$$

Where n is the stoichiometry of the binding reaction, and [M] is the molar concentration of the binding material in the sample cell.

All sample proteins were dialyzed in the same buffer for heat dilution experiments. In addition, all samples were filtered and degassed before setting up an ITC experiment. To measure the interaction between $PP2A_A$ and the full length LCMT1/PME1, 10 μM of the full length $PP2A_A$ was prepared for ITC analysis with 100 μM concentration of full length LCMT1/PME1 and the experiment was initially carried out at 10 ℃. The result suggests that LCMT1

may not associate with $PP2A_A$ because of irregular heat change; however, PME1 may interact with $PP2A_A$ due to the regular heat signal (Figure 5-1). This result did not support the three dimensional arrangement in PME1-PP2A structure. To obtain the thermodynamic parameters, additional ITC experiments were carried out for analysis of the full length PME1 and $PP2A_A$ interaction.

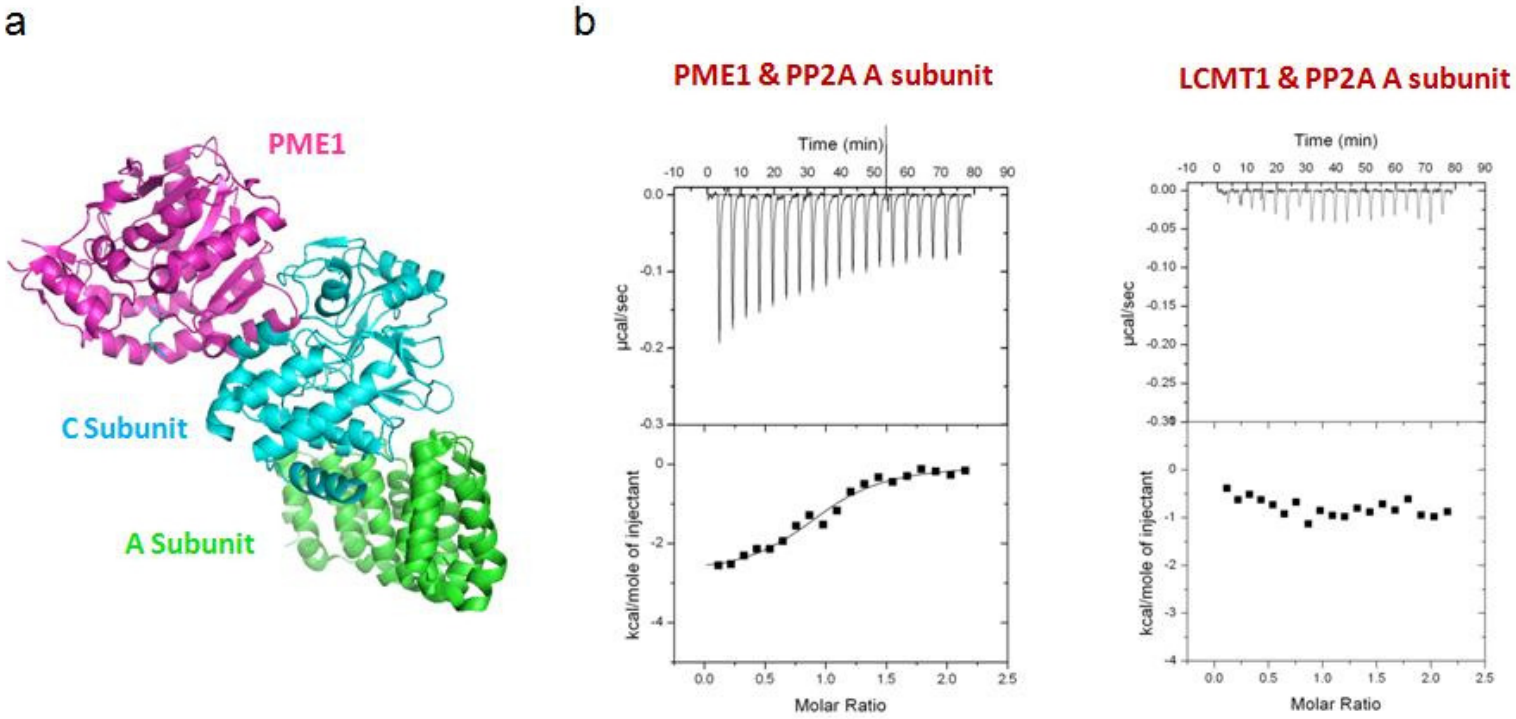

Figure 5-1. Structure of PME1-PP2A Complex and ITC Analysis of the Interaction between $PP2A_A$ and PME1/LCMT1. (a) PME1-PP2A structure suggests that PME1 only interacts with C subunit but not A subunit of PP2A. (b) 10 µM of $PP2A_A$ was titrated by 100 µM PME1 or LCMT1 using ITC. The result shows that PME1 may associate with $PP2A_A$ due to regular heat change; however, LCMT1 may not bind $PP2A_A$ subunit because of irregular heat change.

5.1.1.2 Thermodynamic Parameters of PME1-PP2A$_A$ Interaction

To obtain best Ka fit, the titration curve should exhibit sigmoidal shape and clearly reach saturation at the end of the titration. The sigmoidal region of the binding reaction should contain at least five data points. However, the first data from ITC experiment did not show clear sigmoidal curve nor reach the saturation baseline. Therefore, increasing the concentration of protein in the syringe and modifying the titrating schedules were both tested in order to obtain stronger signals. ITC experiments were carried out using the titration of 10 μM of PP2A$_A$ with 5 x 7-μl, 5 x 10-μl, and 9 x 15-μl injections of PME1 (300 μM) at 10, 15, 20 ℃. Depending of the titration conditions the dissociation constant was estimated to be between 10 and 20 μM. In addition, it was apparent that the value of the dissociation constant (Kd) slightly decreases as temperature raises. However, because the protein concentration of PP2A$_A$ in the cell was 10 μM and very near the estimated value of the Kd, the accuracy in determination of the association constant might be diminished (Figure 5-2). Therefore, in further experiments, the concentration of PP2A$_A$ was increased.

The titration of 30 μM of PP2A$_A$ with 19 x 15 - μl injections of PME1 (295 μM) at 15 ℃ and the titration of 25 μM of PP2A$_A$ with 19 x 15 - μl injections of PME1 (250 μM) at 10, 20, 25 ℃, respectively were performed. ITC curve fitting analysis using one set of sites model, shows that this reaction is exothermic and the stoichiometry (n) indicates that single PME1 molecule may interact with one molecule of PP2A$_A$ subunit. These experiments also suggested that there was a slight decrease in dissociation constant (Kd) value when temperature of the reaction is increased (Figure 5-3). To find out the relationship between

temperature and dissociation constant, all ITC data generated at different temperatures are compared and analyzed (Table 5-1). When the temperature reaches 10, 15, 20, or 25 ℃, the value of Kd is calculated as 20, 12, 10, or 6 μM respectively. This observation implies that PME1 may 'prefer' to interact with $PP2A_A$ at higher temperatures. In addition, data clearly showed that in these experiments it's difficult to reach curve saturation levels due to low value of Ka in combination with relatively low, although maximum practically achievable levels of protein concentration.

The binding reaction can be represented as follow:

$$PME1 + PP2A_A \ <=> PME1\text{-}PP2A_A \qquad (5.3)$$

It is assumed that there is only one binding site for PME1 per $PP2A_A$. The association constant is defined as

$$Ka = [PME1\text{-}PP2A_A] / [PME1][PP2A_A] \qquad (5.4)$$

and the dissociation constant is

$$Kd = [PME1][PP2A_A] / [PME1\text{-}PP2A_A] \qquad (5.5)$$

where $[PP2A_A]_T = [PME1\text{-}PP2A_A] + [PP2A_A]$ is the total concentration of $PP2A_A$. The fractional saturation (F) of $PP2A_A$ sites is

$$F = [PME1\text{-}PP2A_A] / [PP2A_A]_T = [PME1] / Kd + [PME1] \qquad (5.6)$$

The mathematical relationship between the bound and the free PME1 concentrations will be a rectangular hyperbola. Half saturation occurs when [PME1] is equal to Kd. [PME1] = 9 × Kd gives only 0.9 saturation. The 0.99 saturation will be reached only when the concentration of PME1 is equal to 99 Kd.

Based on this formula, if Kd is small (~ nM), even small concentrations of free protein will give F = ~1. The dissociation constant of PME1 and $PP2A_A$ binding reaction is about 6 to 20 μM. Therefore, the final concentration of PME1 in sample cell should be at least 600 μM to reach 99 % saturating curve at 25 ℃. It also means that the concentration of PME1 in the syringe should be about 3 mM due to the volume of sample cell of 1.4 ml being about 4.7 times larger than the volume of the syringe. However, it's impossible to obtain 3 mM PME1 because of the precipitation of PME1 at concentrations approaching mM range.

It could be considered to measure PME1 and $PP2A_A$ binding reaction at higher temperatures in an attempt to obtain saturation of reaction. But unfortunately, when temperature reaches 30 ℃, $PP2A_A$ will start to unfold, judged by the differential scanning calorimetry data (see 5.2.1). It will be difficult to estimate the percentage of well-folded protein in ITC experiments. Therefore, it's not suitable to measure the binding reaction of PME1 and $PP2A_A$ at temperatures above 30 ℃ and further experiments were carried out at the best possible optimal conditions.

$PP2A_A$ (μM)	PME1 (μM)	Salt	Schedule	(°C)	Kd (μM)	N	ΔH (Cal/mol)	ΔS ((Cal/mol)/K)
10	300	50 mM NaCl	5 7-μl, 5 10-μl, and 9 15-μl	10	18 ± 4	1.14 ± 0.27	-9765 ± 2910	-12.7
10	300	50 mM NaCl	5 7-μl, 5 10-μl, and 9 15-μl	15	11.8 ± 1	0.9 ± 0.0794	-7982 ± 846.9	-5.13
10	300	50 mM NaCl	5 7-μl, 5 10-μl, and 9 15-μl	20	10.1 ± 0.8	0.811 ± 0.0672	-6544 ± 657	0.532
25	250	50 mM NaCl	19 15-μl	10	20 ± 2	0.79 ± 0.0479	-8317 ± 699.5	-7.9
25	250	50 mM NaCl	19 15-μl	20	10 ± 1	0.691 ± 0.0351	-4470 ± 307.3	7.83
25	250	50 mM NaCl	19 15-μl	25	6.2 ± 0.6	1.02 ± 0.0197	-4122 ± 122.5	9.99
30	295	50 mM NaCl	19 15-μl	15	14 ± 2	0.908 ± 0.0506	-6041 ± 507.2	1.34

Table 5-1. ITC Analysis of the Interaction between $PP2A_A$ and the Full Length PME1.

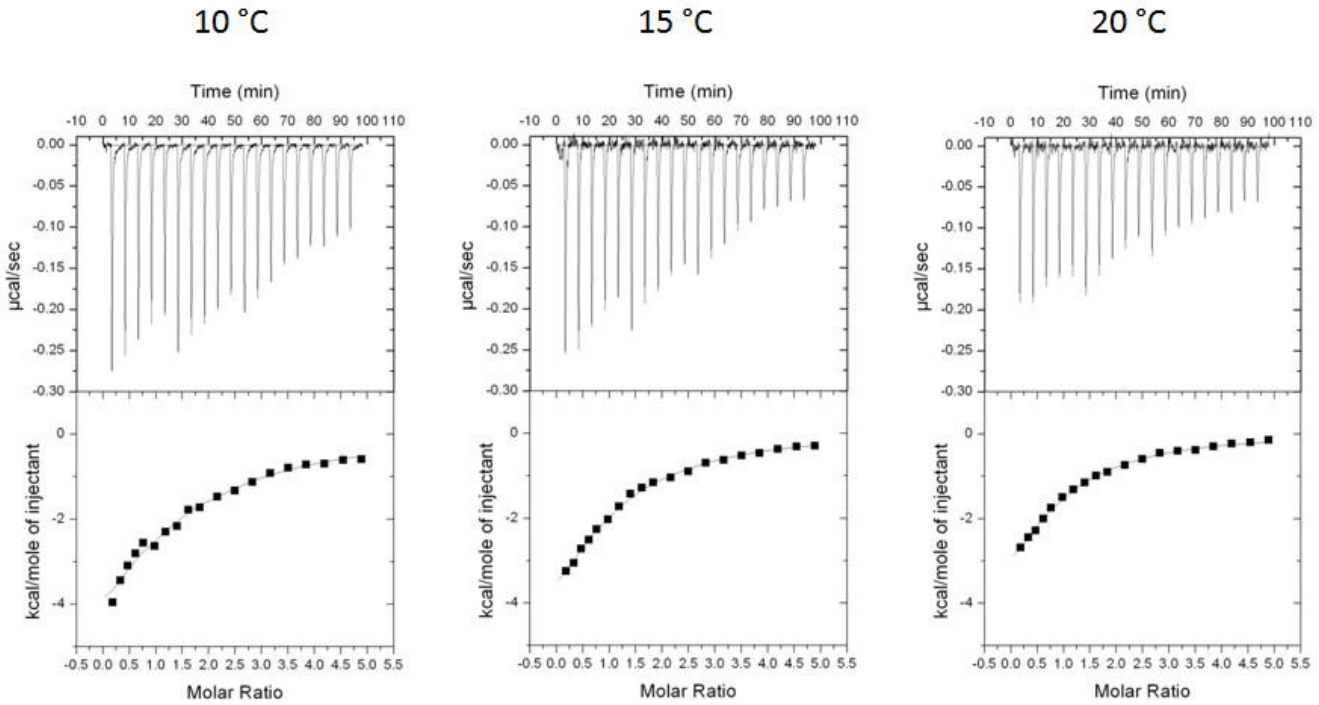

Figure 5-2. ITC Titration Data Describing the Formation of PME1-PP2A$_A$ Complex at Different Temperatures. Titrations were performed in 25 mM Tris (pH 8.0), 50 mM NaCl and 2 mM BME buffer. Raw data show the titration of 10 µM of PP2A$_A$ with 5 7- µl, 5 10 - µl and 9 15 - µl injections of PME1 (300 µM). The solid smooth line represents the best fit of the experimental data to a single binding site model.

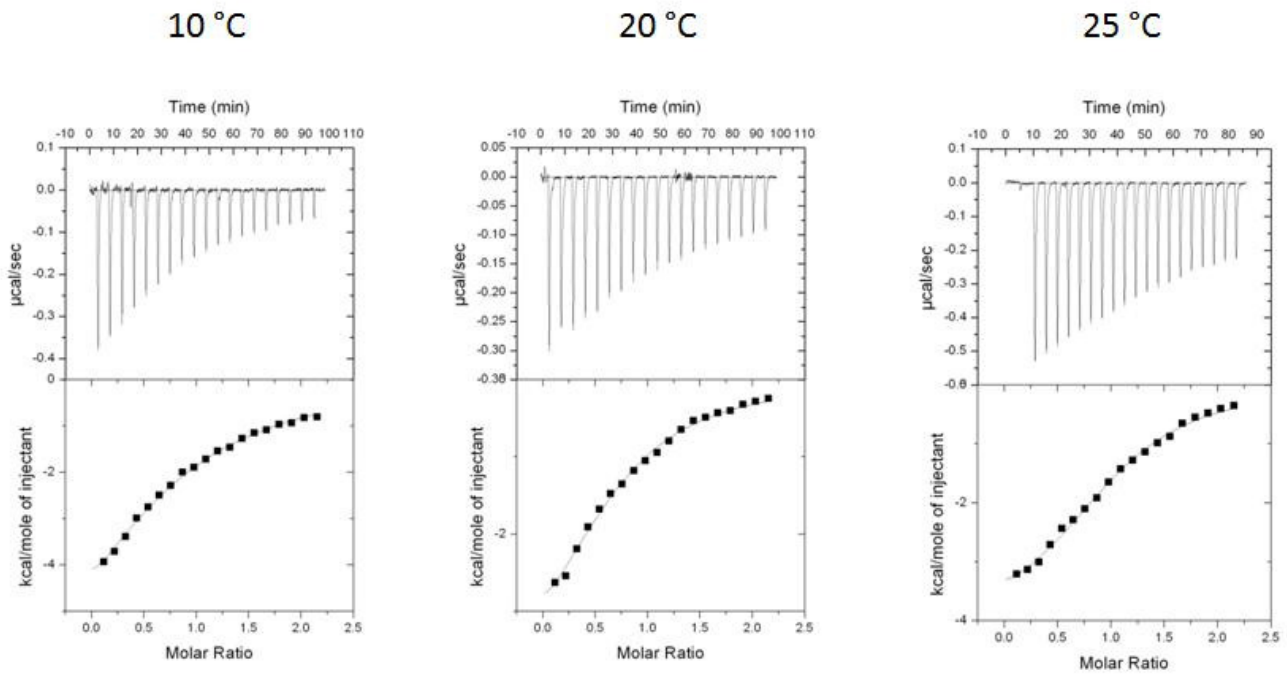

Figure 5-3. ITC Titration Data Describing the Formation of PME1-PP2A$_A$ Complex at Different Temperatures. Titrations were performed in 25 mM Tris (pH 8.0), 50 mM NaCl and 2 mM BME buffer. Raw data show the titration of 25 µM of PP2A$_A$ with 19 15 - µl injections of PME1 (250 µM). The solid smooth line represents the best fit of the experimental data to a single binding site model.

5.1.2 Surface Plasmon Resonance Analysis

Surface plasmon resonance is used to measure the changes in refractive index occurring at the metal surface upon association between the two partners [263]. To confirm the association of PME1 and $PP2A_A$, BIAcore™ X-100 with NTA sensor chip (*GE Healthcare*) was used [264].

BIAcore™ X-100 can detect real-time binding signal enabling kinetic characterization, association constant determination and detection of weak and transient binding events. For protein-protein interaction, the sensitivity of association rate constant (k_{on}) and dissociation rate constant (k_{off}) are 10^3 - 10^7 $M^{-1}s^{-1}$ and 10^{-5} - 10^{-1} s^{-1} respectively. Therefore, the sensitivity of dissociation constant determination (Kd) is 100 µM - 1 pM. Sensor chip NTA is used for immobilization of histidine tagged analytes. The matrix, carboxymethylated dextran, is pre-immobilized with nitrilotriacetic acid (NTA) which will chelate Ni^{2+} to trap molecules containing histidine tag. This method not only controls steric orientation of the immobilized interaction partner for optimum site exposure but also can be easily regenerated by injection of EDTA to remove metal ions.

30 µM of PME1 (42 kDa) and 50 nM of $PP2A_A$ (67 kDa) were prepared for Biacore analysis and 30 µM of LCMT1, which has similar molecular weight (38 kDa) and no interaction with $PP2A_A$ judged by ITC experiment, was used in a control experiment. The binding partner immobilized on the chelating NTA chip was 50 nM $PP2A_A$ and the association with analyte (PME1 or LCMT1) was allowed to occur during 60 sec before dissociation step. The output signal of Biacore is measured in resonance units (RU) proportional to a change in mass

of the immobilized protein. The sensorgram clearly shows that PME1 but not LCMT1 will interact with $PP2A_A$ (Figure 5-4).

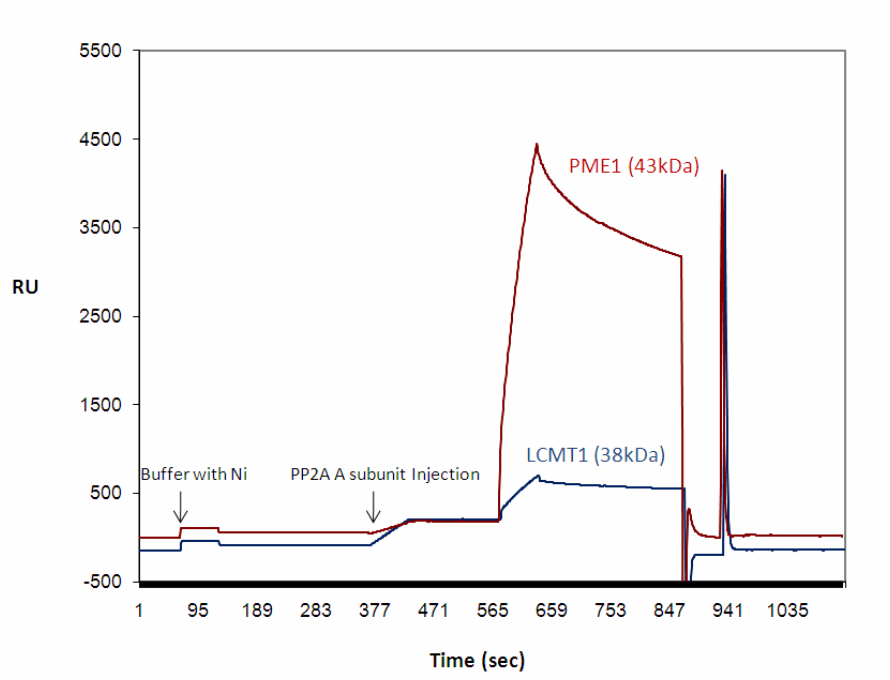

Figure 5-4. BIAcore Analysis of the Interaction between $PP2A_A$ and PME1/LCMT1. Sensorgram showing the evolution of resonance units versus time during association and dissociation measurements performed in BIAcore instrument. The binding partner immobilized on the chip is $PP2A_A$ and the association is individually measured in the presence of 30 μM PME1 (42kDa) or 30 μM LCMT1 (38kDa). The association time is 60 seconds before the flow is changed to analyte-free buffer for dissociation measurements.

5.2 Interpretation of Positive Heat Capacity Change

The heat capacity (Cp), first described in details by Joseph Black, Scottish chemist (1728-1799), is defined as the heat taken up or released per unit change in temperature from a material at constant pressure. This heat capacity is readily measure and it can be used to calculate changes in the enthalpy. The formula can be expressed as follows:

$$H(T_2) = H(T_1) + Cp \times (T_2 - T_1), \tag{5.7}$$

where T_1 is the temperature of the system in state 1 and $H(T_2)$ is the enthalpy of the system in state 2. Another way of writing equation (5.7) is

$$\Delta H = Cp \times \Delta T, \tag{5.8}$$

where $\Delta H = H(T_2) - H(T_1)$ and $\Delta T = T_2 - T_1$. The equation (5.8) can be also written as follows:

$$Cp = \Delta H/\Delta T, \tag{5.9}$$

such that the heat capacity at the constant pressure can be determined from a plot of H versus T in the interval ΔT. When Cp is constant throughout the temperature range, H versus T will be constant. For many molecules including proteins, Cp is effectively constant over small range of temperature in the absence of a change of phase.

For proteins, the heat capacity (Cp) is contributed by the covalent, non-covalent interaction, hydration and the state of protonation terms of charged residues. The burial of polar and non-polar residues in the protein is indeed accompanied by the heat capacity changes that have an opposite sign, negative for non-polar groups and positive for polar groups. The equation describing this relationship was proposed by Makhatadze and Privalov (1995) as follows:

$$\Delta Cp = 2.14\ \Delta ASA_{non\text{-}polar} - 0.88\ \Delta ASA_{polar}, \qquad (5.10)$$

where ΔCp is heat capacity change, $\Delta ASA_{non\text{-}polar}$ is water accessible surface area for non-polar groups, and ΔASA_{polar} is water accessible surface area for polar groups [265].

Most of the protein-protein/DNA/ligand interactions have a negative heat capacity change due to a hydrophobic effect, the removal of non-polar molecules from water [266-268]. However, in our case, a positive heat capacity change is observed in the thermodynamic parameters (Figure 5-5). A positive heat capacity change normally occurs as the protein is unfolding [269-272]. With regard to purified proteins in solution, both folded and unfolded states have their own enthalpy respectively. The heat capacity change between folded and unfolded state at constant pressure is $Cp_{unfold} - Cp_{fold} = \Delta C_{p,d}$ where Cp_{unfold} is the heat capacity of the unfolded state and Cp_{fold} is that of folded state. For the enthalpy difference between the folded and unfolded states of a protein, this equation can also be written as follows:

$$\Delta H_d°(T_2) = \Delta H_d°(T_1) + \Delta C_{p,d} \times (T_2 - T_1), \quad (5.11)$$

$\Delta H_d°$= enthalpy of denaturation

where heat capacity change is temperature independent.

In contrast to most of the protein-protein interactions or protein folding process, positive $\Delta C_{p,d}$ is related to the increase in hydrophobic surface contact with the solvent. The side chains of hydrophobic core are largely sequestered from the solvent in the folded state. Does it mean that PME1 or $PP2A_A$ is unfolding during the ITC experiment? To characterize the melting temperature and unfolding procedure of full length PME1 and $PP2A_A$, the differential scanning calorimeter VP-DSC (*Microcal, LLC*) was used.

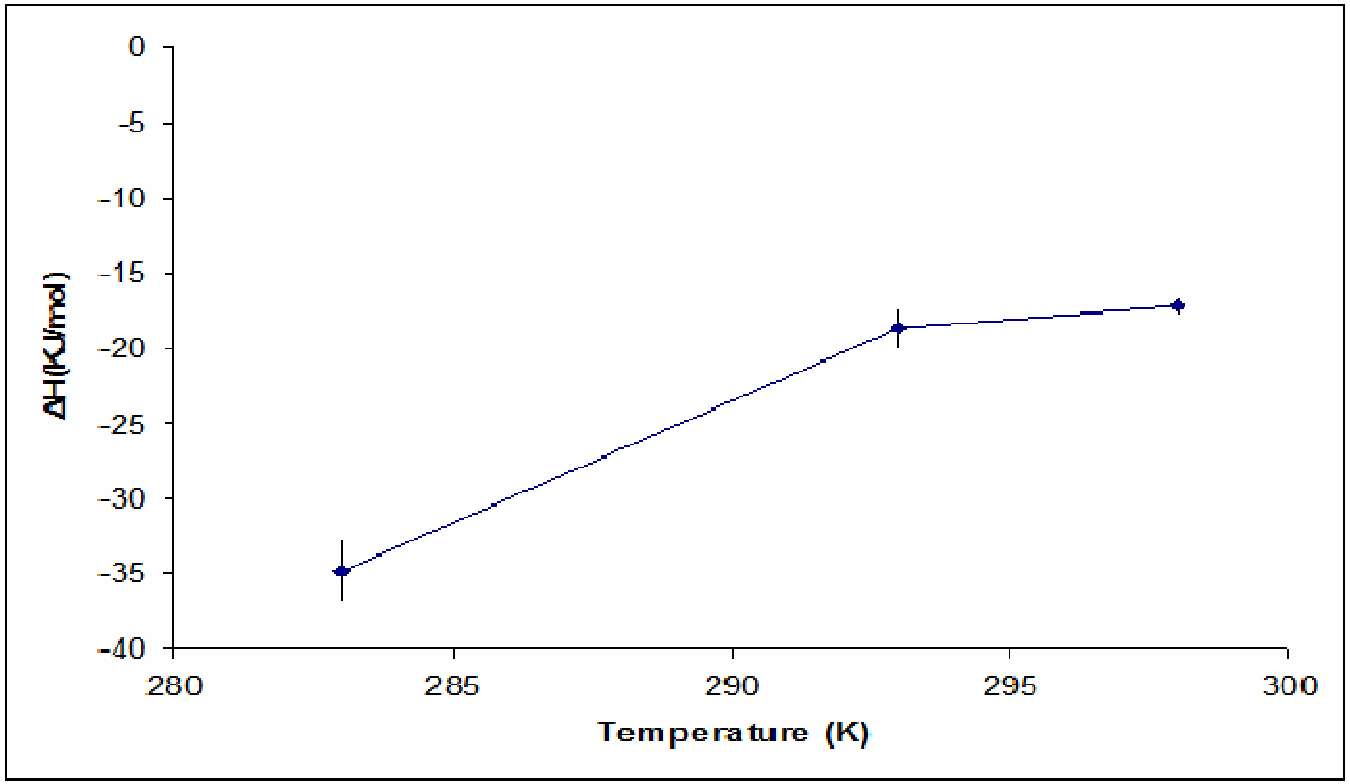

Figure 5-5. Heat Capacity of PME1-PP2A$_A$ Interaction. The positive heat capacity change could be observed in PME1 (250 μM) - PP2A$_A$ (25 μM) interaction.

5.2.1 The Melting Temperature Scan of PME1 and $PP2A_A$

Measuring of ΔH and melting temperature (Tm) can be done with differential scanning calorimetry (DSC), which measures heat absorbed as a function of temperature. Based on the DSC thermograms, it could be concluded that melting process of $PP2A_A$ corresponds to a two-state and irreversible transition model.

$$PP2A_{A,\ fold} \quad => \quad PP2A_{A,\ unfold} \tag{5.12}$$

The $PP2A_A$ started to unfold, when temperature reached 30 ^oC and the melting temperature is about 54.1 ^oC. In contrast to $PP2A_A$, the melting curve for PME1 only fits a non-two-state and irreversible transition model with the melting temperature of 57.7 ^oC. These data indicate that in the process of unfolding PME1 goes through a distinct intermediate state.

$$PME1_{fold} \quad => \quad PME1_I \quad => \quad PME1_{unfold} \tag{5.13}$$

Unlike $PP2A_A$, PME1 was more stable and started to transition at 53 ^oC. Both proteins are well folded below 30 ^oC. Furthermore the measurement of 25 μM of $PP2A_A$ and PME1 mixture in DSC experiment revealed that PME1-$PP2A_A$ complex starts to melt after 42 ^oC (Figure 5-6) with the melting temperature of PME1 and $PP2A_A$ complex reaching only 54 ^oC. In other words no significant additional stabilization of the proteins was observed upon complex formation, compared to the melting temperatures of the individual components.

All ITC measurements of PME1 and $PP2A_A$ interaction were performed between 10 and 25 ^oC. Therefore, PME1 and $PP2A_A$ are both unlikely to unfold in ITC experiments. Thus, not unfolding but another factor dominates PME1 and $PP2A_A$ interaction that contributes to the observed positive heat capacity change.

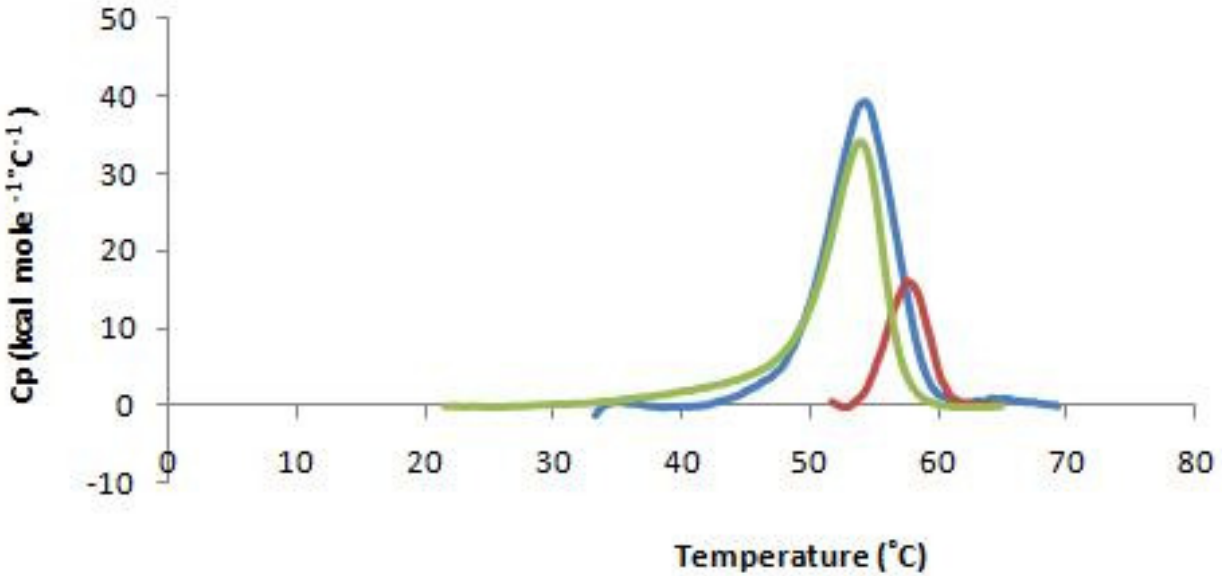

Figure 5-6. Differential Scanning Calorimetry of PME1, PP2A$_A$, and PME1-PP2A$_A$ Complex. DSC transitions for 50 µM of PP2A$_A$ (green), PME1 (red) and PME1-PP2A$_A$ complex (blue) in Tris buffer (25 mM Tris, 50 mM NaCl, pH 8.0) represents the melting temperature (Tm) of each protein and indicates all samples for ITC experiment are stable below 30 ℃.

5.2.2 The Theory of Positive Heat Capacity Change

There are very few examples for positive heat capacity change such as the formation of the phosphofructokinase tetramer [272], the interaction of the brain natruretic peptide with heparin [273], and eIF4E binding to mRNA 5'cap [274]. These studies demonstrated that dehydration of polar molecules will lead to positive heat capacity change and suggest that PME1 may interact with $PP2A_A$ via a polar region. To find out the targeted region for PME1 to interact with $PP2A_A$, the sequence of full length PME1 and $PME1_{39\text{-}376}$ were compared using ClustalW2 (*EMBL-EBI*) [257]. The sequence alignment of full length PME1 and $PME1_{39\text{-}376}$ shows that there are three main segments that have been truncated. The distribution of polar and non-polar residues are equal in the truncated N-terminal segment (residues 1-38) and the C-terminal segment (residues 376-386); however, the middle polypeptide segment (residues 239-282) contains almost 77% polar residues that might potentially be forming $PP2A_A$ subunit interaction surface (Figure 5-7). This interpretation would be in an agreement with an apparent lack interaction of $PME1_{39\text{-}376}$ and $PP2A_A$ in the three-dimensional structure of the complex. But does $PME1_{39\text{-}376}$ really have no site of interaction with $PP2A_A$? To answer this question, $PME1_{39\text{-}376}$ construct was required for isothermal titration calorimetry experiments.

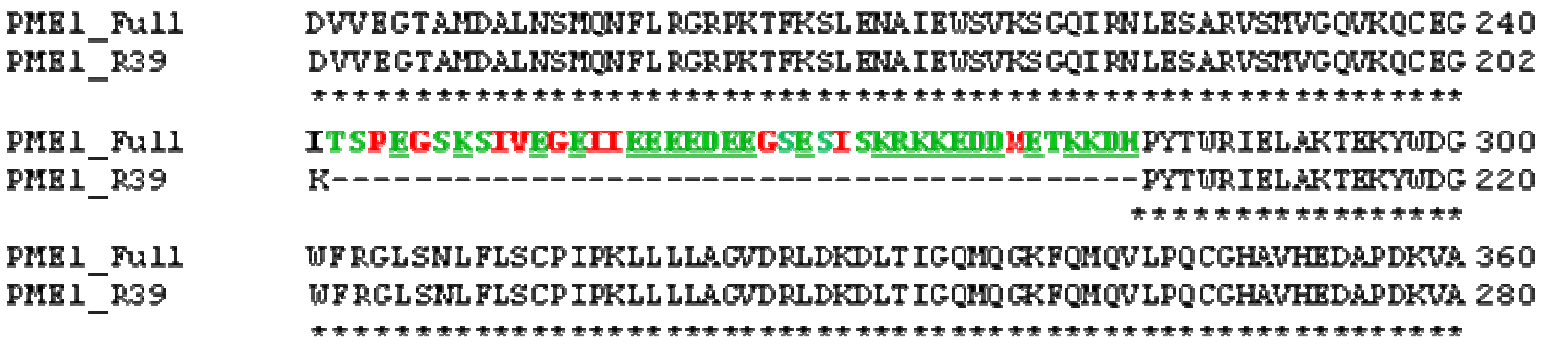

Figure 5-7. Comparison of PME1 and PME1$_{39\text{-}376}$ Protein Sequences. The multiple sequence alignment of full length PME1 and PME1$_{39\text{-}376}$ by ClustalW2 (EMBL-EBI) [257] shows that the sequence segment containing residue 242 to 283 includes 77% polar residues (green) and 23% non-polar residues (red).

5.3 Interaction of $PME1_{39-376}$ and $PP2A_A$

5.3.1 Does $PME1_{39-376}$ Interact with $PP2A_A$?

As the Isothermal titration calorimetry and BIAcore results of full length PME1 and $PP2A_A$ interaction seem to be inconsistent with the crystal structure of the $PME1_{39-376}$-$PP2A_A$ complex solved in 2008 a construct of PME1 ($PME1_{39-376}$), composed of residues 39-238, a small linker EGK, and residues 284-376 was constructed and used in ITC analysis [223]. The measurements was taken by titrating 10 μM of $PP2A_A$ with 5 7- μl, 5 10 - μl and 9 15 - μl injections of $PME1_{1-386}$/$PME1_{39-376}$ (300 μM). Even though the thermodynamic parameters of the association between full length PME1 and $PP2A_A$ were previously obtained, the raw data from this experiment suggested that $PME1_{39-376}$ has lost the capacity to interact with $PP2A_A$ (Figure 5-8). This finding is consistent with the reported three-dimensional X-ray crystal structure of $PME1_{39-376}$-PP2A complex, where $PME1_{39-376}$ indeed exhibited no interaction with $PP2A_A$. The results of the ITC experiment also suggest that the middle polar amino acid segment (residues 239-282) of PME1 may play an important role in PME1-$PP2A_A$ interaction.

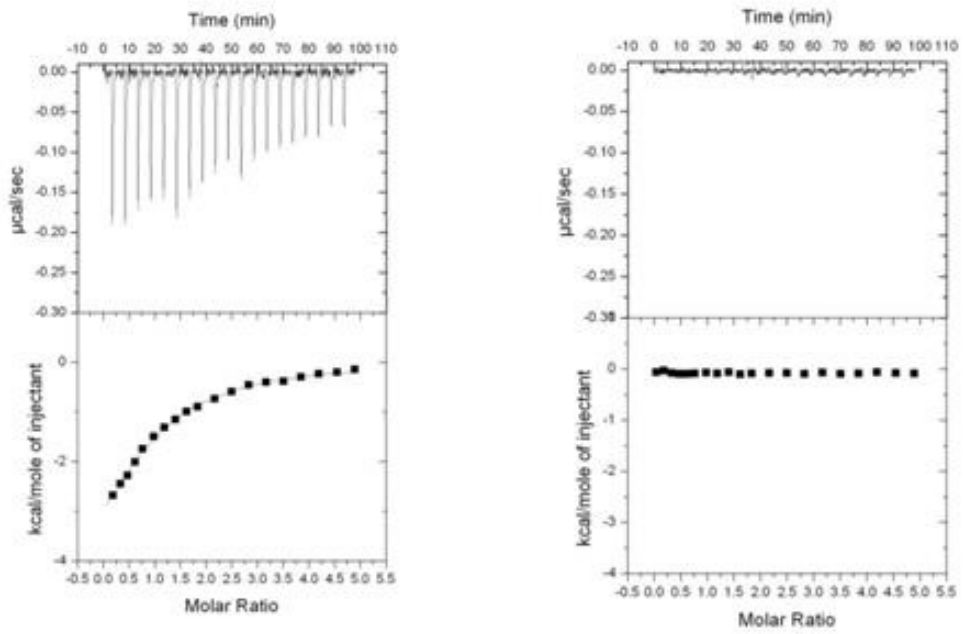

Figure 5-8. ITC Analysis for $PME1_{1\text{-}386}$-$PP2A_A$ or $PME1_{39\text{-}376}$-$PP2A_A$ interaction. 10 µM of $PP2A_A$ was respectively titrated with 5 7- µl, 5 10 - µl and 9 15 - µl injections of 300 µM $PME1_{39\text{-}376}$ (right figure) or full length PME1 (left figure) at 10 ℃. The result suggests no interaction between $PME1_{39\text{-}376}$ and $PP2A_A$ due to the truncation of the putative $PP2A_A$ interacting region..

5.3.2 Electrostatic Interactions

The truncated sequence (residues 239-283) of PME1 not only includes several charged residues, but also contains a highly polar region. Is it possible that PME1 interacts with $PP2A_A$ via electrostatics? To further understand the electrostatic interaction of $PP2A_A$ and PME1, a 25 μM sample of $PP2A_A$ was titrated with 19 15 - μl injections of PME1 (250 μM) under a range of sodium chloride (50, 100, 150, and 500 mM) and magnesium chloride (100 μM) in buffer, 25 mM Tris, pH 8.0, and 1 mM β-mercaptoethanol (Table 5-2). The raw data demonstrated that increasing salt concentration may neutralize the charges in the segment, residue 239 to residue 283, and interfere with the association of PME1 and $PP2A_A$ through electrostatic interaction. This bservation further supports our explanation regarding a loss in capacity of $PME1_{39\text{-}376}$ to interact with $PP2A_A$ (Figure 5-9). Finally, these results are consistent with of the proposed interpretation for the observed positive heat capacity change of PME1 and $PP2A_A$ interaction.

PP2A$_A$ (µM)	PME1 (µM)	Salt	Schedule	(∘ C)	Kd (µM)	N	ΔH (Cal/mol)	ΔS ((Cal/mol)/K)
25	250	50 mM NaCl	19 15-µl	10	20 ± 2	0.79 ± 0.0479	-8317 ± 699.5	-7.9
25	250	100 mM NaCl	19 15-µl	10	31 ± 5	0.833 ± 0.111	-9709 ± 1785	-13.16
25	250	150 mM NaCl	19 15-µl	10	n.d.	n.d.	n.d.	n.d.
25	250	500 mM NaCl	19 15-µl	10	No	No	No	No
25	250	100 µM MgCl2	19 15-µl	10	26 ± 4	0.817 ± 0.1	-11780 ± 2000	-20.5

Table 5-2. The Analysis of PP2A$_A$- PME1 Interaction in Different Salt Conditions Using ITC Instrument.

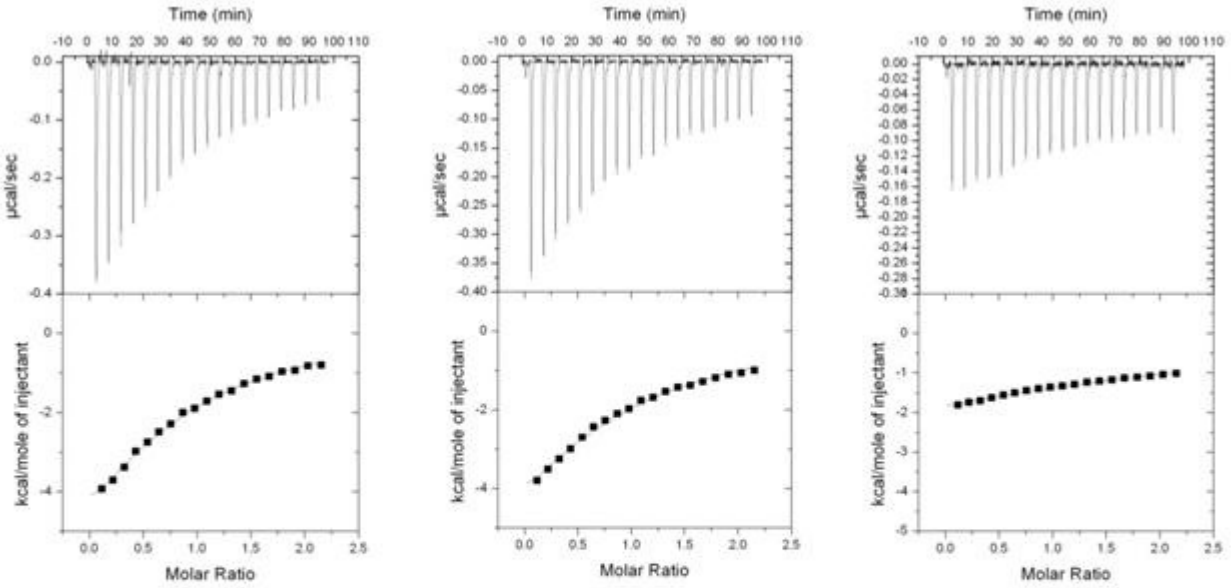

Figure 5-9. The Electrostatic Interaction of PME1-PP2A$_A$ Complex. The figure shows the titration of 25 µM of PP2A$_A$ with 19 15 - µl injections of PME1 (250 µM) at different sodium chloride concentration, 50, 100 and 150 mM and indicates that increasing salt concentration will interfere with the association of PME1 and PP2A$_A$ through electrostatic type of interactions.

5.3.3 The Putative Site of PME1 for PME1-PP2A$_A$ Interaction

Based on the previous experiments, the polar segment (residues 239 to 283) of PME1 may play an important role in dominating PP2A$_A$ and PME1 interaction. Truncation of this segment from PME1 will completely abolish the interaction between PME1 and PP2A$_A$. PP2A$_A$ was shown to interact with other proteins such as regulatory subunits and small T antigen. Do these proteins also contain the similar segment in their protein sequence? The sequence of PME1 was compared with PR61, PR55, and SV40 small T antigen respectively via pairwise sequencing alignment using blastp (*NCBI*) [275] and ClaustalW (*EMBL-EBI*) [257]. Unfortunately, there is no similarity among these proteins. In addition, highly polar region segment was not observed in PR55, PR61, or small T antigen interacting with PP2A$_A$. Although these proteins all interact with PP2A$_A$ at similar region (HEAT repeats 2 to 7), the participating residues from the interacting proteins are very different and it will be difficult to postulate a common mode of interaction.

The next question that was investigated was whether the specific polar amino acid segment (residues 239 to 283) was sufficient for the interaction with PP2A$_A$ to occur even within the context of a different protein (not PME1). Will the protein with the same polypeptide segment engineered be able to associate withPP2A$_A$? To improve the solubility of the polypeptide, glutathione-s-transferase and NusA fusion proteins were created incorporating this segment at the C-terminus. PME1_ET$_{239\text{-}283}$ containing NusA sequence and PME1_GE$_{239\text{-}283}$ including GST tag were made and successfully expressed. In addition, native GST tag and NusA protein were also expressed and purified

to be used in the control ITC experiments.

In order to ensure that glutathione-S-transferase and NusA protein will not interact with $PP2A_A$, 100 μM of glutathione-S-transferase and NusA protein were titrated with with 19 15 - μl injections into the cell containing 10 μM of $PP2A_A$ at 10 ℃. The ITC signal showed that there was no interaction between native GST or NusA protein and $PP2A_A$ due to non-significant heat change (Figure 5-10a).

$PME1\_GE_{239\text{-}283}$ and $PME1\_ET_{239\text{-}283}$ were also prepared for ITC experiment. 150 μM of $PME1\_GE_{239\text{-}283}$ and $PME1\_ET_{239\text{-}283}$ were used to titrate 20 μM $PP2A_A$ at 10 ℃. Unfortunately, no significant heat change signal could be observed in these ITC measurements either (Figure 5-10b). Three explanations for the observed lack of interaction could be put forward. First, the residues 239 to 283 of PME1 may not be the only target site in PME1 and $PP2A_A$ interaction. Second, the residues 239 to 283 are situated in the middle of PME1 polypeptide chain, whereas in $PME1\_GE_{239\text{-}283}$ and $PME1\_ET_{239\text{-}283}$ they were connected with the C terminus of glutathione-S-transferase or NusA protein. The specific protein topology context within the PME1 may thus be required for the formation of the appropriate binding surface and influence the interaction. Finally, native glutathione-S-transferase will form dimer (55.4 kDa) and NusA protein is normally a tetramer (260 kDa). However, when these two proteins were fused with residues 239 to 283 of PME1, $PME1\_GE_{239\text{-}283}$ formed tetramer (126 kDa) while $PME1\_ET_{239\text{-}283}$ still kept original tetrameric form (258 kDa) based on the calibration results of the size exclusion chromatography, Hi Load 16/60 Superdex 200 Prep Grade column (*GE Healthcare*). Interestingly

addition of the polar polypeptide segment seems to have induced further oligomerisation of the glutathione-S-transferase.

Although, the experiments described here clearly showed that PME1 polar residues segment 239-283 is necessary for $PP2A_A$ interaction, current data does not show that the specific polypeptide region is sufficient for the reaction to occur. Perhaps the only way to show details of PME1-PP2A interaction would be by determining the structure of a full length PME1-PP2A complex.

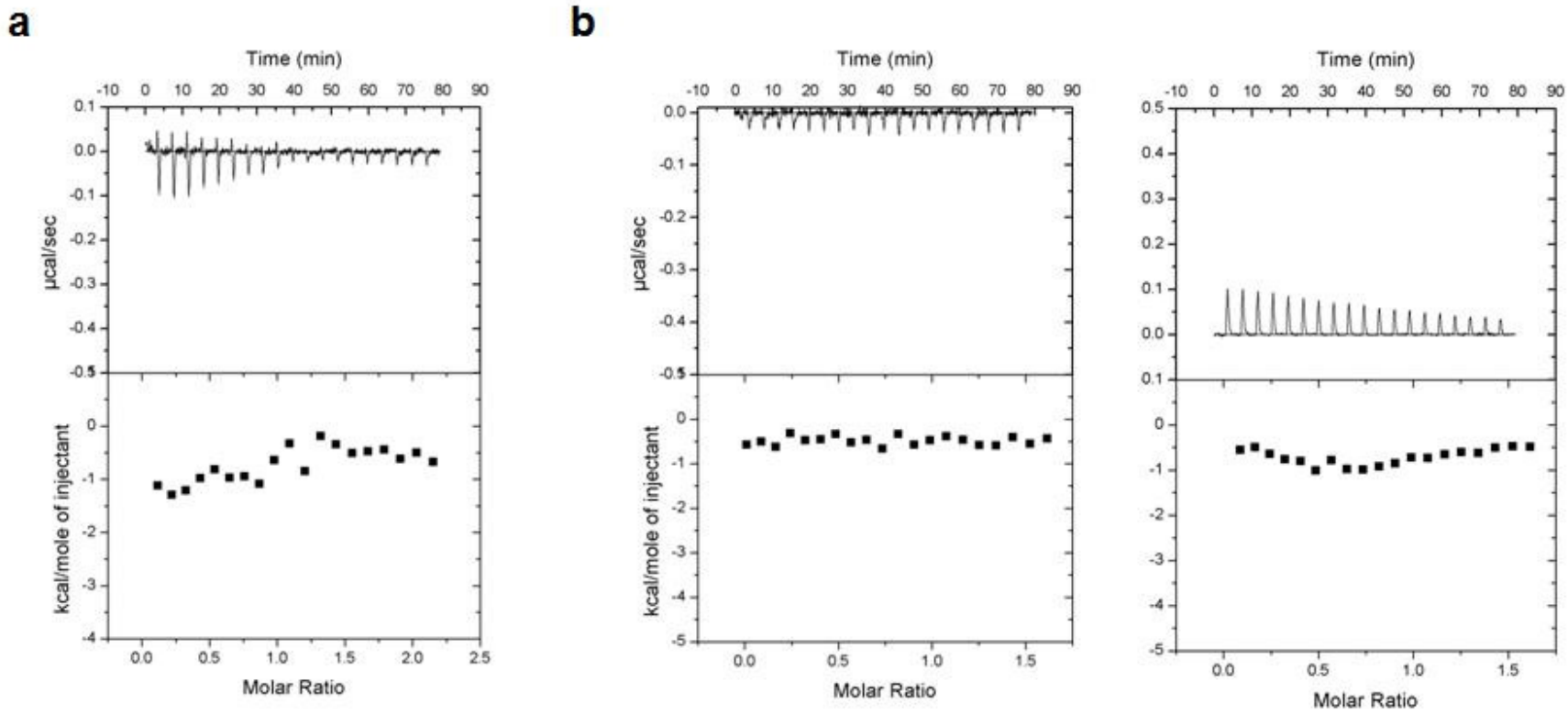

Figure 5-10. The ITC Analysis for PME1_GE$_{239-283}$/PME1_ET$_{239-283}$ and PP2A$_A$ Interactions. (a) The ITC analysis showed that there is no interaction between either NusA or GST protein and PP2A$_A$. (b) No significant heat change was detected in PME1_GE$_{239-283}$/PME1_ET$_{239-283}$ and PP2A$_A$ experiments, suggesting lack of interaction between these molecules.

5.4 A Potential Inhibitor of PME1

The okadaic acid, a toxin found in bivalves, causes diarrhetic shellfish poisoning. The molecular formula of okadaic acid is $C_{44}H_{68}O_{13}$, a derivative of a C_{38} fatty acid [276]. In addition, okadaic acid is a strong inhibitor of PP1, PP2A, and PP2B. The inhibitory effect of okadaic acid is strongest for PP2A, followed by PP1, and then PP2B. *In vitro,* PP2A is inhibited by okadaic acid at a concentration of 1–2 nM and the dissociation constant of the inhibition on protein serine / threonine phosphatase 2A is about 30 pM. Therefore, okadaic acid was a potential tumor promoter through inhibiting PP2A and PP1 [101;277].

Previous studies suggested that PME1 is an okadaic acid-sensitive methylesterase in vivo. Thus, PME1 may associate with okadaic acid. If it's true, okadaic acid would be a good ligand for co-crystallization with PME1. In order to determine the thermodynamic parameters of PME1-okadaic acid interaction, 10 μM of PME1 was prepared for ITC analysis with 19 15 - μl injections of 100 μM okadaic acid at 10 ℃. However, there is no significant heat change in PME1-okadaic acid experiment suggesting that okadaic acid is not PME1 ligand (Figure 5-11). This data is not consistent with the results of an *in vivo* study reported by Stock's group [278]. Previously, it was shown that okadaic acid interferes with the demethylation of PP2A and the author proposed that okadaic acid may be an inhibitor of PME1. Most likely, PME1 not only associates with the C terminus of $PP2A_C$ but also interacts with the active site of $PP2A_C$ at the same time and thus it may compete for binding with the okadaic

acid. This suggestion is supported by the structure of PME1-PP2A complex. The details of PME1 and $PP2A_C$ interaction were described in chapter one (1.2.1). The binding affinity of okadaic acid for $PP2A_C$ is rather high and it either competes PME1 out or it may act as an allosteric inhibitor of $PP2A_C$ and PME1 interaction.

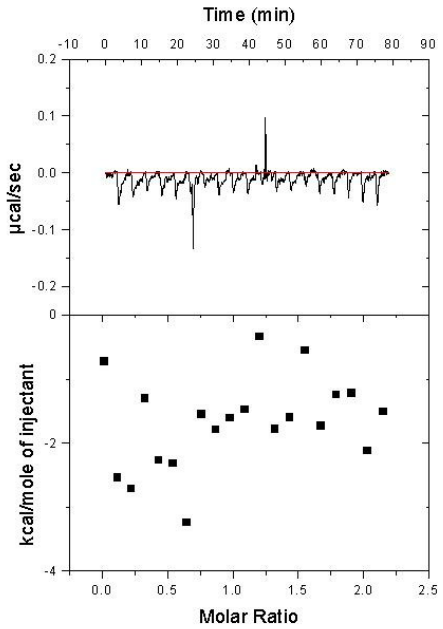

Figure 5-11. Isothermal Titration Calorimeter (ITC) Analysis of PME1 Binding Ability to Okadaic Acid. 300 µl of okadaic acid (100 µM) was prepared for the binding reaction with 1.4 ml PME1 (10 µM). The titration protocol included 19 15 µl injections.This analysis demonstrated that PME1 does not directly interact with okadaic acid.

5.5 Summary

The results of ITC and BIAcore experiments both support the thesis that PME1 but not LCMT1 can interact with $PP2A_A$. This result is not consistent with the reported crystal structure of $PME1_{39-376}$-$PP2A_{HEAT1,11-15}$ complex showing that PME1 only associates with $PP2A_C$. In addition, a positive heat capacity change suggested a highly polar region of dehydration during PME1-$PP2A_A$ interaction. This region was determined to include polar amino acids segment of residues 239 to 283 of PME1. This segment was omitted in the protein used to obtain the crystal structure of $PME1_{39-376}$-$PP2A_{HEAT1, 11-15}$ complex.

The analysis of $PME1_{39-376}$-$PP2A_A$ interaction using ITC equipment also supported the hypothesis that $PME1_{39-376}$ lost its ability to associate with $PP2A_A$. Increasing ionic strength of ITC buffer interferes with the association of PME1 with $PP2A_A$ due to the neutralization of electrostatic interactions through the highly polar region, residues 239 to 283.

Finally, although PME1 was demonstrated an okadaic acid sensitive protein *in vivo*, no interaction was observed between PME1 and okadaic acid in ITC analysis.

Chapter Six

X-ray Crystallography of LCMT1

Although the structure of *Saccharomyces cerevisiae* protein phosphatase methyltransferase 1 (PPM1) was solved in 2004 [223], the structure of human leucine carboxyl methyltransferase 1 (LCMT1) is still unknown. Based on the PSIPRED secondary structure prediction [228,229], several constructs, including $LCMT1_{61\text{-}334}$, $LCMT1_{1\text{-}321}$, $LCMT1_{9\text{-}321}$, $LCMT1_{16\text{-}321}$, and $LCMT1_{20\text{-}321}$, of LCMT1 are accomplished and expressed in *E. coli* cells. Unfortunately, only $LCMT1_{61\text{-}334}$ could express soluble proteins. In addition, only the $LCMT1_{20\text{-}334}$ construct, made by Dr. Roger Geroge in our group, could express soluble protein and form crystals [234]. However, the resolution of the $LCMT1_{20\text{-}334}$ protein crystals (7 Å) is not suitable for structure determination. Several methods were also used for the refinement of crystals from $LCMT1_{20\text{-}334}$ construct. Recently, new constructs, $LCMT1_{7\text{-}232}$, $LCMT1_{7\text{-}334}$ and $LCMT1_{SD20\text{-}334}$, were designed based on limited proteolysis method. The $LCMT1_{7\text{-}334}$ and $LCMT1_{SD20\text{-}334}$ construct could express large amount of soluble protein (6 mg per Liter cells).

In addition, $LCMT1_{SD20\text{-}334}$ construct protein can form crystals. The 2 Å resolution of $LCMT1_{SD20\text{-}334}$ crystal enabled solution of the structure of human LCMT1. This chapter includes the development of $LCMT1_{20\text{-}334}$ and $LCMT1_{SD20\text{-}334}$ crystals and the improvement of crystal quality of $LCMT1_{20\text{-}334}$. In addition, a model of LCMT1 was generated using the bioinformatic program, Modeller 9v2 [231], for molecular replacement. Finally, the structure of human LCMT1 was determined and compared with yeast PPM1. This structure suggested the potential mode of interaction between PP2A and LCMT1.

6.1 Molecular Modelling

Based on the secondary structure comparison of LCMT1 and PPM1 as described in chapter three, the structure of PPM1 and LCMT1 are most likely very similar. In order to understand the catalytic mechanism and predict the structure of human LCMT1, a full length model was generated using the program Modeller (Figure 6-1a) [231]. The yeast protein phosphatase methyltransferase 1 (PPM1) was used as a template. In addition, the generated model of LCMT1 could be used for the molecular replacement methods of phase determination. The model was analyzed using PROCHECK [232] and a summary of the data obtained from PROCHECK is shown in Figure 6-1b.

(a)

(b)

	Human LCMT1 (residues 1-332)
Sequence Identity	**28%**
Ramachandran plot	0.7% disallow (Lys329 & Lys162)
Chi1-Chi2 torsion angle	Two disallow (ILE125 & Trp105)
Residue properties	1. 0 chi value disallow 2. Seven omega torsion angle disallow (Asp19, Arg26, Ser161, Val199, Arg235, Arg247, and Gly253) 3. Max.deviation : 5.6 (Cys184) 4. Bond len/angle: 6.8 (Asn270) 5. Bad contacts: 7
G-factors (above -0.5) (overall average)	-0.06
Main-Chain bond length	98.7% within limits
Main-Chain bond angle	93.4% within limits
Planar groups	100% within limits

Figure 6-1. The Model of Human LCMT1. (a) The overall structure of LCMT1 and PPM1 (PDB: 1RJG) [223] are very similar. (b) The model was further assessed using PROCHECK [232].

6.2 The Refinement of LCMT1$_{20\text{-}334}$ Crystals

The crystallization conditions for LCMT1$_{20\text{-}334}$, mixed with the ligand *S*-adenosylhomocysteine (*Sigma*) in a 1:1 molar ratio, were screened using commercial screen kit by vapour diffusion hanging drop or sitting drop method. Some irregular small crystals could be found in conditions containing ammonium sulphate and PEG as describe in section 3.1.3. This condition was similar to those previously reported by Dr. Roger Geroge in our laboratory [234]. Therefore, this crystallization conditions were further refined. Some methods used for improvement of crystal diffraction quality and the refinement of crystallization conditions, such as dehydration, annealing and seeding are discussed in the following sections.

6.2.1 The Optimal Condition for LCMT1$_{20\text{-}334}$ Crystals

The original condition for LCMT1$_{20\text{-}334}$ crystallization is 0.1 M Na-citrate (pH 5.6), 2 M ammonium sulphate, 0.38 M Na-K tartrate, 2 % PEG 400, 4 % acetone and 5 mM DTT at 22 ^{o}C. However, the crystals from this condition were not only small but also irregular and weakly diffracting. To refine the condition, the pH value, type of buffer, and the concentration of other components were all slightly adjusted. Based on manual hanging drop screening, the optimal pH range for LCMT1$_{20\text{-}334}$ was about pH 6.0 to pH 6.3. Protein was more likely to precipitate at pH value above 6.3 or below 6. The pH range is more important than the type of buffer. Protein was also crystallized in MES, MOPS, and phosphate buffer in different pH range. A lot of small and irregular crystals

(about 0.02 mm) will be easily formed within 24 hours when higher concentration of the main precipitant, ammonium sulphate (1.8-2.0 M) was used. When the concentration of ammonium sulphate is slightly lowered (about 1.6 M -1.4M), the size of protein crystal will reach 0.6 mm and the crystals were well developed after 72 hours (Figure 6-2). Potassium sodium tartrate, PEG 400, and acetone very slightly impacted the size of crystals. Increasing the concentration of these precipitants will lead to the precipitation of protein. Therefore, the optimal crystallization condition for $LCMT1_{20\text{-}334}$ is 0.1 M sodium citrate (pH 6.3), 1.6 M ammonium sulphate, 0.38 M potassium sodium tartrate, 2 % PEG 400, and 4 % acetone at room temperature. Unfortunately even though the crystal size could reach 0.7-0.8 mm, maximum x-ray diffraction resolution for these crystals is only 7 to 7.5 Å. Synchrotron radiation increased the resolution only to maximum of 6.5 Å.

6.2.2 Additive Screening Method for New Crystal Form

To improve the quality of crystal, Additive Screen Kit (*Hampton Research*) and the Opti-Salt Suite (*Qiagen*) were used for additive screening. 0.1 M sodium citrate (pH 6.3), 1.6 M ammonium sulphate, and 2 % PEG 400 were all kept in crystallization reagent for mixing with additives as described in section 2.7.6.3.3. Unfortunately, only similar protein crystals were observed in additive condition, potassium sodium tartrate.

6.2.3 Dehydration of Crystals

The unit cell size may be related to the low resolution of $LCMT1_{20\text{-}334}$ crystals. A

lot of factors such as protein size, the tightness of the protein packing, protein number in asymmetric unit will determine the unite cell size. Therefore, dehydration of crystals could remove the excess solvent content, tighten packing of the protein molecules and reduce the size of the solvent channel. Four methods were employed for $LCMT1_{20-334}$ protein crystals dehydration as described in section 2.7.6.3.1. Due to the high concentration of salt in crystallization reagent, salt crystallized in very short time and reagent condition also changed rapidly. Therefore, the $LCMT1_{20-334}$ crystals were seriously damaged in method I and II. In method III, although the reagent was not exposed to air, directly transferring crystals to higher concentration of precipitants resulted in crystal damage. Finally, $LCMT1_{20-334}$ crystals were tested in the last method, method IV, and analyzed using low temperature x-ray diffraction (-173 ^{o}C). The resolution of crystals was slightly improved but not very significantly (Figure 6-3).

In addition, MicroRT™ Capillaries (*MiTeGen*) were used for salt dehydration of $LCMT1_{20-334}$ crystals as described is section 2.7.6.3.1. Each capillary was filled with each kind of salt resulting in different relative humidity. For dehydrating the protein crystal, the crystal was serially transferred to each capillary for 30 minutes at room temperature to decrease the relative humidity. Each protein crystal was applied to low or room temperature x-ray diffraction. The increased mosaicity of diffraction patterns showed that protein crystals were seriously impaired through this method (Figure 6-4).

Thus, the dehydration method did not significantly improve the resolution of $LCMT1_{20-334}$ crystals and, the protein packing may not be a reason for low

diffraction resolution of crystals.

6.2.4 Annealing Method

The uniformity of the unit cells also plays an important role in scattering pattern. Disordered unit cell will increase mosaicity and reduce the diffraction resolution. Sometimes, crystal annealing method can reduce disorder induced by flash cooling. The methods were described in section 2.7.6.3.2. Unfortunately, both methods did not improve the resolution of the crystals (Figure 6-5). The uniformity of unit cell may not be related to the low resolution problem in $LCMT1_{20\text{-}334}$ crystals.

6.2.5 Seeding Method

All x-ray diffraction experiments showed that there were always very few scattering spots in each diffraction pattern. It may suggest very few unit cells or very large unit cell size in one crystal. The low resolution of the data may be a consequence of a large size of the unit cell which contains a lot of molecules in one asymmetric unit. Therefore, finding a new crystal form may be the only way to solve the problem. To achieve this purpose, a seeding method and generation of new protein constructs were both tested in search for a new crystal form of LCMT1.

To optimize the quality of crystal, seed bead kit (*Hampton Research*) was used in generating seeds of protein crystals. Seeding will assist crystals to form in the

metastable zone which provides reproducibility and improvement of a crystallization experiment. In addition, by placing a seed or solution of seeds in a drop can help crystals, which cannot spontaneously nucleate, to grow from seeds and by performing serial dilutions from a concentrated seed stock, one can control the number of crystals grown in the drop. The detail of seeding method for $LCMT1_{20\text{-}334}$ was described in 2.7.6.3.4. Although a lot of crystals were formed in different conditions, no new crystal form was observed in the screening tray. The hexagon crystals were also analyzed through x-ray diffraction; however, no breakthrough was observed in these experiments.

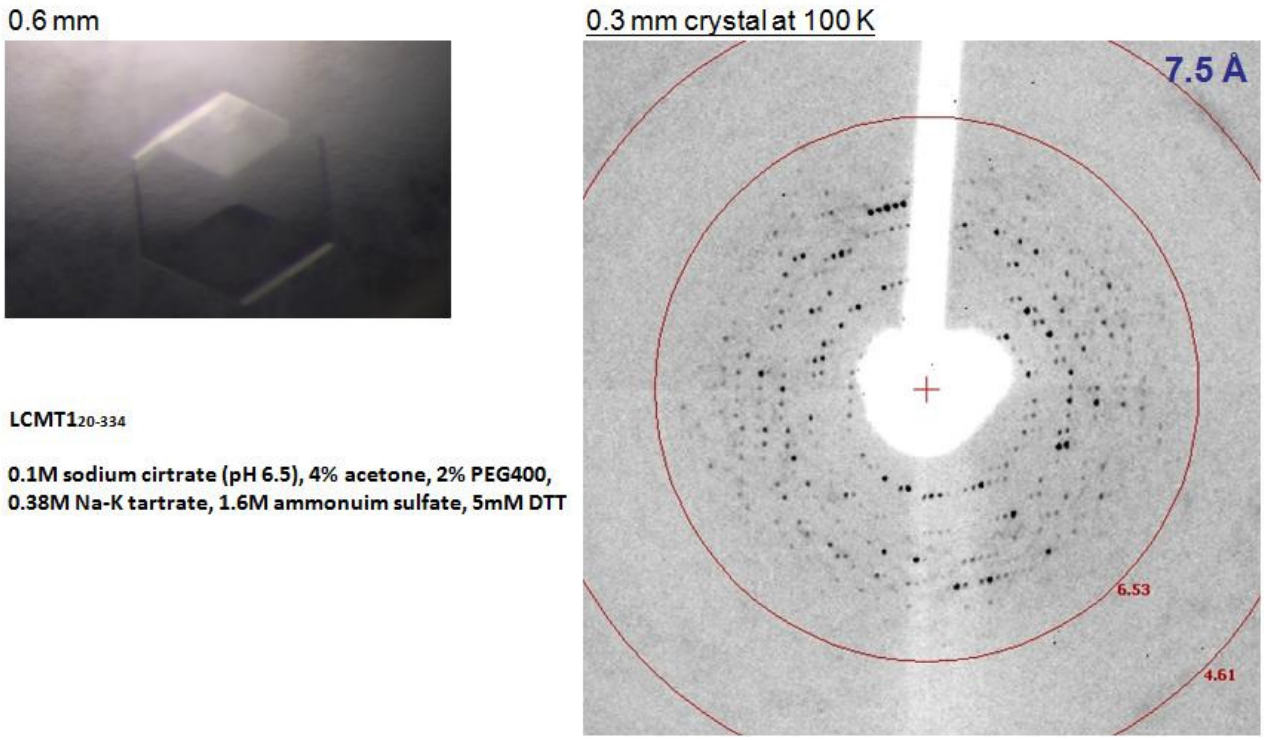

Figure 6-2. The Development of LCMT1$_{20\text{-}334}$ Protein Crystals. The crystallization condition of LCMT1$_{20\text{-}334}$ was refined and optimized. The diameter of largest protein crystal can reach 0.6 to 0.7 mm. However, the resolution of these crystals was not significantly improved.

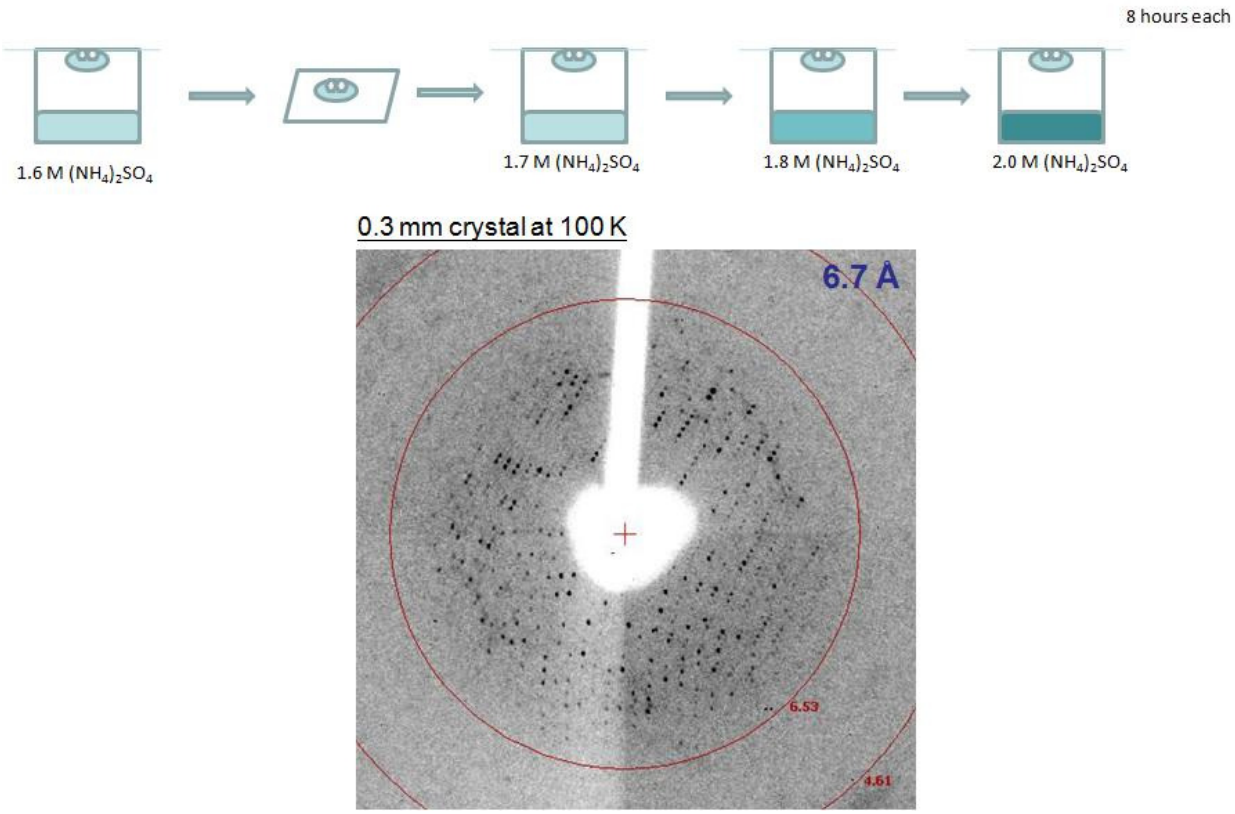

Figure 6-3. The Dehydration Method of LCMT1$_{20-334}$ Crystals through Increasing Precipitants. The protein crystals were dehydrated and equilibrated over reservoir containing serial increase of concentration of precipitant, ammonium sulphate. The x-ray diffraction analysis showed that the resolution of protein crystals was not significantly improved.

Salt	Solubility (g/ml)	r.h.
Sodium Benzoate	0.67	88%
Potassium Chloride	0.40	86%
Cadimonium Chloride	1.41	82%

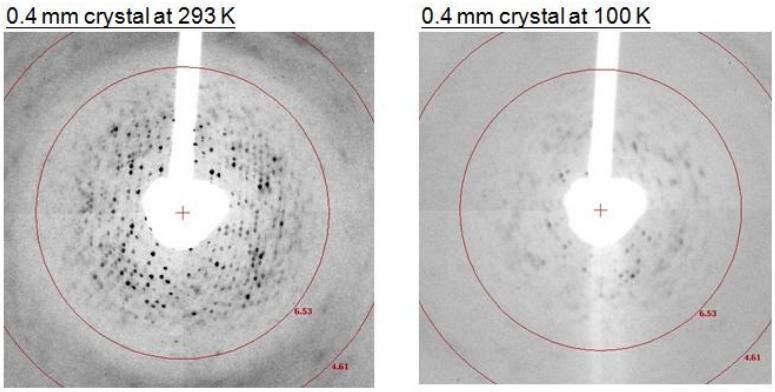

Figure 6-4. The Salt Dehydration Method of LCMT1$_{20\text{-}334}$ Protein Crystals. The protein crystal was serial situated in each capillary, containing different types of salt, for 30 minutes; thus, the relative humidity was serially decreased to dehydrate the protein crystal. Here, when the relative humidity reached 82%, the protein crystals were starting to crack. Therefore, the potassium chloride was used for crystal dehydration. The left and right figure showed the x-ray diffraction of crystals at room and cold temperature respectively. Unfortunately, both results are not satisfactory.

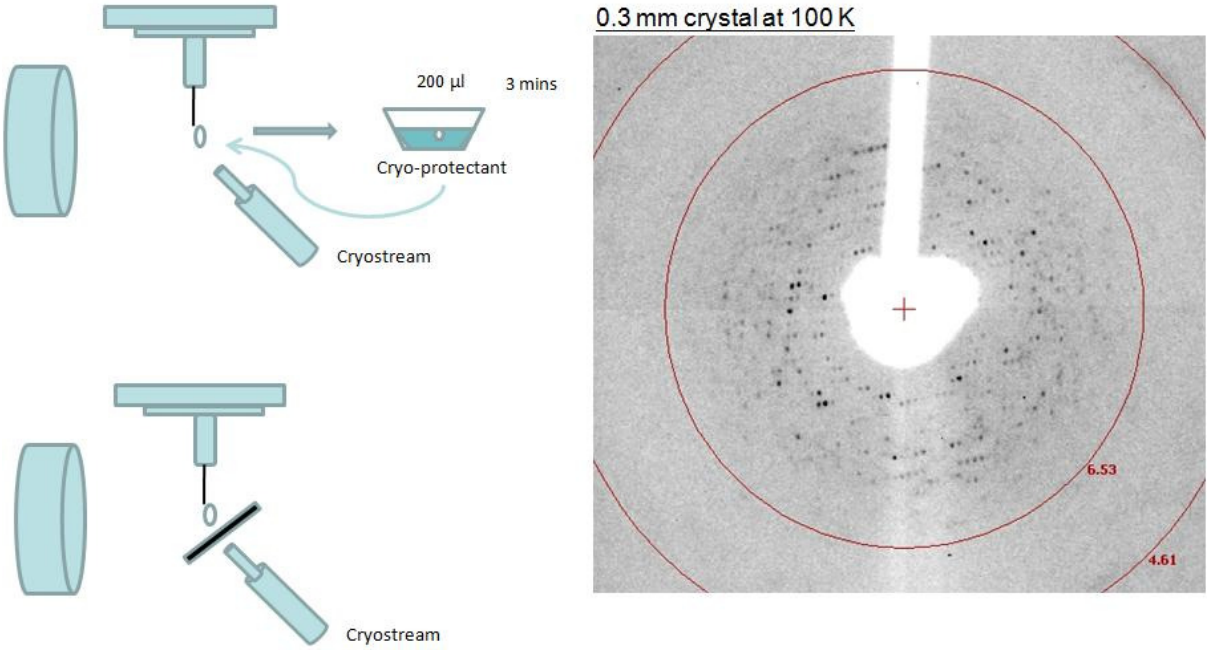

Figure 6-5. Two Anneal Methods for Crystals. Two methods were applied for LCMT1 crystal annealing. The method one (up left corner figure) seriously damaged the crystals. In method two (down left corner figure), the diffraction pattern showed that annealing of crystals did not improve the resolution.

6.3 New Constructs

6.3.1 Crystallization of New Construct Protein

The new constructs were designed based on the limited proteolysis method and well expressed in *E. coli* cells as described in section 3.1.1.2 and 3.1.3 The $LCMT1_{7\text{-}334}$ protein was also set up in crystal trays using the sitting drop method through high throughput screening. However, only phase separation could be observed in some conditions of screening kits, ammonium sulphate suite and PEG suite (*Qiagen*), which is similar with the condition for $LCMT1_{20\text{-}334}$ protein crystallization. The $LCMT1_{20\text{-}334}$ crystallization buffer was also used and adjusted for $LCMT1_{7\text{-}334}$ protein. Unfortunately, no crystal was formed in these conditions.

$LCMT1_{20\text{-}334}$ was not very soluble but could form crystals, whereas $LCMT1_{7\text{-}334}$ was very soluble but no protein crystallization occurred. Combining both characters in one construct may be helpful for protein solubility and crystal growth. $LCMT1_{SD20\text{-}334}$ was designed based on these two constructs. Like $LCMT1_{7\text{-}334}$, large amount of $LCMT1_{SD20\text{-}334}$ protein could be harvested from *E. coli* cells. As prediction, this protein could successfully form crystals in several conditions with different precipitants (PEG 3350, PEG 5000, PEG 8000, ammonium sulfate, or Jeffamine ED-2001) (Fig 3-7). The resolution of crystals (1.7 to 2 Å) was also greatly improved. The pentaerythritol ethoxylate was a good cryoprotectant for low temperature X-ray diffraction. The crystal from the condition, 0.05 M Bis-Tris pH 6.5, 0.05 M ammonium sulfate and 30%

pentaerythritol ethoxylate, was chosen for X-ray data collection.

6.3.2 Structure Determination

The images from charged-coupled device (CCD) detectors were processed using the program, d*TREK (*Rigaku*) [246]. A list of Bragg reflections contains their Miller indices (*h, k, l*), the integrated intensities *I* (*hkl*), and standard deviations, sigma (*I*). The summary of data collection was list in Table 6.1.

The crystal structure of the human LCMT1 was determined through molecular replacement program, Phaser/CCP4 suite [233]. The homology model for the core structure of LCMT1 as the starting model was described in section 6.1. The initial model covered ~75 % of the amino acid residues, including residues 62-108, residues 114-137, residues 157-231 and residues 258-321, present in the polypeptide chain used to obtain crystals.

After molecular replacement, the structure was refined using RefMac/CCP4 suite [233]. The final refinement statistics are also listed in Table 6.1.

	$LCMT1_{SD20-334}$
Data	
Space group	$P2_12_12_1$
Unit cells (Å) (a, b, c)	49.09, 63.30, 81.8
Resolution (Å)	17.53-2.0 (2.07-2.0)
Measured reflections	76195 (4418)
Unique reflections	17062 (1587)
Completeness (%)	96 (91.2)
R_{merge}	0.057 (0.335)
I/σ (I)	17.5 (2.2)
Refinement Statistics	
Resolution Range	17.53-2.0 (2.07-2.0)
R_{cryst}	0.20
R_{free}	0.26
Mean B factors (Å^2)	32.8
Water molecules	138
r.m.s.d.bond length (Å)	0.016
r.m.s.d. bond angles (°)	1.6
Ramachandran plot (%) (Favored, allowed, disallowed)	(98.6, 100, 0)

†R_{merge}= $\sum_h\sum_i$ | Ih,i - <Ih> | / $\sum_h\sum_i$ <Ih> where Ih,i is the ith used observation for unique hkl h, and <Ih> is the mean intensity for unique hkl h. ‡ With respect to Engh and Hubber parameters (Engh & Hubber, 1991).

Table 6.1 Data Collection and Refinement Statistics

6.4 The Crystal Structure of Human LCMT1

6.4.1 The Overall Structure of Human LCMT1

Human LCMT1 belongs to the Class I AdoMet-dependent MTase family, a member of the FAD/NAD(P) binding Rossmann fold superfamily (Figure 6-6a) [279]. The main structural feature of LCMT1 is a seven-stranded β-sheet flanked by α-helices, with the core β-strands arranged in the following order, β3, β2, β1, β4, β5, β7, and β6. The strands (β1 to β5 and β6) surrounded by the six α-helices (αZ and αA to αE) are parallel, whereas β7 is anti-parallel (Figure 6-6a). In addition to the core domain, several insertions were observed in the human LCMT1 structure. Structural insertions in members of the Rossmann fold superfamily contain substrate recognition motifs and variations in these insertions amongst the methyltransferases are associated with their observed differences in substrate specificities [280]. Even orthologous proteins from different species exhibit significant differences in these embellishments to the core protein fold. Based on the spatial arrangement around the central β-sheet in human LCMT1, variations to the core topology can be grouped into three regions: the β3-β2 region, the β1-β4-β5 region and the β7-β6 region. In the β3-β2 region, helix α3 and strand βA join helix αB to αC to pack against strands β3 and β2. Although, other proteins might have embellishments at this site, their structures differ significantly. For example, in the structure of the bacterial protein methyltransferase CheR, there is a small subdomain at this position, which serves as a point of the attachment to its membrane associated substrate [281]. In the β1-β4-β5 region, helices α4, α1 and α2 are placed at the

C-terminal edge of the central β-sheet, near the entrance to the enzyme active site. Location of the N-terminal helices α1 and α2 is similar to the location of the N-terminal regions in other methyltransferases, where they have been implicated in substrate recognition [281]. In the β7-β6 region, three helices, α5, α6 and α7, create a topological insertion arranged in a triangular fashion, while packing against helix αZ through hydrophobic interactions. Helices α1, α5, α6 and α7, as well as the associated connecting loops, are all in the vicinity of helix αZ such that they completely bury the N-terminal end of the helix αZ inside the hydrophobic core of the protein (Figure 6-6b). The role of the described topological additions and insertions to the Rossmann fold is dual: it is both structural, in providing the stabilizing hydrophobic environment for the central β-sheet, and functional, in creating the platform for the site of the specific interactions with the substrate, in this case the PP2A molecule. The crystal structure of human LCMT1 is missing a 26-residues long polypeptide fragment that would represent the fourth site of the topological insertions, located between strand β5 and the helix αE and this part of the structure would also be placed at the C-terminal edge of the central β-sheet thus forming the entrance to the active site together with other described inserted structural elements (Figure 6-7). The corresponding region in the yeast structure, labeled αY in Figure 6-7, exhibited great flexibility and it is tempting to postulate that this domain acts as a lid for the active site that enables substrate interaction and that might become ordered upon binding of PP2A. Superimposition of PPM1 structure including that region on the structure of LCMT1 indicates that the region could not be accommodated within the same crystal form of LCMT1, as it would interfere with crystal packing, which might explain the difficulty in

crystallizing the full-length form of the protein.

a

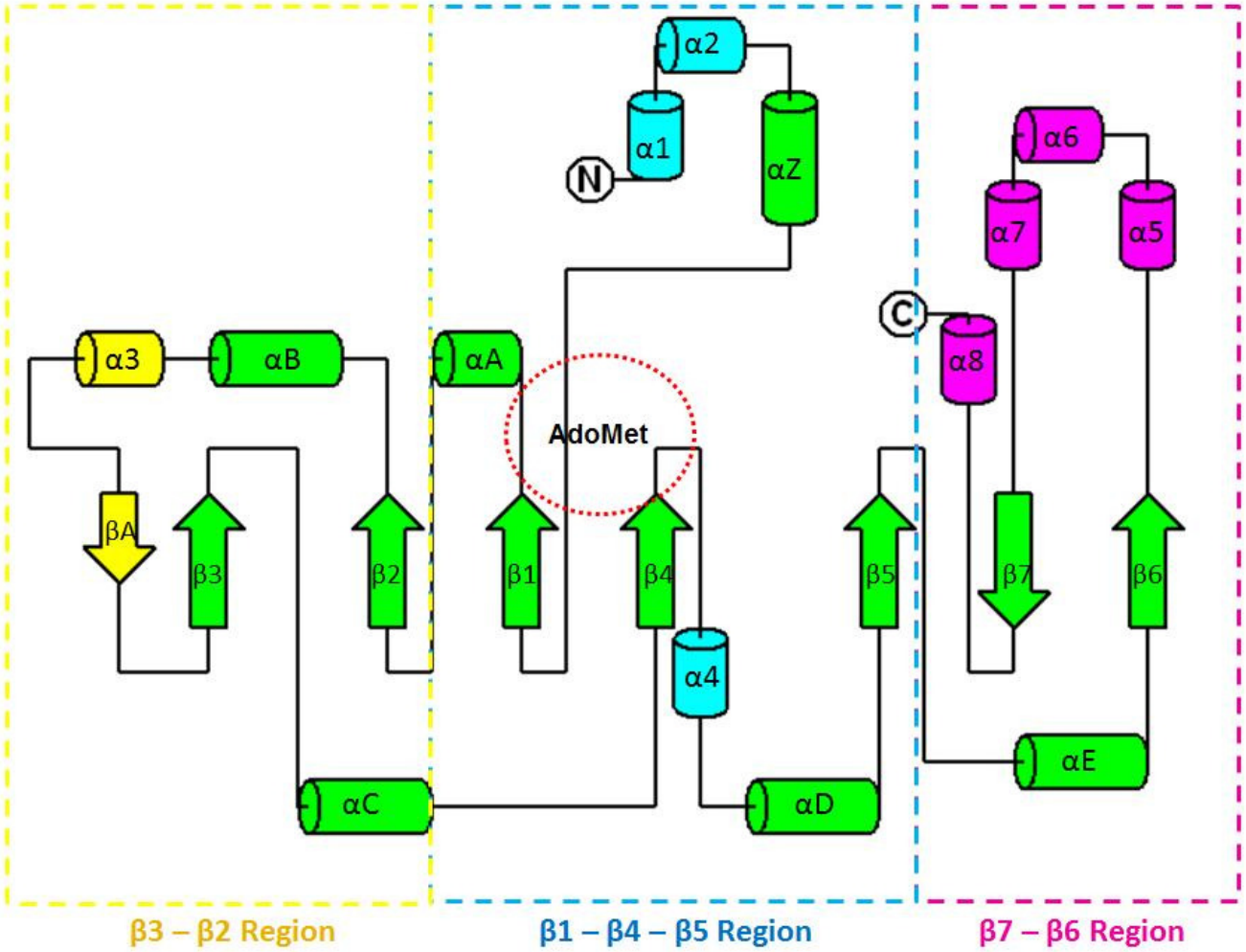
α2
α1
N
αZ
α6
α7
α5
C
α8
α3
αB
αA
AdoMet
βA
β3
β2
β1
β4
β5
β7
β6
α4
αE
αC
αD
β3 – β2 Region
β1 – β4 – β5 Region
β7 – β6 Region

b

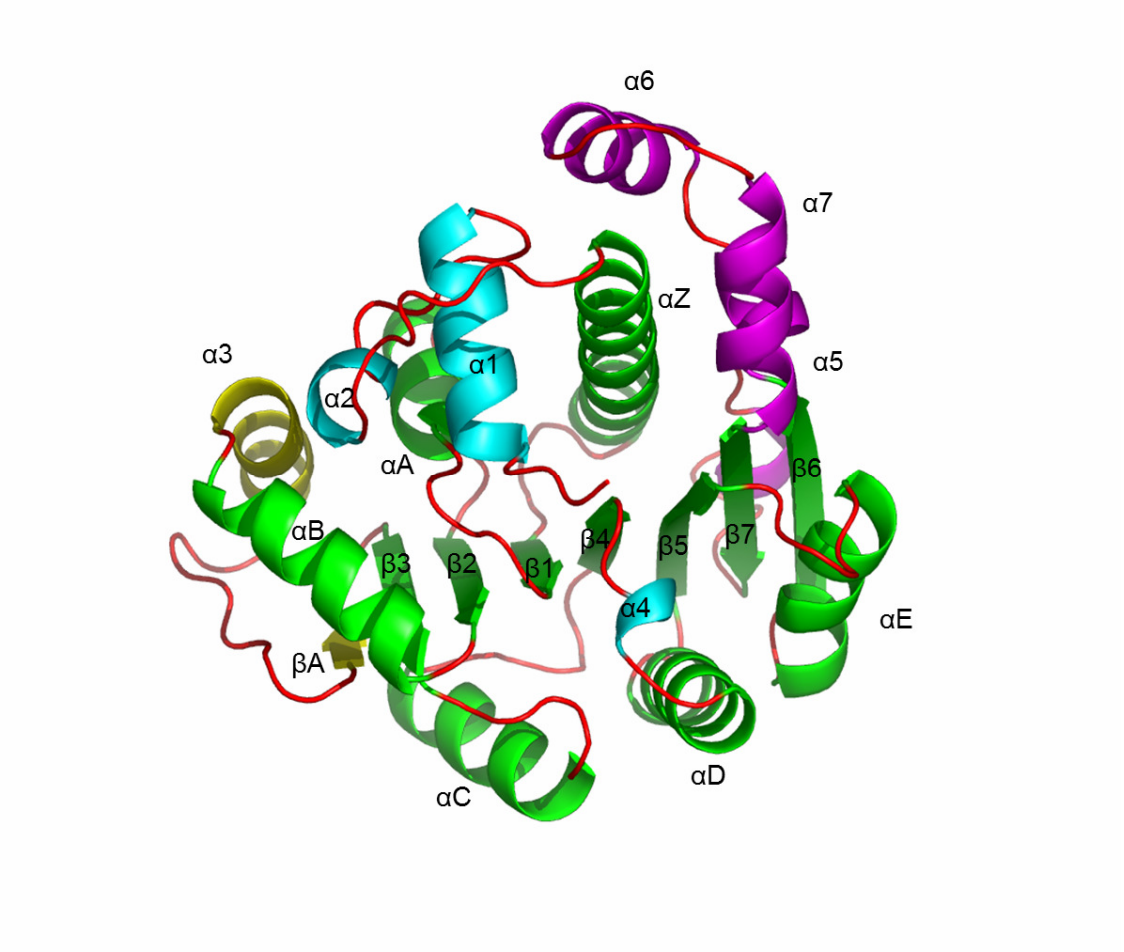

C

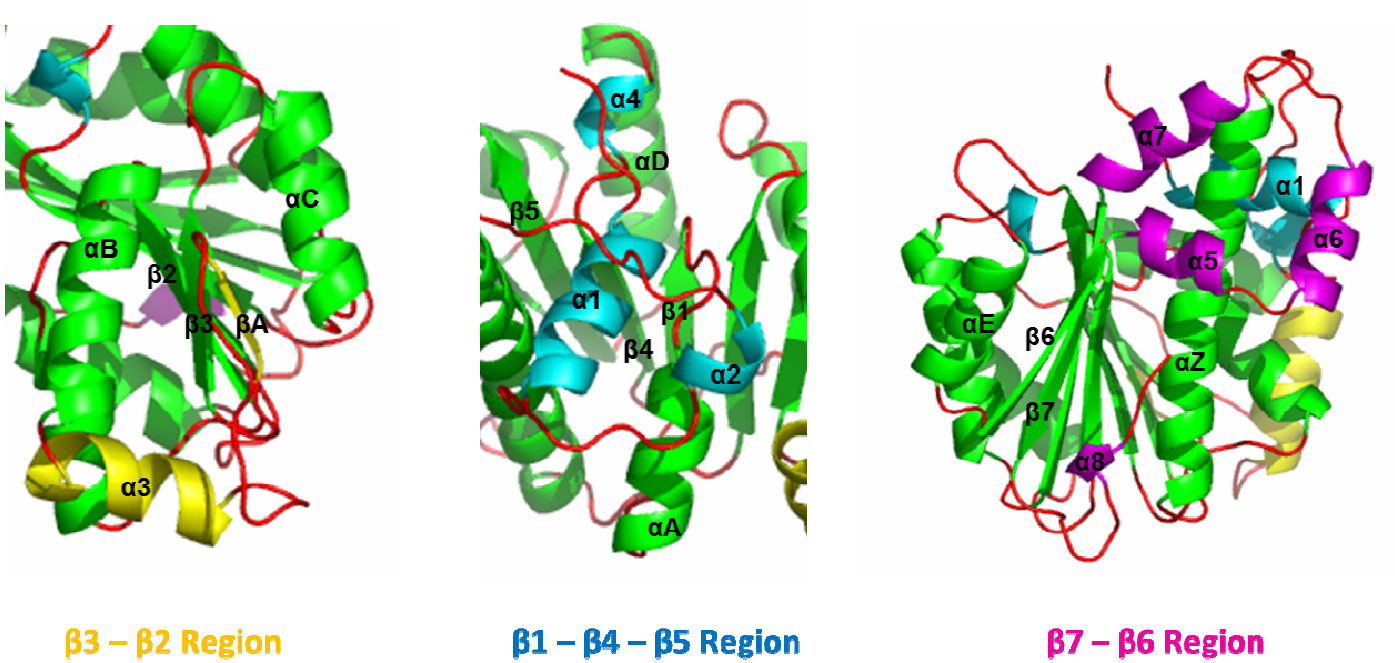

Figure 6-6. The Overall Structure of LCMT1. (a) Topology diagram of human leucine carboxyl methyltransferase 1. (b) The core structure of LCMT1 containing a seven-stranded β sheet (β3, β2, β1, β4, β5, β7, and β6) flanked by six α-helices (αZ and αA to αE) belongs to the Class I AdoMet-dependent methyltransferase 1 family. The colours of secondary structure elements are represented as follows: the core structure of methyltransferases, green; insertions in the β3-β2 region, yellow; the insertion in the β1-β4-β5 region, cyan; the insertion in the β7-β6 region, pink. A ribbon diagram of LCMT1 generated with PyMOL viewer (*DeLano Scientific LLC*). The

same colour scheme was used as in Fig. 1A. (c) Detailed view of the structural embellishments to the core methyltransferase domain: region β3-β2 (α3 and βA), β1-β4-β5 (α1, α2 and α4), and β7-β6 (α5, α6, α7 and α8).

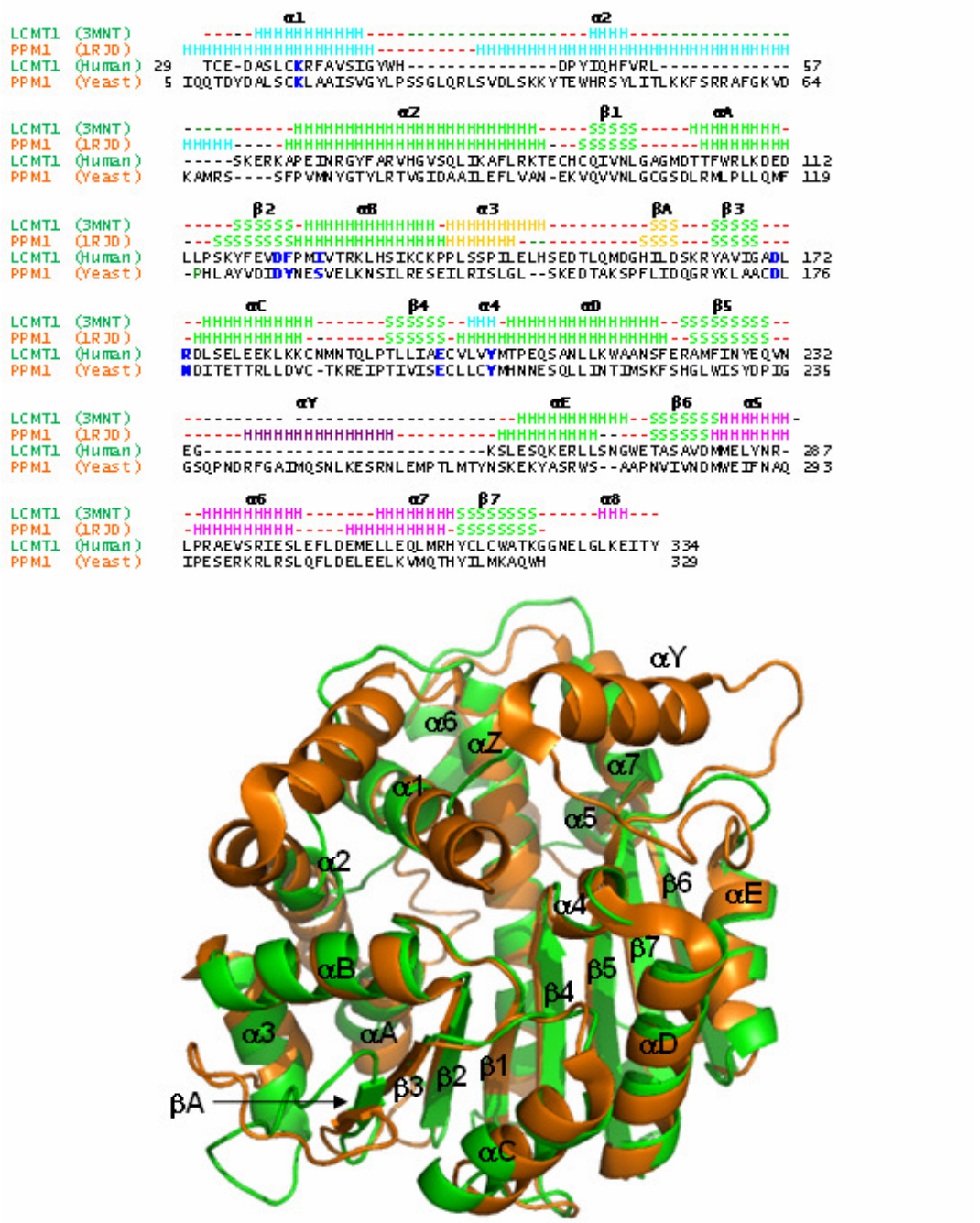

Figure 6-7. Comparison of Human LCMT1 and Yeast PPM1. The sequence alignment, based on the superimposition of yeast PPM1 and human LCMT1 structure, is shown on the top of the figure. The secondary structure elements of human LCMT1 and yeast PPM1 are indicated above the aligned sequences. The colour assignment for the secondary structure of human LCMT1 is the same as in Fig.1. Dashed lines coloured black and red represent gaps in the sequence alignment or protein loops, respectively. The amino acid residues coloured in blue are associated with AdoMet. The *Saccharomyces cerevisiae* PPM1(1RJD) (orange) and human LCMT1 (green) structures were superimposed using Coot 0.6.1. Helix αY in the yeast PPM1 structure is absent from the LCMT1 structure and it was replaced by the EG dipeptide.

6.4.2 Comparison of Human LCMT1 with Yeast PPM1

The molecular replacement method was utilized to solve the crystal structure of human LCMT1 using the crystal structure of yeast PPM1 (PDB id 1RJG) [223] to generate a starting model for the rotation/translation function searches. Initial attempts to solve the structure with a PPM1-based homology model of LCMT1 failed and the successful solution was obtained only with a greatly stripped model of LCMT1. Specifically, the successful molecular replacement model contained the core structure corresponding to the residues 61-321 with all loop/insertion regions removed. The omitted residues were subsequently built into the electron density maps during the process of model building and refinement. The superimposition of the structures of human LCMT1 and *S. cerevisiae* PPM1 (1RJD), using the program Coot 0.6.1 [253], shows that the core regions of the two proteins are very similar, with a root mean square distance of 1.3 Å for 231 Ca-atoms of the aligned residues despite a relatively low sequence identity for the overlapping sequence (~30 %) (Figure 6-7). As expected, the structures exhibit main differences within the associated variable segment. For example, in the β1-β4-β5 region of the human LCMT1 core structure, a short helix α2 is flanked by two flexible long loops, whereas in the same area of yeast PPM1, this part is replaced by a long α helix with a sharp kink in the middle giving the appearance of two helices (Figure 6-7). In contrast, helix α1 within this insertion is strongly conserved in its topology and sequence between LCMT1 and PPM1, most likely due to the direct participation of this helix in the formation of the AdoMet binding site. Additional variations include conformational differences of the α3-loop-βA connection between the helix αB

and strand β3, significant differences in lengths and relative orientation of the C-terminal helices α5, α6, and α7, and the presence of an additional single helical turn α8 at the C-terminal end of LCMT1 (Figure 6-7). Clearly, the structural differences reflect species-specific determinants of protein-protein interactions with the respective partner substrates or potential regulatory proteins.

6.4.3 S-adenosylmethionine Binding Site

An initial electron density map, following the successful molecular replacement solution, was examined for any un-modeled electron density within the core of the LCMT1 structure and we could clearly identify the position and conformation of the AdoMet molecule that was included in the crystallization (Figure 6-8a). The cofactor adopts an extended conformation that is commonly found in AdoMet-dependent methyltransferases and the superimposition of AdoMet binding sites of human LCMT1 and that of yeast PPM1 shows that residues interacting with AdoMet are highly conserved between two proteins (Figure 6-8b). The adenine ring of the bound AdoMet is sandwiched between hydrophobic residues Phe123 and Leu172 in LCMT1, while the equivalent residues in the PPM1 structure are Tyr129 and Leu176. Similarly, as it is the case in many other nucleotide-binding proteins, hydroxyl oxygen atoms from the ribose moiety are positioned in the active site through interaction with the acidic residue, Asp122 in LCMT1, specifically. At the other end of the AdoMet molecule, the carboxylate group is engaged in an ionic interaction with the conserved residues Lys37 (α1) and Arg73 (αZ) while the amino group forms

hydrogen bonds with the backbone carbonyl oxygen from Gly98 (β1-αA connection) and Glu198 (β4) (Figure 6-8b). However, further away from the zone of direct interaction with AdoMet but lining the cavity that creates the binding pocket for the cofactor, there are some significant differences such as the presence of Ile126 in LCMT1 in place of Ser132 in PPM1, Val200 in LCMT1 instead of Leu203 in PPM1, or Arg173 at the top of the adenine ring in LCMT1, compared to Asn177 at the equivalent position of PPM1.

In the structure of human LCMT1 presented here, AdoMet does not appear fully buried into the active site with the side of the cofactor containing the activated methyl group being relatively exposed – AdoMet has a contact area of 17 $Å^2$ as calculated by AreaMol/CCP4 [233]. In contrast, in the structure of yeast PPM1 (1RJD), AdoMet is covered by the beginning of the N-terminal helix α1, which is partially unraveled in the structure of LCMT1. Although the full-length LCMT1 protein contains an additional 20 residues at the N-terminus, the sequence content of that N-terminal segment, dominated by Ser and Cys residues, would suggest that the region is unstructured, at least in the absence of substrate, and, thus, we do not anticipate that the N-terminal residues would be occluding AdoMet in the context of the full-length protein. Partially exposed AdoMet and the surrounding funnel shaped opening indicate an entry site for the carboxyl terminal motif of the PP2A catalytic subunit (T^{304}PDYFL^{309}) which is methylated by LCMT1 on the terminal carboxyl group to form an alpha-leucine ester modification (Figure 6-8c). Examination of a molecular surface of PPM1 identifies a deep and narrow grove that leads toward the only exposed side of the cofactor – an activated methyl group of the bound AdoMet molecule (Figure

6-9a). The equivalent orientation of the human LCMT1 molecular surface reveals a similar groove, strongly suggesting that an extended form of the $PP2A_C$ C-terminus might approach AdoMet through that site.

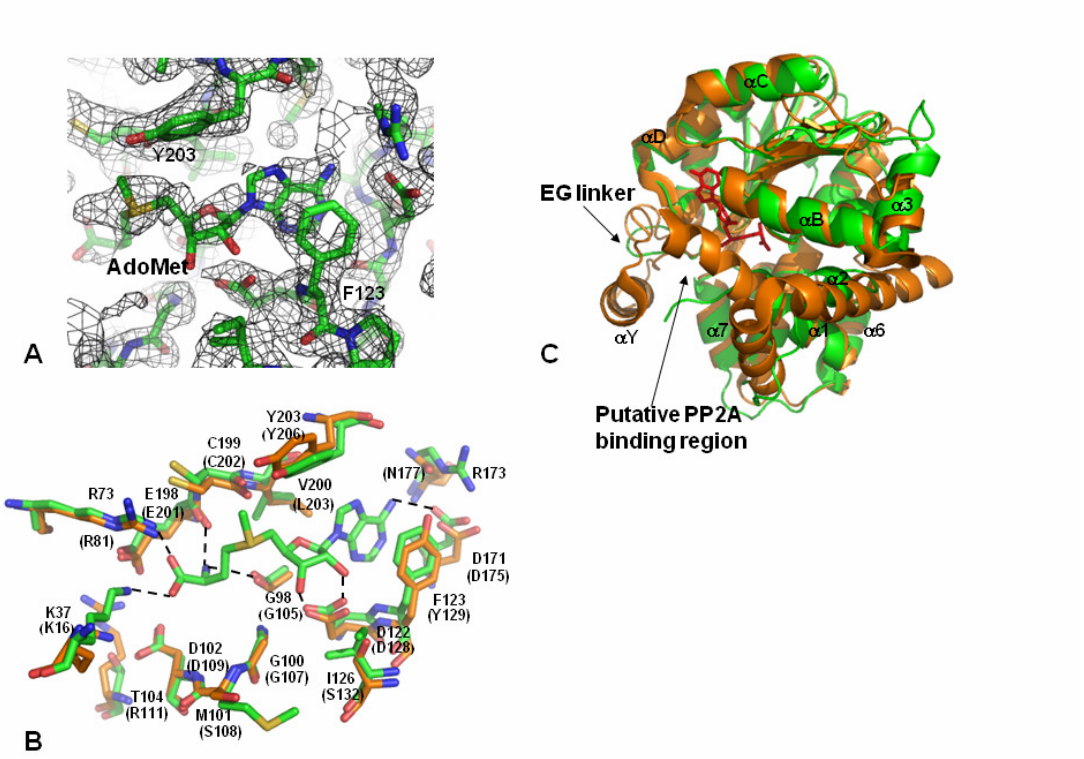

Figure 6-8. Active Site of Human LCMT1. (a) The electron density of AdoMet can be clearly observed in the sigma-weighted ($2mF_o$-DF_c, α_c) electron density map calculated with the initial model after the molecular replacement solution was obtained. The model at that stage included only 75 % of the residues and no AdoMet. The map is shown at a level of 1.0 σ (0.33e/Å^3) with the final refined coordinates for LCMT1 overlaid. (b) Superimposition of the human LCMT1 (green) and yeast PPM1 (orange) structures shows conservation of the AdoMet binding site. Several hydrogen bonds between AdoMet and human LCMT1 residues are indicated in dashed lines. Residue numbers corresponding to PPM1 are shown in brackets. (c) The putative PP2A binding site is indicated on the superimposed structures of human LCMT1 and yeast PPM1. The site of excision of residues 232 to 259 and replacement by EG linker in human LCMT1 is also indicated.

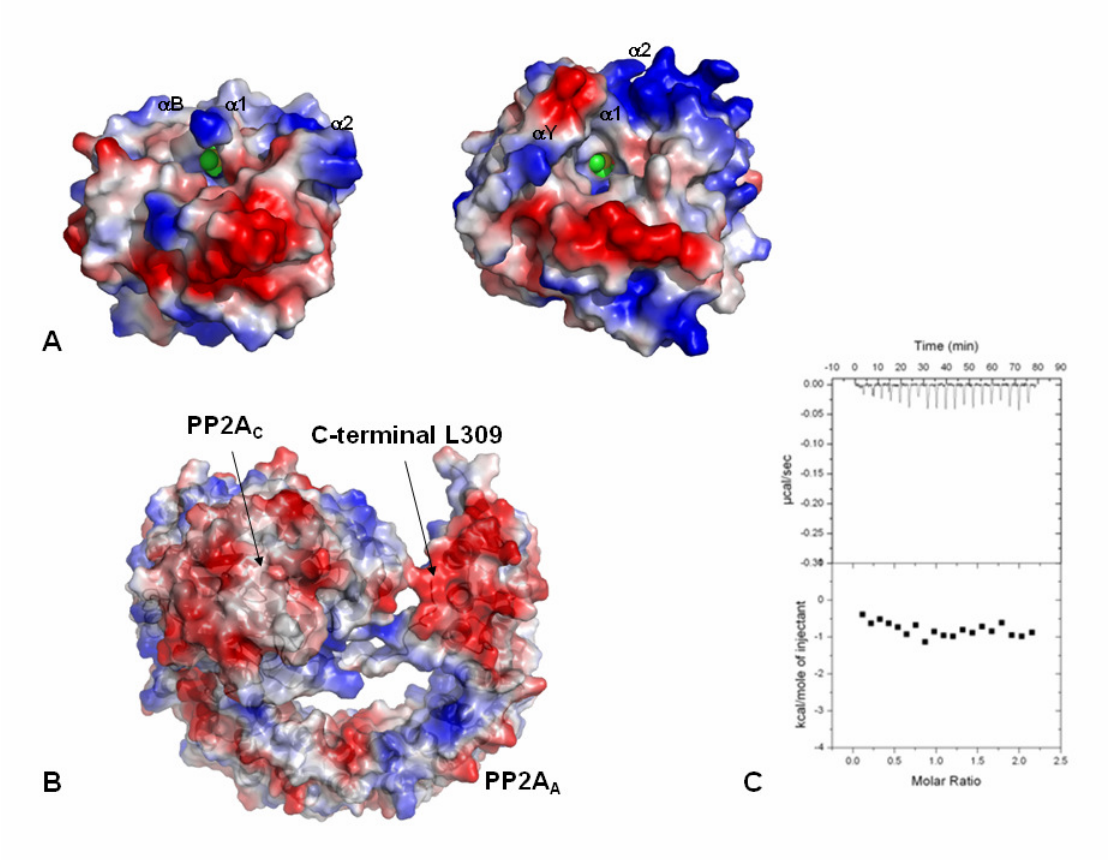

Figure 6-9. Model of the protein-protein interaction with PP2A. (a) Qualitative representation of the surface electrostatic potential of LCMT1 was generated in PyMOL viewer (*DeLano Scientific LLC*). Molecular surfaces of yeast PPM1 (left) and human LCMT1 (right) shown in the equivalent orientations reveal narrow grooves providing access to the cofactor. AdoMet is shown as van der Waals spheres representation with atoms of carbon, sulphur, oxygen and nitrogen coloured green, yellow, red and blue respectively. In both images an activated methyl group bound to the sulphur atom is visible. Above the active sites in both molecules, there are areas of positively charged surface (blue region) suggesting an additional site of association with PP2A. (b) Areas of negative surface potential of $PP2A_D$ (red) that might be involved in binding LCMT1. (c) Isothermal titration calorimetry experiments revealed no effective binding between $PP2A_A$ subunit and LCMT1.

6.4.4 Putative Mode of PP2A Interaction with LCMT1

Over the past several years, the structures of several proteins forming complexes with PP2A have been determined, including the structure of the holoenzyme with the B' (PR61) [17,19] or B (PR55) subunits [24], the structure of SV40 small-T antigen in complex with the PP2A scaffolding subunit ($PP2A_A$) [217] and methylesterase PME1 with the PP2A core enzyme ($PP2A_D$) [221], and these structures can provide some clues regarding LCMT1 interaction with PP2A. While B' (PR61), B (PR55) and SV40 small-T antigen associate with both catalytic $PP2A_C$ and scaffolding $PP2A_A$ subunits, PME1 was observed to interact only with $PP2A_C$. The $PP2A_A$ subunit, which is composed of HEAT repeats, uses different sets of these repeats for intermolecular interactions with various partners, such that HEAT repeats 2, 4 and 5 are involved in the PR61-$PP2A_A$ interaction, whereas HEAT repeats 3 to 7 are associated with the PR55-$PP2A_A$ interaction. The SV40 small-T antigen, on the other hand, interacts with the intra-HEAT-repeat loops of HEAT repeats 3-7 of the $PP2A_A$ subunit. The association of $PP2A_C$ with various regulatory proteins is even more diverse, due to the different functions that these proteins perform.

Although it is the C-terminal carboxyl group of the $PP2A_C$ subunit that is methylated, the substrate for the LCMT1 enzyme is a $PP2A_D$ core enzyme – a complex between the A and C subunits. Furthermore, LCMT1 does not exhibit any activity towards the synthetic peptide corresponding to the conserved C-terminal motif of the $PP2A_C$, suggesting that LCMT1 would also need to recognize other molecular features of PP2A in addition to Leu309. LCMT1

might use protein/protein interactions to orient its active site appropriately towards the C-terminus of $PP2A_C$ which, otherwise, would be a poor substrate and this mode of interaction might involve recognition of specific surfaces on the A subunit or a direct interaction with the C subunit at a site additional to that of the C-terminus, in a fashion similar to that seen for the methylesterase PME1 [221]. Qualitative examination of the electrostatic surface potential of LCMT1 reveals a positively charged area of the protein (Figure 6-9a) just above the deep groove leading to the cofactor. This surface is formed by the helices α2, αB and the flexible loop linking α2 to αZ of human LCMT1. Examination of the electrostatic surface potential of the core $PP2A_D$ enzyme reveals two complementary negatively charged regions, one on the C subunit and another formed by the C-terminus of $PP2A_C$ and the N-terminal HEAT repeats of the A subunit, suggesting that either of these regions might be involved in protein/protein interaction with LCMT1 (Figure 6-9b). However, isothermal titration calorimetry experiments with 100 μM full length LCMT1 did not detect any association between LCMT1 and $PP2A_A$ as no significant heat change was observed (Figure 6-9c). Thus, we would suggest that either the binding constant for $PP2A_A$ is very low, contrary to what would be expected for the proposed charge-charge surface interaction, or that LCMT1 might only associate with $PP2A_C$. Further verification of this model is needed.

6.5 Summary

$LCMT1_{20-334}$ was the only protein product that was crystalized in complex with the co-factor, *S*-adenosylmethionine from the optimized crystallization

conditions of 0.1 M Na-citrate (pH 6.5), 1.6 M ammonium sulphate, 0.38 M Na-K tartrate, 2 % PEG 400, 4 % acetone and 5 mM DTT at 22 ^{o}C. However, these crystals diffracted only to 7 Å and were not suitable for structure determination. Several methods were used to improve diffraction quality of the crystals including additive screening method (*Hampton Research*), dehydration using MicroRT™ Capillaries (*MiTeGen*), crystal annealing and seeding method (*Hampton Research*) but neither method was successful in improving diffraction pattern suggesting that additional protein constructs would need to be considered for crystallization in order to obtain a different crystal form.

New constructs were designed based on secondary structure prediction and limited proteolysis. The crystals from the variant LCMT1$_{SD20-334}$ protein were also successfully developed in various precipitant buffers. A single crystal from one of the conditions (0.05 ammonium sulphate, 0.05 M Bis-Tris chloride pH 6.5, 30 % pentaerythritol ethoxylate) was used to collect diffraction data that were used to solve the structure.

Crystal structure of human LCMT1 exhibits strong conservation of the core of the globular structure including the AdoMet binding site. Unique structural elements that represent variation to the common topology are most likely involved in protein/protein interactions with its substrate – the catalytic subunit of the key cellular phosphatase PP2A. LCMT1 is involved in regulation of methylation-dependent PP2A holoenzyme assembly however the full implications of this modification are not well understood. The crystal structure of LCMT1 could be exploited for the development of the specific inhibitors that

would be used as molecular tools for investigation of PP2A methylation *in vivo*. The truncated form of enzyme that we described here is very soluble and crystallized under a range of conditions thus it would provide an excellent platform for the crystallographic studies of the putative inhibitors.

Chapter Seven

Conclusions and Discussion

Protein phosphatase 2A is an important protein involved in several essential cellular mechanisms that has been a subject of investigation for many years [10,74,75]. Cancers and Alzheimer's disease were related to de-regulation of PP2A [96-100]. In addition, two main modes of regulation of PP2A, phosphorylation and methylation, were studied for almost two decades. Phosphorylation at Tyr307 of $PP2A_C$ leads to the inactivation of PP2A [50-53]; however, the role of methylation and demethylation, carried out by LCMT1 and PME1 respectively, at Leu309 of $PP2A_C$ was debated for several years. More recently, it was demonstrated that the methylation state of the catalytic subunit is a key mechanism for the assembly of a PP2A holoenzyme [72].

Tight binding of PME1 to PP2A was demonstrated *in vivo* several years ago together with the role of PME1 in de-methylation and stabilization of $PP2A_C$ [63]. Recently, the three-dimensional structure of PME1 and PP2A was determined suggesting that in the trimeric complex of $PP2A_A$, $PP2A_C$ and PME1, as expected, $PP2A_C$ is in contact with the methylesterase but there was no interaction observed between $PP2A_A$ and PME1 [221]. In contrast, our SPR and ITC studies showed direct association of $PP2A_A$ with PME1 and the thermodynamic parameters of this interaction were obtained. To gain an insight into the molecular characteristics of PME1 interaction with $PP2A_A$, ITC experiments were carried out at different temperatures and saline buffers. Positive heat capacity change suggests that interaction between PME1 and $PP2A_A$ is via polar residues. Increasing the concentration of salt interferes with the electrostatic nature of interaction between PME1 and $PP2A_A$. Finally, the truncated PME1, $PME1_{39\text{-}376}$, loses its ability to associate with $PP2A_A$ due to the

deletion of an important amino acid segment (residues 239-282) that is most likely required for interaction.

In the crystallographic structure of PME1-PP2A complex, a large space between truncated PME1 and $PP2A_A$ can be clearly observed and, in the context of a complex that would be formed between the full-length PME1 and $PP2A_A$, it might accommodate the truncated polypeptide segment (residues 239-282) of PME1. To support this assumption, the structure of PP2A–PR61 [17,19], SV40 small t antigen-$PP2A_A$ [217] and PP2A-PME1 complex [221] were superimposed and analyzed (Fig 7-1). Although no structural similarity was found among PR61, SV40 small t antigen and PME1, PR61 and SV40 small t antigen interact with $PP2A_A$ at similar HEAT repeats region. HEAT repeats 2, 4 and 5 are involved in PR61-PP2A interaction and SV40 small t antigen interacts with the intra-loops of HEAT repeats 3-7 of $PP2A_A$. HEAT repeats 3 to 7 are positioned beneath the proposed space for the truncated segment (residues 239-282) of PME1. Additionally, the superimposition shows that this space bellow the residues 238 and 283 of PME1 is occupied by two α helices of PR61 in a structure of a complex of PP2A with PR61. Secondary structure prediction of PME1 using PSIPRED indicates that the truncated segment (residues 239-282) of PME1 is composed of two α helices connected by a loop. Thus I would propose that HEAT repeats 3 to 7 of $PP2A_A$ are not only the target for PR61 and SV 40 small t antigen, but also the site of $PP2A_A$ interaction with for PME1.

It would be necessary to determine the three-dimensional structure of the full

length PME1 in a complex with PP2A in order to fully describe molecular basis of their interaction. Further efforts will be made to isolate full length PME1-PP2A$_A$ complex for crystallization studies. Data described in this thesis imply that PME1 which can interact individually with either PP2A$_A$ or PP2A$_C$ may play additional role in the mechanism of PP2A regulation.

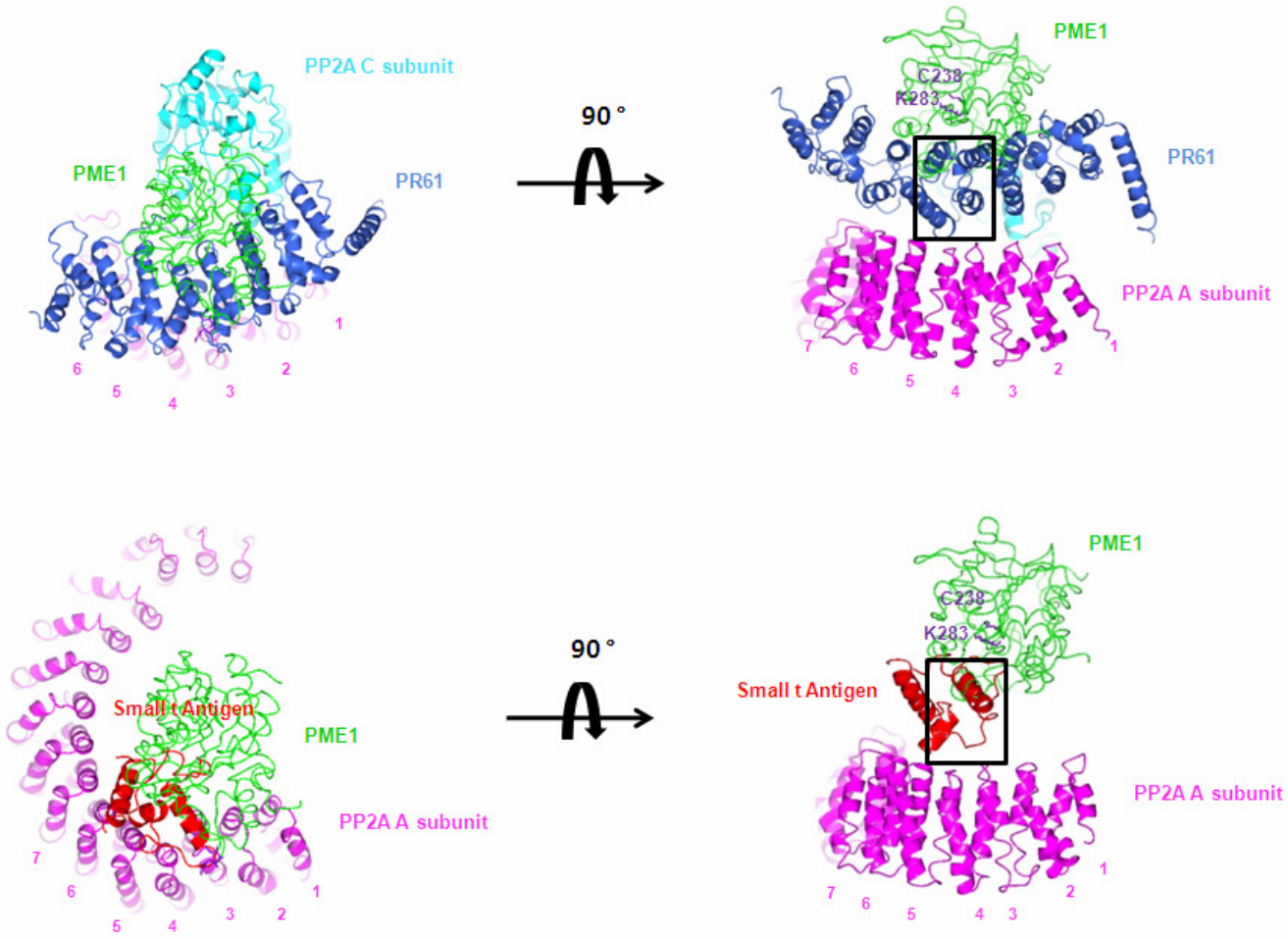

Figure 7-1. The superimposition and comparison of PP2A complexes. The structure of PP2A–PR61 (PDB: 2NYM), SV40 small t antigen-PP2A$_A$ (PDB: 2PKG) and PP2A-PME1 (PDB: 3C5W) complex were superimposed using CCP4mg program. PR61 and SV40 small t antigen interact with PP2A$_A$ at similar region, HEAT repeats 3 to 7. A large space (black square) observed beneath the residues cys238 and lys283 may be occupied by the missing polypeptide segment (residues 239-282) in a complex between the full-length PME1 and PP2A. Hence, PME1 may also interact with PP2A$_A$ at HEAT repeats 3 to 7.

High resolution diffracting crystals of human LCMT1 crystals were generated. The crystal structure of human PP2A LCMT1 exhibits strong conservation of the core of the globular structure including the AdoMet binding site. Unique structural elements that represent variation to the common topology are most likely involved in protein/protein interactions with its substrate – the catalytic subunit of the key cellular phosphatase PP2A. The crystal structure of LCMT1 could be exploited for the development of the specific inhibitors that would be used as molecular tools for investigation of PP2A methylation *in vivo*. The truncated form of the enzyme that we described here is very soluble and crystallized under a range of conditions thus it would provide an excellent platform for the crystallographic studies of the putative inhibitors. Furthermore inhibition of LCMT1 might have therapeutic potential in cancer, as it was shown that LCMT1 is required for cell cycle progression and cell survival.

References

1 Barford D (1995) Protein phosphatases. *Curr. Opin. Struct. Biol.*, **5,** 728-734.

2 Venter JC, Adams MD, Myers EW, Li PW, Mural RJ, Sutton GG, Smith HO, Yandell M, Evans CA, Holt RA, Gocayne JD, Amanatides P, Ballew RM, Huson DH, Wortman JR, Zhang Q, Kodira CD, Zheng XH, Chen L, Skupski M, Subramanian G, Thomas PD, Zhang J, Gabor Miklos GL, Nelson C, Broder S, Clark AG, Nadeau J, McKusick VA, Zinder N, Levine AJ, Roberts RJ, Simon M, Slayman C, Hunkapiller M, Bolanos R, Delcher A, Dew I, Fasulo D, Flanigan M, Florea L, Halpern A, Hannenhalli S, Kravitz S, Levy S, Mobarry C, Reinert K, Remington K, bu-Threideh J, Beasley E, Biddick K, Bonazzi V, Brandon R, Cargill M, Chandramouliswaran I, Charlab R, Chaturvedi K, Deng Z, Di F, V, Dunn P, Eilbeck K, Evangelista C, Gabrielian AE, Gan W, Ge W, Gong F, Gu Z, Guan P, Heiman TJ, Higgins ME, Ji RR, Ke Z, Ketchum KA, Lai Z, Lei Y, Li Z, Li J, Liang Y, Lin X, Lu F, Merkulov GV, Milshina N, Moore HM, Naik AK, Narayan VA, Neelam B, Nusskern D, Rusch DB, Salzberg S, Shao W, Shue B, Sun J, Wang Z, Wang A, Wang X, Wang J, Wei M, Wides R, Xiao C, Yan C, Yao A, Ye J, Zhan M, Zhang W, Zhang H, Zhao Q, Zheng L, Zhong F, Zhong W, Zhu S, Zhao S, Gilbert D, Baumhueter S, Spier G, Carter C, Cravchik A, Woodage T, Ali F, An H, Awe A, Baldwin D, Baden H, Barnstead M, Barrow I, Beeson K, Busam D, Carver A, Center A, Cheng ML, Curry L, Danaher S, Davenport L, Desilets R, Dietz S, Dodson K, Doup L, Ferriera S, Garg N, Gluecksmann A, Hart B, Haynes J, Haynes C, Heiner C, Hladun S, Hostin D, Houck J, Howland T, Ibegwam C, Johnson J, Kalush F, Kline L, Koduru S, Love A, Mann F, May D, McCawley S, McIntosh T, McMullen I, Moy M, Moy L, Murphy B, Nelson K, Pfannkoch C, Pratts E, Puri V, Qureshi H, Reardon M, Rodriguez R, Rogers YH, Romblad D, Ruhfel B, Scott R, Sitter C, Smallwood M, Stewart E, Strong R, Suh E, Thomas R, Tint NN, Tse S, Vech C, Wang G, Wetter J, Williams S, Williams M, Windsor S, Winn-Deen E, Wolfe K, Zaveri J, Zaveri K, Abril JF, Guigo R, Campbell MJ, Sjolander KV, Karlak B, Kejariwal A, Mi H, Lazareva B, Hatton T, Narechania A, Diemer K, Muruganujan A, Guo N, Sato S, Bafna V, Istrail S, Lippert R, Schwartz R, Walenz B, Yooseph S, Allen D, Basu A, Baxendale J, Blick L, Caminha M, Carnes-Stine J, Caulk P, Chiang YH, Coyne M, Dahlke C, Mays A, Dombroski M, Donnelly M, Ely D, Esparham S, Fosler C, Gire H, Glanowski S, Glasser K, Glodek A, Gorokhov M, Graham K, Gropman B, Harris M, Heil J, Henderson S, Hoover J, Jennings D, Jordan C, Jordan J, Kasha J, Kagan L, Kraft C, Levitsky A, Lewis M, Liu X, Lopez J, Ma D, Majoros W, McDaniel J, Murphy S, Newman M, Nguyen T, Nguyen N, & Nodell M (2001) The sequence of the human genome. *Science*, **291,** 1304-1351.

3 Lander ES, Linton LM, Birren B, Nusbaum C, Zody MC, Baldwin J, Devon K, Dewar K, Doyle M, FitzHugh W, Funke R, Gage D, Harris K, Heaford A, Howland J, Kann L, Lehoczky J, LeVine R, McEwan P, McKernan K, Meldrim J, Mesirov JP, Miranda C, Morris W, Naylor J,

Raymond C, Rosetti M, Santos R, Sheridan A, Sougnez C, Stange-Thomann N, Stojanovic N, Subramanian A, Wyman D, Rogers J, Sulston J, Ainscough R, Beck S, Bentley D, Burton J, Clee C, Carter N, Coulson A, Deadman R, Deloukas P, Dunham A, Dunham I, Durbin R, French L, Grafham D, Gregory S, Hubbard T, Humphray S, Hunt A, Jones M, Lloyd C, McMurray A, Matthews L, Mercer S, Milne S, Mullikin JC, Mungall A, Plumb R, Ross M, Shownkeen R, Sims S, Waterston RH, Wilson RK, Hillier LW, McPherson JD, Marra MA, Mardis ER, Fulton LA, Chinwalla AT, Pepin KH, Gish WR, Chissoe SL, Wendl MC, Delehaunty KD, Miner TL, Delehaunty A, Kramer JB, Cook LL, Fulton RS, Johnson DL, Minx PJ, Clifton SW, Hawkins T, Branscomb E, Predki P, Richardson P, Wenning S, Slezak T, Doggett N, Cheng JF, Olsen A, Lucas S, Elkin C, Uberbacher E, Frazier M, Gibbs RA, Muzny DM, Scherer SE, Bouck JB, Sodergren EJ, Worley KC, Rives CM, Gorrell JH, Metzker ML, Naylor SL, Kucherlapati RS, Nelson DL, Weinstock GM, Sakaki Y, Fujiyama A, Hattori M, Yada T, Toyoda A, Itoh T, Kawagoe C, Watanabe H, Totoki Y, Taylor T, Weissenbach J, Heilig R, Saurin W, Artiguenave F, Brottier P, Bruls T, Pelletier E, Robert C, Wincker P, Smith DR, Doucette-Stamm L, Rubenfield M, Weinstock K, Lee HM, Dubois J, Rosenthal A, Platzer M, Nyakatura G, Taudien S, Rump A, Yang H, Yu J, Wang J, Huang G, Gu J, Hood L, Rowen L, Madan A, Qin S, Davis RW, Federspiel NA, Abola AP, Proctor MJ, Myers RM, Schmutz J, Dickson M, Grimwood J, Cox DR, Olson MV, Kaul R, Raymond C, Shimizu N, Kawasaki K, Minoshima S, Evans GA, Athanasiou M, Schultz R, Roe BA, Chen F, Pan H, Ramser J, Lehrach H, Reinhardt R, McCombie WR, de la BM, Dedhia N, Blocker H, Hornischer K, Nordsiek G, Agarwala R, Aravind L, Bailey JA, Bateman A, Batzoglou S, Birney E, Bork P, Brown DG, Burge CB, Cerutti L, Chen HC, Church D, Clamp M, Copley RR, Doerks T, Eddy SR, Eichler EE, Furey TS, Galagan J, Gilbert JG, Harmon C, Hayashizaki Y, Haussler D, Hermjakob H, Hokamp K, Jang W, Johnson LS, Jones TA, Kasif S, Kaspryzk A, Kennedy S, Kent WJ, Kitts P, Koonin EV, Korf I, Kulp D, Lancet D, Lowe TM, McLysaght A, Mikkelsen T, Moran JV, Mulder N, Pollara VJ, Ponting CP, Schuler G, Schultz J, Slater G, Smit AF, Stupka E, Szustakowski J, Thierry-Mieg D, Thierry-Mieg J, Wagner L, Wallis J, Wheeler R, Williams A, Wolf YI, Wolfe KH, Yang SP, Yeh RF, Collins F, Guyer MS, Peterson J, Felsenfeld A, Wetterstrand KA, Patrinos A, Morgan MJ, de JP, Catanese JJ, Osoegawa K, Shizuya H, Choi S, & Chen YJ (2001) Initial sequencing and analysis of the human genome. *Nature*, **409,** 860-921.

4 Shi Y (2009) Serine/threonine phosphatases: mechanism through structure. *Cell*, **139,** 468-484.

5 Alonso A, Sasin J, Bottini N, Friedberg I, Friedberg I, Osterman A, Godzik A, Hunter T, Dixon J, & Mustelin T (2004) Protein tyrosine phosphatases in the human genome. *Cell*, **117,** 699-711.

6 Barford D, Das AK, & Egloff MP (1998) The structure and mechanism of protein phosphatases: insights into catalysis and regulation. *Annu. Rev. Biophys. Biomol. Struct.*, **27,** 133-164.

7 Hemmings BA, ms-Pearson C, Maurer F, Muller P, Goris J, Merlevede W, Hofsteenge J, & Stone SR (1990) alpha- and beta-forms of the 65-kDa subunit of protein phosphatase 2A have a similar 39 amino acid repeating structure. *Biochemistry*, **29,** 3166-3173.

8 Arino J, Woon CW, Brautigan DL, Miller TB, Jr., & Johnson GL (1988) Human liver phosphatase 2A: cDNA and amino acid sequence of two catalytic subunit isotypes. *Proc. Natl. Acad. Sci U. S. A*, **85,** 4252-4256.

9 Stone SR, Hofsteenge J, & Hemmings BA (1987) Molecular cloning of cDNAs encoding two isoforms of the catalytic subunit of protein phosphatase 2A. *Biochemistry*, **26,** 7215-7220.

10 Janssens V & Goris J (2001) Protein phosphatase 2A: a highly regulated family of serine/threonine phosphatases implicated in cell growth and signalling. *Biochem. J.*, **353,** 417-439.

11 Lechward K, Awotunde OS, Swiatek W, & Muszynska G (2001) Protein phosphatase 2A: variety of forms and diversity of functions. *Acta Biochim. Pol.*, **48,** 921-933.

12 Groves MR, Hanlon N, Turowski P, Hemmings BA, & Barford D (1999) The structure of the protein phosphatase 2A PR65/A subunit reveals the conformation of its 15 tandemly repeated HEAT motifs. *Cell*, **96,** 99-110.

13 Wang C, Chua K, Seghezzi W, Lees E, Gozani O, & Reed R (1998) Phosphorylation of spliceosomal protein SAP 155 coupled with splicing catalysis. *Genes Dev.*, **12,** 1409-1414.

14 Malik HS, Eickbush TH, & Goldfarb DS (1997) Evolutionary specialization of the nuclear targeting apparatus. *Proc. Natl. Acad. Sci U. S. A*, **94,** 13738-13742.

15 Walter G, Ferre F, Espiritu O, & Carbone-Wiley A (1989) Molecular cloning and sequence of cDNA encoding polyoma medium tumor antigen-associated 61-kDa protein. *Proc. Natl. Acad. Sci U. S. A*, **86,** 8669-8672.

16 Gusella JF & MacDonald ME (1998) Huntingtin: a single bait hooks many species. *Curr. Opin. Neurobiol.*, **8,** 425-430.

17 Cho US & Xu W (2007) Crystal structure of a protein phosphatase 2A heterotrimeric holoenzyme. *Nature*, **445,** 53-57.

18 Xing Y, Xu Y, Chen Y, Jeffrey PD, Chao Y, Lin Z, Li Z, Strack S, Stock JB, & Shi Y (2006) Structure of protein phosphatase 2A core enzyme bound to tumor-inducing toxins. *Cell*, **127,** 341-353.

19 Xu Y, Xing Y, Chen Y, Chao Y, Lin Z, Fan E, Yu JW, Strack S, Jeffrey PD, & Shi Y (2006) Structure of the protein phosphatase 2A holoenzyme. *Cell*, **127,** 1239-1251.

20 Ruediger R, Pham HT, & Walter G (2001) Alterations in protein phosphatase 2A subunit interaction in human carcinomas of the lung and colon with mutations in the A beta subunit gene. *Oncogene*, **20,** 1892-1899.

21 Cohen P (1989) The structure and regulation of protein phosphatases. *Annu. Rev. Biochem.*, **58,** 453-508.

22 Orgad S, Brewis ND, Alphey L, Axton JM, Dudai Y, & Cohen PT (1990) The structure of protein phosphatase 2A is as highly conserved as that of protein phosphatase 1. *FEBS Lett.*, **275,** 44-48.

23 Mumby M (2007) The 3D structure of protein phosphatase 2A: new insights into a ubiquitous regulator of cell signaling. *ACS Chem. Biol.*, **2,** 99-103.

24 Xu Y, Chen Y, Zhang P, Jeffrey PD, & Shi Y (2008) Structure of a protein phosphatase 2A holoenzyme: insights into B55-mediated Tau dephosphorylation. *Mol. Cell*, **31,** 873-885.

25 Mayer RE, Hendrix P, Cron P, Matthies R, Stone SR, Goris J, Merlevede W, Hofsteenge J, & Hemmings BA (1991) Structure of the 55-kDa regulatory subunit of protein phosphatase 2A: evidence for a neuronal-specific isoform. *Biochemistry*, **30,** 3589-3597.

26 Healy AM, Zolnierowicz S, Stapleton AE, Goebl M, Paoli-Roach AA, & Pringle JR (1991) CDC55, a Saccharomyces cerevisiae gene involved in cellular morphogenesis: identification, characterization, and homology to the B subunit of mammalian type 2A protein phosphatase. *Mol. Cell Biol.*, **11,** 5767-5780.

27 Zolnierowicz S, Csortos C, Bondor J, Verin A, Mumby MC, & Paoli-Roach AA (1994) Diversity in the regulatory B-subunits of protein phosphatase 2A: identification of a novel isoform highly expressed in brain. *Biochemistry*, **33,** 11858-11867.

28 Neer EJ, Schmidt CJ, Nambudripad R, & Smith TF (1994) The ancient regulatory-protein family of WD-repeat proteins. *Nature*, **371,** 297-300.

29 Griswold-Prenner I, Kamibayashi C, Maruoka EM, Mumby MC, & Derynck R (1998) Physical and functional interactions between type I transforming growth factor beta receptors and Balpha, a WD-40 repeat subunit of phosphatase 2A. *Mol. Cell Biol.*, **18,** 6595-6604.

30 Batut J, Schmierer B, Cao J, Raftery LA, Hill CS, & Howell M (2008) Two highly related regulatory subunits of PP2A exert opposite effects on TGF-beta/Activin/Nodal signalling. *Development*, **135,** 2927-2937.

31 Zolnierowicz S, Van HC, Andjelkovic N, Cron P, Stevens I, Merlevede W, Goris J, & Hemmings BA (1996) The variable subunit associated with protein phosphatase 2A0 defines a novel multimember family of regulatory subunits. *Biochem. J.*, **317 (Pt 1),** 187-194.

32 McCright B & Virshup DM (1995) Identification of a new family of protein phosphatase 2A regulatory subunits. *J. Biol. Chem.*, **270,** 26123-26128.

33 Csortos C, Zolnierowicz S, Bako E, Durbin SD, & Paoli-Roach AA (1996) High complexity in the expression of the B' subunit of protein phosphatase 2A0. Evidence for the existence of at least seven novel isoforms. *J. Biol. Chem.*, **271,** 2578-2588.

34 Tehrani MA, Mumby MC, & Kamibayashi C (1996) Identification of a novel protein phosphatase 2A regulatory subunit highly expressed in muscle. *J. Biol. Chem.*, **271,** 5164-5170.

35 McCright B, Rivers AM, Audlin S, & Virshup DM (1996) The B56 family of protein phosphatase 2A (PP2A) regulatory subunits encodes differentiation-induced phosphoproteins that target PP2A to both nucleus and cytoplasm. *J. Biol. Chem.*, **271,** 22081-22089.

36 Bhasin N, Cunha SR, Mudannayake M, Gigena MS, Rogers TB, & Mohler PJ (2007) Molecular basis for PP2A regulatory subunit B56alpha targeting in cardiomyocytes. *Am. J. Physiol Heart Circ. Physiol*, **293,** H109-H119.

37 Hendrix P, Mayer-Jackel RE, Cron P, Goris J, Hofsteenge J, Merlevede W, & Hemmings BA (1993) Structure and expression of a 72-kDa regulatory subunit of protein phosphatase 2A. Evidence for different size forms produced by alternative splicing. *J. Biol. Chem.*, **268,** 15267-15276.

38 Ahn JH, Sung JY, McAvoy T, Nishi A, Janssens V, Goris J, Greengard P, & Nairn AC (2007) The B"/PR72 subunit mediates Ca2+-dependent dephosphorylation of DARPP-32 by protein phosphatase 2A. *Proc. Natl. Acad. Sci U. S. A*, **104,** 9876-9881.

39 Voorhoeve PM, Hijmans EM, & Bernards R (1999) Functional interaction between a novel protein phosphatase 2A regulatory subunit, PR59, and the retinoblastoma-related p107 protein. *Oncogene*, **18,** 515-524.

40 Stillman B (1996) Cell cycle control of DNA replication. *Science*, **274,** 1659-1664.

41 Stillman B (1994) Smart machines at the DNA replication fork. *Cell*, **78,** 725-728.

42 Yan Z, Fedorov SA, Mumby MC, & Williams RS (2000) PR48, a novel regulatory subunit of protein phosphatase 2A, interacts with Cdc6 and modulates DNA replication in human cells. *Mol. Cell Biol.*, **20,** 1021-1029.

43 Castets F, Bartoli M, Barnier JV, Baillat G, Salin P, Moqrich A, Bourgeois JP, Denizot F, Rougon G, Calothy G, & Monneron A (1996) A novel calmodulin-binding protein, belonging to the WD-repeat family, is localized in dendrites of a subset of CNS neurons. *J. Cell Biol.*, **134,**

1051-1062.

44 Muro Y, Chan EK, Landberg G, & Tan EM (1995) A cell-cycle nuclear autoantigen containing WD-40 motifs expressed mainly in S and G2 phase cells. *Biochem. Biophys. Res. Commun.*, **207,** 1029-1037.

45 Moreno CS, Park S, Nelson K, Ashby D, Hubalek F, Lane WS, & Pallas DC (2000) WD40 repeat proteins striatin and S/G(2) nuclear autoantigen are members of a novel family of calmodulin-binding proteins that associate with protein phosphatase 2A. *J. Biol. Chem.*, **275,** 5257-5263.

46 Westphal RS, Anderson KA, Means AR, & Wadzinski BE (1998) A signaling complex of Ca2+-calmodulin-dependent protein kinase IV and protein phosphatase 2A. *Science*, **280,** 1258-1261.

47 Tian L, Knaus HG, & Shipston MJ (1998) Glucocorticoid regulation of calcium-activated potassium channels mediated by serine/threonine protein phosphatase. *J. Biol. Chem.*, **273,** 13531-13536.

48 Zhou XB, Ruth P, Schlossmann J, Hofmann F, & Korth M (1996) Protein phosphatase 2A is essential for the activation of Ca2+-activated K+ currents by cGMP-dependent protein kinase in tracheal smooth muscle and Chinese hamster ovary cells. *J. Biol. Chem.*, **271,** 19760-19767.

49 Chen J, Martin BL, & Brautigan DL (1992) Regulation of protein serine-threonine phosphatase type-2A by tyrosine phosphorylation. *Science*, **257,** 1261-1264.

50 Chen J, Parsons S, & Brautigan DL (1994) Tyrosine phosphorylation of protein phosphatase 2A in response to growth stimulation and v-src transformation of fibroblasts. *J. Biol. Chem.*, **269,** 7957-7962.

51 Srinivasan M & Begum N (1994) Regulation of protein phosphatase 1 and 2A activities by insulin during myogenesis in rat skeletal muscle cells in culture. *J. Biol. Chem.*, **269,** 12514-12520.

52 Begum N & Ragolia L (1996) cAMP counter-regulates insulin-mediated protein phosphatase-2A inactivation in rat skeletal muscle cells. *J. Biol. Chem.*, **271,** 31166-31171.

53 Begum N & Ragolia L (1999) Role of janus kinase-2 in insulin-mediated phosphorylation and inactivation of protein phosphatase-2A and its impact on upstream insulin signalling components. *Biochem. J.*, **344 Pt 3,** 895-901.

54 Usui H, Inoue R, Tanabe O, Nishito Y, Shimizu M, Hayashi H, Kagamiyama H, & Takeda M (1998) Activation of protein phosphatase 2A by cAMP-dependent protein kinase-catalyzed phosphorylation of the 74-kDa B'' (delta) regulatory subunit in vitro and identification of the phosphorylation sites. *FEBS Lett.*, **430,** 312-316.

55 Xu Z & Williams BR (2000) The B56alpha regulatory subunit of protein

phosphatase 2A is a target for regulation by double-stranded RNA-dependent protein kinase PKR. *Mol. Cell Biol.*, **20,** 5285-5299.

56 Lee J & Stock J (1993) Protein phosphatase 2A catalytic subunit is methyl-esterified at its carboxyl terminus by a novel methyltransferase. *J. Biol. Chem.*, **268,** 19192-19195.

57 Xie H & Clarke S (1993) Methyl esterification of C-terminal leucine residues in cytosolic 36-kDa polypeptides of bovine brain. A novel eucaryotic protein carboxyl methylation reaction. *J. Biol. Chem.*, **268,** 13364-13371.

58 Xie H & Clarke S (1994) Protein phosphatase 2A is reversibly modified by methyl esterification at its C-terminal leucine residue in bovine brain. *J. Biol. Chem.*, **269,** 1981-1984.

59 Xie H & Clarke S (1994) An enzymatic activity in bovine brain that catalyzes the reversal of the C-terminal methyl esterification of protein phosphatase 2A. *Biochem. Biophys. Res. Commun.*, **203,** 1710-1715.

60 Lee J, Chen Y, Tolstykh T, & Stock J (1996) A specific protein carboxyl methylesterase that demethylates phosphoprotein phosphatase 2A in bovine brain. *Proc. Natl. Acad. Sci U. S. A*, **93,** 6043-6047.

61 Kalhor HR, Luk K, Ramos A, Zobel-Thropp P, & Clarke S (2001) Protein phosphatase methyltransferase 1 (Ppm1p) is the sole activity responsible for modification of the major forms of protein phosphatase 2A in yeast. *Arch. Biochem. Biophys.*, **395,** 239-245.

62 De B, I, Derua R, Janssens V, Van HC, Waelkens E, Merlevede W, & Goris J (1999) Purification of porcine brain protein phosphatase 2A leucine carboxyl methyltransferase and cloning of the human homologue. *Biochemistry*, **38,** 16539-16547.

63 Ogris E, Du X, Nelson KC, Mak EK, Yu XX, Lane WS, & Pallas DC (1999) A protein phosphatase methylesterase (PME-1) is one of several novel proteins stably associating with two inactive mutants of protein phosphatase 2A. *J. Biol. Chem.*, **274,** 14382-14391.

64 Favre B, Zolnierowicz S, Turowski P, & Hemmings BA (1994) The catalytic subunit of protein phosphatase 2A is carboxyl-methylated in vivo. *J. Biol. Chem.*, **269,** 16311-16317.

65 Zhu T, Matsuzawa S, Mizuno Y, Kamibayashi C, Mumby MC, Andjelkovic N, Hemmings BA, Onoe K, & Kikuchi K (1997) The interconversion of protein phosphatase 2A between PP2A1 and PP2A0 during retinoic acid-induced granulocytic differentiation and a modification on the catalytic subunit in S phase of HL-60 cells. *Arch. Biochem. Biophys.*, **339,** 210-217.

66 Bryant JC, Westphal RS, & Wadzinski BE (1999) Methylated C-terminal leucine residue of PP2A catalytic subunit is important for binding of

regulatory Balpha subunit. *Biochem. J.*, **339 (Pt 2),** 241-246.

67 Wu J, Tolstykh T, Lee J, Boyd K, Stock JB, & Broach JR (2000) Carboxyl methylation of the phosphoprotein phosphatase 2A catalytic subunit promotes its functional association with regulatory subunits in vivo. *EMBO J.*, **19,** 5672-5681.

68 Guo CY, Brautigan DL, & Larner JM (2002) ATM-dependent dissociation of B55 regulatory subunit from nuclear PP2A in response to ionizing radiation. *J. Biol. Chem.*, **277,** 4839-4844.

69 Longin S, Jordens J, Martens E, Stevens I, Janssens V, Rondelez E, De B, I, Derua R, Waelkens E, Goris J, & Van HC (2004) An inactive protein phosphatase 2A population is associated with methylesterase and can be re-activated by the phosphotyrosyl phosphatase activator. *Biochem. J.*, **380,** 111-119.

70 Jordens J, Janssens V, Longin S, Stevens I, Martens E, Bultynck G, Engelborghs Y, Lescrinier E, Waelkens E, Goris J, & Van HC (2006) The protein phosphatase 2A phosphatase activator is a novel peptidyl-prolyl cis/trans-isomerase. *J. Biol. Chem.*, **281,** 6349-6357.

71 Ikehara T, Ikehara S, Imamura S, Shinjo F, & Yasumoto T (2007) Methylation of the C-terminal leucine residue of the PP2A catalytic subunit is unnecessary for the catalytic activity and the binding of regulatory subunit (PR55/B). *Biochem. Biophys. Res. Commun.*, **354,** 1052-1057.

72 Longin S, Zwaenepoel K, Louis JV, Dilworth S, Goris J, & Janssens V (2007) Selection of protein phosphatase 2A regulatory subunits is mediated by the C terminus of the catalytic Subunit. *J. Biol. Chem.*, **282,** 26971-26980.

73 Paoli-Roach AA, Park IK, Cerovsky V, Csortos C, Durbin SD, Kuntz MJ, Sitikov A, Tang PM, Verin A, & Zolnierowicz S (1994) Serine/threonine protein phosphatases in the control of cell function. *Adv. Enzyme Regul.*, **34,** 199-224.

74 Zolnierowicz S (2000) Type 2A protein phosphatase, the complex regulator of numerous signaling pathways. *Biochem. Pharmacol.*, **60,** 1225-1235.

75 Goldberg Y (1999) Protein phosphatase 2A: who shall regulate the regulator? *Biochem. Pharmacol.*, **57,** 321-328.

76 Wang Y & Ng TY (2006) Phosphatase 2A negatively regulates mitotic exit in Saccharomyces cerevisiae. *Mol. Biol. Cell*, **17,** 80-89.

77 Perdiguero E & Nebreda AR (2004) Regulation of Cdc25C activity during the meiotic G2/M transition. *Cell Cycle*, **3,** 733-737.

78 Karaiskou A, Jessus C, Brassac T, & Ozon R (1999) Phosphatase 2A

and polo kinase, two antagonistic regulators of cdc25 activation and MPF auto-amplification. *J. Cell Sci*, **112 (Pt 21),** 3747-3756.

79 Gabel S, Benefield J, Meisinger J, Petruzzelli GJ, & Young M (1999) Protein phosphatases 1 and 2A maintain endothelial cells in a resting state, limiting the motility that is needed for the morphogenic process of angiogenesis. *Otolaryngol. Head Neck Surg.*, **121,** 463-468.

80 Lee TH (1995) The role of protein phosphatase type-2A in the Xenopus cell cycle: initiation of the G2/M transition. *Semin. Cancer Biol.*, **6,** 203-209.

81 Arroyo JD & Hahn WC (2005) Involvement of PP2A in viral and cellular transformation. *Oncogene*, **24,** 7746-7755.

82 Lin XH, Walter J, Scheidtmann K, Ohst K, Newport J, & Walter G (1998) Protein phosphatase 2A is required for the initiation of chromosomal DNA replication. *Proc. Natl. Acad. Sci U. S. A*, **95,** 14693-14698.

83 Cho DH, Choi YJ, Jo SA, Ryou J, Kim JY, Chung J, & Jo I (2006) Troglitazone acutely inhibits protein synthesis in endothelial cells via a novel mechanism involving protein phosphatase 2A-dependent p70 S6 kinase inhibition. *Am. J. Physiol Cell Physiol*, **291,** C317-C326.

84 Andjelkovic N, Zolnierowicz S, Van HC, Goris J, & Hemmings BA (1996) The catalytic subunit of protein phosphatase 2A associates with the translation termination factor eRF1. *EMBO J.*, **15,** 7156-7167.

85 Petritsch C, Beug H, Balmain A, & Oft M (2000) TGF-beta inhibits p70 S6 kinase via protein phosphatase 2A to induce G(1) arrest. *Genes Dev.*, **14,** 3093-3101.

86 Jiang Y & Broach JR (1999) Tor proteins and protein phosphatase 2A reciprocally regulate Tap42 in controlling cell growth in yeast. *EMBO J.*, **18,** 2782-2792.

87 Millward TA, Zolnierowicz S, & Hemmings BA (1999) Regulation of protein kinase cascades by protein phosphatase 2A. *Trends Biochem. Sci*, **24,** 186-191.

88 Anderson NG, Maller JL, Tonks NK, & Sturgill TW (1990) Requirement for integration of signals from two distinct phosphorylation pathways for activation of MAP kinase. *Nature*, **343,** 651-653.

89 Gomez N & Cohen P (1991) Dissection of the protein kinase cascade by which nerve growth factor activates MAP kinases. *Nature*, **353,** 170-173.

90 Xin M & Deng X (2006) Protein phosphatase 2A enhances the proapoptotic function of Bax through dephosphorylation. *J. Biol. Chem.*, **281,** 18859-18867.

91 Chen CL, Lin CF, Chiang CW, Jan MS, & Lin YS (2006) Lithium inhibits

ceramide- and etoposide-induced protein phosphatase 2A methylation, Bcl-2 dephosphorylation, caspase-2 activation, and apoptosis. *Mol. Pharmacol.*, **70,** 510-517.

92 Chatfield K & Eastman A (2004) Inhibitors of protein phosphatases 1 and 2A differentially prevent intrinsic and extrinsic apoptosis pathways. *Biochem. Biophys. Res. Commun.*, **323,** 1313-1320.

93 Azam S, Drobetsky E, & Ramotar D (2007) Overexpression of the cis/trans isomerase PTPA triggers caspase 3-dependent apoptosis. *Apoptosis.*, **12,** 1243-1255.

94 varado-Kristensson M & Andersson T (2005) Protein phosphatase 2A regulates apoptosis in neutrophils by dephosphorylating both p38 MAPK and its substrate caspase 3. *J. Biol. Chem.*, **280,** 6238-6244.

95 Chiang CW, Kanies C, Kim KW, Fang WB, Parkhurst C, Xie M, Henry T, & Yang E (2003) Protein phosphatase 2A dephosphorylation of phosphoserine 112 plays the gatekeeper role for BAD-mediated apoptosis. *Mol. Cell Biol.*, **23,** 6350-6362.

96 Sontag E, Hladik C, Montgomery L, Luangpirom A, Mudrak I, Ogris E, & White CL, III (2004) Downregulation of protein phosphatase 2A carboxyl methylation and methyltransferase may contribute to Alzheimer disease pathogenesis. *J. Neuropathol. Exp. Neurol.*, **63,** 1080-1091.

97 Tanimukai H, Grundke-Iqbal I, & Iqbal K (2005) Up-regulation of inhibitors of protein phosphatase-2A in Alzheimer's disease. *Am. J. Pathol.*, **166,** 1761-1771.

98 Vafai SB & Stock JB (2002) Protein phosphatase 2A methylation: a link between elevated plasma homocysteine and Alzheimer's Disease. *FEBS Lett.*, **518,** 1-4.

99 Janssens V, Goris J, & Van HC (2005) PP2A: the expected tumor suppressor. *Curr. Opin. Genet. Dev.*, **15,** 34-41.

100 Schonthal AH (2001) Role of serine/threonine protein phosphatase 2A in cancer. *Cancer Lett.*, **170,** 1-13.

101 Bialojan C & Takai A (1988) Inhibitory effect of a marine-sponge toxin, okadaic acid, on protein phosphatases. Specificity and kinetics. *Biochem. J.*, **256,** 283-290.

102 Smith JA & Martin L (1973) Do cells cycle? *Proc. Natl. Acad. Sci U. S. A*, **70,** 1263-1267.

103 Dunphy WG (1994) The decision to enter mitosis. *Trends Cell Biol.*, **4,** 202-207.

104 Felix MA, Cohen P, & Karsenti E (1990) Cdc2 H1 kinase is negatively regulated by a type 2A phosphatase in the Xenopus early embryonic cell

cycle: evidence from the effects of okadaic acid. *EMBO J.*, **9,** 675-683.

105 Yamashita K, Yasuda H, Pines J, Yasumoto K, Nishitani H, Ohtsubo M, Hunter T, Sugimura T, & Nishimoto T (1990) Okadaic acid, a potent inhibitor of type 1 and type 2A protein phosphatases, activates cdc2/H1 kinase and transiently induces a premature mitosis-like state in BHK21 cells. *EMBO J.*, **9,** 4331-4338.

106 Lee TH, Solomon MJ, Mumby MC, & Kirschner MW (1991) INH, a negative regulator of MPF, is a form of protein phosphatase 2A. *Cell*, **64,** 415-423.

107 Picard A, Labbe JC, Barakat H, Cavadore JC, & Doree M (1991) Okadaic acid mimics a nuclear component required for cyclin B-cdc2 kinase microinjection to drive starfish oocytes into M phase. *J. Cell Biol.*, **115,** 337-344.

108 Lee TH, Turck C, & Kirschner MW (1994) Inhibition of cdc2 activation by INH/PP2A. *Mol. Biol. Cell*, **5,** 323-338.

109 Gould KL, Moreno S, Owen DJ, Sazer S, & Nurse P (1991) Phosphorylation at Thr167 is required for Schizosaccharomyces pombe p34cdc2 function. *EMBO J.*, **10,** 3297-3309.

110 Borgne A & Meijer L (1996) Sequential dephosphorylation of p34(cdc2) on Thr-14 and Tyr-15 at the prophase/metaphase transition. *J. Biol. Chem.*, **271,** 27847-27854.

111 Karaiskou A, Cayla X, Haccard O, Jessus C, & Ozon R (1998) MPF amplification in Xenopus oocyte extracts depends on a two-step activation of cdc25 phosphatase. *Exp. Cell Res.*, **244,** 491-500.

112 Lawson R, Cohen P, & Lane DP (1990) Simian virus 40 large T-antigen-dependent DNA replication is activated by protein phosphatase 2A in vitro. *J. Virol.*, **64,** 2380-2383.

113 Virshup DM, Kauffman MG, & Kelly TJ (1989) Activation of SV40 DNA replication in vitro by cellular protein phosphatase 2A. *EMBO J.*, **8,** 3891-3898.

114 Scheidtmann KH, Virshup DM, & Kelly TJ (1991) Protein phosphatase 2A dephosphorylates simian virus 40 large T antigen specifically at residues involved in regulation of DNA-binding activity. *J. Virol.*, **65,** 2098-2101.

115 Cegielska A, Shaffer S, Derua R, Goris J, & Virshup DM (1994) Different oligomeric forms of protein phosphatase 2A activate and inhibit simian virus 40 DNA replication. *Mol. Cell Biol.*, **14,** 4616-4623.

116 Liu J, Smith CL, DeRyckere D, DeAngelis K, Martin GS, & Berger JM (2000) Structure and function of Cdc6/Cdc18: implications for origin recognition and checkpoint control. *Mol. Cell*, **6,** 637-648.

117 Borlado LR & Mendez J (2008) CDC6: from DNA replication to cell cycle checkpoints and oncogenesis. *Carcinogenesis*, **29,** 237-243.

118 Helliwell SB, Wagner P, Kunz J, uter-Reinhard M, Henriquez R, & Hall MN (1994) TOR1 and TOR2 are structurally and functionally similar but not identical phosphatidylinositol kinase homologues in yeast. *Mol. Biol. Cell*, **5,** 105-118.

119 Hay N & Sonenberg N (2004) Upstream and downstream of mTOR. *Genes Dev.*, **18,** 1926-1945.

120 Avruch J, Hara K, Lin Y, Liu M, Long X, Ortiz-Vega S, & Yonezawa K (2006) Insulin and amino-acid regulation of mTOR signaling and kinase activity through the Rheb GTPase. *Oncogene*, **25,** 6361-6372.

121 Wullschleger S, Loewith R, & Hall MN (2006) TOR signaling in growth and metabolism. *Cell*, **124,** 471-484.

122 Yang Q & Guan KL (2007) Expanding mTOR signaling. *Cell Res.*, **17,** 666-681.

123 Hall MN (2008) mTOR-what does it do? *Transplant. Proc.*, **40,** S5-S8.

124 Schmidt A, Kunz J, & Hall MN (1996) TOR2 is required for organization of the actin cytoskeleton in yeast. *Proc. Natl. Acad. Sci U. S. A*, **93,** 13780-13785.

125 Di Como CJ & Arndt KT (1996) Nutrients, via the Tor proteins, stimulate the association of Tap42 with type 2A phosphatases. *Genes Dev.*, **10,** 1904-1916.

126 Yan G, Shen X, & Jiang Y (2006) Rapamycin activates Tap42-associated phosphatases by abrogating their association with Tor complex 1. *EMBO J.*, **25,** 3546-3555.

127 Oficjalska-Pham D, Harismendy O, Smagowicz WJ, Gonzalez de PA, Boguta M, Sentenac A, & Lefebvre O (2006) General repression of RNA polymerase III transcription is triggered by protein phosphatase type 2A-mediated dephosphorylation of Maf1. *Mol. Cell*, **22,** 623-632.

128 Murata K, Wu J, & Brautigan DL (1997) B cell receptor-associated protein alpha4 displays rapamycin-sensitive binding directly to the catalytic subunit of protein phosphatase 2A. *Proc. Natl. Acad. Sci U. S. A*, **94,** 10624-10629.

129 Inui S, Sanjo H, Maeda K, Yamamoto H, Miyamoto E, & Sakaguchi N (1998) Ig receptor binding protein 1 (alpha4) is associated with a rapamycin-sensitive signal transduction in lymphocytes through direct binding to the catalytic subunit of protein phosphatase 2A. *Blood*, **92,** 539-546.

130 Boudreau RT, Sangster SM, Johnson LM, Dauphinee S, Li AW, & Too

CK (2002) Implication of alpha4 phosphoprotein and the rapamycin-sensitive mammalian target-of-rapamycin pathway in prolactin receptor signalling. *J. Endocrinol.*, **173,** 493-506.

131 Thomas G & Hall MN (1997) TOR signalling and control of cell growth. *Curr. Opin. Cell Biol.*, **9,** 782-787.

132 Nien WL, Dauphinee SM, Moffat LD, & Too CK (2007) Overexpression of the mTOR alpha4 phosphoprotein activates protein phosphatase 2A and increases Stat1alpha binding to PIAS1. *Mol. Cell Endocrinol.*, **263,** 10-17.

133 Stansfield I, Jones KM, Kushnirov VV, Dagkesamanskaya AR, Poznyakovski AI, Paushkin SV, Nierras CR, Cox BS, Ter-Avanesyan MD, & Tuite MF (1995) The products of the SUP45 (eRF1) and SUP35 genes interact to mediate translation termination in Saccharomyces cerevisiae. *EMBO J.*, **14,** 4365-4373.

134 Zhouravleva G, Frolova L, Le G, X, Le GR, Inge-Vechtomov S, Kisselev L, & Philippe M (1995) Termination of translation in eukaryotes is governed by two interacting polypeptide chain release factors, eRF1 and eRF3. *EMBO J.*, **14,** 4065-4072.

135 Andjelkovic M, Jakubowicz T, Cron P, Ming XF, Han JW, & Hemmings BA (1996) Activation and phosphorylation of a pleckstrin homology domain containing protein kinase (RAC-PK/PKB) promoted by serum and protein phosphatase inhibitors. *Proc. Natl. Acad. Sci U. S. A*, **93,** 5699-5704.

136 Ricciarelli R & Azzi A (1998) Regulation of recombinant PKC alpha activity by protein phosphatase 1 and protein phosphatase 2A. *Arch. Biochem. Biophys.*, **355,** 197-200.

137 Ballou LM, Jeno P, & Thomas G (1988) Protein phosphatase 2A inactivates the mitogen-stimulated S6 kinase from Swiss mouse 3T3 cells. *J. Biol. Chem.*, **263,** 1188-1194.

138 DeRemer MF, Saeli RJ, Brautigan DL, & Edelman AM (1992) Ca(2+)-calmodulin-dependent protein kinases Ia and Ib from rat brain. II. Enzymatic characteristics and regulation of activities by phosphorylation and dephosphorylation. *J. Biol. Chem.*, **267,** 13466-13471.

139 Barnes GN, Slevin JT, & Vanaman TC (1995) Rat brain protein phosphatase 2A: an enzyme that may regulate autophosphorylated protein kinases. *J. Neurochem.*, **64,** 340-353.

140 Park IK & Soderling TR (1995) Activation of Ca2+/calmodulin-dependent protein kinase (CaM-kinase) IV by CaM-kinase kinase in Jurkat T lymphocytes. *J. Biol. Chem.*, **270,** 30464-30469.

141 Barisic S, Strozyk E, Peters N, Walczak H, & Kulms D (2008) Identification of PP2A as a crucial regulator of the NF-kappaB feedback

loop: its inhibition by UVB turns NF-kappaB into a pro-apoptotic factor. *Cell Death Differ.*, **15,** 1681-1690.

142 Chiang CW, Yan L, & Yang E (2008) Phosphatases and regulation of cell death. *Methods Enzymol.*, **446,** 237-257.

143 Song G, Ouyang G, & Bao S (2005) The activation of Akt/PKB signaling pathway and cell survival. *J. Cell Mol. Med.*, **9,** 59-71.

144 Whiteman EL, Cho H, & Birnbaum MJ (2002) Role of Akt/protein kinase B in metabolism. *Trends Endocrinol. Metab*, **13,** 444-451.

145 Alessi DR, Deak M, Casamayor A, Caudwell FB, Morrice N, Norman DG, Gaffney P, Reese CB, MacDougall CN, Harbison D, Ashworth A, & Bownes M (1997) 3-Phosphoinositide-dependent protein kinase-1 (PDK1): structural and functional homology with the Drosophila DSTPK61 kinase. *Curr. Biol.*, **7,** 776-789.

146 Pullen N, Dennis PB, Andjelkovic M, Dufner A, Kozma SC, Hemmings BA, & Thomas G (1998) Phosphorylation and activation of p70s6k by PDK1. *Science*, **279,** 707-710.

147 Alessi DR, Kozlowski MT, Weng QP, Morrice N, & Avruch J (1998) 3-Phosphoinositide-dependent protein kinase 1 (PDK1) phosphorylates and activates the p70 S6 kinase in vivo and in vitro. *Curr. Biol.*, **8,** 69-81.

148 Westphal RS, Coffee RL, Jr., Marotta A, Pelech SL, & Wadzinski BE (1999) Identification of kinase-phosphatase signaling modules composed of p70 S6 kinase-protein phosphatase 2A (PP2A) and p21-activated kinase-PP2A. *J. Biol. Chem.*, **274,** 687-692.

149 Mellor H & Parker PJ (1998) The extended protein kinase C superfamily. *Biochem. J.*, **332 (Pt 2),** 281-292.

150 Hansra G, Bornancin F, Whelan R, Hemmings BA, & Parker PJ (1996) 12-O-Tetradecanoylphorbol-13-acetate-induced dephosphorylation of protein kinase Calpha correlates with the presence of a membrane-associated protein phosphatase 2A heterotrimer. *J. Biol. Chem.*, **271,** 32785-32788.

151 Ricciarelli R, Tasinato A, Clement S, Ozer NK, Boscoboinik D, & Azzi A (1998) alpha-Tocopherol specifically inactivates cellular protein kinase C alpha by changing its phosphorylation state. *Biochem. J.*, **334 (Pt 1),** 243-249.

152 Soderling TR (1999) The Ca-calmodulin-dependent protein kinase cascade. *Trends Biochem. Sci*, **24,** 232-236.

153 Colomer J & Means AR (2007) Physiological roles of the Ca2+/CaM-dependent protein kinase cascade in health and disease. *Subcell. Biochem.*, **45,** 169-214.

154 Means AR (2008) The Year in Basic Science: calmodulin kinase cascades. *Mol. Endocrinol.*, **22,** 2759-2765.

155 Ishida A, Sueyoshi N, Shigeri Y, & Kameshita I (2008) Negative regulation of multifunctional Ca2+/calmodulin-dependent protein kinases: physiological and pharmacological significance of protein phosphatases. *Br. J. Pharmacol.*, **154,** 729-740.

156 Anderson KA, Noeldner PK, Reece K, Wadzinski BE, & Means AR (2004) Regulation and function of the calcium/calmodulin-dependent protein kinase IV/protein serine/threonine phosphatase 2A signaling complex. *J. Biol. Chem.*, **279,** 31708-31716.

157 Wolff RA, Dobrowsky RT, Bielawska A, Obeid LM, & Hannun YA (1994) Role of ceramide-activated protein phosphatase in ceramide-mediated signal transduction. *J. Biol. Chem.*, **269,** 19605-19609.

158 Santoro MF, Annand RR, Robertson MM, Peng YW, Brady MJ, Mankovich JA, Hackett MC, Ghayur T, Walter G, Wong WW, & Giegel DA (1998) Regulation of protein phosphatase 2A activity by caspase-3 during apoptosis. *J. Biol. Chem.*, **273,** 13119-13128.

159 Deng X, Ito T, Carr B, Mumby M, & May WS, Jr. (1998) Reversible phosphorylation of Bcl2 following interleukin 3 or bryostatin 1 is mediated by direct interaction with protein phosphatase 2A. *J. Biol. Chem.*, **273,** 34157-34163.

160 Ito T, Deng X, Carr B, & May WS (1997) Bcl-2 phosphorylation required for anti-apoptosis function. *J. Biol. Chem.*, **272,** 11671-11673.

161 Xin M & Deng X (2005) Nicotine inactivation of the proapoptotic function of Bax through phosphorylation. *J. Biol. Chem.*, **280,** 10781-10789.

162 Zha J, Harada H, Yang E, Jockel J, & Korsmeyer SJ (1996) Serine phosphorylation of death agonist BAD in response to survival factor results in binding to 14-3-3 not BCL-X(L). *Cell*, **87,** 619-628.

163 Ruvolo PP, Deng X, Ito T, Carr BK, & May WS (1999) Ceramide induces Bcl2 dephosphorylation via a mechanism involving mitochondrial PP2A. *J. Biol. Chem.*, **274,** 20296-20300.

164 Aggarwal BB (2000) Apoptosis and nuclear factor-kappa B: a tale of association and dissociation. *Biochem. Pharmacol.*, **60,** 1033-1039.

165 Poppelmann B, Klimmek K, Strozyk E, Voss R, Schwarz T, & Kulms D (2005) NF{kappa}B-dependent down-regulation of tumor necrosis factor receptor-associated proteins contributes to interleukin-1-mediated enhancement of ultraviolet B-induced apoptosis. *J. Biol. Chem.*, **280,** 15635-15643.

166 DiDonato JA, Hayakawa M, Rothwarf DM, Zandi E, & Karin M (1997) A cytokine-responsive IkappaB kinase that activates the transcription

factor NF-kappaB. *Nature*, **388,** 548-554.

167 Pearson G, Robinson F, Beers GT, Xu BE, Karandikar M, Berman K, & Cobb MH (2001) Mitogen-activated protein (MAP) kinase pathways: regulation and physiological functions. *Endocr. Rev.*, **22,** 153-183.

168 Davis RJ (2000) Signal transduction by the JNK group of MAP kinases. *Cell*, **103,** 239-252.

169 Raman M, Chen W, & Cobb MH (2007) Differential regulation and properties of MAPKs. *Oncogene*, **26,** 3100-3112.

170 Roux PP & Blenis J (2004) ERK and p38 MAPK-activated protein kinases: a family of protein kinases with diverse biological functions. *Microbiol. Mol. Biol. Rev.*, **68,** 320-344.

171 Weston CR & Davis RJ (2007) The JNK signal transduction pathway. *Curr. Opin. Cell Biol.*, **19,** 142-149.

172 Silverstein AM, Barrow CA, Davis AJ, & Mumby MC (2002) Actions of PP2A on the MAP kinase pathway and apoptosis are mediated by distinct regulatory subunits. *Proc. Natl. Acad. Sci U. S. A*, **99,** 4221-4226.

173 Ballif BA & Blenis J (2001) Molecular mechanisms mediating mammalian mitogen-activated protein kinase (MAPK) kinase (MEK)-MAPK cell survival signals. *Cell Growth Differ.*, **12,** 397-408.

174 Rubinfeld H & Seger R (2005) The ERK cascade: a prototype of MAPK signaling. *Mol. Biotechnol.*, **31,** 151-174.

175 Meloche S & Pouyssegur J (2007) The ERK1/2 mitogen-activated protein kinase pathway as a master regulator of the G1- to S-phase transition. *Oncogene*, **26,** 3227-3239.

176 McKay MM & Morrison DK (2007) Integrating signals from RTKs to ERK/MAPK. *Oncogene*, **26,** 3113-3121.

177 Wellbrock C, Karasarides M, & Marais R (2004) The RAF proteins take centre stage. *Nat. Rev. Mol. Cell Biol.*, **5,** 875-885.

178 Alessi DR, Gomez N, Moorhead G, Lewis T, Keyse SM, & Cohen P (1995) Inactivation of p42 MAP kinase by protein phosphatase 2A and a protein tyrosine phosphatase, but not CL100, in various cell lines. *Curr. Biol.*, **5,** 283-295.

179 Sonoda Y, Kasahara T, Yamaguchi Y, Kuno K, Matsushima K, & Mukaida N (1997) Stimulation of interleukin-8 production by okadaic acid and vanadate in a human promyelocyte cell line, an HL-60 subline. Possible role of mitogen-activated protein kinase on the okadaic acid-induced NF-kappaB activation. *J. Biol. Chem.*, **272,** 15366-15372.

180 Sontag E, Fedorov S, Kamibayashi C, Robbins D, Cobb M, & Mumby M (1993) The interaction of SV40 small tumor antigen with protein phosphatase 2A stimulates the map kinase pathway and induces cell proliferation. *Cell*, **75,** 887-897.

181 Jaumot M & Hancock JF (2001) Protein phosphatases 1 and 2A promote Raf-1 activation by regulating 14-3-3 interactions. *Oncogene*, **20,** 3949-3958.

182 Kubicek M, Pacher M, Abraham D, Podar K, Eulitz M, & Baccarini M (2002) Dephosphorylation of Ser-259 regulates Raf-1 membrane association. *J. Biol. Chem.*, **277,** 7913-7919.

183 Strack S (2002) Overexpression of the protein phosphatase 2A regulatory subunit Bgamma promotes neuronal differentiation by activating the MAP kinase (MAPK) cascade. *J. Biol. Chem.*, **277,** 41525-41532.

184 Ory S, Zhou M, Conrads TP, Veenstra TD, & Morrison DK (2003) Protein phosphatase 2A positively regulates Ras signaling by dephosphorylating KSR1 and Raf-1 on critical 14-3-3 binding sites. *Curr. Biol.*, **13,** 1356-1364.

185 Van Kanegan MJ, Adams DG, Wadzinski BE, & Strack S (2005) Distinct protein phosphatase 2A heterotrimers modulate growth factor signaling to extracellular signal-regulated kinases and Akt. *J. Biol. Chem.*, **280,** 36029-36036.

186 Letourneux C, Rocher G, & Porteu F (2006) B56-containing PP2A dephosphorylate ERK and their activity is controlled by the early gene IEX-1 and ERK. *EMBO J.*, **25,** 727-738.

187 Raingeaud J, Gupta S, Rogers JS, Dickens M, Han J, Ulevitch RJ, & Davis RJ (1995) Pro-inflammatory cytokines and environmental stress cause p38 mitogen-activated protein kinase activation by dual phosphorylation on tyrosine and threonine. *J. Biol. Chem.*, **270,** 7420-7426.

188 Li SP, Junttila MR, Han J, Kahari VM, & Westermarck J (2003) p38 Mitogen-activated protein kinase pathway suppresses cell survival by inducing dephosphorylation of mitogen-activated protein/extracellular signal-regulated kinase kinase1,2. *Cancer Res.*, **63,** 3473-3477.

189 Tanaka N, Kamanaka M, Enslen H, Dong C, Wysk M, Davis RJ, & Flavell RA (2002) Differential involvement of p38 mitogen-activated protein kinase kinases MKK3 and MKK6 in T-cell apoptosis. *EMBO Rep.*, **3,** 785-791.

190 Porras A, Zuluaga S, Black E, Valladares A, Alvarez AM, Ambrosino C, Benito M, & Nebreda AR (2004) P38 alpha mitogen-activated protein kinase sensitizes cells to apoptosis induced by different stimuli. *Mol. Biol.*

Cell, **15,** 922-933.

191 Grethe S & Porn-Ares MI (2006) p38 MAPK regulates phosphorylation of Bad via PP2A-dependent suppression of the MEK1/2-ERK1/2 survival pathway in TNF-alpha induced endothelial apoptosis. *Cell Signal.*, **18,** 531-540.

192 Prickett TD & Brautigan DL (2007) Cytokine activation of p38 mitogen-activated protein kinase and apoptosis is opposed by alpha-4 targeting of protein phosphatase 2A for site-specific dephosphorylation of MEK3. *Mol. Cell Biol.*, **27,** 4217-4227.

193 Gotz J, Probst A, Ehler E, Hemmings B, & Kues W (1998) Delayed embryonic lethality in mice lacking protein phosphatase 2A catalytic subunit Calpha. *Proc. Natl. Acad. Sci U. S. A*, **95,** 12370-12375.

194 Gotz J, Probst A, Mistl C, Nitsch RM, & Ehler E (2000) Distinct role of protein phosphatase 2A subunit Calpha in the regulation of E-cadherin and beta-catenin during development. *Mech. Dev.*, **93,** 83-93.

195 Barker N & Clevers H (2000) Catenins, Wnt signaling and cancer. *Bioessays*, **22,** 961-965.

196 Patturajan M, Nomoto S, Sommer M, Fomenkov A, Hibi K, Zangen R, Poliak N, Califano J, Trink B, Ratovitski E, & Sidransky D (2002) DeltaNp63 induces beta-catenin nuclear accumulation and signaling. *Cancer Cell*, **1,** 369-379.

197 Seeling JM, Miller JR, Gil R, Moon RT, White R, & Virshup DM (1999) Regulation of beta-catenin signaling by the B56 subunit of protein phosphatase 2A. *Science*, **283,** 2089-2091.

198 Li X, Yost HJ, Virshup DM, & Seeling JM (2001) Protein phosphatase 2A and its B56 regulatory subunit inhibit Wnt signaling in Xenopus. *EMBO J.*, **20,** 4122-4131.

199 Creyghton MP, Roel G, Eichhorn PJ, Vredeveld LC, Destree O, & Bernards R (2006) PR130 is a modulator of the Wnt-signaling cascade that counters repression of the antagonist Naked cuticle. *Proc. Natl. Acad. Sci U. S. A*, **103,** 5397-5402.

200 Aulehla A & Herrmann BG (2004) Segmentation in vertebrates: clock and gradient finally joined. *Genes Dev.*, **18,** 2060-2067.

201 Tian Q & Wang J (2002) Role of serine/threonine protein phosphatase in Alzheimer's disease. *Neurosignals.*, **11,** 262-269.

202 Zhang CE, Tian Q, Wei W, Peng JH, Liu GP, Zhou XW, Wang Q, Wang DW, & Wang JZ (2008) Homocysteine induces tau phosphorylation by inactivating protein phosphatase 2A in rat hippocampus. *Neurobiol. Aging*, **29,** 1654-1665.

203 Sontag E, Nunbhakdi-Craig V, Sontag JM, az-Arrastia R, Ogris E, Dayal S, Lentz SR, Arning E, & Bottiglieri T (2007) Protein phosphatase 2A methyltransferase links homocysteine metabolism with tau and amyloid precursor protein regulation. *J. Neurosci.*, **27,** 2751-2759.

204 Tsujio I, Zaidi T, Xu J, Kotula L, Grundke-Iqbal I, & Iqbal K (2005) Inhibitors of protein phosphatase-2A from human brain structures, immunocytological localization and activities towards dephosphorylation of the Alzheimer type hyperphosphorylated tau. *FEBS Lett.*, **579,** 363-372.

205 Van HC & Goris J (2004) PP2A fulfills its promises as tumor suppressor: which subunits are important? *Cancer Cell*, **5,** 105-106.

206 Ruediger R, Pham HT, & Walter G (2001) Alterations in protein phosphatase 2A subunit interaction in human carcinomas of the lung and colon with mutations in the A beta subunit gene. *Oncogene*, **20,** 1892-1899.

207 Tamaki M, Goi T, Hirono Y, Katayama K, & Yamaguchi A (2004) PPP2R1B gene alterations inhibit interaction of PP2A-Abeta and PP2A-C proteins in colorectal cancers. *Oncol. Rep.*, **11,** 655-659.

208 Ito A, Koma Y, Watabe K, Nagano T, Endo Y, Nojima H, & Kitamura Y (2003) A truncated isoform of the protein phosphatase 2A B56gamma regulatory subunit may promote genetic instability and cause tumor progression. *Am. J. Pathol.*, **162,** 81-91.

209 Deichmann M, Polychronidis M, Wacker J, Thome M, & Naher H (2001) The protein phosphatase 2A subunit Bgamma gene is identified to be differentially expressed in malignant melanomas by subtractive suppression hybridization. *Melanoma Res.*, **11,** 577-585.

210 Junttila MR, Puustinen P, Niemela M, Ahola R, Arnold H, Bottzauw T, Ia-aho R, Nielsen C, Ivaska J, Taya Y, Lu SL, Lin S, Chan EK, Wang XJ, Grenman R, Kast J, Kallunki T, Sears R, Kahari VM, & Westermarck J (2007) CIP2A inhibits PP2A in human malignancies. *Cell*, **130,** 51-62.

211 Okamoto K, Li H, Jensen MR, Zhang T, Taya Y, Thorgeirsson SS, & Prives C (2002) Cyclin G recruits PP2A to dephosphorylate Mdm2. *Mol. Cell*, **9,** 761-771.

212 Haupt Y, Maya R, Kazaz A, & Oren M (1997) Mdm2 promotes the rapid degradation of p53. *Nature*, **387,** 296-299.

213 Dohoney KM, Guillerm C, Whiteford C, Elbi C, Lambert PF, Hager GL, & Brady JN (2004) Phosphorylation of p53 at serine 37 is important for transcriptional activity and regulation in response to DNA damage. *Oncogene*, **23,** 49-57.

214 Li HH, Cai X, Shouse GP, Piluso LG, & Liu X (2007) A specific PP2A regulatory subunit, B56gamma, mediates DNA damage-induced

dephosphorylation of p53 at Thr55. *EMBO J.*, **26,** 402-411.

215 Manning BD & Cantley LC (2007) AKT/PKB signaling: navigating downstream. *Cell*, **129,** 1261-1274.

216 Chen W & Hahn WC (2003) SV40 early region oncoproteins and human cell transformation. *Histol. Histopathol.*, **18,** 541-550.

217 Chen Y, Xu Y, Bao Q, Xing Y, Li Z, Lin Z, Stock JB, Jeffrey PD, & Shi Y (2007) Structural and biochemical insights into the regulation of protein phosphatase 2A by small t antigen of SV40. *Nat. Struct. Mol. Biol.*, **14,** 527-534.

218 Longin S, Zwaenepoel K, Martens E, Louis JV, Rondelez E, Goris J, & Janssens V (2008) Spatial control of protein phosphatase 2A (de)methylation. *Exp. Cell Res.*, **314,** 68-81.

219 Kelley LA, MacCallum RM, & Sternberg MJ (2000) Enhanced genome annotation using structural profiles in the program 3D-PSSM. *J. Mol. Biol.*, **299,** 499-520.

220 Finn RD, Mistry J, Schuster-Bockler B, Griffiths-Jones S, Hollich V, Lassmann T, Moxon S, Marshall M, Khanna A, Durbin R, Eddy SR, Sonnhammer EL, & Bateman A (2006) Pfam: clans, web tools and services. *Nucleic Acids Res.*, **34,** D247-D251.

221 Xing Y, Li Z, Chen Y, Stock JB, Jeffrey PD, & Shi Y (2008) Structural mechanism of demethylation and inactivation of protein phosphatase 2A. *Cell*, **133,** 154-163.

222 Lee JA & Pallas DC (2007) Leucine carboxyl methyltransferase-1 is necessary for normal progression through mitosis in mammalian cells. *J. Biol. Chem.*, **282,** 30974-30984.

223 Leulliot N, Quevillon-Cheruel S, Sorel I, de La Sierra-Gallay IL, Collinet B, Graille M, Blondeau K, Bettache N, Poupon A, Janin J, & van TH (2004) Structure of protein phosphatase methyltransferase 1 (PPM1), a leucine carboxyl methyltransferase involved in the regulation of protein phosphatase 2A activity. *J. Biol. Chem.*, **279,** 8351-8358.

224 Wang Y & Burke DJ (1997) Cdc55p, the B-type regulatory subunit of protein phosphatase 2A, has multiple functions in mitosis and is required for the kinetochore/spindle checkpoint in Saccharomyces cerevisiae. *Mol. Cell Biol.*, **17,** 620-626.

225 Gil-Bernabe AM, Romero F, Limon-Mortes MC, & Tortolero M (2006) Protein phosphatase 2A stabilizes human securin, whose phosphorylated forms are degraded via the SCF ubiquitin ligase. *Mol. Cell Biol.*, **26,** 4017-4027.

226 Kitajima TS, Sakuno T, Ishiguro K, Iemura S, Natsume T, Kawashima SA, & Watanabe Y (2006) Shugoshin collaborates with protein phosphatase

2A to protect cohesin. *Nature*, **441,** 46-52.

227 Schultz J, Milpetz F, Bork P, & Ponting CP (1998) SMART, a simple modular architecture research tool: identification of signaling domains. *Proc. Natl. Acad. Sci U. S. A*, **95,** 5857-5864.

228 Bryson K, McGuffin LJ, Marsden RL, Ward JJ, Sodhi JS, & Jones DT (2005) Protein structure prediction servers at University College London. *Nucleic Acids Res.*, **33,** W36-W38.

229 Jones DT (1999) Protein secondary structure prediction based on position-specific scoring matrices. *J. Mol. Biol.*, **292,** 195-202.

230 Fontana A, de Laureto PP, Spolaore B, Frare E, Picotti P, & Zambonin M (2004) Probing protein structure by limited proteolysis. *Acta Biochim. Pol.*, **51,** 299-321.

231 Fiser A & Sali A (2003) Modeller: generation and refinement of homology-based protein structure models. *Methods Enzymol.*, **374,** 461-491.

232 Morris AL, MacArthur MW, Hutchinson EG, & Thornton JM (1992) Stereochemical quality of protein structure coordinates. *Proteins*, **12,** 345-364.

233 (1994) The CCP4 suite: programs for protein crystallography. *Acta Crystallogr. D Biol. Crystallogr.*, **50,** 760-763.

234 George RR, Harris R, Nunn CM, Cramer R, & Djordjevic S (2002) Chaperonin assisted overexpression, purification, and characterisation of human PP2A methyltransferase. *Protein Expr. Purif.*, **26,** 266-274.

235 Myles T, Schmidt K, Evans DR, Cron P, & Hemmings BA (2001) Active-site mutations impairing the catalytic function of the catalytic subunit of human protein phosphatase 2A permit baculovirus-mediated overexpression in insect cells. *Biochem. J.*, **357,** 225-232.

236 Jin LT, Hwang SY, Yoo GS, & Choi JK (2004) Sensitive silver staining of protein in sodium dodecyl sulfate-polyacrylamide gels using an azo dye, calconcarboxylic acid, as a silver-ion sensitizer. *Electrophoresis*, **25,** 2494-2500.

237 Provencher SW & Glockner J (1981) Estimation of globular protein secondary structure from circular dichroism. *Biochemistry*, **20,** 33-37.

238 Velazquez-Campoy A, Leavitt SA, & Freire E (2004) Characterization of protein-protein interactions by isothermal titration calorimetry. *Methods Mol. Biol.*, **261,** 35-54.

239 Pierce MM, Raman CS, & Nall BT (1999) Isothermal titration calorimetry of protein-protein interactions. *Methods*, **19,** 213-221.

240 Sanchez-Ruiz JM, Lopez-Lacomba JL, Cortijo M, & Mateo PL (1988) Differential scanning calorimetry of the irreversible thermal denaturation of thermolysin. *Biochemistry*, **27,** 1648-1652.

241 Spink CH (2008) Differential scanning calorimetry. *Methods Cell Biol.*, **84,** 115-141.

242 Boussaad S, Pean J, & Tao NJ (2000) High-resolution multiwavelength surface plasmon resonance spectroscopy for probing conformational and electronic changes in redox proteins. *Anal. Chem.*, **72,** 222-226.

243 Wang S, Boussaad S, Wong S, & Tao NJ (2000) High-sensitivity stark spectroscopy obtained by surface plasmon resonance measurement. *Anal. Chem.*, **72,** 4003-4008.

244 Gugliotti M, Rodrigues TS, Baptista MS, & Politi MJ (2004) Large increase in the heat transfer through monolayers detected by beam deflection. *Langmuir*, **20,** 5648-5650.

245 Ericsson UB, Hallberg BM, Detitta GT, Dekker N, & Nordlund P (2006) Thermofluor-based high-throughput stability optimization of proteins for structural studies. *Anal. Biochem.*, **357,** 289-298.

246 Pflugrath JW (1999) The finer things in X-ray diffraction data collection. *Acta Crystallogr. D Biol. Crystallogr.*, **55,** 1718-1725.

247 Kuo A, Bowler MW, Zimmer J, Antcliff JF, & Doyle DA (2003) Increasing the diffraction limit and internal order of a membrane protein crystal by dehydration. *J. Struct. Biol.*, **141,** 97-102.

248 Heras B, Edeling MA, Byriel KA, Jones A, Raina S, & Martin JL (2003) Dehydration converts DsbG crystal diffraction from low to high resolution. *Structure*, **11,** 139-145.

249 Heras B & Martin JL (2005) Post-crystallization treatments for improving diffraction quality of protein crystals. *Acta Crystallogr. D Biol. Crystallogr.*, **61,** 1173-1180.

250 McCoy AJ, Grosse-Kunstleve RW, Adams PD, Winn MD, Storoni LC, & Read RJ (2007) Phaser crystallographic software. *J. Appl. Crystallogr.*, **40,** 658-674.

251 Vagin A & Teplyakov A (2010) Molecular replacement with MOLREP. *Acta Crystallogr. D Biol. Crystallogr.*, **66,** 22-25.

252 Murshudov GN, Vagin AA, & Dodson EJ (1997) Refinement of macromolecular structures by the maximum-likelihood method. *Acta Crystallogr. D Biol. Crystallogr.*, **53,** 240-255.

253 Emsley P & Cowtan K (2004) Coot: model-building tools for molecular graphics. *Acta Crystallogr. D Biol. Crystallogr.*, **60,** 2126-2132.

254 Laskowski RA, Moss DS, & Thornton JM (1993) Main-chain bond lengths and bond angles in protein structures. *J. Mol. Biol.*, **231,** 1049-1067.

255 Chen VB, Arendall WB, III, Headd JJ, Keedy DA, Immormino RM, Kapral GJ, Murray LW, Richardson JS, & Richardson DC (2010) MolProbity: all-atom structure validation for macromolecular crystallography. *Acta Crystallogr. D Biol. Crystallogr.*, **66,** 12-21.

256 Berman HM, Battistuz T, Bhat TN, Bluhm WF, Bourne PE, Burkhardt K, Feng Z, Gilliland GL, Iype L, Jain S, Fagan P, Marvin J, Padilla D, Ravichandran V, Schneider B, Thanki N, Weissig H, Westbrook JD, & Zardecki C (2002) The Protein Data Bank. *Acta Crystallogr. D Biol. Crystallogr.*, **58,** 899-907.

257 Larkin MA, Blackshields G, Brown NP, Chenna R, McGettigan PA, McWilliam H, Valentin F, Wallace IM, Wilm A, Lopez R, Thompson JD, Gibson TJ, & Higgins DG (2007) Clustal W and Clustal X version 2.0. *Bioinformatics*, **23,** 2947-2948.

258 de Marco A (2006) Two-step metal affinity purification of double-tagged (NusA-His6) fusion proteins. *Nat. Protoc.*, **1,** 1538-1543.

259 Ikehara T, Shinjo F, Ikehara S, Imamura S, & Yasumoto T (2006) Baculovirus expression, purification, and characterization of human protein phosphatase 2A catalytic subunits alpha and beta. *Protein Expr. Purif.*, **45,** 150-156.

260 Brandt H, Capulong ZL, & Lee EY (1975) Purification and properties of rabbit liver phosphorylase phosphatase. *J. Biol. Chem.*, **250,** 8038-8044.

261 Martin BL, Shriner CL, & Brautigan DL (1994) Concurrent purification of type-1 and type-2A protein phosphatase catalytic subunits. *Protein Expr. Purif.*, **5,** 211-217.

262 Kloeker S, Reed R, McConnell JL, Chang D, Tran K, Westphal RS, Law BK, Colbran RJ, Kamoun M, Campbell KS, & Wadzinski BE (2003) Parallel purification of three catalytic subunits of the protein serine/threonine phosphatase 2A family (PP2A(C), PP4(C), and PP6(C)) and analysis of the interaction of PP2A(C) with alpha4 protein. *Protein Expr. Purif.*, **31,** 19-33.

263 Malmqvist M & Karlsson R (1997) Biomolecular interaction analysis: affinity biosensor technologies for functional analysis of proteins. *Curr. Opin. Chem. Biol.*, **1,** 378-383.

264 Nieba L, Nieba-Axmann SE, Persson A, Hamalainen M, Edebratt F, Hansson A, Lidholm J, Magnusson K, Karlsson AF, & Pluckthun A (1997) BIACORE analysis of histidine-tagged proteins using a chelating NTA sensor chip. *Anal. Biochem.*, **252,** 217-228.

265 Makhatadze GI & Privalov PL (1995) Energetics of protein structure. *Adv.*

Protein Chem., **47,** 307-425.

266 Gomez J, Hilser VJ, Xie D, & Freire E (1995) The heat capacity of proteins. *Proteins*, **22,** 404-412.

267 Eftink MR, Anusiem AC, & Biltonen RL (1983) Enthalpy-entropy compensation and heat capacity changes for protein-ligand interactions: general thermodynamic models and data for the binding of nucleotides to ribonuclease A. *Biochemistry*, **22,** 3884-3896.

268 Spolar RS, Livingstone JR, & Record MT, Jr. (1992) Use of liquid hydrocarbon and amide transfer data to estimate contributions to thermodynamic functions of protein folding from the removal of nonpolar and polar surface from water. *Biochemistry*, **31,** 3947-3955.

269 Privalov PL & Gill SJ (1988) Stability of protein structure and hydrophobic interaction. *Adv. Protein Chem.*, **39,** 191-234.

270 Privalov PL & Makhatadze GI (1990) Heat capacity of proteins. II. Partial molar heat capacity of the unfolded polypeptide chain of proteins: protein unfolding effects. *J. Mol. Biol.*, **213,** 385-391.

271 Dill KA (1990) Dominant forces in protein folding. *Biochemistry*, **29,** 7133-7155.

272 Luther MA, Cai GZ, & Lee JC (1986) Thermodynamics of dimer and tetramer formations in rabbit muscle phosphofructokinase. *Biochemistry*, **25,** 7931-7937.

273 Hileman RE, Jennings RN, & Linhardt RJ (1998) Thermodynamic analysis of the heparin interaction with a basic cyclic peptide using isothermal titration calorimetry. *Biochemistry*, **37,** 15231-15237.

274 Niedzwiecka A, Stepinski J, Darzynkiewicz E, Sonenberg N, & Stolarski R (2002) Positive heat capacity change upon specific binding of translation initiation factor eIF4E to mRNA 5' cap. *Biochemistry*, **41,** 12140-12148.

275 McGinnis S & Madden TL (2004) BLAST: at the core of a powerful and diverse set of sequence analysis tools. *Nucleic Acids Res.*, **32,** W20-W25.

276 Dickey RW, Bobzin SC, Faulkner DJ, Bencsath FA, & Andrzejewski D (1990) Identification of okadaic acid from a Caribbean dinoflagellate, Prorocentrum concavum. *Toxicon*, **28,** 371-377.

277 Garcia A, Cayla X, Guergnon J, Dessauge F, Hospital V, Rebollo MP, Fleischer A, & Rebollo A (2003) Serine/threonine protein phosphatases PP1 and PP2A are key players in apoptosis. *Biochimie*, **85,** 721-726.

278 Lee J, Chen Y, Tolstykh T, & Stock J (1996) A specific protein carboxyl methylesterase that demethylates phosphoprotein phosphatase 2A in

bovine brain. *Proc. Natl. Acad. Sci U. S. A*, **93,** 6043-6047.

279 Schubert HL, Blumenthal RM, & Cheng X (2003) Many paths to methyltransfer: a chronicle of convergence. *Trends Biochem. Sci*, **28,** 329-335.

280 Martin JL & McMillan FM (2002) SAM (dependent) I AM: the S-adenosylmethionine-dependent methyltransferase fold. *Curr. Opin. Struct. Biol.*, **12,** 783-793.

281 Djordjevic S & Stock AM (1997) Crystal structure of the chemotaxis receptor methyltransferase CheR suggests a conserved structural motif for binding S-adenosylmethionine. *Structure*, **5,** 545-558.